INVESTIGATING THE ROLES OF AQUAPORIN 4 IN INTRACELLULAR AND EXTRACELLULAR VESICLES IN MODELS OF TRAUMATIC INJURY

CHARLOTTE ELIZABETH CLARKE-BLAND

Doctor of Philosophy

ASTON UNIVERSITY

September 2023

Thesis Summary

Investigating the roles of Aquaporin 4 in intracellular and extracellular vesicles in models of traumatic injury

Charlotte Clarke-Bland, Doctor of Philosophy, Aston University 2023

Recent findings indicate that Aquaporins (AQP) play important roles in intracellular and extracellular Vesicles (EV). Intracellular vesicular trafficking of vesicles causes increased AQP concentration in the plasma membrane and increased water uptake by cells. It has recently been shown that AQP are released in EV, multiple roles for AQP in EV have been suggested, such as volumetric control of cells, uptake of AQP by recipient cells, and more. Both mechanisms have been identified in cells expressing AQP4 and have been linked to the pathological uptake and accumulation of water (oedema) in the central nervous system following injury.

This study aims to understand the role of AQP4 in intracellular and extracellular vesicles. We ask: 1) Does AQP4 traffic to the endfeet of astrocytes following injury? 2) Does extracellular hypotonicity (as seen in CNS oedema) promote EV release? 3) Is AQP4 present in these EV? and 4) what is the role of AQP4 in these EV?

A rat spinal crush injury model was used to investigate the role of calmodulin (CaM) and protein kinase A (PKA) in AQP4 trafficking to astrocytic endfeet *in vivo*, a mechanism previously only investigated in an *in vitro* model. Inhibition of CaM and PKA reduced AQP4 expression and trafficking to endfeet.

An EV release model was developed to produced AQP4-positive EV *in vitro,* using stably transfected cell lines expressing AQP4, changes in extracellular tonicity impacted both EV release and EV cargo. Changes in EV populations were measured using ultraviolet side scatter flow cytometry and western blotting.

These results indicate that AQP4 plays an important role in astrocytic vesicles and could be a therapeutic target to cerebral oedema.

Keywords: Aquaporin 4, Extracellular Vesicles, CNS injury, TFP, H89, Hypotonicity

Acknowledgements

Firstly, it is important to acknowledge the use of HeLa cells in this project. The HeLa cell line was established from the tumour cells of Henrietta Lacks without her knowledge or consent in 1951. Use of these cells has made significant contributions to scientific progress and advances in human health. I am grateful to Henrietta Lacks, now deceased, and to her surviving family members for their contributions to biomedical research, and this project. Researchers involved in this project have made donations to the Henrietta Lacks Foundation™ to acknowledge and express gratitude for this contribution.

I would like to thank Professors Asif Ahmed and Chris Hewitt, who initiated and facilitated my PhD journey. Thanks also to Aston University Biosciences and Health & Life Sciences for funding and support.

A huge thanks goes to my PhD supervisors, Professors Roslyn Bill and Andrew Devitt who have supported me, not only during my PhD but throughout my career. They have shared their experience and expertise and have been generous with their time. They have also taken me to some amazing places and provided me with endless opportunities to learn and grow. I feel very lucky to have had them as my supervisors.

Special thanks go to Dr John Simms, who helped me settle back into lab work after eight years away. His patience and understanding certainly made the process easier for me. Also, to Drs Phillip Kitchen and Ivana Milic, I have learned a lot, thanks to their knowledge, attention to detail, and willingness to help.

Thanks also go to everyone on #TeamAQP, past and present, and everyone in the EV lab. Thank you for all the bits of training, sharing, discussions and fun.

Thank you to my family and friends who have believed in me and lifted me up, especially my mum Julie, Philly, Beth, Nathan, Christina, Gabby, and Lo.

I am unbelievably grateful for the love and support of my partner Craig who has held my world steady.

And of course, my final words go to my son Archie, my forever motivation.

Publications

Kitchen, P., Salman, M. M., Halsey, A. M., **Clarke-Bland, C**., MacDonald, J. A., Ishida, H., Vogel, H. J., Almutiri, S., Logan, A., Kreida, S., Al-Jubair, T., Winkel Missel, J., Gourdon, P., Törnroth-Horsefield, S., Conner, M. T., Ahmed, Z., Conner, A. C., & Bill, R. M. (2020). Targeting Aquaporin-4 Subcellular Localization to Treat Central Nervous System Edema. *Cell*, 181(4), 784–799.e19. https://doi.org/10.1016/j.cell.2020.03.037

Clarke-Bland, C. E., Bill, R. M., & Devitt, A. (2022). Emerging roles for AQP in mammalian extracellular vesicles. *Biochimica et Biophysica Acta. Biomembranes*, *1864*(3), 183826. https://doi.org/10.1016/j.bbamem.2021.183826

Contents

List of Tables

Abbreviations

AD	Alzheimer's Disease
Alix	ALG-2-interacting protein X
ANOVA	Analysis of variance
APO	Apochromatic
AQP	Aquaporin/s
ATP	Adenosine Triphosphate
AVP	Arginine Vasopressin
BBB	Blood-brain-barrier
BSA	Bovine serum albumin
CaM	Calmodulin
cDNA	Complementary DNA
CNS	Central Nervous System
CryoTEM	Cryogenic transmission electron microscopy
CSF	Cerebrospinal fluid
DAPI	4',6-diamidino-2-phenylindole
DMEM	Dulbecco's Modified Eagle Medium
DMSO	Dimethyl sulfoxide
Duc	Differential ultracentrifugation
EDTA	Ethylenediaminetetraacetic acid
EAAT1/2	Excitatory amino acid transporter 1/2
ESCRT	Endosomal sorting complex
EV	Extracellular Vesicle/s
FC	Flow cytometry
GBM	Glioblastoma multiforme
GFAP	Glial fibrillary acidic protein
gMFI	Geometric mean fluorescence intensity
H-89	N-[2-(p-Bromocinnamylamino)ethyl]-5-isoquinolinesulfonamide
IHC	Immunohistochemistry
ISF	Interstitial fluid
mFI	Median fluorescence intensity
NMOSD	Neuromyelitis Optica spectrum disorders
NPA	Asparagine-proline-alanine
OAP	Orthogonal arrays of particles
PBS	Phosphate buffered saline
PDL	Poly-D-Lysine
PDVF	Immobilon-P polyvinylidene fluoride
PEI	Polyethyleneimine
PFA	Paraformaldehyde
PKA	Protein Kinase A
PKC	Protein Kinase C
RECA-1	Rat endothelia cell Antigen -1
REE	Relative endfoot expression
RME	Relative membrane expression
ROI	Region of interest
ROS	Reactive oxygen Species
SC	Spinal cord

SCI	Spinal Cord Injury
SEC	Size exclusion chromatography
SED	Stress induced exhaustion disorder
siRNA	Small interfering RNAs
TBI	Traumatic Brain Injury
TEM	Transmission electron microscopy
TFP	Trifluoperazine
TGN-020	2-(nicotinamide)-1,3,4-thiadiazole
TSG101	Tumour susceptibility gene 101
uEV	Urinary Extracellular vesicles
UV-SSC	Ultraviolet side scatter
VPS4	Vacuolar protein sorting-associated protein
VR2	Type 2 vasopressin receptor
WT	Wild Type

Chapter 1 Introduction[1]

1.1 Aquaporin proteins

1.1.1 Water homeostasis

Maintaining proper water and solute balance is fundamental for the normal functioning of all living organisms. The rapid movement of water is an important mechanism by which water/solute balances are maintained. The diffusion of water across membranes via osmosis is a well characterised concept (Loeb, 1920) but does not account for the rapid transcellular water movement essential for maintaining homeostasis. Though a number of theories were explored (Flamion and Spring, 1990, Sidel and Solomon, 1957, Solomon et al., 1983), aquaporins (AQP) have been identified as the channels via which rapid water transport occurs.

1.1.2 Aquaporin expression and function

AQP are a family of small (~30 kDa), integral, transmembrane water channel proteins (Verkman and Mitra, 2000). AQP have been identified in all kingdoms of life including thirteen mammalian AQP (AQP 0–12). In mammals, AQP typically reside in the plasma membrane of cells (Denker et al., 1988) where they form pores and facilitate the rapid, passive and bi-directional movement of water, small neutral solutes, and some ions, into and out of cells in response to osmotic or concentration gradients (Bai et al., 1999). Selected AQP exhibit different subcellular localisation (Nozaki et al., 2008); and some are found in intracellular vesicles which can traffic to the plasma membrane in response to external stimuli including hormones, hypotonicity and hypoxia (Conner et al., 2012, Kitchen et al., 2015b, Salman et al., 2017)

[1] Parts of this chapter have been adapted from the published literature review: Clarke-Bland, C. et al. (2022). “Emerging roles for Aquaporins in Extracellular Vesicles”. *Biochimica et Biophysica Acta. Biomembranes*, *1864*(3), 183826.

1.1.3 Aquaporin structure

AQP are characterised by their structural components. They comprise six transmembrane helices, intracellular N- and C- termini and five loop domains (Figure 1.1). *In vivo*, AQP predominantly assemble as homotetramers (de Groot et al., 2001) with each AQP monomeric unit featuring a functional central pore that facilitates water permeability (Jung et al., 1994). The narrowest point of this pore measures approximately 2.8Å (Agre et al., 2002, Cui and Bastien, 2011) and contains the distinctive AQP NPA (asparagine-proline-alanine) motif (Eriksson et al., 2013, Beitz et al., 2006), integral for the selective transport of water. Variations in this NPA domain give rise to differential permeability profiles and subclasses of AQP (Kitchen et al., 2015a). Orthodox AQPs (0,1,2,4,5,6 and 10) are permeable to water (and some also act as ion channels), aquaglyceroporins (AQPs 3, 7 and 9) are permeable to glycerol, urea and some other solutes, whilst super or unorthodox aquaporins (AQPs 11 and 12) are the most recently and incompletely defined family members (AQP8 is an ammonia-permeable AQP related to the orthodox sub-group (Kitchen et al., 2015a).

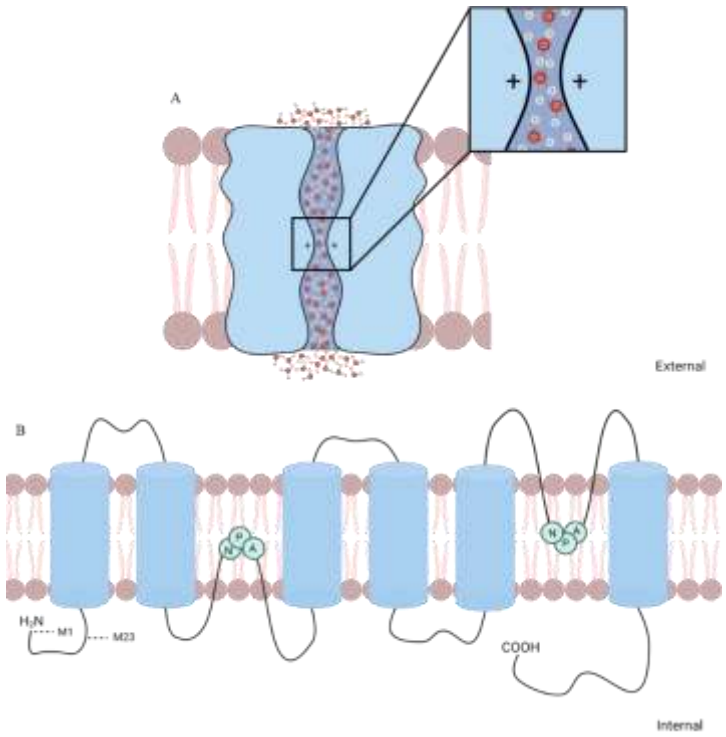

Figure 1.1 AQP structure

(A) Schematic cross section of an AQP monomer in a plasma membrane. Water molecules move through the central pore in single file at the narrowest point. Positive charges in the pore facilitate selective water transport. Zoomed selection shows the narrowest point in more detail. (B) Schematic representation of AQP4 components in a lipid bilayer. AQP are characterised by their NPA motif, intracellular N- and C- termini and transmembrane helices. AQP4 has two isoforms, M1 and M23, named after their initial methionine residues. Schematic representations of AQP structures were made using Biorender.com.

The thirteen mammalian AQP are expressed ubiquitously throughout the human body; they have been identified in every tissue (Figure 1.2) (Day et al., 2014). AQP are expressed preferentially in specific tissues and organs. The structure and localisation of AQP largely determines their function (Horsefield et al., 2008, Magni et al., 2006), for example the orthodox AQP, AQP4 is the primary water channel in the central nervous system (CNS) (Manley et al., 2004) while AQP7, an aquaglyceroporin permeable to water, glycerol, urea and some other solutes. It expressed by adipocytes where it functions primarily as a glycerol transporter (Kishida et al., 2000).

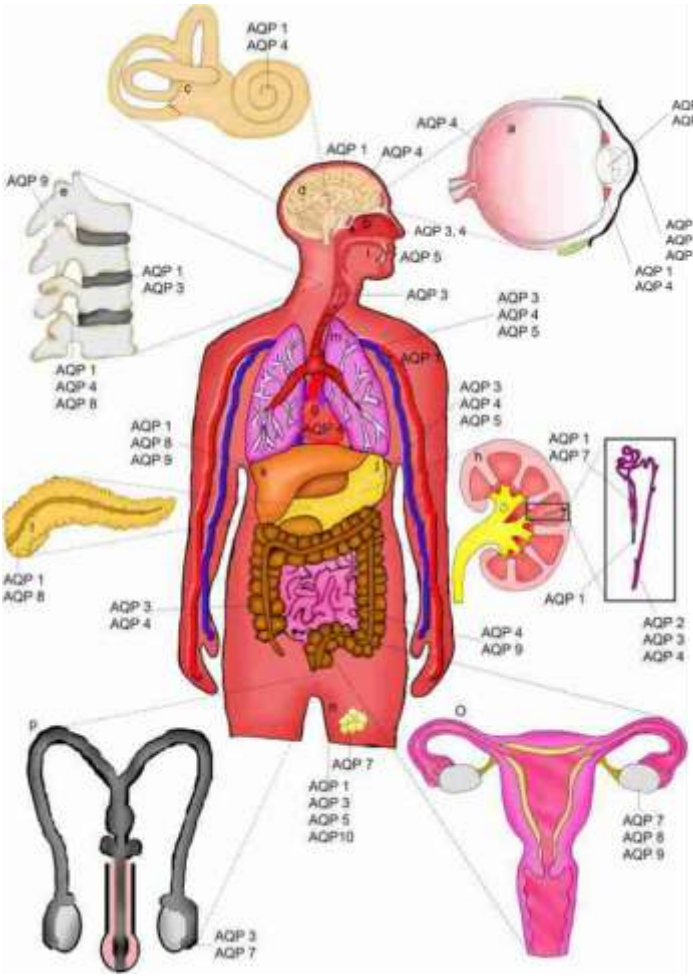

Figure 1.2 Human AQP expression

Schematic representation of AQP expression in the human body. (A) Eye: AQP 0, 1, 3, 4 & 5. (B) Olfactory: AQP 4 & 5 (C) Inner Ear: AQP 1 & 4 (D) Brain: AQP 1 & 4 (E) Spinal cord: AQP 1, 4 & 8. Intervertebral disk: AQP 1 & 3, Osteoclast: AQP 9. (F) Blood vessels: AQP 1. (G) Heart: AQP4. (H) Kidney: AQP 1, 2, 3, 4 & 7. (I) Salivary Glands: AQP5. (J) Gastrointestinal Tract: AQP 3, 4, 5 & 9. (K) Liver: AQP 1, 8 & 9. (L) Pancreas: AQP 1 & 8. (M) Lung: AQP 3, 4 & 5. (N) Adipose Tissue: AQP 7. (O) Reproductive AQP3, 7, 8 & 9. Schematic from (Day, et al., 2014); reproduced with permission.

1.1.4 Aquaporin trafficking

The water channel function of AQP is dependent on their localisation in the plasma membrane. Many AQP are constitutively expressed at the plasma membrane, but some are also stored in intracellular vesicles and relocalised to the plasma membrane in response to external stimuli. The membrane trafficking mechanisms of AQP2 are the most well documented. Expression of AQP2 at the plasma membrane is selectively controlled by the anti-diuretic hormone, arginine vasopressin (AVP). AQP2 is primarily a water channel protein, important for the reabsorption of water into the bloodstream. AQP2 is expressed by principal cells in the kidney and is located in connecting tubules and collecting ducts of the nephron (Nielsen et al., 1993b). AQP2 is expressed only at the apical membrane and in sub-apical vesicles at the plasma membrane of principal cells.

The AVP-AQP2 pathway has been established as an important mechanism in physiological water balance and related disorders (Figure 1.3) (Marples et al., 1995, Nielsen et al., 1995). AVP secretion by the pituitary gland increases in response to increased blood plasma osmolality and decreases in blood volume. AVP binds the type 2 vasopressin receptor (V2R) in the kidney resulting in increased water absorption through AQP2. AVP-V2R binding results in increased phosphorylation of AQP2 by protein kinase A (PKA) and an increase in intracellular calcium ions, required for AQP2 trafficking (Jung and Kwon, 2016). Upon phosphorylation, AQP2 traffics from intracellular vesicles to the apical plasma membrane, resulting in increased membrane porosity and water reabsorption (Knepper et al., 2015).

Discovery of this trafficking mechanism inspired studies of potential, similar trafficking mechanisms for other AQP. AQP1 is another highly expressed renal water channel protein but its relocalisation is not regulated by AVP. *In vitro* studies identified AQP1 trafficking to the plasma membrane of cells in response to extracellular hypotonicity. Similar to the AVP-AQP2 mechanism, increases in intracellular calcium ions were observed. AQP1 is phosphorylated by protein kinase C (PKC) and relocalises to the plasma membrane and increases cell water permeability (Conner et al., 2012, Conner et al., 2010).

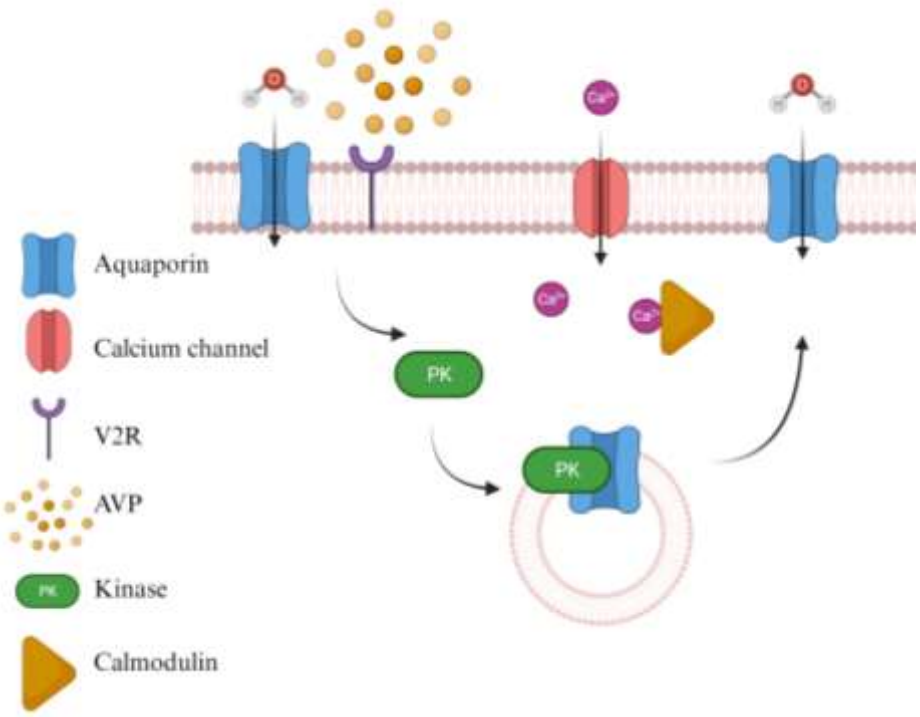

Figure 1.3 AQP trafficking mechanisms

The schematic shows the trafficking mechanisms observed for AQP 1, 2 & 4. Intracellular AQP are stored in intracellular vesicles. They traffic to the plasma membrane in response to external triggers such as hypotonicity (caused by hypoxia; AQP 1 & 4) and AVP binding to V2R (AQP2). These triggers cause calcium ion influx and phosphorylation by protein kinases C (AQP1) or A (AQP 2 & 4). Calmodulin activation has been identified in the AQP4 pathway. Water influx increases following increased AQP localisation to the cell surface. Schematic created using Biorender.com.

A similar mechanism for AQP4 has been identified in an *in vitro* cell model (Kitchen et al., 2015b). AQP4 in intracellular vesicles relocalises to the plasma membrane in response to extracellular changes such as hypotonicity. As AQP4 relocalises to the plasma membrane, water re-uptake increases, and cell swelling is observed. As with AQP1 relocalisation, intracellular calcium ion levels increase, and PKA phosphorylates AQP4. Calmodulin (CaM) is activated by increased intracellular calcium ions. Mutation of PKA phosphorylation sites, and inhibition of CaM with W-7 hydrochloride or Trifluoperazine (TFP) prevented AQP4 membrane trafficking in response to extracellular stimuli. This suggests that AQP4 phosphorylation and inhibition of CaM are potential targets to prevent AQP4 localisation to the plasma membrane *in vivo*.

1.1.5 Aquaporins of the central nervous system

AQP 1 & 4 are expressed in the CNS and function primarily as water channels. AQP1 is located in the apical membrane of epithelial cells within the choroid plexus (King and Agre, 1996). Its role involves facilitating water secretion into the cerebral spinal fluid (CSF) (Nielsen et al., 1993b). AQP4, the protein of interest for this project, is the most abundantly expressed AQP in the CNS (Hasegawa et al., 1994, Rash, 1998). It is expressed by astrocytes, a glial cell subtype with important roles such as, mediation of cerebral blood flow rate, the control of solute transport across the blood brain barrier (BBB) and cell to cell communication (Solenov et al., 2004). Their morphology is polyhedron (Ogata and Kosaka, 2002) consisting of a cell body, multiple processes and endfeet that surround blood vessels and form the BBB, the blood -spinal cord barrier. While AQP4 is expressed throughout astrocyte membranes, it is at the endfeet that AQP4 is most highly expressed (Figure 1.4) (Nielsen et al., 1997a). It is believed that the endfoot localisation of AQP4 is significant in the process of both healthy and pathological water transport in the CNS.

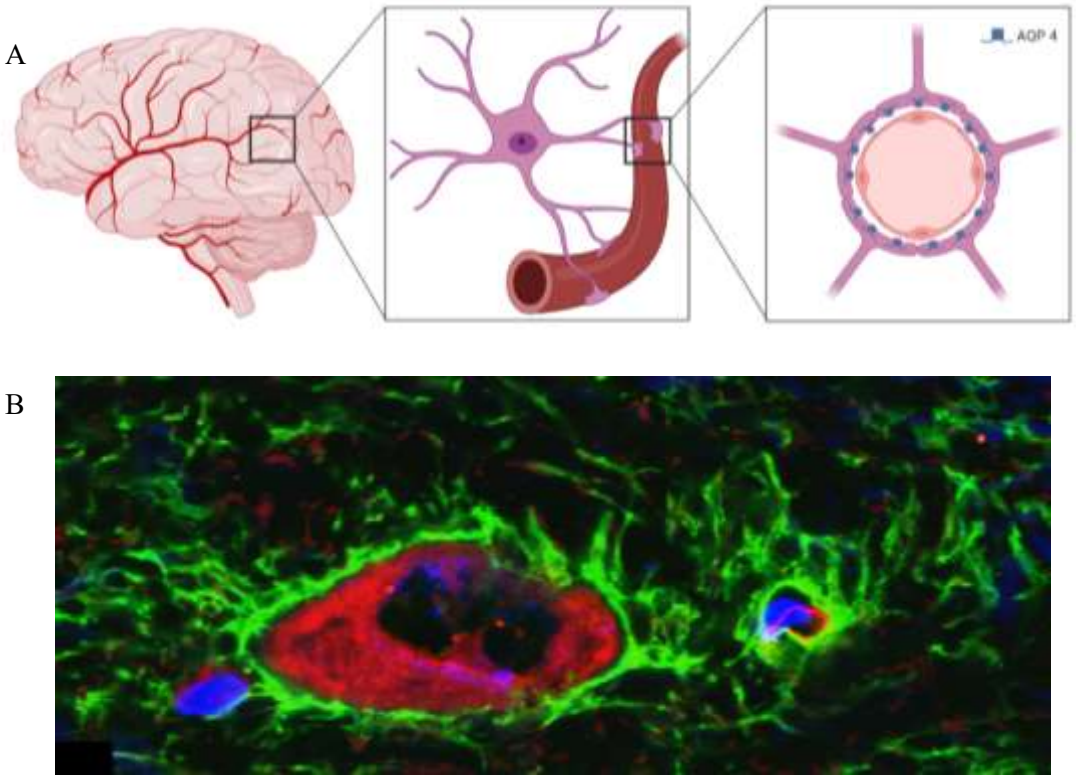

Figure 1.4 AQP4 expression in the Central Nervous System

(A) Schematic shows AQP4 localisation in the CNS. Blood vessels surround the brain tissue. Astrocytic endfeet wrap around blood vessels, forming the BBB. AQP4 is expressed in the endfeet of astrocytes. (B) Confocal image overlay shows AQP4 expression in astrocytic endfeet (green) surrounding vascular endothelial cells (red) and cell nuclei (blue). Schematic created using Biorender.com. Fluorescence image captured for this project.

AQP4 has been shown to play a pathophysiological role in diseases characterised by excess water accumulation in the CNS (oedema), such as tumour growth (Papadopoulos et al., 2001), ischemic stroke (Manley et al., 2000a) and traumatic injury (Ke et al., 2002, Kiening et al., 2002, Sun et al., 2003). It is now widely accepted AQP4 is responsible for rapid water transport and that inhibition of AQP4 is key in the therapeutic prevention of oedema following traumatic brain Injury (TBI). The search for AQP4 inhibitors has focussed largely on the prevention of water flow through AQP4, by blocking the pore. So far, this approach has shown little success (Abir-Awan et al., 2018), the most promising AQP4 inhibitor identified is currently TGN-020 (2-(nicotinamide)-1,3,4-thiadiazole) but it is yet to be trialled clinically (Igarashi et al., 2011). More recently studies have sought to understand and identify components of an AQP4 trafficking mechanism, based on the hypothesis that the plasma membrane localisation of AQP4 is essential to its function as a water channel. AQP4 trafficking is a potential target for prevention of oedema.

1.2 CNS injury

CNS injury, including spinal cord injury (SCI) and TBI can have long term detrimental effects on patients. While both conditions require further investigation to find successful therapeutic interventions, this study uses an SCI model to elucidate pathological mechanisms also observed in TBI. In the hope of preventing the onset of secondary injury in TBI and development of the associated symptoms.

TBI is a leading cause of death; affecting around 10 million people each year (Hyder et al., 2007). TBI is most commonly caused by road traffic accidents, falls and suicide attempts (Cassidy et al. (2004). It is defined as a direct or indirect physical trauma to the brain resulting in brain tissue injury. TBI includes primary injury, the physical and mechanical damage to brain tissue caused by the initial trauma, including damage to brain tissue and blood vessels, and secondary injury, tissue damage incurred as a result of water accumulation, via AQP4 In the brain (oedema) and increased intracranial pressure, bleeding and/ or prolonged inflammation. The pathophysiology of TBI is complex and patient outcome depends on both the severity of the primary injury and the level of damage caused by secondary injury. The prevention of secondary injury caused by oedema is the current focus of TBI therapeutics. Over 30 TBI clinical trials have been conducted but no success has yet been seen and further understanding of the mechanisms behind secondary injury is needed if successful

therapies are to be discovered. AQP4 remains a promising target but further understanding of its role in TBI is required.

1.2.1 CNS oedema

Following CNS injury, increased levels of water move into, and accumulate in the brain. This occurs via different mechanisms; in vasogenic oedema, blood vessels become compromised as endothelial tight junctions break down. Cytotoxic oedema is characterised by increased permeability of brain cells to solutes, causing disruption of osmotic gradients and the rapid influx of water into cells (Stiefel et al., 2005). Injury-related oedema is complex and vasogenic and cytotoxic oedemas often happen simultaneously.

Oedema is observed following both brain and spinal cord injury. The mechanisms of oedema are similar in both tissues of the CNS (Dumont et al., 2001). TBI and SCI are associated with secondary injury caused by swelling of CNS tissue caused by increases in intracranial or intraspinal pressure, as tissue volume increases within a fixed space defined by the cranium or dura of the spinal column (Ghajar, 2000, Yang et al., 2022, Maikos et al., 2008). Secondary injury exacerbates tissue injury and associated symptoms.

In TBI even slight changes in intracranial pressure can cause adverse symptoms including nausea, loss of vision, severe headaches, irreversible brain damage and even death (Jennett, 1998). Current treatments options are limited and invasive; diuretic drugs can be administered to reduce total tissue water content with limited and sometimes counteractive effects (Pathomporn et al., 2018). Craniectomy, the partial removal of the skull, is used to relieve intracranial pressure but is extremely invasive and introduces complications such as risk of infection, long recovery periods and low survival rates (Stiver, 2009). While it has been established that AQP4 is important in CNS oedema in both the brain and spinal cord, attempts to target AQP4 therapeutically have been unsuccessful. Further understanding the role of AQP4, and the mechanisms behind its function, including its subcellular localisation, is required.

1.2.2 CNS Inflammation

Injuries, such as TBI, elicit an immune response (Das et al., 2012). The primary purpose of this response is to resolve injury but, in an environment, where injury increases over time, such as TBI, inflammation is prolonged, causing further tissue

damage (Kriz, 2006). Microglia and astrocytes migrate into areas of injury become activated and secrete pro-inflammatory cytokines (Lozano et al., 2015), and secretion of anti-inflammatory cytokines decreases (Loane and Kumar, 2015). This creates an inflammatory and cytotoxic environment, which causes cell death and recruitment of circulating inflammatory cells. Inflammation is currently mediated therapeutically by corticosteroids but further understanding of the causes and progression of inflammation following TBI could lead to enhanced therapies (Postolache et al., 2020). AQP4 plays a key role in CNS inflammation. It is required for the migration of activated astrocytes to sites of injury (Auguste et al., 2007) and has been proposed to promote inflammation (Li et al., 2011).

1.3 Extracellular vesicles

Extracellular vesicles (EV) are naturally occurring nano- or micro- sized particles (Wolf, 1967) released by cells into their extracellular environment (Trams et al., 1981). The composition of EV can vary greatly as EV mirror the properties and condition of the cell from which they are derived, carrying cell cargoes such as functional nucleic acids, proteins, and lipid-based components (van der Pol et al., 2012, Yanez-Mo et al., 2015). As such, EV play roles in diverse processes, including the transport of enzymes (Peters et al., 1991), microRNAs (Arroyo et al., 2011), antigens, and membrane proteins (Raposo et al., 1996).

Both healthy and diseased cells release EV into their surrounding environment, although the cargoes of EV can differ based on the cellular condition (van der Pol et al., 2012). For instance, EV released by stressed or activated cells may contain molecules associated with either pro- or anti-inflammatory responses. While EV have been linked to cellular waste disposal, it is also thought that they play important roles in more complex processes, such as cell communication, carrying information about the condition of the cell from which they are released. As such EV have been identified as biomarkers for disease. EV can be isolated from bodily fluids such as CSF, saliva, breast milk, blood, amniotic fluid, menstrual fluid, and semen, allowing for collection of liquid biopsies with minimal invasion, especially when compared to alternatives such as tissue biopsy (Yanez-Mo et al., 2015).

Two main classes of EV are widely acknowledged, categorized based on their subcellular origin. Whilst nomenclature within the field can vary, these classes are most

commonly named exosomes and microvesicles/microparticles (Figure 1.5). Exosomes, typically sized between 30 to 150 nm, derive from intracellular multivesicular bodies via the endosomal pathway. Microvesicles, on the other hand, bud directly from the cell's plasma membrane and are generally larger (100 to 2000 nm), although there is some overlap in size (Gould and Raposo, 2013).

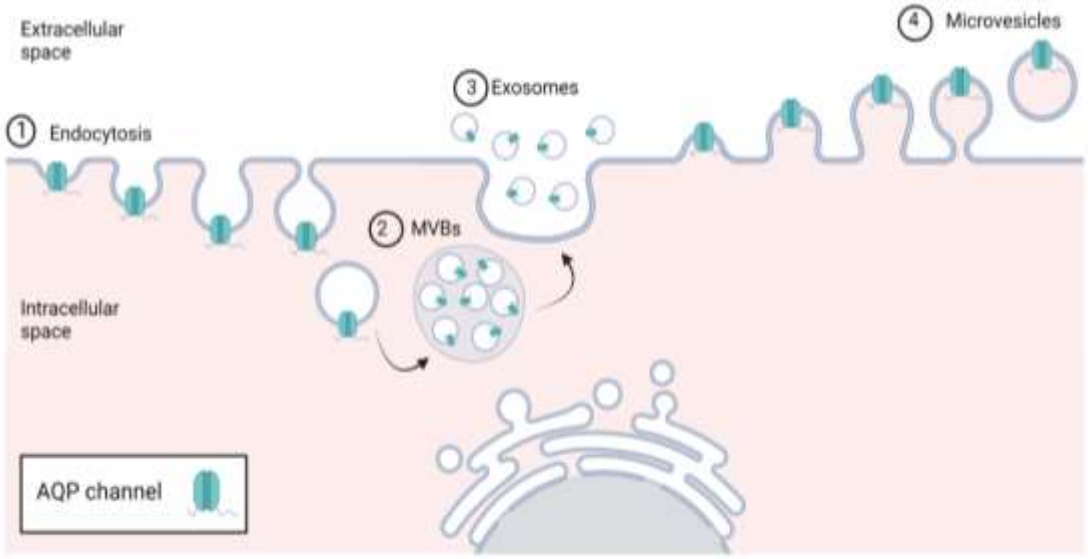

Figure 1.5 Pathways of Extracellular Vesicle Production

Schematic shows extracellular vesicle production via two independent pathways. (1) Endocytosis of the plasma membrane and components, such as membrane proteins. (2) Formation of multivesicular bodies. (3) release of exosomes into the extracellular space. (4) Release of microsomes into the extracellular space directly from the plasma membrane. Schematic created using Biorender.com.

1.3.1 Aquaporins in extracellular vesicles

1.3.1.1 Aquaporins in CNS-derived extracellular vesicles

To date the mammalian AQP 1, 2, 3, 4, 5, 7 and 9 have been identified in EV, in a variety of organisms and cell types (Vesiclepedia, 2023). EV originating from the CNS, (CNS-EV) have been detected in CSF, which surrounds the brain and spinal cord, and blood in various physiological and pathological states (Akers et al., 2015, Lee et al., 2016), including brain tumours (D'Asti et al., 2016), stroke (Hayakawa et al., 2016), and TBI (Nekludov et al., 2017). CNS-EV have shown potential as biomarkers for assessing injury severity (Beard et al., 2020, Goetzl et al., 2019, Cheng et al., 2019). Recent studies have demonstrated that astrocyte-derived EV carry functional proteins that are taken up by neighbouring cells (Gosselin et al., 2013). Based on the expression and

localisation of AQP in cells of the CNS, and their adjacent CNS fluids, it is possible to predict where AQP-positive EV will be released (Figure 1.6).

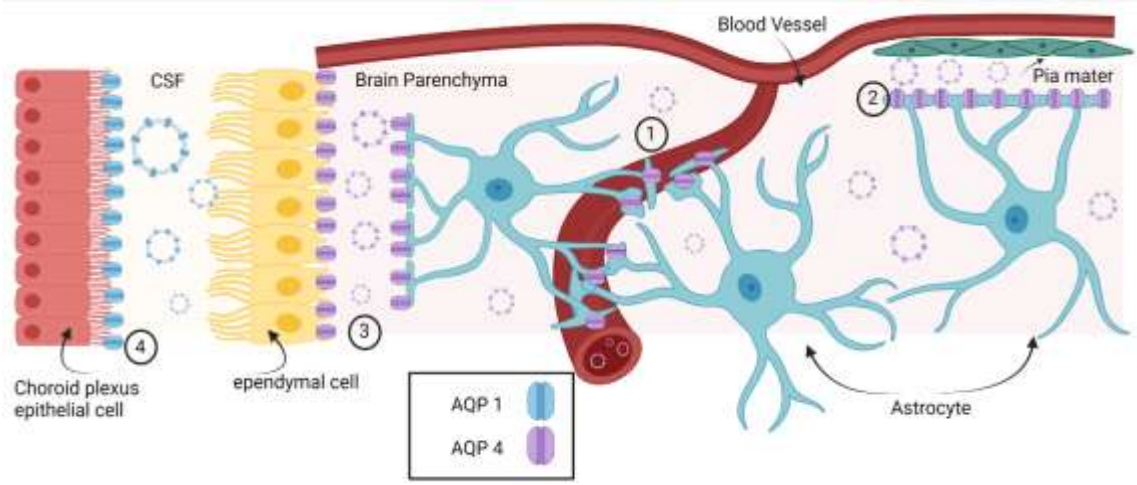

Figure 1.6 AQP release in extracellular vesicles in the CNS

Schematic shows the predicted release of AQP 1 and 4 in EV in fluids of the CNS. AQP1 is located in the apical membrane of choroid plexus epithelial cells. AQP4 is expressed by astrocytes, in perivascular endfeet (1) at the pia mater (2) and in the basolateral membrane of ependymal cells (3). Therefore, it is expected the AQP4-positive EV are secreted into the interstitial fluid, blood, and cerebro-spinal fluid near the pia mater. (4) AQP1 is expressed by the epithelial cells of the choroid plexus and are secreted into the surrounding CSF. Schematic drawn using Biorender.com

Complications arising from CNS pathologies often involve secondary injury caused by inflammation and/or tissue swelling as a consequence of the rapid and excessive accumulation of water in CNS tissue. AQP4 has been implicated as the water channel responsible for the movement in water in these pathologies. CNS-EV have also been identified in CNS pathologies such as, viral infection (Sampey et al., 2014), prion disorders (Coleman et al., 2012), neurodegenerative conditions (Denver et al., 2019), multiple sclerosis (Von Bartheld and Altick, 2011), CNS cancer (Ciregia et al., 2017), and injury. Notably, CNS-EV that are AQP-positive have been identified in several of these pathologies (Nekludov et al., 2017, Bejerot et al., 2019, Gonzalez-Molina et al., 2021, Denver et al., 2019, Wallensten et al., 2023). Many CNS pathologies are associated with tissue injury and oedema. APQ4 has been shown to play a leading role in CNS oedema formation and resolution, allowing rapid movement of water into and out of the CNS. AQP4 and EV have been implicated in a number of CNS injury-related pathologies.

1.3.2.1 Stroke

Ischemic stroke is a condition characterised by the blockage of arterial blood supply and subsequent oxygen deprivation and hypoxia. It leads to cell death and can cause brain damage or even fatality. Following ischemic stroke, brain oedema is reduced in AQP4 knock-out mice, compared to WT mice (Manley et al., 2004). This suggests that AQP4 plays a role in oedema associated with ischemic stroke. EV derived from astrocytes are released following ischemic stroke. Although no attempt has been made to identify AQP4 in these EV, it is likely that they contain AQP4, as they are derived from astrocytes. It has been hypothesised that these EV play a protective role against further neuronal damage (Fruhbeis et al., 2013). More recently, microglia-derived EV, exposed to hypoxia, appear to have protective effects on astrocytes following ischemic injury (Xin et al., 2023), suggesting that EV produced in hypoxic conditions may confer properties to astrocytes that prevent cell damage.

1.3.2.2 Traumatic brain injury

TBI is either direct or indirect damage to brain tissue and can result in various outcomes, including loss of BBB integrity, vascular damage, cell injury and death, inflammation, and oedema (Ghajar, 2000). Depending on the severity of the injury, TBI can trigger secondary injury, which is associated with the onset of more severe symptoms such as poor patient prognosis, permanent brain impairment, and even loss of life. In response to injury, AQP4 expression levels in the brain are elevated and an increase in brain water content is observed (Guo et al., 2006). Inhibition of AQP4 function may mitigate cerebral oedema following TBI, underscoring the potential significance of AQP4 as a potential drug target.

Following TBI, activated astrocytes and microglia release EV (Hazelton et al., 2018). These ‘response’ EV contain pro-inflammatory cargoes and are believed to propagate damaging inflammation (Kumar et al., 2017). The levels of these response EV may correlate with injury severity, potentially serving as valuable biomarkers. EV carrying AQP4 have been identified in the blood stream of TBI patients. AQP4 has been implicated as a biomarker for severe TBI due to its increased presence in EV from TBI patients compared to those without injury (Nekludov et al., 2017). Moreover, the release of AQP4 in EV has been proposed as a potential mechanism to protect astrocytes from further oedema, as observed following ischemic damage (Xin et al., 2021).

Astrocytes that interface with blood vessels form a critical component of the BBB (Figure 1.4). When astrocytic endfeet swell or undergo cell death, the integrity of the BBB is compromised. This breach allows immune cells, previously unable to enter the CNS, to infiltrate the brain. Although immune cells contribute to the removal of dead and dying cells, they also release reactive oxygen species (ROS), causing further damage, and attracting more immune cells. This cascade causes inflammation resulting in secondary injury to tissue.

AQP4 expression not only increases in the region of injured tissue but also in other uninjured parts of the brain following focal injury (Chen et al., 2016). Considering this, it is conceivable that AQP4, released in EV, is taken up and expressed by neighbouring cells. This suggests a form of intercellular communication, potentially involving EV transferring AQP4 to different regions of the brain. Moreover, AQP4 might play a role in maintaining the membrane integrity of CNS-EV, potentially contributing to the prolonged circulation of EV. Particularly following CNS injury, alterations in water and solute levels are known to occur. AQP4 may allow CNS-EV to adapt to osmolar changes in their environment, preventing excessive swelling or shrinkage of EV and therefore, a longer half-life.

1.3.2.3 Glioma

Astrocytes expressing AQP4, like other cell types, can undergo neoplastic transformation. The most common and malignant glial cancer is glioblastoma multiforme (GBM). High-grade tumours often exhibit increased AQP4 expression, and this elevated expression of AQP4 has been linked to a variety of roles, including increased water permeability (Saadoun et al., 2002) and glial cell migration. Notably, research has indicated that AQP4-knockout glial cells exhibit reduced migratory and invasive capabilities (Ding et al., 2011). Given these findings, it is plausible that targeting cerebral AQP4 could be a promising strategy in the treatment of glioma. The potential involvement of AQP4 in various aspects of glioma biology, coupled with its increased expression in high-grade tumours, suggests that modulating AQP4 function might hold therapeutic value in managing these aggressive brain cancers. AQP4 has been identified in glioma-derived EV. M1 and M23 AQP4-positive EV effect their surrounding environment, driving a migratory phenotype, or apoptosis respectively (Simone et al., 2022). This suggests a possible role for AQP4-positive EV in intercellular communication.

1.3.2.4 Neuromyelitis Optica spectrum disorders

Neuromyelitis Optica spectrum disorders (NMOSD) represent autoimmune conditions characterised by the presence of brain lesions. Patients afflicted with NMOSD often exhibit autoimmunity against AQP4, producing antibodies known as NMOSD-Ab that specifically target and bind to the AQP4 protein (Lennon et al., 2005, Sato et al., 2013). This antibody binding triggers an inflammatory cascade response, which subsequently leads to processes such as demyelination of nerves, cellular damage, and cell death. Encephalitis is also a phenomenon observed in NMOSD, although it occurs less frequently.

In vitro studies suggest the existence of multiple epitopes on AQP4 to which NMOSD-Ab bind, resulting in diverse consequences. These include endolysosomal degradation, breakdown of the BBB, and changes in water transport via AQP4 (Hinson et al., 2012). Studies propose that the binding of NMOSD-Ab could lead to the internalisation of AQP4, initiating a complement cascade. Interestingly, AQP4-positive microparticles have been identified in patients with NMOSD. AQP4-positive EV have been shown to cause widespread inflammation and the production of autoantibodies (Bejerot et al., 2019). Though exosomes derived from the CSF of patients with NMOSD, or multiple sclerosis, where AQP4 immunoreactivity is not observed, did not show any differences in AQP4 content (Lee et al., 2016). Exploring the inflammatory properties of AQP4-positive EV, derived from glial cells, could potentially provide further insight into the complex mechanisms underlying CNS immune diseases like NMOSD.

1.3.2.5 Alzheimer's disease

(AD) is a form of dementia, characterised by beta-amyloid plaques and tangles composed of the tau protein. Within the CNS, it is well established that cells release EV, and there is a suggestion that these EV contribute both to physiological functions and pathological processes. EV have been reported in Alzheimer's disease, as well as conditions linked to tau-related pathology and dementia with Lewy bodies, important characteristics of AD. Studies report that EV may transmit pathology (Eitan et al., 2016, Ngolab et al., 2020). The role of EV within neurodegeneration is complicated and, at times, paradoxical. For instance, in AD, neurons release beta-amyloid within EV (Rajendran et al., 2006). This has been suggested as a mechanism for waste disposal (Yuyama et al., 2015). Neuronal-derived EV have also been proposed to reduce the accumulation of amyloid plaques, potentially through their transfer of beta-amyloid to microglia, thereby displaying a neuroprotective function (Yuyama et al., 2012, Yuyama et al., 2014). It is not clear, however whether all EV function in a

comparable manner; microglia, for example, release neurotoxic forms of beta-amyloid in EV, exerting a harmful effect (Gonzalez-Molina et al., 2021). Other cells of the CNS, such as astrocytes and pericytes (Sagare et al., 2013), with varied outcomes.

AQP4 has been linked to AD pathogenesis it is suggested it plays a role in the clearance of beta-amyloid and tau. In AD the polarisation of AQP4 to astrocytic endfeet is disrupted, and AQP4 expression is dispersed. Furthermore, the release of AQP4 in exosomes, isolated from rat blood serum, is increased significantly in rats with Alzheimer's disease, compared to wild type (WT) rats (Denver et al., 2019). These findings are supported by recent findings in an AD mouse model, where increased levels of AQP4-positive EV were observed (Gonzalez-Molina et al., 2021). Further work is needed to determine whether EV released in AD has a neuroprotective function. Considering AQP4's influence on macrophage motility, it is plausible that AQP4 in EV possesses functional significance yet to be fully understood.

1.3.2.6 Stress induced exhaustion disorder

Stress induced exhaustion disorder (SED), often referred to as clinical burnout, is characterised by chronic fatigue and cognitive dysfunction. SED patients exhibit symptoms similar to those observed in TBI, including long-term cognitive dysfunction and memory issues (Beser et al., 2014). SED patients have elevated levels of circulating astrocyte-derived EV containing AQP4, in contrast to individuals with depressive disorders such as major depressive disorder (Wallensten et al., 2023). Notably, the levels of AQP4-EV in SED patients show a close correlation with those previously seen in TBI patients (Wallensten et al., 2023). This finding underscores a potential connection between SED and TBI, suggesting a shared mechanism or pathway involving AQP4-positive EVs.

1.4 Potential roles for aquaporins in extracellular vesicles

When considering the function of EV, the benefit of EV release to host cells and/or the effects EV have upon recipient cells are typically primary considerations. EV are characterised based on their cargo, which can indicate the cell type from which EV are derived and may provide insight to their potential destination and/or function. The presence of AQP in has been shown to be important in a number of processes, including in EV release by host cells, communication, and uptake of EV by recipient cells and also, roles in EV integrity that may extend their half-life upon release.

AQP-EV are likely to be released in all body fluids. It is hypothesised that the nature and role of the bodily fluid can provide insight into the potential function of EV contents. For example, the role of breast milk is to deliver nutrients and immunity to infants, it is probable that the role of EV in breast milk is associated with this function. Conversely, urine is released by the body to excrete waste products and water, implying that urinary EV and their cargo are likely to support waste and water regulation and/or elimination.

Existing evidence shows that the components of EV can be altered by the extracellular environment. EV release may increase or decrease in response to various stimuli, and the composition and concentration of EV can also change. The presence of AQP in EV is not solely consequential to their presence in the plasma membrane, or intracellular vesicles. For example, AQP2 release in urinary EV (uEV) is reflective of urine concentration. Low urine concentration is observed alongside an increase in AQP2 in uEV. However, this is not observed in the case of AQP1 uEV in hypoosmolar urine, even though cellular expression of AQP1 increases (Elliot et al., 1996). This suggests that AQP presence in EVs is subject to regulation beyond their presence in the plasma membrane.

1.4.1 Roles for AQP in EV - Host cells

1.4.1.1 AQP release in EV as a mechanism for regulation of water transport

Originally it was thought that the primary function of EV release was a form of 'waste disposal' to remove unwanted cellular components. While there is some evidence supporting this notion, it has become clear that there are other, more complex roles for EV. Nonetheless, the beneficial effects of AQP removal from the plasma membrane may be one explanation for their presence in EV (Figure 1.7).

In the plasma membrane, AQP primarily function as water and/or solute channels, facilitating the movement of water and/or small solutes into and out of cells. Endogenous regulation of AQP can involve their trafficking to and from the plasma membrane, thereby determining membrane porosity and water permeability (Nielsen et al., 1995, Conner et al., 2010, Kitchen et al., 2015b). Thus, the concentration of AQP in the plasma influences cell volume regulation. AQP are trafficked from intracellular

vesicles. For example, AQP2 is relocalised upon vasopressin secretion (Nielsen et al., 1993a), AQP1 and AQP4 are relocalised to the plasma membrane in response to extracellular hypotonicity (Conner et al., 2012, Kitchen et al., 2015b). It is possible that following trafficking, the plasma membrane and its components are released as EV to the extracellular environment. Depending on the specific AQP's function, this process could either decrease water reabsorption or reduce water secretion, features that may be beneficial or detrimental depending upon the local microenvironment.

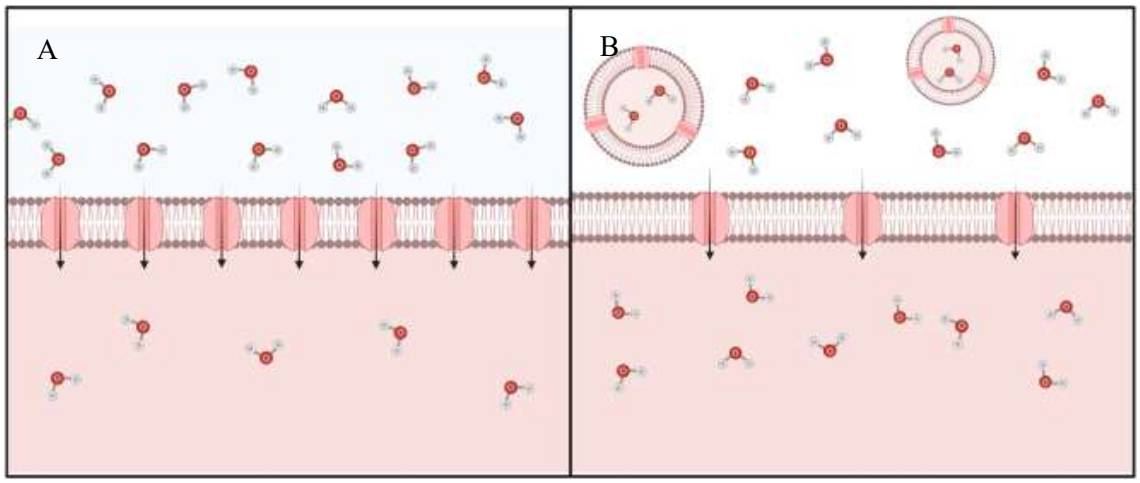

Figure 1.7 Release of AQP4 in EV for Volumetric Regulation

Schematic shows AQP release in EV following water influx via AQP water channels (A) Water moves into the intracellular space along an osmotic gradient. (B) AQP water channels and water molecules are secreted in EV. Intracellular water content is reduced, and water influx is limited. Schematic was created using Biorender.com.

1.4.1.2 AQP in EV production and release

The presence of AQP in phospholipid membranes can influence membrane fluidity and membrane dynamics. Increased membrane protein density reduces lipid packing, thus reducing plasma membrane lipid density. Cells and vesicles that are more water permeable increasing membrane fluidity, which is important for cell motility (Loitto et al., 2002). Increased AQP abundance in the plasma membrane increases cell motility, with AQP being polarised at the leading edge of motile cells. Although the exact mechanisms by which AQP contribute to cell membrane fluidity and dynamics remain incompletely understood, several hypotheses have been proposed.

During EV production, whether via endocytic or exocytic pathways, AQP facilitate localised water movement across the plasma membrane. During endocytosis, AQP might enable water movement out of the cell, leading to a reduction in cell volume.

This, in turn, could aid the formation and internalization of plasma membrane components into the cytoplasm without a notable increase in overall cell volume (Figure 1.8).

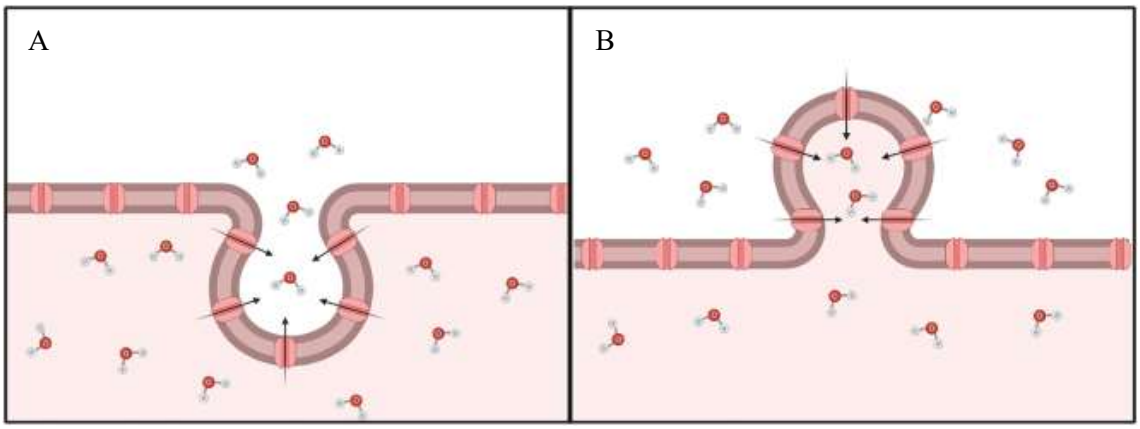

Figure 1.8 AQP water channels facilitate localised volumetric regulation and subsequent EV formation.

Schematic shows possible roles for AQP water channels in EV formation. (A) AQP expression in the plasma membrane allows rapid excretion of water and a reduction in cell volume, facilitating endocytosis and formation of exosomes. (B) AQP expression in the plasma membrane allows rapid uptake of water and an increase in cell volume, facilitating exocytosis and formation of microvesicles. Schematic created using Biorender.com.

Microvesicles, which originate directly from the plasma membrane, also contain AQP (Asvapromtada et al., 2018, Abdeen et al., 2014, Oliveira et al., 2011). It is plausible that localised water influx into the intracellular space augments intracellular volume and assists vesicle formation aimed at the extracellular space volume and aids vesicle formation toward to extracellular space. This could potentially contribute to the dynamic process of vesicle formation and release.

In summary, AQP appear to play multifaceted roles in influencing membrane properties, cell motility, and the biogenesis of EV. Their impact on localized water movement and volume changes likely contributes to the intricate processes of membrane dynamics and vesicle formation. Further research is needed to fully unravel the mechanisms underlying AQP involvement in these cellular processes.

1.4.2 Roles for AQP in EV - Recipient cells

EV carry cell cargo such as functional DNA, microRNAs (Arroyo et al., 2011), functional proteins (Raposo et al., 1996), enzymes (Andrei et al., 1999), and lipid-based

components (van der Pol et al., 2012, Yanez-Mo et al., 2015). Evidence shows that these cargoes can be taken up and utilised by recipient cells.

1.4.2.1 AQP in EV communication – protein delivery to recipient cells

EV play a crucial role in intercellular communication by transmitting cargoes. This cargo can influence and modify recipient cells upon uptake. EV can transport AQP proteins to neighbouring cells. AQP can be integrated into recipient cell proteomes; functional AQP have been observed in AQP-negative cells incubated with AQP-positive EV (Street et al., 2011). Based on these findings, there arises a potential scenario where AQP could contribute to intercellular communication. In this speculative scenario, AQP are transferred from AQP-positive cells to neighbouring AQP-negative cells via EV (Figure 1.9).

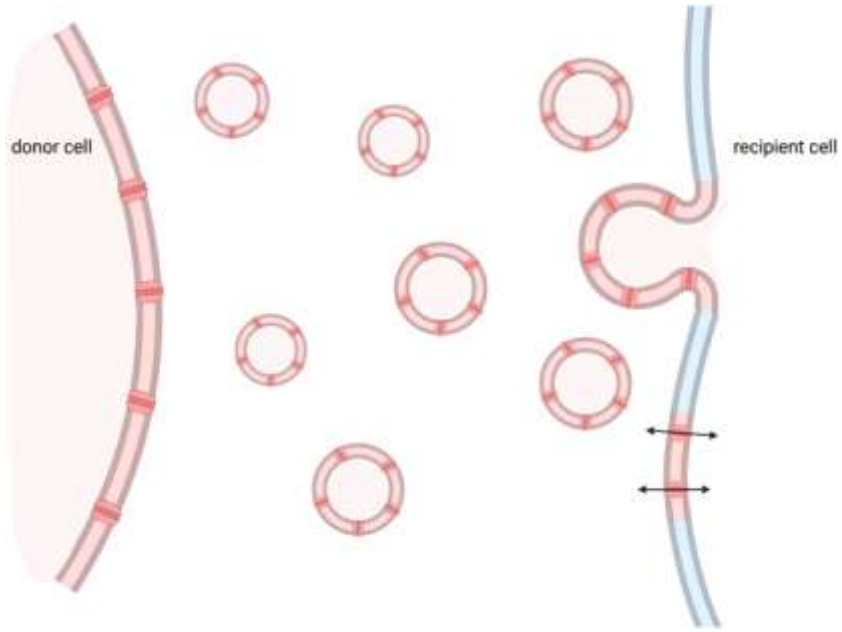

Figure 1.9 Intercellular Transfer of AQP in EV

Schematic shows release of AQP positive EV by donor cells. These EV move through the extracellular environment and can be taken up and integrated into recipient cells. Schematic created using Biorender.com.

Elevated levels of AQP in EV could function as signalling molecules to neighbouring cells, possibly leading to an increase in AQP expression in recipient cells. From a physiological perspective, this mechanism could offer certain advantages. Notably, the rate at which EV are generated, released, and delivered to recipient cells is quick in comparison to the time it takes for AQP proteins to be synthesised via transcription. AQP sharing via EV could therefore be a rapid solution for cells requiring increased AQP levels.

1.4.2.2 Communication – bystander effect

The bystander effect, a phenomenon in which a cell's phenotype is communicated to neighbouring cells via EV, is an interesting aspect of intercellular communication. This concept has been observed in various contexts, including cases where irradiated cells transfer radiation-induced damage to non-irradiated cells (Szatmari et al., 2017). Similarly, the bystander effect has been documented in response to heat shock, suggesting that cells experiencing a stressor can induce a state of heightened preparedness in nearby cells (Bewicke-Copley et al., 2017). If this phenomenon is coupled with the prolonged half-life of EV, it could potentially enable a protective response to occur in more distal cells, contributing to a networked cellular response to stress or injury.

It is intriguing to consider the possibility that AQP in EV might play a role in facilitating a bystander effect in intercellular communication. If AQP-containing EV are capable of transmitting cargoes that prompt neighbouring cells to modulate their AQP expression, this could lead to increased or decreased water permeability in those recipient cells. Such a mechanism could facilitate a coordinated response to changes in the cellular environment, where AQP function as molecular messengers. However, it is important to note that this idea is speculative and would necessitate further experimental investigation to ascertain its validity. Exploring the potential role of AQP in EV-mediated bystander effects could provide new insights into how cells collectively respond to stressors or changes in their surroundings, and how they work together to adapt and maintain homeostasis.

1.4.2.3 Communication – inflammation

The impact of EV on immune function and inflammatory responses is complex and context dependent. EV can exhibit both pro-inflammatory and anti-inflammatory effects based on their cargo and the specific context (Thery et al., 2009). In different scenarios, EV can contribute to the recruitment of macrophages, important innate immune cells that possess the ability to trigger both pro-inflammatory and anti-inflammatory responses, as well as modulating those responses (Grant et al., 2019). Effective control of this response is critical in the resolution of inflammation (Lo Sicco et al., 2017).

AQP have been implicated in multiple immune processes, such as phagocytic cup formation and immune cell migration (Tollis et al., 2010, Loitto et al., 2002). This raises

the possibility that the presence of AQP in EV may mediate these important immune-related effects. Specifically, AQP1 has been identified as a crucial factor in the process of macrophage phenotype switching, determining their inflammatory properties. Of note, is the suggestion that EV derived from GBM cells can modulate microglial phenotypes, potentially supporting tumour growth by supressing the onset of inflammation (Abels et al., 2019, Maas et al., 2020). This suggests that EV, such as those containing AQP, could have significant implications for immune responses and their interplay with various pathological conditions. Further research in this area is needed to gain a more comprehensive understanding of the roles played by AQP in EV and their potential impact on immune function and inflammation.

1.4.2.4 Communication- protein orientation

Research has demonstrated that the process of exosome production, including endocytosis of the plasma membrane components and their release as exosomes can cause orientation switching of membrane proteins (Cvjetkovic et al., 2016). In the context of AQP, this could result in the exposure of regions that are normally situated intracellularly, such as the N- and C- termini and intracellular loops (Figure 1.10). These regions contain phosphorylation sites and regions crucial for protein-protein interactions (Nesverova and Tornroth-Horsefield, 2019).

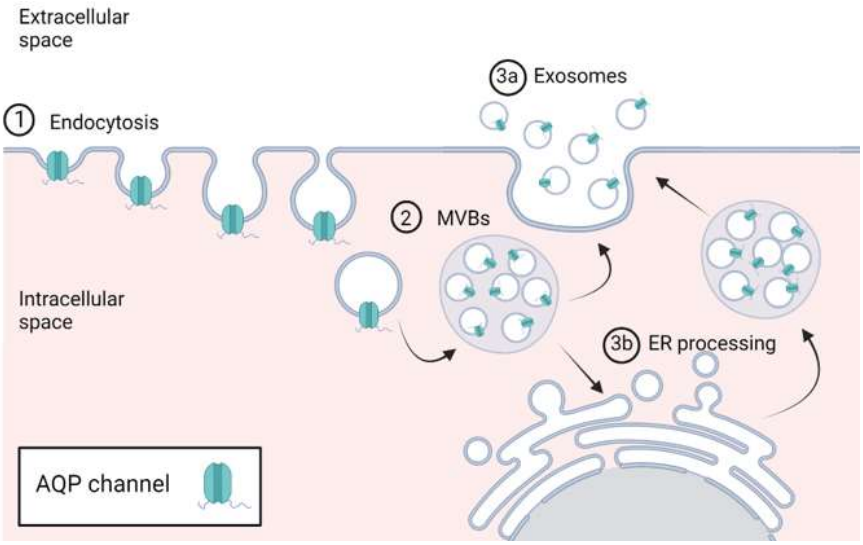

Figure 1.10 Processing of Multivesicular bodies in the Endoplasmic Reticulum

Schematic shows a possible pathway for the production of EV containing 'inside out' AQP. (1) The plasma membrane and components are endocytosed. (2) Formation of multivesicular bodies. (3a) release of exosomes into the extracellular space. (3b) Processing of MVB and release of processed exosomes. Schematic created using Biorender.com.

This dynamic reorientation of AQP during the process of endocytosis and exosome formation has the potential to alter their functional properties and regulatory mechanisms. Phosphorylation, which often occurs at these intracellular regions, can impact the activity and localization of AQP. Furthermore, interactions with other proteins or molecules in the extracellular space could be influenced by the exposure of these intracellular domains.

The exposure of these regions upon incorporation into exosomes might also have implications for intercellular communication and the interactions of recipient cells with AQP-containing exosomes. This phenomenon highlights the complexity of AQP's roles and the multifaceted effects of their presence in EV. Further exploration of these mechanisms could provide valuable insights into the functions and regulation of AQP and their potential roles in intercellular signalling.

1.4.3 Roles for AQP in EV - EV delivery

1.4.3.1 AQP in EV membrane integrity and volumetric regulation

Upon release by host cells, EV journey through fluid environments with differing osmolarities to their host cell. These environments may be prone to significant fluctuations in osmolarity, and EV must possess the ability to adjust and safeguard their structural integrity. AQP-positive cells are able to regulate membrane integrity and it is anticipated that AQP play a similar role in EV, preventing rapid swelling or shrinkage in response to tonic changes, as seen for example in sperm cells (Chen and Duan, 2011).

Shrinking or swelling of EV could result in unsuccessful delivery of EV cargo to recipient cells and subsequent release of cargo into the extracellular space may have undesired consequences such as onset of inflammation. AQP1 is released into exosomes as erythrocytes mature, suggesting a role for volumetric control (Blanc et al., 2009). This raises the possibility that the role of AQP in helping to maintain volumetric control in EV may underpin EV resilience to environmental change and, consequently, their half-life. This will enable longer journeys within the body to impact more distant recipient cells and/or enter more distant recipient cells for sampling as biomarkers.

1.4.3.2 EV deformability

In order to travel through the extracellular environment, especially within the intricate network of the extracellular matrix, EV must be able to squeeze through narrow spaces often smaller than their own diameter. Thus, EV must exhibit a certain degree of deformability, as they have been found in locations distant from their point of

origin (Lenzini et al., 2020). AQP1-positive EV have the ability to move through narrow spaces more easily than EV containing AQP1 with reduced functionality. It is hypothesised that the water permeability of EV dictates their capacity to deform though volumetric adjustments. Given that deformability is required for EV to move though tight spaces, the presence of AQP in EV could be essential for their successful migration. Moreover, the increased membrane fluidity of AQP-positive EV is likely to contribute to their ability to deform and move through such spaces.

1.4.3.3 AQP in EV interaction and fusion with recipient cells

There could be a significant role for AQP in the uptake of EV, specifically for EV swelling which, could facilitate their fusion with the plasma membrane of recipient cells. It has been shown that AQP re important in the fusion of secretory vesicles with plasma membranes for successful secretion of vesicle contents (Kelly et al., 2004). AQP-positive vesicles are able to swell and fuse with the plasma membrane, subsequently releasing their secretory components. This same concept could be applied to the fusion of circulating EV with the plasma membrane of recipient cells where AQP-positive EV have the ability to swell in response to osmolar changes near the plasma membrane, aiding fusion and allowing uptake of EV by recipient cells and therefore facilitating integration of EV cargo (Figure 1.11).

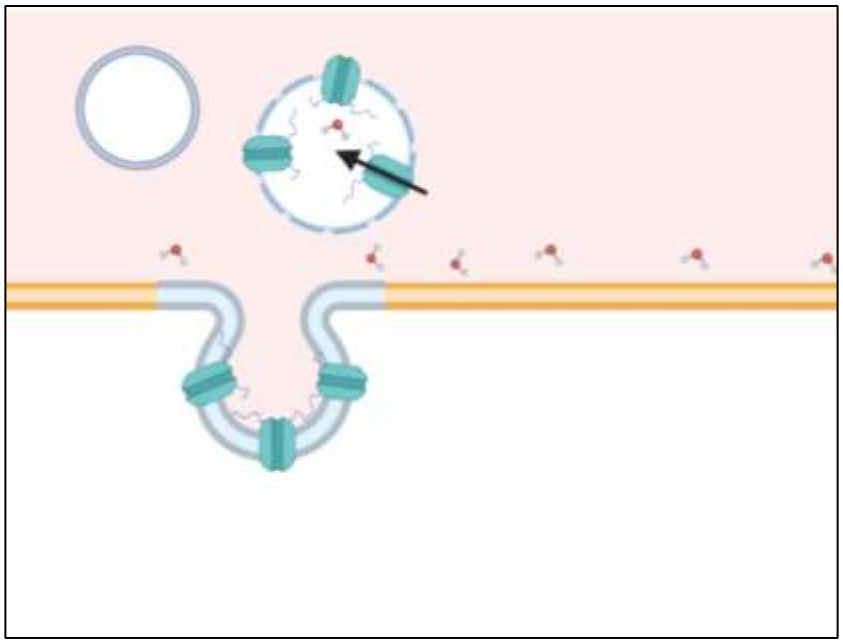

Figure 1.11 AQP facilitate EV swelling and uptake by recipient cells.

Schematic shows a possible role for AQP in EV uptake. AQP4 positive EV swell in response to increased hypotonicity at the plasma membrane of recipient cells. Cell swelling causes EV membrane changes that facilitate fusion of EV with recipient cells and subsequent uptake of EV and their cargo. Schematic created using Biorender.com.

1.4.4 AQP in EV as biomarkers for disease

Changes in AQP expression levels and localisation have been observed in a wide range of pathological conditions, affecting both cellular and EV AQP. These conditions encompass diverse diseases such as various cancers, tissue injuries, ischemia, and inflammatory diseases. Differences in AQP expression can be measured and serve as biomarkers for disease in both cells and EV. While measuring cellular AQP expression typically involves invasive methods such as tissue biopsies, CSF collection, or blood sampling, the extraction of EV-containing fluids offers a less invasive alternative. For example, EV can be harvested from saliva and urine. By delving deeper into the study of AQP concentration and functionality in EV, it may be possible to advance clinical diagnostic techniques and procedures, thereby enhancing the accuracy and effectiveness of disease detection and monitoring, and patient experience.

1.4.5 AQP in EV as drug targets

Given the involvement of AQP in various pathological conditions, they are being recognized as significant and promising drug targets. Despite this potential, efforts to develop AQP inhibitors for clinical use have yielded limited success in clinical trials. As an alternative approach, some studies have focused on utilizing small interfering RNAs (siRNAs) encapsulated in EVs to target and modulate AQP expression (Fukuda et al., 2013, Mughees et al., 2021). This is a potentially promising area for AQP targeted therapeutics. This avenue of research into AQP-targeted therapeutics through EV-mediated siRNA delivery could offer new possibilities for effective interventions in various diseases.

1.4.6 AQP in EV in drug delivery

The therapeutic potential of endogenous EV has gained significant attention as a novel avenue for promoting tissue healing and recovery in various organisms. This emerging field of research offers exciting prospects for therapeutic applications (Batrakova and Kim, 2015). EV can be isolated from suitable bodily fluids, purified, and administered to individuals with specific injuries or conditions. Enhancing our understanding of the active components in EV is crucial for advancing this field, enabling the development of exogenously synthesized EV that can potentially reduce reliance on host organisms. Given that the composition of EV membranes plays a pivotal role in successful delivery, as demonstrated in plants (Martinez-Ballesta et al., 2018), we hypothesise

AQP would be essential components of synthesised EV membranes in EV engineered for therapeutic purposes.

1.5 Aim and objectives

1.5.1 Aim

The overall aim of this thesis is to characterise AQP4 in both intracellular and extracellular vesicles. Identifying AQP4 trafficking between the astrocyte cell surface and intracellular vesicles *in vivo* was particularly challenging and required the development of robust imaging and analysis methods. The characterisation of AQP4 in EV required the development of *in vitro* models that would enable the first quantitative analysis of EV from AQP4-positive cells.

1.5.2 Objectives

1) Determine whether there are any observable differences in the subcellular localization of AQP4 in an *in vivo* CNS oedema model and investigate whether treatment with inhibitors of AQP4 relocalisation prevent these observable differences (Chapter 3).

2) Create and confirm a stably transfected AQP4-GFP -positive HeLa cell line to use in an EV release model (Chapter 4)

3) Create a tonicity-linked EV release model, determine the conditions of the model, and a successful isolation protocol (Chapter 4).

4) Confirm AQP4 presence in EV derived from AQP4-positive cells and investigate possible roles for AQP4 in EV (Chapter 5).

Chapter 2 : Materials and Methods

2.1 Materials

2.1.1 Hardware

Epifluorescence microscopy

EVOS FL, ThermoFisher Scientific Inc

DMI400B, Leica Microsystems

Confocal Microscopy

TCS SP5 II, Leica Microsystems

Cryogenic Electron Microscopy

Lacey carbon grids, EMResolutions

GP2 plunge freezer, Leica Microsystems

JEOL2100Plus TEM, JEOL Ltd

Flow Cytometry

CytoFLEX S, Beckman Coulter Inc

Nano-flow cytometer, Nano FCM

Centrifugation

Microcentrifuge: Eppendorf Centrifuge 5418, Eppendorf Ltd.

AccuSpin tm 400, Fisher Scientific Ltd (2000g)

Megafuge 8R Heraeus, ThermoFisher Scientific

Western Blot Visualisation

G:Box Chemi HR 1.4, Synoptics Ltd

DNA quantification

Nanodrop, ThermoFisher Scientific

Tissue culture

class II biological safety cabinet (MSC Advantage, ThermoFisher Scientific)

Media Osmolarity

Micro-Digital Osmometer Type 7M: Loser

2.1.2 Software

Epifluorescence Imaging Software: Leica Application Suite, Advanced Fluorescence. Version 2.7.3.9723. Leica Microsystems GmbH

Flow cytometry software: CytExpert, Version 2.3.1.22. Beckman Coulter, Inc

G:Box software: GeneSys Version 1.3.3.0, Synoptics Ltd

Image data analysis software: Image J, National Institutes of Health & the Laboratory for Optical and Computational Instrumentation

: LASAF, Leica Microsystems

2.1.3 Tissue Culture

24 well plates: CoStar, Corning inc.

6 well plates: Corning inc.

T25 Flasks: Nunc™ EasyFlask Nunclon delta surface 25cm^2, ThermoFisher Scientific

T75 Flasks: nunc™ easyflask Nunclon delta surface 75cm^2, Thermo Fisher Scientific

35mm glass bottomed dishes: FluoroDish, WPI World Precision Instruments

Stripettes: 5mL, 10mL, 25mL, ThermoFisher Scientific

50mL tubes: ThermoFisher Scientific

15mL tubes: Corning Inc

PBS: Sigma-Aldrich (Merck)

Trypsin EDTA: Sigma Life Science

PEI: Sigma Aldrich (Merck)

FBS: Gibco, ThermoFisher

DMEM: Sigma-Aldrich (Merck)

RPMI: Sigma-Aldrich (Merck)

L-Glutamine 2mM: Sigma- Aldrich (Merck)

Penicillin Streptomycin: 100 I.U./mL penicillin and 100µg/mL streptomycin, Sigma-Aldrich (Merck)

G418 Sulphate (Gibco)

0.45 filters: Nylon, Thermo Fisher Scientific

0.2 filters: PTFE, Merck Millipore

Micropipette tips: SureOne 10µL, 300µL, 1000µL, Thermo Fisher Scientific

Microcentrifuge tubes: 500µL, Starlabs Ltd

: 1.5mL, Greiner bio-one GmbH

: 2mL, Starlabs Ltd

HeLa cells: ATCC

THP-1 cells: ATCC

Stable AQP4-GFP MDCK cells: Dr Phillip Kitchen

2.1.4 Western Blot

Propan-2-ol: 99.5%, ThermoFisher Scientific

Ethanol absolute: 99.8%, ThermoFisher Scientific

Methanol 99.8%: ThermoFisher Scientific

2-Mercaptoethanol, 98%, Sigma-Aldrich (Merck)

Tris Glycine, 0.25M Tris, 1.92M glycine (10×), National Diagnostics, Inc

Tris Glycine SDS, 0.25M Tris, 1.92M glycine, 1% SDS (10×), National Diagnostics, Inc

Chemiluminescence reagents: SuperSignal West Pico PLUS Chemiluminescent Substrate, ThermoFisher Scientific

TEMED: National Diagnostics Inc

Acrylamide: ProtoGel 0.8% w/v, National Diagnostics, Inc

EGTA 97%: Sigma-Aldrich (Merck)

EDTA sodium salt: Melford Laboratories Ltd

Milk Powder: dried skimmed milk, Tesco PLC

TRIS HCl: Melford Laboratories Ltd

TRIS Base: Melford Laboratories Ltd

Gel casting: (Bio-Rad)

Protein Ladder: Page Ruler, ThermoScientific

RIPA buffer, 1% v/v triton X-100, 0.5% w/v sodium deoxycholate, 0.1% SDS, 150 mM NaCl, 50 mM tris, pH 8) supplemented with a protease inhibitor cocktail (2 mM AEBSF, 0.3 μM aprotinin, 16 μM bestatin, 14 μM E-64, 1 μM leupeptin, 1 mM EDTA, (Sigma))

Polyclonal Anti-Rabbit HRP-linked secondary antibody (sc2313, Santa Cruz)

Rabbit Anti-GFP primary antibody

Monoclonal Rabbit Anti-AQP4 primary antibody (ab128906, Abcam)

2.1.5 Antibody labelling

Mounting Medium: Fluoroshield TM with DAPI, Sigma-Aldrich (Merck)

Triton X-100: Sigma-Aldrich (Merck)

BSA: Sigma-Aldrich (Merck)

Goat serum: ThermoFisher Scientific

Tween: Sigma-Aldrich (Merck)

Monoclonal Rabbit Anti-AQP4 primary antibody (ab128906, Abcam)

anti-GFAP: G3893, Sigma-Aldrich

anti-RECA-1: ab9774, Abcam

polyclonal anti-rabbit Alexafluor-488 secondary antibody: A21206, Invitrogen

polyclonal anti-mouse Alexafluor-594 secondary antibody: A21203, Invitrogen

2.1.6 EV production

SEC columns: qEV original 70nm Gen 2, IZON Science PLC

D-mannitol: Melford Laboratories Ltd

Sodium hydroxide 97%: Sigma-Aldrich, Merck

30kDa centrifugal concentration filters: Amicon Ultra, Millipore

10kDa centrifugal concentration filters: Amicon Ultra, Millipore

BODIPY FL Maleimide: ThermoFisher Scientific

Fluorescent polystyrene calibration beads: MegaMix Plus FSC and SSC, BioCytex

Annexin-V APC, BioLegend Inc.

2.1.7 Molecular techniques

Lysogeny Broth: Miller, ThermoFisher Scientific

pcDNA-DEST47 construct: Invitrogen

XL-10 gold competent cells: David Nagel, Aston University

Ampicillin Sulphate (Gibco)

Maxiprep kit: Qiagen

Sequencing Primers: BGH & T7, ThermoFisher Scientific)

2.2 Methods

2.2.1 AQP4 Relocalisation

2.2.1.1 Rat spinal cord tissue preparation

All animal surgeries described in this section were conducted by Dr Andrea Halsey and Professor Zubair Ahmed (Birmingham University, UK) and are included here to provide details of the methods used to generate the rat tissue samples that were analysed in this project. This section has been adapted from the methods published in Andrea Halsey's PhD thesis "Investigating the Role of Subcellular Localisation of Aquaporin 4 in Astrocytes After Traumatic Spinal Cord Injury", 2021, University of Birmingham.

Animal Surgeries were licensed by the UK Home Office and all experimental protocols were approved by the University of Birmingham's Animal Welfare and Ethical Review Board in strict accordance with the guidelines of the UK Animals Scientific Procedures Act, 1986 and the Revised European Directive 1010/63/EU and conformed to the guidelines and recommendation of the use of animals by the Federation of the European Laboratory Animal Science Associations.

A dorsal column (DC) crush at level T8 of the spinal cord was performed (Ahmed et al., 2010; Lagord et al., 2002) on female Sprague Dawley rats (Charles River) weighing between 175-225 g were used. First, the rats were subcutaneously injected with 0.2 mL of Buprenorphine and anaesthetised with 2.5-5% isoflurane and 2 L/mg of oxygen. A partial laminectomy of the T8 vertebrae was performed, to expose the spinal cord. A bilateral DC crush the spinal cord dorsal column at level T8 level was using a calibrated watchmaker's forceps, at a depth and width of 1 mm × 1 mm. Following recovery, rats were killed by increasing CO_2 concentrations.

Immediately following DC, rats were given an intraspinal injection of 2.5 µL of either 1×PBS, 4.9 mM TFP or 10 µM H89. Uninjured control rats were not injected. Injections were performed using glass micropipettes, attached to the rubber tubing from butterfly needles secured to a 5 mL syringe. The tip of the micropipette was inserted into the lesion site and solutions were pushed through slowly over a 1-minute period.

For tissue sample preservation, animals were intracardially perfused with 4% paraformaldehyde in phosphate buffered saline (PBS). Spinal cords were dissected ±5 mm from the lesion site and cryogenically protected in increasing sucrose concentrations in PBS, before being embedded in OCT Compound (ThermoFisher Scientific) and snap frozen on dry ice. Tissue was sectioned onto Superfrost Plus

Slides (ThermoFisher Scientific) at 15 µm using a Bright cryostat (Bright Instrument) through the parasagittal plane of the cord and stored at -20°C.

2.2.2 Antibody labelling

Spinal cord tissue sections were thawed for 30 minutes at room temperature and washed in PBS for 10 minutes. Non-specific binding was blocked by incubation of sections in blocking solution (0.5% w/v bovine serum albumin (BSA) (Sigma-Aldrich) and 3% v/v normal goat serum (ThermoFisher Scientific) in 0.5% Tween 20 in PBS (Sigma-Aldrich)) for 30 minutes. Spinal cord sections were incubated with combinations of either anti-AQP4 (ab128906, Abcam) and anti-Glial fibrillary acidic protein (GFAP) (G3893, Sigma-Aldrich) or anti-AQP4 (ab128906, Abcam) and anti-rat endothelial cell antigen (RECA-1) (ab9774, Abcam) primary antibodies, diluted in blocking solution at 1:1000 (AQP4), 1:200 (GFAP) and 1:50 (RECA-1). Sections were incubated with primary antibodies overnight at 4°C in a humidified chamber.

For subsequent labelling with fluorescently conjugated secondary antibodies, sections were washed in PBS for 10 minutes and incubated with secondary antibodies in blocking solution for 1 hour at room temperature. AQP4 was detected with an anti-rabbit Alexafluor-488 antibody (A21206, Invitrogen). RECA-1 and GFAP were detected using an anti-mouse Alexafluor-594 antibody (A21203, Invitrogen). Secondary antibodies were used at a 1:400 dilution in PBS. Following labelling with secondary antibodies, sections were washed with PBS for 10 minutes and mounted in Fluoroshield™ containing 4',6-diamidino-2-phenylindole (DAPI) (Sigma-Aldrich (Merck)). Primary and secondary antibody details are presented in Table 1.

2.2.3 Confocal Microscopy

Imaging was performed using an upright SP5 Tandem Confocal Scanning II system (Leica Microsystems, GmBH). Tissue samples were imaged using a 63x oil lens with APO correction. AQP4-AlexaFluor 488 was excited using a 488 nm Argon laser at 20% power. GFAP- AlexaFluor 594 was excited with a 594 nm Helium Neon laser at 29% power and RECA1- AlexaFluor 633 with a 633 nm Helium Neon laser. DAPI was excited using a two-photon near-infrared laser at 800 nm (SpectraPhysics). Images were captured in a square, 1024 x 1024-pixel format (x,y). To facilitate accurate acquisition and analysis to process expression of AQP4, smart gain and offset were

adjusted using the quick LUT, glow over and under setting, to create a dynamic fluorescence range (0-255).

2.2.4 Quantification of antibody labelling

Following imaging of spinal cord tissue with confocal microscopy, images were analysed and fluorescence intensity of AQP4 labelling was quantified using LASAF software (Leica Microsystems GmbH). For quantification of AQP4 expression in samples, regions of interest (ROI) were drawn around entire fields images and the

mean fluorescence value calculated. For quantification of AQP4 localisation to endfeet, linear ROIs were drawn along AQP4-positive areas around endothelial cell labelling and compared with mean fluorescence values of linear regions drawn along cell processes and bodies (Figure 2.1).

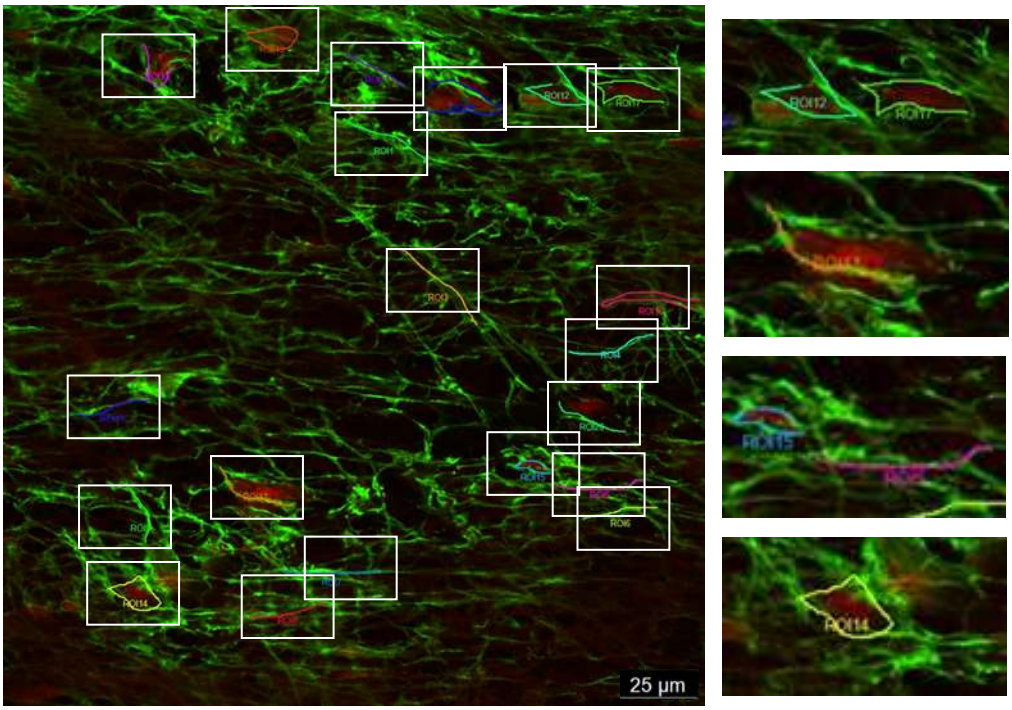

Figure 2.1 Relative endfoot expression quantification protocol

Representative confocal histogram overlay shows AQP4 expression (green) and endothelial cell localisation (red) in rat spinal cord tissue. ROI were drawn manually around endothelial cells and along astrocytic processes for comparison of mean fluorescence values (Relative endfoot expression). White boxes highlight linear areas drawn to measure fluorescence intensities. Zoomed images show a selection of these areas in more detail.

2.2.5 Stable cell-line generation

2.2.5.1 AQP4 cDNA construct

The mammalian expression plasmid pcDNA-DEST47 (Invitrogen) encoding human AQP4 cDNA was gifted by Dr Matthew Conner (Wolverhampton University). This vector contains AQP4 and GFP cDNA, for production of an AQP4-GFP fusion protein, an ampicillin resistance gene for bacterial transformants selection and a Neomycin/G418 resistance gene for selection of stable mammalian transfectants. The full sequence of the pDEST47 vector is included in Appendix 1.

2.2.5.2 Amplification and confirmation of AQP4-GFP cDNA

XL-10 gold competent cells, gifted by Dr David Nagel (Aston University) were thawed on ice and transferred to pre-chilled 1.5 mL microcentrifuge tubes. 10 ng of plasmid DNA was added to 100 µL of cells. Cells were subjected to heat shock at 42°C for 30 seconds in a heat block and cooled on ice for 5 minutes. Cells were made up to 1 mL with lysogeny broth (LB) (Miller, ThermoFisher Scientific) and incubated on a roller shaker at 37 °C for 1 hour. Cells were centrifuged pelleted by centrifugation and resuspended in 100 µL of LB for plating onto 100 µg/mL ampicillin LB agar plates. Plates were incubated overnight at 37 °C. Single colonies of transformed competent cells were selected using a sterile loop and transferred to 100 mL of 100 µg/mL ampicillin in LB on an orbital shaker for 16 hours. This then transferred to 500 mL ampicillin in LB and grown on an orbital shaker overnight. Transformed cells were processed for maxiprep (Qiagen) following the manufacturer's instructions. Maxiprep protein concentrations were quantified using a Nanodrop (ThermoFisher) prior to further use. AQP4-GFP in PDEST-47 was confirmed by sequencing in forward and reverse directions using T7 and BGH sequencing primers, respectively. Sequencing was done by Functional Genomics (University of Birmingham). Sequence data was confirmed using ExPASy software (Swiss Informatics Research Portal) (Figure 2.2).

2.2.6 Mammalian Cell culture

2.2.6.1 HeLa cells

HeLa cells used for stable cell line generation were from the American Type Culture Collection (ATCC). HeLa cells were used up to a passage number of 75 and were cultured in Dulbecco's modified Eagle's medium (DMEM) (Sigma- Aldrich (Merck)), supplemented with 10% v/v foetal bovine serum (FBS) (Gibco, ThermoFisher

Scientific), penicillin (100 units/mL) and streptomycin (100 µg/mL) (Sigma- Aldrich (Merck)).

2.2.6.2 MDCK cells

WT, and stably transfected M1 and M23 -AQP4 Madin-Darby canine kidney (MDCK) cells were a kind gift from Dr Phillip Kitchen. Stable M1 MDCK express the full M1-AQP4-GFP construct. M23 MDCK stably expressed only M23-AQP4. This was achieved by M1I mutation, removing the first methionine, required for M1 production. Without this mutation, MDCK cells expressed only M1-AQP4. MDCK cells were used up to passage 40. MDCK cells were routinely cultured in Dulbecco's modified Eagle's medium (DMEM) (Sigma-Aldrich (Merck) supplemented with 10% v/v foetal bovine serum (FBS) (Gibco, ThermoFisher Scientific), penicillin (100 units/mL) and streptomycin (100 µg/mL) (Sigma-Aldrich (Merck)).

2.2.6.3 THP-1 cells

THP-1 cells were purchased from ATCC. These cells were used up to passage 98. THP-1 cells were cultured in RPMI-1640 culture medium (Sigma-Aldrich (Merck)) supplemented with 10% v/v foetal bovine serum (FBS) (Gibco, ThermoFisher Scientific), penicillin (100 units/mL) and streptomycin (100 µg/mL) (Sigma-Aldrich (Merck)). 10 mL of medium to deactivate trypsin and dilute cells. 1.5 mL of cells were reseeded for continued growth. THP-1 monocytes were harvested every 2 days, 5 mL of cell suspension was removed and replaced with 5 mL of medium.

Table 1. Antibodies used in Immunohistochemistry of rat spinal cord samples

Primary Antibody					Secondary Antibody				
Target	**Host**	**Dilution**	**Manufacturer**	**Identifier**	**Host/ Target**	**Fluorophore**	**Dilution**	**Manufacturer**	**Identifier**
Aquaporin-4 C terminus (AQP4)	Monoclonal-Rabbit	1:1000	Abcam	ab128906	Polyclonal Donkey/Rabbit IgG	Alexafluor-488	1:400	Invitrogen	A21206
Rat endothelial cells (RECA-1)	Monoclonal-Mouse	1:200	Abcam	ab9774	Polyclonal Donkey/Mouse IgG	Alexafluor-594			A21203
Glial fibrillary acidic protein (GFAP)	Monoclonal-Mouse	1:50	Sigma-Aldrich	G3893					

2.2.6.4 General cell culture

All work with live cells was done in a class II biological safety cabinet (MSC Advantage, ThermoFisher Scientific). Cells were cultured in a humidified 37°C incubator with 5% CO2. HeLa and MDCK cells were routinely cultured in Dulbecco's modified Eagle's medium (DMEM) (Sigma- Aldrich (Merck)). THP-1 cells were cultured in RPMI-1640 (Sigma- Aldrich (Merck)). For routine culture, all media were supplemented with 10% v/v foetal bovine serum (FBS) (Gibco, ThermoFisher Scientific), penicillin (100 units/mL) and streptomycin (100 µg/mL) (Sigma- Aldrich (Merck)). All media were pre-warmed to 37 °C before use. HeLa and MDCK cells were grown in a total volume of 10 mL in Nunc T75 flasks (ThermoFisher Scientific). THP-1 were grown in a total volume of 10 mL in Nunc T25 flasks (ThermoFisher Scientific). HeLa and MDCK cells were routinely cultured at ~70% confluency by washing with 5 mL PBS (Sigma- Aldrich (Merck)) and incubation with 2 mL 0.25% trypsin Ethylenediaminetetraacetic acid (EDTA) (Sigma Life Science) at 37°C until cells became visibly rounded under a brightfield microscope. Cells were resuspended in 10 mL of complete medium and diluted 10× for continued growth in a 10 mL total volume.

2.2.7 Transfection

2.2.7.1 Transient transfection

Transient transfections were performed using polyethyleneimine (PEI). For transfection of HeLa cells in 24 well plates (Corning inc.), HeLa cells were seeded into wells at a concentration of 5×10^4 cells in 1 mL complete medium per well. For transfection of HeLa cell in 35mm glass-bottomed dishes (World Precision Instruments), cells were seeded at a concentration of 3×10^5 cells per dish. Cells were incubated for 24h prior to transfection. pcDNA and PEI were used at a 1:3 ratio. pcDNA (AQP4-GFP in PDEST-47) was diluted 50× in serum-free DMEM and mixed by pipetting. PEI was added in a dropwise manner, mixed and incubated at room temperature for 15 minutes. This protocol was scaled up or down, keeping all concentrations the same for different sized culture vessels. Successful transfection was confirmed using epifluorescence microscopy (Leica Microsystems GmbH) for green fluorescence.

```
Query  1
MSDRPTARRWGKCGPLCTRENIMVAFKGVWTQAFWKAVTAEFLAMLIFVLLSLGSTINWG  60

MSDRPTARRWGKCGPLCTRENIMVAFKGVWTQAFWKAVTAEFLAMLIFVLLSLGSTINWG

Sbjct  1
MSDRPTARRWGKCGPLCTRENIMVAFKGVWTQAFWKAVTAEFLAMLIFVLLSLGSTINWG  60


Query  61
GTEKPLPVDMVLISLCFGLSIATMVQCFGHISGGHINPAVTVAMVCTRKISIAKSVFYIA  120

GTEKPLPVDMVLISLCFGLSIATMVQCFGHISGGHINPAVTVAMVCTRKISIAKSVFYIA

Sbjct  61
GTEKPLPVDMVLISLCFGLSIATMVQCFGHISGGHINPAVTVAMVCTRKISIAKSVFYIA  120


Query  121
AQCLGAIIGAGILYLVTPPSVVGGLGVTMVHGNLTAGHGLLVELIITFQLVFTIFASCDS  180

AQCLGAIIGAGILYLVTPPSVVGGLGVTMVHGNLTAGHGLLVELIITFQLVFTIFASCDS

Sbjct  121
AQCLGAIIGAGILYLVTPPSVVGGLGVTMVHGNLTAGHGLLVELIITFQLVFTIFASCDS  180


Query  181
KRTDVTGSIALAIGFSVAIGHLFAINYTGASMNPARSFGPAVIMGNWENHWIYWVGPIIG  240

KRTDVTGSIALAIGFSVAIGHLFAINYTGASMNPARSFGPAVIMGNWENHWIYWVGPIIG

Sbjct  181
KRTDVTGSIALAIGFSVAIGHLFAINYTGASMNPARSFGPAVIMGNWENHWIYWVGPIIG  240


Query  241
AVLAGGLYEYVFCPDVEFKRRFKEAFSKAAQQTKGSYMEVEDNRSQVETDDLILKPGVVH  300

AVLAGGLYEYVFCPDVEFKRRFKEAFSKAAQQTKGSYMEVEDNRSQVETDDLILKPGVVH

Sbjct  241
AVLAGGLYEYVFCPDVEFKRRFKEAFSKAAQQTKGSYMEVEDNRSQVETDDLILKPGVVH  300


Query  301  VIDVDRGEEKKGKDQSGKGLSS  322

             VIDVDRGEEKKGKDQSG+ LSS

Sbjct  301  VIDVDRGEEKKGKDQSGEVLSS  322
```

Figure 2.2 AQP4 sequence alignment

Alignment of an AQP4-GFP cDNA FASTA 5'-to-3' sequence with known AQP4 DNA sequence (UniProt, ExPASy). Top sequence labelled 'Query' is the sequence of cDNA generated by PCR of the PDEST-47 construct using the T7 primer. The bottom sequence labelled 'Sbjct,' is the known AQP4 DNA sequence provided by UniProt. The middle sequence represents sequence alignment.

2.2.8 Stable cell line generation

2.2.8.1 G418 optimisation

Stable transfection of HeLa cells was possible as pcDNA-DEST47 contained a neomycin/G418 resistance gene. To determine an appropriate concentration of the G418 antibiotic for selection of successfully transfected cells, non-transfected HeLa cells were seeded in a 24 well plate at 5×10^4 cells per well, in duplicate, and incubated with increasing concentrations of G418 (0, 50, 100, 200, 300, 400, 500, 600, 700, 800, 900 and 1,000 µg/mL). Cells were grown in these conditions for two weeks and media were replaced every two days, maintaining G418 concentrations. The lowest concentration of G418 required to kill all non-transfected cells, determined using brightfield microscopy (EVOS, ThermoFisher Scientific), was chosen for further selection of successfully transfected cells.

2.2.8.3 Stable transfection

HeLa cells were transiently transfected as described above, in T75 flasks for increased yield. A non-transfected 6 well plate was used as a control for cell death. After 48 hours, cells were resuspended in culture medium containing 500 µg/mL G418. G418-supplemented medium was refreshed every two days. After 14 days, colonies were visualised using an epifluorescence microscope (Leica Microsystems GmbH) for live cells and AQP4-GFP expression. Live cell colonies were harvested using trypsin EDTA and reseeded into 96 well plates at an average concentration of one cell per well in 100 µL G418 medium. Colonies were grown to confluence, trypsinized and transferred to a 24 well plate (Corning), grown to confluence and transferred to a six well plate (Corning), then a T75 flask (Nunc). Upon reaching confluence three colonies were transferred to T75 flasks for freezing. All steps were performed with 500 µg/mL G418 in culture medium.

2.2.9 EV release model

2.2.9.1 Generation of media for tonic stress

For EV production in tonic stress, isotonic, hypotonic, and hypertonic media were made. Isotonic medium contained serum-free DMEM, L-glutamine and penicillin-streptomycin solution (pen-strep). Hypotonic medium contained two parts sterile deionised water with one-part isotonic medium. Hypertonic medium contained 200mOsm mannitol in isotonic medium. The final osmolarity of media was measured with an osmometer (Loeser), following the manufacturer's instructions. Osmolarity of media were: Isotonic ~340mOsm, hypotonic ~110mOsm and hypertonic ~790mOsm.

2.2.9.2 Tonic stress incubation

Stably transfected HeLa and MDCK cells were grown to confluence in T75 flasks, washed with 5 mL of calcium and magnesium-free PBS and incubated at 37˚C in 5% CO_2 for four hours in 10 mL of either isotonic, hypotonic, or hypertonic medium. Media were harvested and centrifuged at 2000×g for 10 minutes to pellet cell debris. Media were transferred to 15 mL 30kDa centrifugal concentration filters (Amicon Ultra, Millipore) and centrifuged at 3200×g for a minimum of 10 minutes at 4˚C. Media were concentrated to ~200 µL volume, transferred to sterile 1.5 mL microfuge tubes and made up to 500 µL volume with sterile PBS. For BODIPY FL Maleimide labelling 1 µL of 5 mM BODIPY Maleimide was added to each sample and incubated at incubated 4˚C overnight.

2.2.9.3 Size exclusion chromatography isolation of EV

EV were isolated using size exclusion chromatography (SEC) columns (qEV original 70nm Gen 2, IZON Science PLC) following the manufacturer's instructions. Fraction volumes were optimised for EV isolation. 13 small, 0.5 µL fractions were collected and analysed individually for EV content using UV-SSC FC. Once EV presence was confirmed, EV positive fractions were combined or collected as larger fractions.

2.2.10 Epifluorescence Microscopy

2.2.10.1. AQP4-GFP Expression

Stably transfected cells were regularly monitored for AQP4-GFP expression. Cells were visualised using an inverted DMI400B epifluorescence microscope (Leica Microsystems GmbH). Cells were imaged using phase contrast microscopy and 488 nm excitation with a 'GFP' filter cube for green fluorescence.

2.2.10.2 Tonicity-mediated AQP4-GFP translocation

Stably transfected HeLa cells were seeded in 35 mm glass bottomed dishes (World Precision Instruments) at a 3×10^5/mL concentration and incubated for 24 hours prior to imaging. Cells were imaged using an inverted epifluorescence microscope (DMI400B, Leica Microsystems GmbH) in temperature controlled environmental chamber, warmed to 37 °C. Cells were imaged using phase contrast microscopy and 488 nm excitation with a 'GFP' filter cube for green fluorescence. Cells were imaged at 63× magnification using an oil apochromatic (APO) objective. ROI were selected and maintained while extracellular tonicity was altered. Initially, cells were imaged in 500 µL of DMEM (Isotonic). Increasing amounts of sterile water was added to the dish (500 µL) each time, to create increasing hypotonic environments. Water was added to DMEM to

create final dilutions of 1:1, 2:1 and 3:1 water: DMEM. The relative membrane expression of AQP4-GFP in each condition was quantified by ImageJ (National Institutes of Health & the Laboratory for Optical and Computational Instrumentation). Line profiles were drawn across cells, including the plasma membrane, cytoplasm and extracellular space giving the relative fluorescence intensities of pixels at different points along the line, and therefore distinct parts of the cell (Figure 2.3 A). Plasma membrane fluorescence values and cytoplasmic values identified using line intensity profiles and line length (Figure 2.3 B). Average fluorescence values of the cell cytoplasm and cell membrane were compared and quantified as the percentage membrane expression. A minimum of three cells were imaged for each condition and ten lines were drawn per cell.

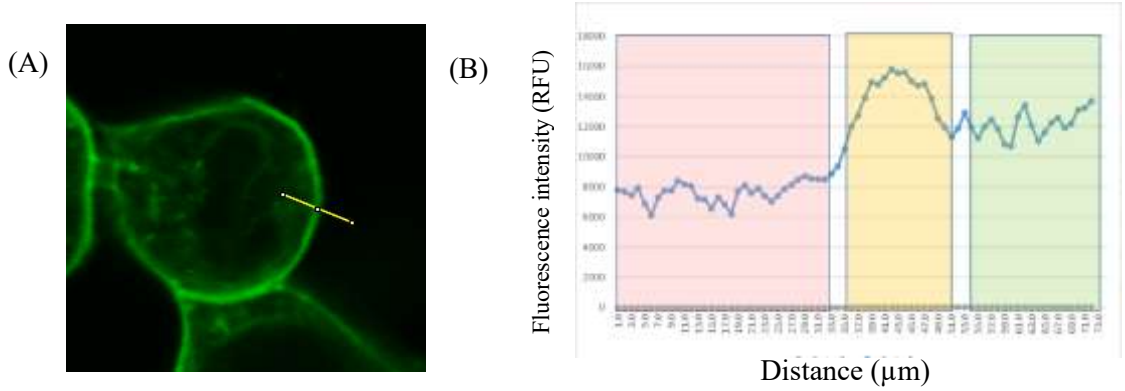

Figure 2.3 Hypotonic relocalisation quantification method

(A) The representative epifluorescence micrograph shows transfected cells, expressing AQP4-GFP in hypotonic medium. The yellow line demonstrates how line profiles were created to measure fluorescence intensity at different points, crossing the plasma membrane into the cell cytoplasm, with similar distance measured either side of the plasma membrane. (B) Line profiles were used to generate fluorescence intensity histograms. Membrane fluorescence values are highlighted as yellow. Intracellular values are green and extracellular values are red. Fluorescence values were used to calculate percentage membrane fluorescence (Sum membrane fluorescence/ (Sum membrane fluorescence + sum cytoplasmic fluorescence) *100)

2.2.11 Flow Cytometry

All flow cytometry analyses were performed using a CytoFLEX S cytometer (Beckman Coulter).

2.2.11.1 Flow cytometry analyses of cell lines

2.2.10.1.1 Cell counting

MDCK and HeLa cells were counted using flow cytometry for normalisation of EV counts. THP-1 cells were counted before incubation with EV to ensure consistent cell numbers between experiments. Adherent cell lines (MDCK and HeLa) were harvested using trypsin EDTA and resuspended in 10 mL of DMEM. THP-1 cells were mixed by pipetting and transferred to 5 mL flow cytometry tubes for counting. For HeLa and MDCK cell counting, 20 µL of cell suspension was analysed. A slow flow rate was used, (10 µL per minute). Forward scatter (FSC) and side scatter (SSC) properties were used to identify cell populations. FSC gain was set to 145 and SSC to 360. For THP-1 cell counting, a medium flow rate was used (30 µL per minute). FSC was set to 200 and SSC to 700. Cell populations appeared as a dense cloud of dots, where each dot represented an 'event,' where the laser was disrupted. Small events, with low FSC and SSC values were excluded from counting by drawing a 2D gate around a distinct population of dots with larger FSC and SSC events. These gates are explained in more detail in Chapter 4.

2.2.11.1.2 Cell fluorescence

MDCK and HeLa cell populations were analysed for GFP expression using flow cytometry. Cell populations were identified as described in section 2.5.1.1. AQP4-GFP expression was detected using a 488 nm laser and corresponding filter cube. The gain for this channel was set to 150. THP-1 cells were analysed for green fluorescence following incubation with BODIPY (BODIPY FL Maleimide) labelled EV. Following identification of cell populations, 5000 cells were analysed for green fluorescence. A medium flow rate was used. The gain for GFP detection was set to 200.

2.2.11.1.3 EV-THP-1 cell interaction

48 hours prior to analysis, THP-1 monocytes were differentiated using dihydroxy vitamin D3 (VD3) in RPMI (Sigma-Aldrich (Merck)) at a 100 nM final concentration. THP-1 cells were counted using flow cytometry as described above (CytoFLEX, Beckman Coulter). A background level of fluorescence was established prior to incubation with EV by drawing a fluorescence positive gate above background fluorescence levels. THP-1 cells were incubated with BODIPY labelled EV at a 1:10 ratio, where the concentration of EV was 10× the concentration of THP-1 cells. For each condition, at least 2500 THP-1 cells were counted at a slow flow rate (10 µL/min).

THP-1 cells were analysed for green fluorescence intensity to measure EV interaction and /or uptake.

2.2.11.2 Flow Cytometry analyses of EV

Following SEC isolation, EV were identified and analysed by ultraviolet side scatter flow cytometry (UV-SSC) (CytoFLEX, Beckman Coulter) using a 405 nm laser to excite nano-sized green particles for detection. Green, fluorescent polystyrene calibration beads (BioCytex) of known sizes (diameters of 100 nm, 160 nm, 200 nm, 240 nm, 300 nm, 500 nm, 900 nm) were used to define EV detection parameters. At least 5 µL of EV suspension was analysed. Flow rates between 10 µL and 60 µL per minute were used. BODIPY labelled EV were detected using UV-SSC and green (BODIPY) labelling. UV-SSC gain was set 500 and BODIPY (FITC channel) to 2000. Sample thresholding was used to remove background signal. FSC, set to 1, was used as the primary threshold trigger. UV-SSC, set to 20,000, was used as a secondary trigger. Unlabelled EV were analysed for cell-derived GFP fluorescence to confirm AQP4-GFP presence in EV using the same method. A 2D 'EV' gate was drawn around fluorescent particles within the expected size range, described in more detail in Figure 5.6. Events that fell within this gate were predicted to be EV and analysed further.

BODIPY labelled EV were defined using the method described above and analysed for Annexin-V labelling. Annexin-V-APC was centrifuged at 10,000×g for 1 minute in a microfuge to pellet any dye aggregates. 5 µL of Annexin-V-APC (BioLegend) was added to 200 µL of EV suspension and 200µL of Annexin-V binding buffer (BioLegend) before incubation in the dark for 15 minutes. Annexin-V-APC labelling of EV was determined using excitation with a 638 nm laser and collection of peak fluorescence emission at 660 nm. Positive Annexin-V EV were defined using a linear gate, as described more detail in Figure 5.6.

2.2.11.2.1 Hypotonic tolerance

EV were counted using UV-SSC FC (CytoFLEX, Beckman Coulter) as described above. EV samples were diluted to equal concentrations in sterile PBS, then further diluted with either sterile PBS or sterile water at a 1:1 ratio. EV were then counted again. EV counts in sterile water were compared to EV in PBS by calculating the percentage of EV in water, compared to PBS.

2.2.12 Calcein AM cell swelling assay

This work was undertaken by Lucas Unger, Aston University. The method is included here to describe the procedure used to generate the Calcein AM data included in Chapter 4, which supports HeLa cell relocalisation findings.

Stably transfected MDCK and HeLa cells were seeded overnight into black 96-well clear-bottomed plates at a concentration of 6×10^3 and 8×10^3 cells per well respectively, in 100 µL complete medium. Cells were loaded with 5µM of calcein AM (ThermoFisher), a membrane permeant fluorescent dye for 90 min at 37°C. Cells were washed with PBS and immersed in 75 µL of HEPES-buffered DMEM Media were supplemented with 0.75 mM of Probenecid to minimise calcein AM leakage from cells. Plates were transferred to the plate reader (Fluostar Omega, BMG) for measurement. Pure water was injected into wells, creating an osmotic gradient. The fluorescence signal of calcein AM was measured by exciting with a 485 nm laser with emission at 525 nm measured. The osmotic-triggered cell volume changes due to water transport leads to alterations of the fluorescence signal quenching and can be quantified by calculating the rate constant k through kinetic curve fitting (shrinkage C+A*exp(-k*x), swelling C-A*exp(-k*x)). The constant k is proportional to the water permeability.

2.2.13 SDS-PAGE & Western blotting

2.2.13.1 SDS-PAGE

Cell samples were prepared by lysing a confluent 35 mm dish of cells in 250 µL of ice-cold RIPA buffer. Lysates were centrifuged at 21,000 × g for 10 minutes at 4 °C.

EV samples were produced using the technique described in section 2.2.9 In order to obtain enough protein to detect via western blot, EV production was amplified 10x and a further concentration step was completed following SEC isolation; 2 mL of isolated EV were concentrated into a final 100 µL volume using 1.5 mL, 10kDa centrifugal concentration filters (Amicon). Prior to loading, samples were mixed with 4× laemmli buffer and 20 mL of sample was loaded.

SDS-PAGE was performed following a standard protocol. 0.75mm thick gels were cast using standard equipment (Bio-Rad). Separating gels were 8% acrylamide, stacking gels were 4% acrylamide. Prior to loading, samples were mixed with 4× laemmli buffer. 20 µL of each sample was loaded. Electrophoresis was done at 200V for 45 minutes. The molecular weights of samples were estimated using a protein marker (Page Ruler, ThermoScientific).

2.2.13.2 Western blotting

Following separation on polyacrylamide gels, proteins were transferred to methanol activated PVDF membranes using a wet electroblotting system (Bio-Rad). Electrophoresis was done at 100V for one hour. Membranes were blocked using 20% w/v powdered skimmed milk (Tesco PLC) in 0.1% v/v PBS-tween for one hour on an orbital shaker at RT. Membranes were washed for 10 minutes in PBS-tween and incubated in either 5 mL of anti-AQP4 (ab128906, Abcam) at 1:1000 dilution or anti-GFP (Santa Cruz) at 1:5000 dilution, primary antibodies in 5% BSA PBS-tween overnight on a roller mixer at 4°C. Membranes were washed in PBS-tween for 10 minutes and incubated with anti-rabbit HRP conjugated secondary antibody in PBS-tween at room temperature for one hour.

2.2.14 Cryogenic transmission electron microscopy

EV release was confirmed by cryogenic electron transmission microscopy (CryoTEM) with the kind help of Dr Saskia Bakker at the Advanced Biomedical Imaging Facility (Warwick University). Imaging was funded by the Engineering and Physical Sciences Research Council (EPSRC) grant EP/V007688/1. We acknowledge the Midlands Regional Cryo-EM Facility, supported by Medical Research Council award reference MC_PC_17136.

EV samples were prepared following the method described in section 2.4.1.2. HeLa EV samples were made using hypertonic medium, and MDCK EV using hypotonic medium, for maximum EV release. Following SEC isolation samples were concentrated to 100 µL volume using 10kDa centrifugal concentration filters. Samples were prepared 24h prior to cryoTEM imaging and transported on ice.

Prior to imaging carbon grids were prepared in a glow discharger. EV samples were blotted and frozen onto Lacey carbon grids (EMResolutions, UK) using a Leica GP2 plunge freezer. EV were imaged using a JEOL2100Plus transmission electron microscope (TEM) with a Gatan OneView camera. Samples were imaged at 30,000/ 60,000× magnification.

Chapter 3 : Analysis of AQP4 expression and localization in rat spinal cord tissue

3.1 Introduction

AQP4 is expressed in the CNS (Papadopoulos and Verkman, 2013), specifically in astrocytes (Oklinski et al., 2014). It is responsible for the rapid transport of water into, and out of, the CNS in both healthy and pathological processes, such as TBI. AQP4-negative mice have been demonstrated to have reduced oedema following ischemic injury (Manley et al., 2000b) and investigations into the role of AQP4 in SCI show important roles for AQP4 in both oedema formation and resolution (Saadoun et al., 2008, Kimura et al., 2010). This suggests that AQP4 is a possible target for reduction of oedema following CNS injury, and that a short-term and/or reversible solution is required. Previous studies that target AQP4 function through pore-blocking have been unsuccessful at clinical trial, while others have identified components of an AQP4 trafficking mechanism in an *in vitro*, mammalian cell model (Kitchen et al., 2015b). In this chapter, confocal microscopy was used to demonstrate, for the first time, that this mechanism can be seen in mammalian tissue.

The work in this chapter expanded on the AQP4 trafficking mechanism identified *in vitro* (Kitchen et al., 2015b). It was hypothesised that the inhibition of CaM or inhibition of PKA phosphorylation of AQP4 would prevent AQP4 localisation to astrocytic endfeet following CNS injury and therefore prevent subsequent tissue oedema. Analysis by confocal microscopy of rat tissue from animals subjected to SCI was used to investigate AQP4 expression and localisation with and without CaM (TFP) and PKA (H89) inhibitors. The main objective of this work was to develop a robust analysis method that could quantify AQP4 levels at the astrocyte cell surface within tissue; a much more challenging context than that of primary cell culture. This work was performed in collaboration with Dr Andrea Halsey, University of Birmingham, who provided tissue samples and participated in imaging experiments.

3.2 AQP4 labelling in rat spinal cord tissue

3.2.1. Optimisation of immunohistochemical labelling of AQP4

Rat spinal cord samples, subjected to SCI (as described in Section 2.2), and non-injured control samples, were analysed for AQP4 expression using immunohistochemical (IHC) labelling and confocal microscopy. This IHC process presented several challenges; following the crush injury, tissue integrity suffered, making samples fragile and prone to breakage. The IHC labelling process required multiple labelling steps and therefore multiple washes, which disturbed tissues and, at times, caused tissue to break at the site of injury, making imaging unreliable. issue thickness was optimised, and successful labelling was performed on 15 µm slices, taking great care with samples so as not to damage tissue further. The integrity of tissue at the site of injury was especially important as imaging of astrocytes and AQP4 expression was carried out in the vicinity of the crush site. Imaging was not performed directly in the crush area, as cell integrity was often compromised and individual cells, and cell morphology could not be reliably identified (Figure 3.1).

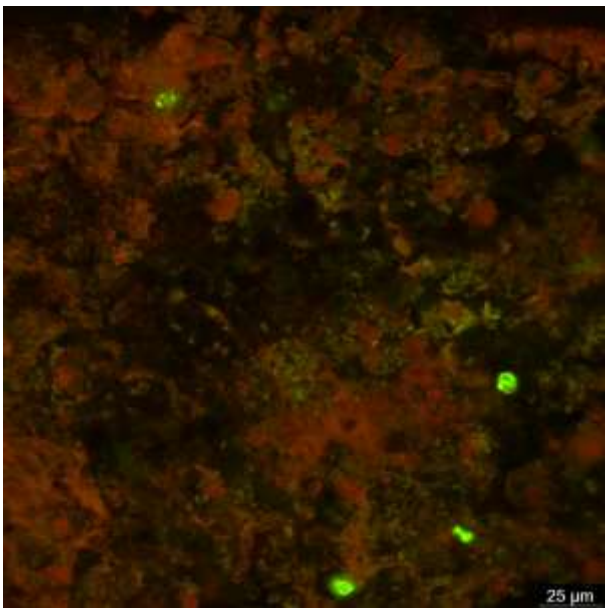

Figure 3.1 IHC labelling of AQP4 and GFAP within the site of injury

Representative confocal histogram overlay shows IHC labelling of AQP4 (green) and GFAP (red) in rat spinal cord tissue following SCI. The image is taken within the crush site.

Antibody labelling was optimised for IHC; the anti-AQP4 antibody used had been used successfully to detect AQP4 by western blot but had not been used for AQP4 detection in tissue samples. Once tissue thickness had been optimised, the concentration of anti-AQP4 antibody required for staining was determined.

While the primary aim of this study was to investigate the actions of CaM and PKA inhibitors, TFP and H89, in relation to AQP4 localisation to astrocytic endfeet, as these had been identified as important components of the AQP4 trafficking pathway, it was important to first investigate whether overall AQP4 expression levels were altered.

Rat spinal cord tissue samples (No injury control, Injury + PBS, Injury + TFP, and Injury + H89) were labelled for AQP4 expression with a monoclonal anti-AQP4 rabbit primary antibody (Abcam, ab128906) and a polyclonal anti-rabbit Alexafluor488 secondary antibody (Invitrogen, A21206) (Table 1) and imaged using confocal microscopy (Figure 3.2).

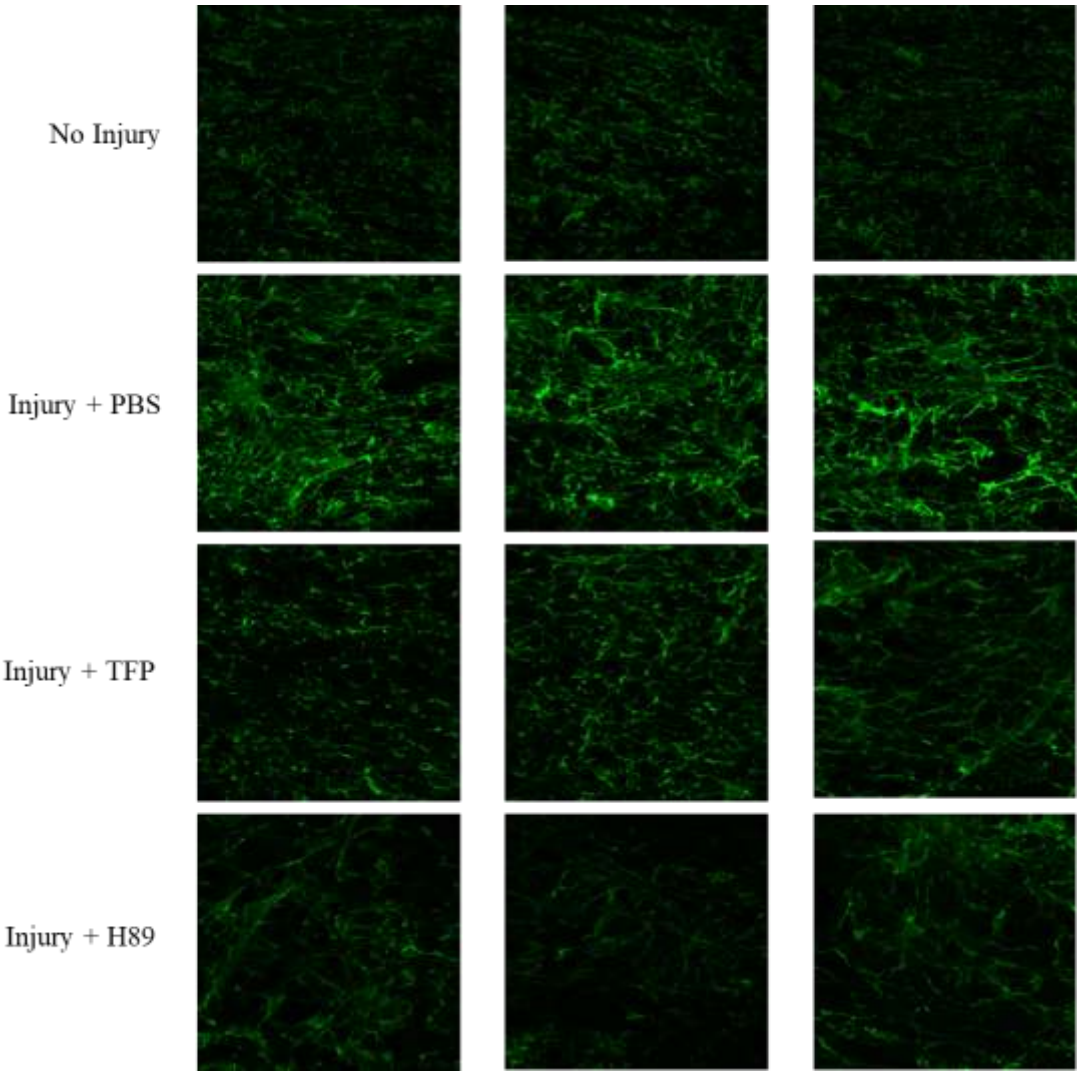

Figure 3.2 Confocal microscopy of AQP4 expression in rat spinal cord tissue

Representative fluorescence confocal micrographs show AQP4 expression (green) in rat spinal cord tissue samples following spinal crush injury, with and without treatment with CaM and H89 inhibitors. Samples included uninjured rat spinal cord tissue (no injury), untreated injured tissue (Injury +PBS), injured tissue + CaM inhibition (Injury+ TFP), and injured tissue + PKA inhibition (Injury + H89). Three representative images are shown per treatment. Images were taken at a 63x magnification.

Qualitative analysis of AQP4 labelling in rat spinal cord tissue suggested there were differences in AQP4 between treatments. Comparison of injured, untreated tissue (Injury +PBS) with uninjured tissue showed an increase in overall AQP4 expression following injury. This observation was not observed in tissue from animals treated with TFP or H89.

In order to confirm these findings, AQP4 fluorescence was quantified. Using LASAF image analysis software (Leica Microsystems), entire fields of view were selected as ROI to be included in analysis (Figure 3.3). Qualitative analysis of images suggested differences in AQP4 expression between treatments. From these image data, the mean intensity of green fluorescence values for each treatment condition were calculated and recorded as a scatter plot (Figure 3.4).

.

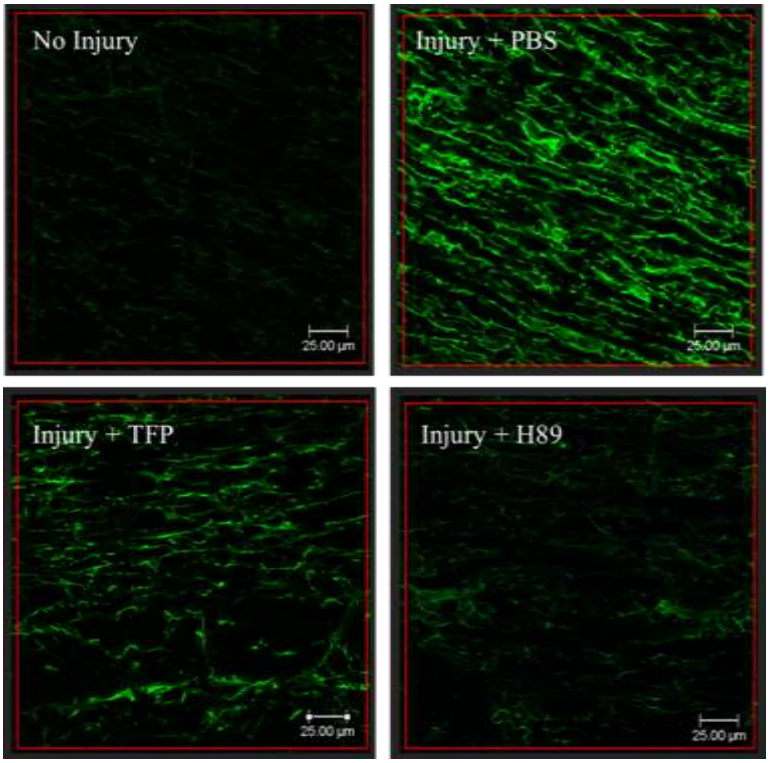

Figure 3.3 Quantification of AQP4 expression in rat spinal cord tissue following SCI

Representative confocal images show green fluorescence labelling (AQP4) in rat spinal cord tissue following SCI. Samples included uninjured rat spinal cord tissue (no injury), untreated injured tissue (Injury +PBS), injured tissue + CaM inhibition (Injury+ TFP), and injured tissue + PKA inhibition (H89). Images were taken at a 63x magnification. Red boxes define ROIs used for quantification of green fluorescence. Scale bars = 25 µm

3.3 AQP4 and GFAP labelling of astrocytes

Rat spinal cord samples, subjected to a crush injury (as described in Chapter 2), and non-injured control samples were analysed for AQP4 and GFAP expression. GFAP is a filament protein expressed in abundance by astrocytes. GFAP is a common target for antibody labelling of astrocytes (Middeldorp and Hol, 2011). Differences in AQP4 expression levels between samples treated with CaM and PKA inhibitors, and those without treatment, could identify a possible mechanism for the reduction of AQP4 expression following injury. GFAP labelling of samples identifies astrocytes within tissue samples and may allow for the application of AQP4 quantification. In order to analyse and quantify AQP4 expression, and identify astrocytes within spinal cord tissue, samples were labelled with green (AQP4) and red (GFAP) fluorophores and analysed using confocal microscopy (Figure 3.4) Optimisation of co-staining with anti-GFAP was straightforward, a reliable anti-GFAP antibody was easily sourced and secondary antibodies, with distinct excitation and emission profiles were readily available.

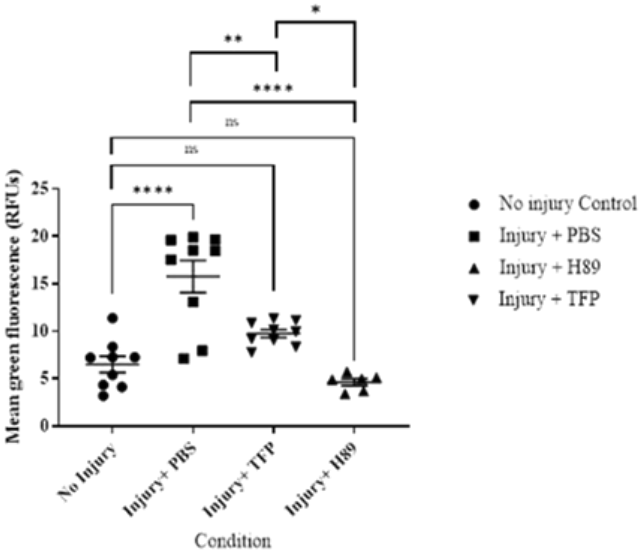

Figure 3.4 Quantification of AQP4 expression in rat spinal cord tissue

Scatter plot shows the mean green fluorescence values of images acquired using confocal microscopy where green fluorescence correlates with AQP4 expression. Uninjured rat spinal cord tissue (no injury), untreated injured tissue (Injury +PBS), injured tissue + CaM inhibition (Injury+ TFP), and injured tissue + PKA inhibition (H89) were plotted. Values are given in relative fluorescence units (RFUs). A one-way ANOVA followed by a Bonferroni *post hoc* test was applied to assess statistical significance. n=6. *=p<0.05, **=p<0.01,****=p<0.001.

Analysis of rat spinal cord tissue samples showed successful IHC labelling of AQP4 and GFAP. Astrocytes were clearly identified by red fluorescence labelling of GFAP. AQP4 was present in the cell membranes of astrocytes (green), not only in astrocytic endfeet but also in cell bodies and processes. Astrocytic bodies were identified by the presence of nuclei (DAPI, blue). Astrocytic processes were identified by absence of nuclei and morphology. It was determined that the method used for AQP4 labelling was appropriate, as AQP4 signal was clear and appeared to be specific, with a low signal to noise ratio, and could be used for further imaging, as the signal to noise ratio was high, labelling appeared to be specific and bright. Thought it was not possible to clearly identify astrocytic endfeet using this method, there were some areas of brighter green fluorescence, where GFAP staining was absent and nuclear morphology appeared endothelial that may have been endfoot labelling (Figure 3.5).

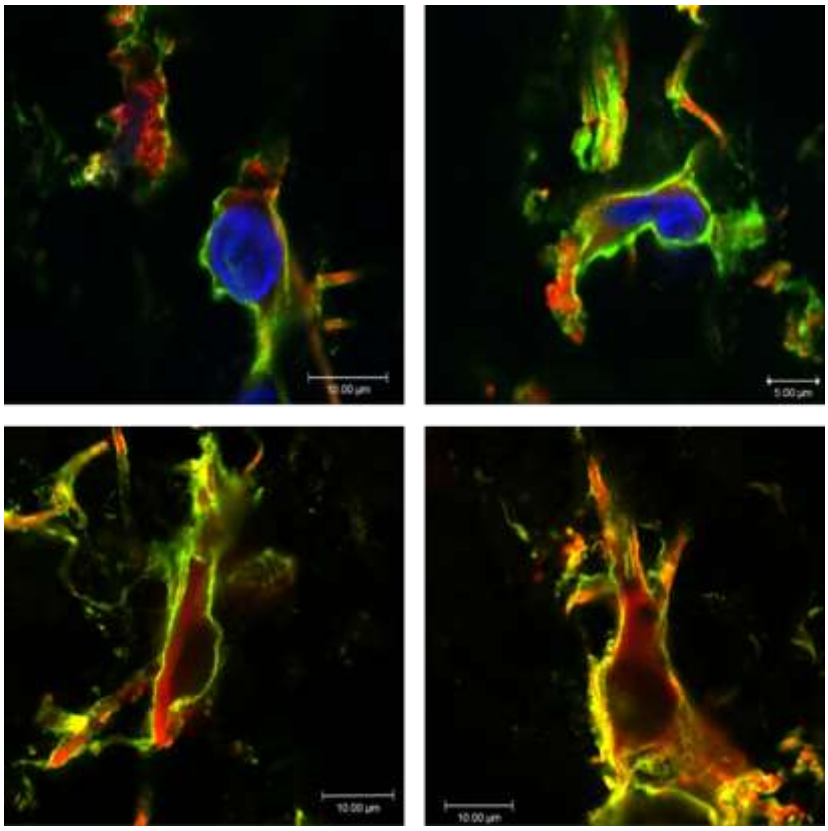

Figure 3.5 Identification of astrocytes

Representative overlay confocal micrographs show AQP4 (green), GFAP (red) and DAPI (blue) labelling of rat spinal cord tissue following SCI. Images show GFAP expression by astrocytes and AQP4 expression in astrocytic plasma membranes. DAPI is included only in the top two images.

It was also observed that some of these structures appeared to have multiple, distinct nuclei and were therefore believed to be multicellular rather than one individual cell per structure. This also suggests that these structures are not made up of astrocytes as, astrocytes are mono-nucleic and AQP4-containing membranes would be observed between nuclei. Structures of various sizes were observed, this is evident from the scale bars included in Figure 3.6. and further suggested that these structures were not individual cells. It is known that astrocytes interface with multiple cell types in the CNS.

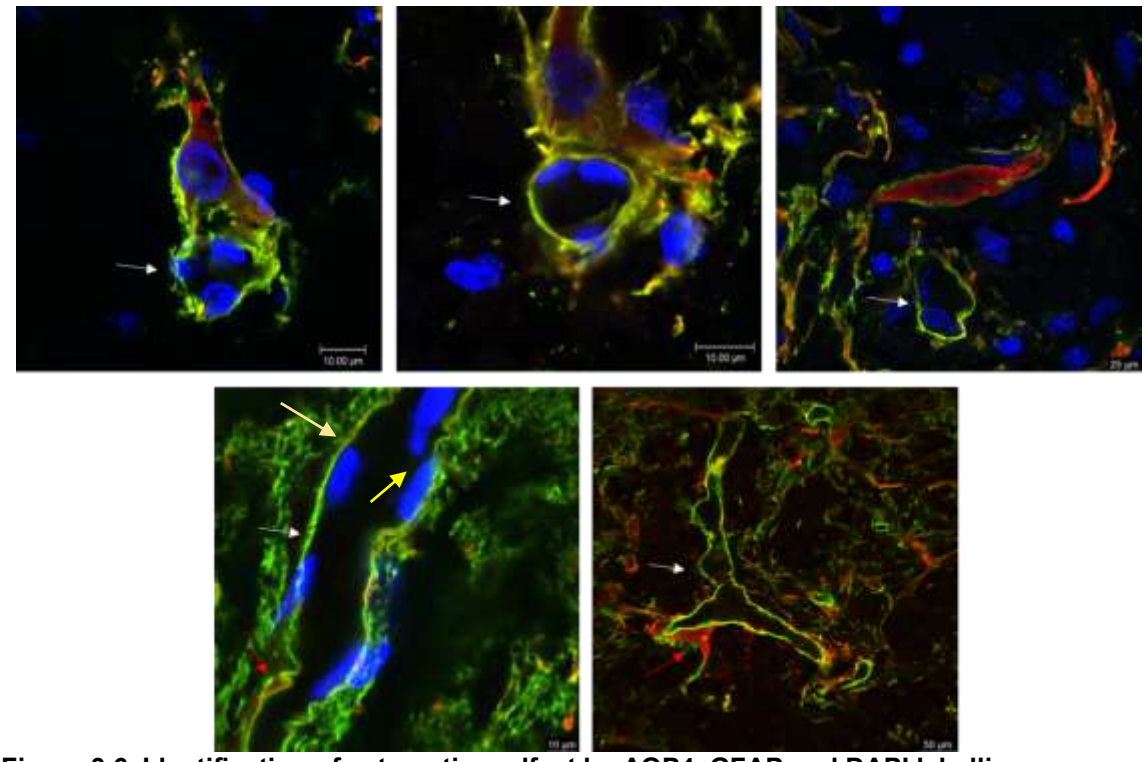

Figure 3.6 Identification of astrocytic endfeet by AQP4, GFAP and DAPI labelling

Representative confocal micrographs show labelling of AQP4 (green), GFAP (red) and Nuclei (blue). White arrows point to areas of green fluorescence labelling around GFAP-negative areas. Red arrows identify areas of GFAP labelling in direct or close contact with areas identified by white arrows. Squamous-like nuclei are present in large unlabelled areas (yellow arrow).

It was presumed that these structures are blood vessels, based on their shape, and the increased AQP4 fluorescence intensity observed in some of the structures, expected at astrocytic endfeet which interface with blood vessels (Figure 3.6). In addition, the shape of some nuclei suggest that the structures are composed of squamous endothelial cells. The differences observed between examples of these structures suggest that they may not all be composed of the same cells. As no other cell markers were used to identify other CNS cell types in this protocol, it was not possible to say for sure which cell type/s these structures contain, and further investigation was required. Therefore, endfeet were not easy to identify and quantification using this method was not possible.

3.4 Identification of astrocytic endfeet

Analysis of tissue samples labelling for AQP4 and GFAP provided important insight into the levels of AQP4 expression and the possible presence of activated astrocytes in samples following injury and allowed comparison of samples with and without treatments. This method did not however, allow for accurate identification of astrocytic endfeet, due to AQP4 labelling throughout astrocytic membranes, and so quantification of AQP4 localisation to endfeet was not possible. In order to further identify the cellular composition of tissues and allow identification of blood vessels and therefore endfeet another IHC method was required.

Initially, the possibility of using other astrocytic endfoot markers was investigated. Alternative astrocyte markers such as excitatory amino acid transporters 1/2 (EAAT1/2) were considered but these can be found in intracellular vesicles and throughout the plasma of activated astrocytes and would therefore not help in the identification of endfeet. In fact, no other markers that specifically labelled astrocytic endfeet could be identified; AQP4 appeared to be the most reliable endfoot marker available. Another marker was therefore required to confirm endfoot localisation. If treatment with CaM or PKA inhibitors reduced AQP4 endfoot localisation, then endfeet may not be clearly identifiable, and quantification of AQP4 localisation would not be possible. The identification of AQP4, in the proximity of blood vessels, was explored as an effective alternative. A suitable endothelial cell marker was sought, and, after an extensive search, an anti-rat endothelial cell antigen antibody (RECA-1) was identified. This antibody had been shown to label endothelial cells consistently and effectively in different tissues, and three different strains of rat. Initially, it was hoped that AQP4, GFAP, DAPI and RECA-1 could be labelled simultaneously. Unfortunately, at the time, any RECA-1 antibodies that had been used to successfully label RECA-1 in rat tissue using IHC were produced in mice and would not have been distinguishable from the anti-GFAP antibody used, which was also raised in mice. In addition, the confocal system used to image tissue samples was equipped with fixed laser lines, which limited the conjugated fluorophores that could be used. In essence, thorough optimisation had been required for antibody labelling to this point and new antibody combinations, requiring further optimisation, would have been necessary for successful simultaneous labelling of all four antigens. It was therefore decided that GFAP labelling would be replaced with RECA-1. RECA-1 labelling was performed and optimised for labelling of rat spinal cord tissue.

3.5 AQP4 and RECA-1 labelling of rat spinal cord tissue.

Injured rat spinal cord tissue was labelled using IHC for AQP4 (green) following the protocol established earlier in this chapter, and GFAP labelling was replaced RECA-1 labelling. Astrocytic endfeet were identified as green fluorescence labelling directly around red fluorescent endothelial cells, (Figure 3.7).

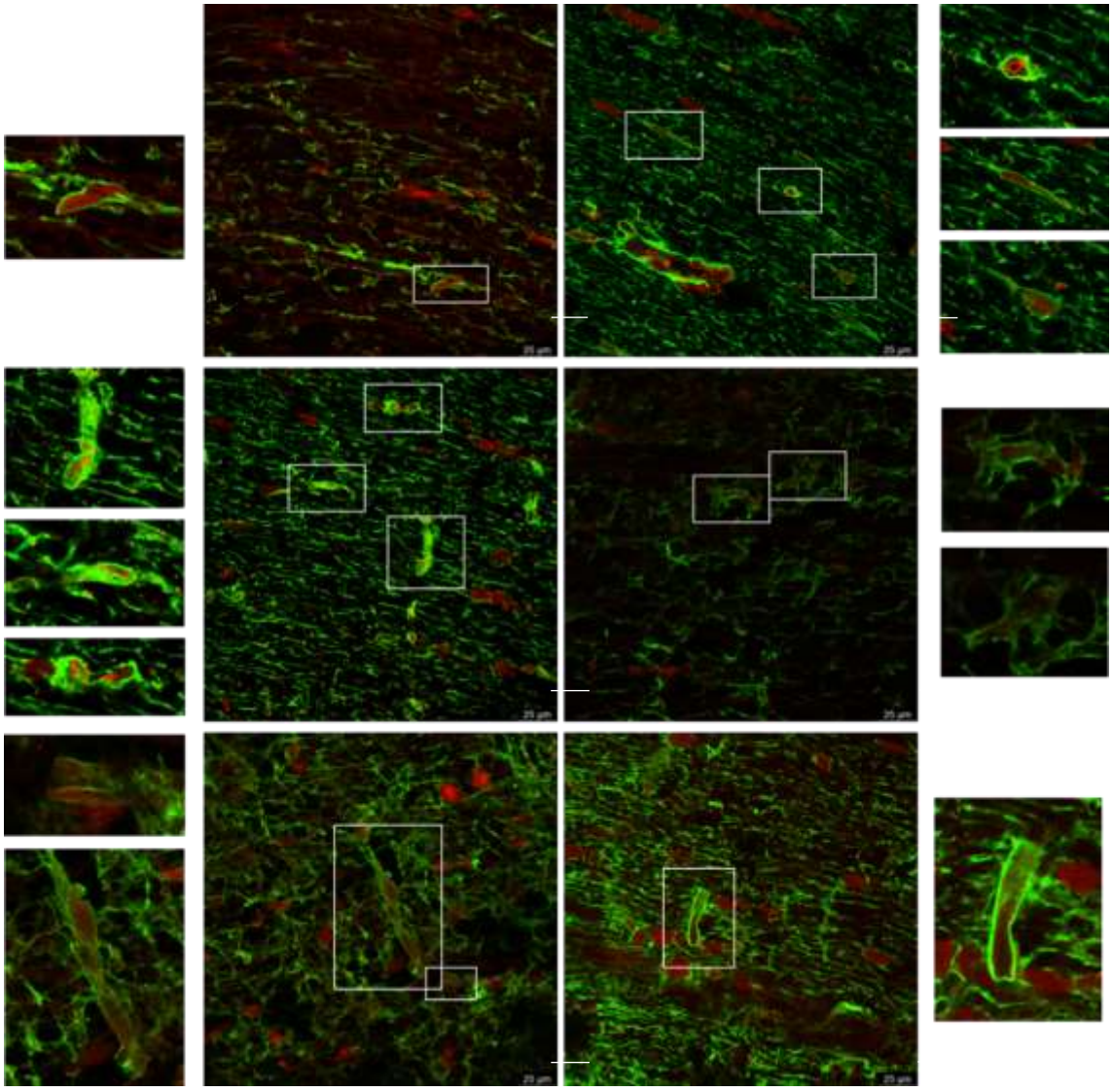

Figure 3.7 Identification of astrocytic endfeet

Representative confocal overlay micrographs show IHC labelling of AQP4 (green) and RECA-1 (red). White boxes and corresponding zoomed images show examples of areas of RECA-1 labelling surrounded by AQP4 labelling. Representative images are taken from a variety of conditions. Images were taken at 63x magnification. Zoomed images are not to scale.

Qualitative analysis of images from samples labelled for AQP4 and RECA-1 made identification of endfeet clearer. As seen earlier, AQP4 and therefore astrocytic membranes labelled clearly (green). Endothelial cells were visible after labelling of RECA-1 (red). Areas of red labelling, surrounded by green fluorescence were identified. These areas of green fluorescence were previously presumed to be endfeet. Localisation of endfeet was confirmed following the addition of RECA-1 labelling. These data did not include nuclear staining, so it was not possible to discuss nuclear morphology and compare findings with the nuclear morphology seen in the previous figure. The sizes and shape of the RECA-1 positive structures resembled the structures identified in figure 3.4. The AQP4 labelling around these structures also appeared the same. As RECA-1 labels endothelial cells, and AQP4 is concentrated in membranes around RECA-1 positive areas, these were determined to be astrocytic endfeet. In order to ascertain whether there were any differences in AQP4 localisation to endfeet following treatment with TFP or H89, AQP4 expression at endfeet was compared between conditions (Figure 3.8).

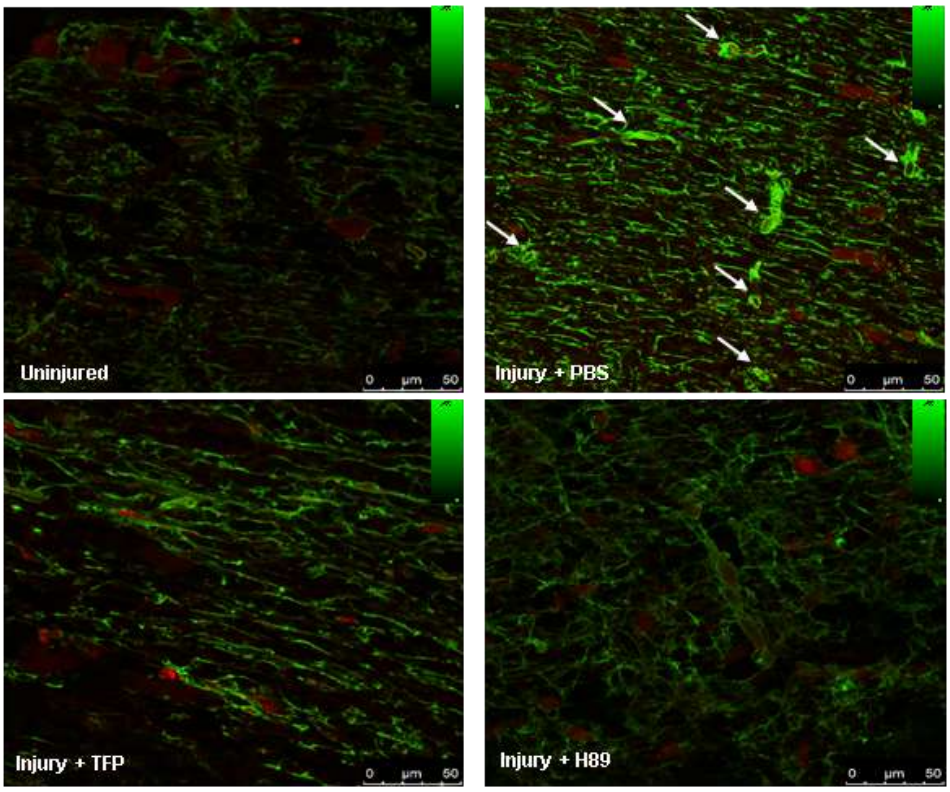

Figure 3.8 Identification of endfeet in rat spinal cord tissue

Representative overlay confocal micrographs show AQP4 (green) and RECA-1 (red) labelling in rat spinal cord tissue with and without treatment with CaM and PKA inhibitors. Samples included uninjured rat spinal cord tissue (no injury), untreated injured tissue (Injury +PBS), injured tissue + CaM inhibition (Injury + TFP), and injured tissue + PKA inhibition (Injury + H89). Images were taken at a 63x magnification.

Qualitative analysis of AQP4 expression in astrocytic endfeet suggested there were differences between treatments (Figure 3.8). When comparing the amount of AQP4 expressed at endfeet with AQP4 expression in other parts of astrocytes, such as cell bodies and processes (Relative endfoot expression (REE)), it appeared that there was more AQP4 expressed in the endfeet in the injured, untreated conditions when compared with uninjured and treated controls as AQP4 appeared brightest in this area. In order to confirm these observations, the REE was quantified.

3.5 Quantification of AQP4 expression in endfeet

A quantification protocol was designed to allow quantification of AQP4 expression in specific areas of astrocytes, namely in astrocytic endfeet versus processes and cell bodies. AQP4 is primarily expressed in endfeet *in vivo* (Nielsen et al., 1997b) and it is anticipated that this localisation is important for AQP4 function in water influx and subsequent oedema following ischemic injury. In order to investigate whether AQP localisation to endfeet is altered by treatment with TFP or H89, AQP4 expression was quantified. Areas for measurement were defined by manually drawing linear ROIs on areas of AQP4 expression next to (endfeet) and away from (processes and cell bodies) areas of RECA-1 expression using LASAF image data analysis software (Leica Microsystems) (Figure 3.9).

A mean fluorescence value was given for each ROI drawn. These values were categorised as either endfoot expression or cell expression and compared (mean endfoot expression/ mean cell expression = REE) (Figure 3.10). Where REE is greater than 1, AQP4 expression is higher in endfeet than cell bodies and processes.

Statistical analyses for differences between the REE expression of AQP between different treatments showed that there was a significant increase in AQP4 localisation to astrocytic endfeet following spinal cord injury. In addition, rats treated with either TFP or H89 did not show this increase. Instead, a significant decrease was seen in REE when rats were treated with TFP or H89, compared to injured rats with no treatment. These data suggest that both TFP and H89 play a role in the localisation of AQP4 to astrocytic endfeet following spinal cord injury.

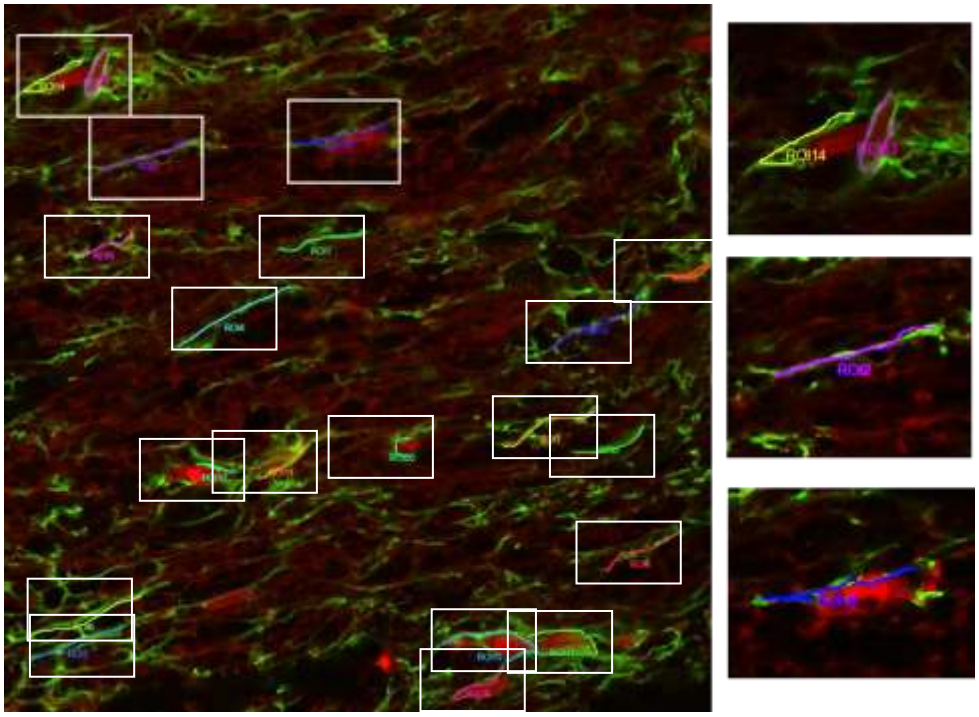

Figure 3.9 Quantification method of endfoot AQP4 expression

The representative confocal micrograph overlays show IHC labelling of AQP4 (green) and RECA-1 (red) expression in injured rat spinal cord tissue. Multiple ROIs (ROI 1-20) were drawn along areas of green fluorescence in close proximity to, and away from areas of red fluorescence. White boxes highlight ROIs drawn to measure green fluorescence intensities. Zoomed images show a selection of ROIs in more detail.

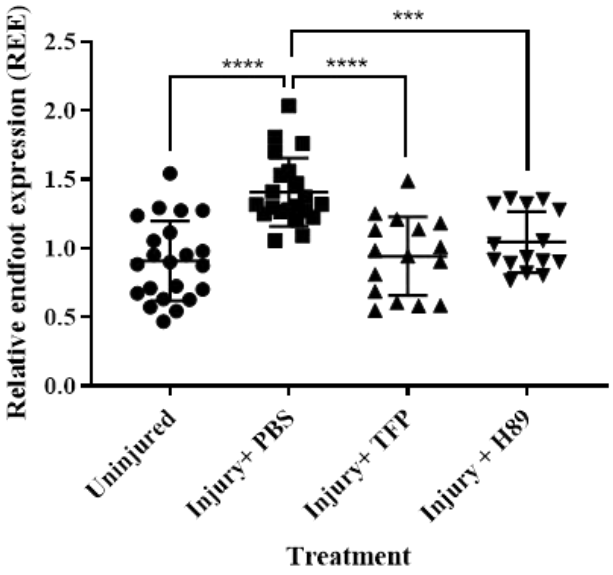

Figure 3.10 Quantification of AQP4 relative endfoot expression (REE)

Scatter plot shows the REE values of AQP4 in rat injured spinal cord tissue with and without treatment with CaM and PKA inhibitors. Samples included uninjured rat spinal cord tissue (no injury), untreated injured tissue (Injury +PBS), injured tissue + CaM inhibition (Injury + TFP), and injured tissue + PKA inhibition (injury + H89). Each icon represents a relative fluorescence value calculated from a single image and 20 ROIs. The mean and SD of each group is shown. 6 rats were used per condition. Statistical significance was determined using a 1-way ANOVA and a Bonferroni *post hoc* test. ***=p< 0.005, ****=p< 0.001.

3.6 Oedema in rat spinal cord tissue following SCI

The data presented in this chapter were published as part of a bigger study where the effect of TFP and H89 treatments on tissue oedema (Kitchen et al., 2020). Published data are shown here as they describe the physiological consequences of SCI and treatment with TFP and H89, these data were collected by Dr Andrea Halsey (Birmingham University). The original hypothesis presented at the start of this chapter suggested that TFP and H89 prevent AQP4 localisation to astrocytic endfeet following SCI and subsequent oedema. The following data complete the story by describing the effect of SCI and treatments on spinal cord oedema.

Water content of spinal columns was measured following SCI by weighing spinal cord tissue (Figure 3.11). The 'wet' weight of spinal cords was normalised to the dry weight and data were presented as water content as a percentage of the mass.

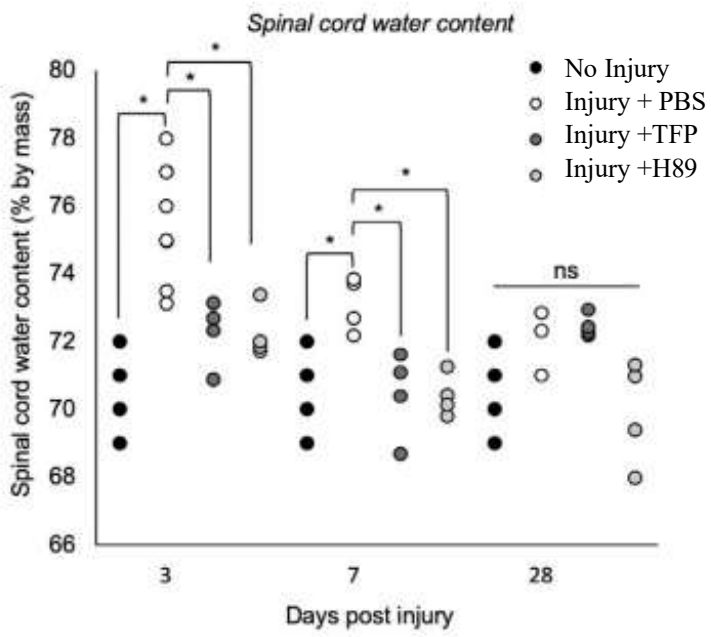

Figure 3.11 Water content of the thoracic spinal cord

Chart shows water content (% mass) of injured rat spinal cord tissue 3-, 7- and 28-days following injury. Data shown include uninjured tissue (No injury), injured tissue with no treatment (Injury + PBS), and injured tissue with either TFP or H89 treatments. Tissue samples were weighed before and after drying and water content was calculated as a percentage of tissue mass, by subtracting the dry weight from the wet weight of tissue. For statistical comparisons ANOVA was followed by *post hoc* Bonferroni-corrected t tests. *$p < 0.05$, ns represents $p > 0.05$

The data show a significant increase in spinal tissue water content in injured tissue with no treatment compared with uninjured tissue three days after injury. This increase was not observed in tissue from injured rats treated with either TFP or H89. After 7 days the water content of injured untreated tissue decreased, as oedema subsided but was still significantly higher than the water content of uninjured tissue and injured tissue from rats treated with TFP or H89. After 28 days, no differences in water content were observed. These data confirm the ability of TFP and H89 to prevent oedema following injury.

3.7 Discussion

The aim of this chapter was to create an IHC labelling, imaging and analysis protocol that allowed for quantification of AQP4 expression in astrocytic endfeet, in order to ascertain whether CaM and PKA played a role in AQP4 localisation to astrocytic endfeet following injury, a mechanism first observed *in vitro*, mammalian cell studies (Kitchen et al., 2015b). IHC was successful as AQP4 was identified in samples, an imaging protocol for tissue imaging was established using confocal microscopy and an AQP4 quantification protocol was designed that allowed quantification of AQP4 in endfeet versus processes and cell bodies. It was observed that there is an increase in both AQP4 expression and endfoot localisation following injury but not when animals are treated with TFP or H89. This was of interest as AQP4 expression and relocalisation was identified as a potential target for oedema following injury.

Combined with the increase in spinal water content observed only in injured, untreated tissue. these findings support the hypothesis that AQP4 localisation is important the onset of CNS oedema following injury and supports the idea that TFP and H89 inhibit oedema caused by increased expression and trafficking of AQP4.

Chapter 4 : Development of a tonicity-linked EV release model in MDCK and HeLa cells

4.1 Introduction

AQP have been identified in EV derived from healthy, stressed and activated cells from a wide variety of organisms. The properties of EV, and their AQP cargo are often altered in disease states (Clarke-Bland et al., 2022).

AQP4 has been identified in CNS-derived EV in a small number of studies, including *ex vivo* and *in vitro* techniques (Bejerot et al., 2019, Denver et al., 2019, Gonzalez-Molina et al., 2021, Nekludov et al., 2017, Simone et al., 2022, Wallensten et al., 2023). These studies cover only a few CNS pathologies and, to date, only one publication attempts to identify AQP4 in EV associated with TBI (Nekludov et al., 2017). This study concludes that there is more AQP4-positive EV in human patient blood following TBI, suggesting that AQP4 is a biomarker for injury severity. While promising, this result is yet to be reproduced, and requires further investigation.

The use of blood samples for EV studies comes with complications. Patient variables must be considered, such as age, sex, diet, and medication. TBI classification is also important, TBI type, localisation, cause, and physiological responses could all cause sample variation. It is difficult to attain samples; both ethical approval and patient consent are required. Additionally, circulating CNS-derived EV are mixed with blood serum and other tissues (Nekludov et al., 2017). EV isolation techniques are often dependent on the size and density of EV, CNS-derived EV cannot be reliably isolated from a mixed population; and additional steps are required to detect known markers, many of which are yet to be identified (Witwer et al., 2013). An *in vitro* model was therefore developed for this project to avoid complications encountered in the use of biological samples and enable investigation into the role of AQP4 in EV, and links with tonic stress. Immortalised cells produce EV *in vitro*, and release of EV can be optimised to produce the high numbers of EV often needed for accurate analysis, especially in discovery and protein analysis studies (Hahm, 2021). Issues with low EV counts include inaccurate analysis of EV populations, such as reliable counting, and characterisation of EV. For EV cargo analyses, large numbers of EV are often required to detect molecules of interest. The amount of cargo EV can hold is limited by EV size. Furthermore, as EV may be lost during isolation, it is advantageous to optimise EV release (Konoshenko, 2018).

This chapter describes the development of an *in vitro* EV release model that used tonic stress to trigger EV release by AQP4-positive and AQP4-negative cells. An EV release model was developed using MDCK stable cell lines; the effects of tonic stress were measured, and EV release was confirmed. A stable cell line expressing AQP4-GFP was generated using HeLa cells. AQP4-GFP expression and function was confirmed using western blot, flow cytometry and fluorescence microscopy. EV release by these cells was analysed.

4.2 Development of an EV release model in MDCK cells

A tonicity-linked EV release model was created to study and compare EV release by MDCK cells. Cells had been stably transfected with either M1-AQP4-GFP (M1 MDCK) or M23-AQP4-GFP (M23 MDCK). The cDNA for the M23 isoform of AQP4 had been generated by single point mutation of the first start codon (M1I) thus removing this start codon and allowing initiation of transcription only at the next methionine, in position 23 (M23). M1-AQP4-GFP were stably transfected using the full-length AQP4-GFP sequence. MDCK cells selectively expressed the M1 isoform of AQP4 and so no further interventions were required to ensure isolation of M1-AQP4 expression. WT MDCK were not transfected. Both M23 MDCK and M1 MDCK were transfected with the pDEST47 mammalian transfection vector introduced in Chapter 2.

4.2.1 Confirmation of AQP4-GFP expression in MDCK cells

Expression of M1 and M23 AQP4-GFP in stable MDCK cell lines had been published previously. AQP4-GFP expression, and their translocation in response to extracellular hypotonicity had been confirmed using western blot and fluorescence microscopy (Kitchen, 2015). In the present study AQP4-GFP expression in M1 MDCK, M23 MDCK and WT MDCK was reconfirmed by epifluorescence microscopy and flow cytometry (Figure 4.1).

An anticipated, qualitative analysis of epifluorescence images confirmed M1 and M23 AQP4-GFP expression in stably transfected MDCK cells. Quantitative analysis of flow cytometry data showed increased GFP expression in cells transfected with AQP4-GFP compared to non-transfected cells (Figure 4.1). GFP expression in M1 MDCK was also significantly higher than in M23 MDCK. The percentage of cells expressing AQP4-GFP was around 99% for M1-AQP4 and around 80% for M23-AQP4, both were significantly higher than WT MDCK, expressing no AQP4-GFP. The high expression and

transfection levels for this cell line made it a suitable candidate for an EV release model.

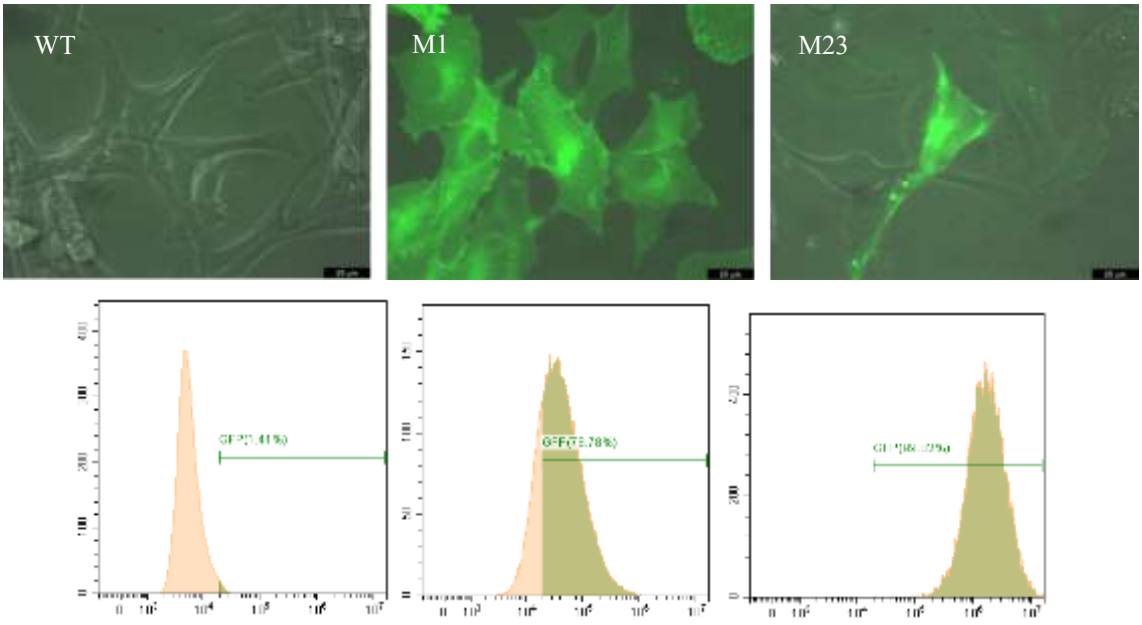

Figure 4.1 Confirmation of AQP4-GFP expression in stably transfected MDCK cells

(A) Representative fluorescence overlay micrographs show AQP4-GFP expression in MDCK cells. Stable transfectants express either M1 or M23 isoforms of AQP4 (M1 MDCK and M23 MDCK). Cells were imaged using epifluorescence microscopy to detect green fluorescence emission. (B) Representative flow cytometry frequency histograms show the CORRESPONDING percentage of WT MDCK, M1 MDCK, and M23 MDCK cell populations that emitted green fluorescence.

4.2.2 Development of EV release conditions in MDCK cells

WT, M1, and M23 MDCK cells were grown to confluence in T75 flasks in complete DMEM. Prior to tonic stress, growth medium was removed, and cells were washed with PBS. Cells were then incubated with 10 mL of either isotonic ~340 mOsm, hypotonic-~110 mOsm and hypertonic ~790 mOsm media. The conditions used to make EV are summarized below (Table 2). To collect EV, growth media were removed and centrifuged to pellet any large debris. Media were then concentrated using 30kDa centrifugal concentration filters (Amicon) and stained with BODIPY. EV were isolated from concentrated media by size exclusion chromatography (SEC). Cell health was analysed following tonic stress. EV release was confirmed and AQP4-GFP presence in EV was established.

Table 2 Conditions used in the tonicity-linked EV release model -MDCK cells

Cell Line	AQP4 content	Tonic condition
MDCK	WT	isotonic
		hypotonic
		hypertonic
	M1	isotonic
		hypotonic
		hypertonic
	M23	isotonic
		hypotonic
		hypertonic

4.2.3. Development of a flow cytometry gating protocol for cell detection

Cell properties were analysed using flow cytometry. Each cell was detected by a laser and represented as a dot on a plot based on the forward and SSC of the laser by the cell. Cells in a single population often have similar forward and SSC properties and appear as a 'cloud' of dots (Figure 4.2). A gate two-dimensional gate was manually drawn around the 'cloud,' of events with a similar forward and SSC properties to define a cell population and remove background noise (Figure 4.2 B). All cell data presented from here analyse cell populations defined using this gating method. GFP expression in cell populations was defined using a second, linear gate incorporating fluorescence intensities higher than those observed in control, GFP negative cell populations. This 'GFP' gate was defined using WT HeLa (Figure 4.2 C). GFP expression in AQP4 HeLa populations was then measured using the same gate, cells that were positive for GFP expression fell within the 'GFP gate' (Figure 4.2 D).

This project uses geometric mean fluorescence intensity (gMFI) to quantify fluorescence. This average value was chosen to quantify fluorescence over other average values as it is a more accurate value to use when data spans across a log scale, in comparison to the arithmetic mean, which is more appropriate for data that can be presented on a linear scale, or where the range of values within a data set is not broad (Illingworth, 2023). The gMFI were calculated by multiplying all values within a data set and finding the root value, rather than adding values and dividing by the number of values in the data set (arithmetic mean). This was an appropriate method to

use as there were large differences between the largest and smallest values in data sets, as is often observed in fluorescence emission analyses.

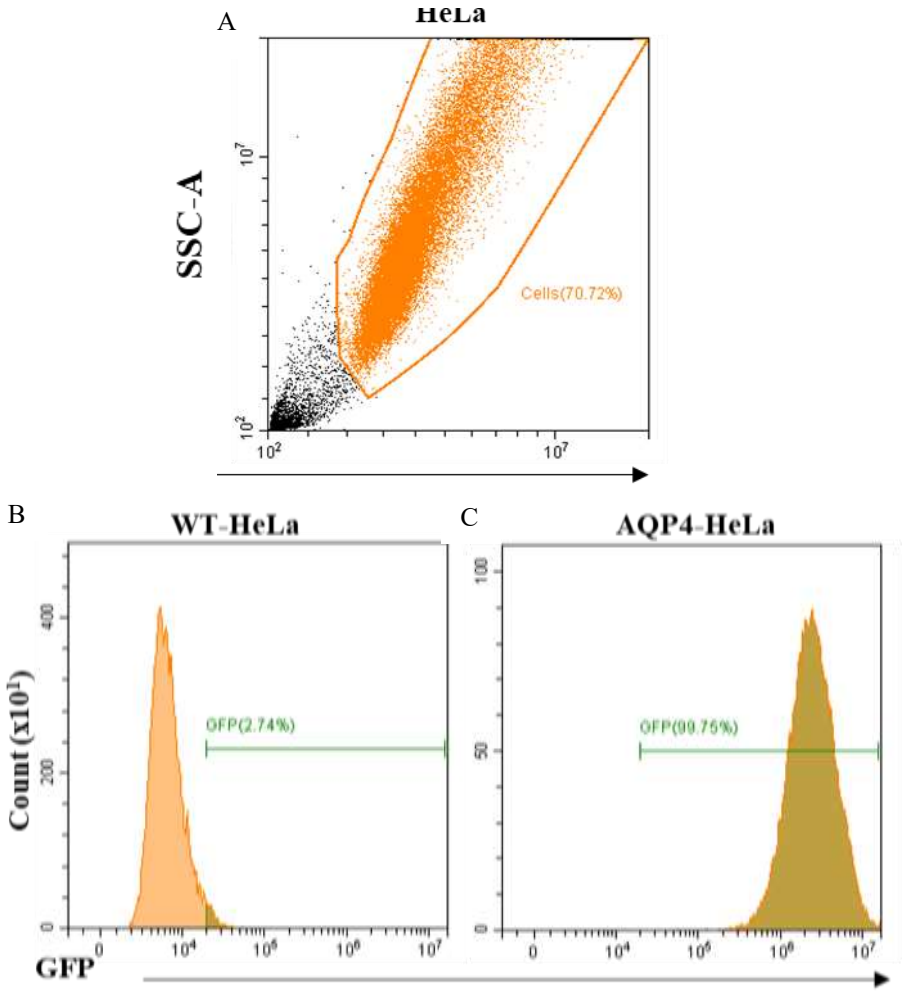

Figure 4.3 Identification and gating cell populations using flow cytometry.

(A) Representative flow cytometry dot plot shows 'cloud' of cells. 'Cells' gate shows how background noise was excluded. (B&C) Representative flow cytometry frequency histograms show linear GFP gate drawn to distinguish positive GFP expression in cell populations. (B) Representative frequency histogram shows percentage of cells expressing GFP WT (AQP4 negative) HeLa cell populations. (C) Representative frequency histogram shows percentage of cells expressing GFP in AQP4 HeLa populations.

The median fluorescence intensity (mFI) is also commonly used to represent fluorescence intensity data, as it provides an accurate representation of average fluorescence values of a population when subpopulations are present (Illingworth, 2023). When deciding which average value to use, both the gMFI and mFI were calculated (Figure 4.3). gMFI and mFI values were similar and showed a similar pattern. The EV data analysed did not appear to contain distinguishable

subpopulations of EV, and it was decided that gMFI was an appropriate measure of average fluorescence intensity.

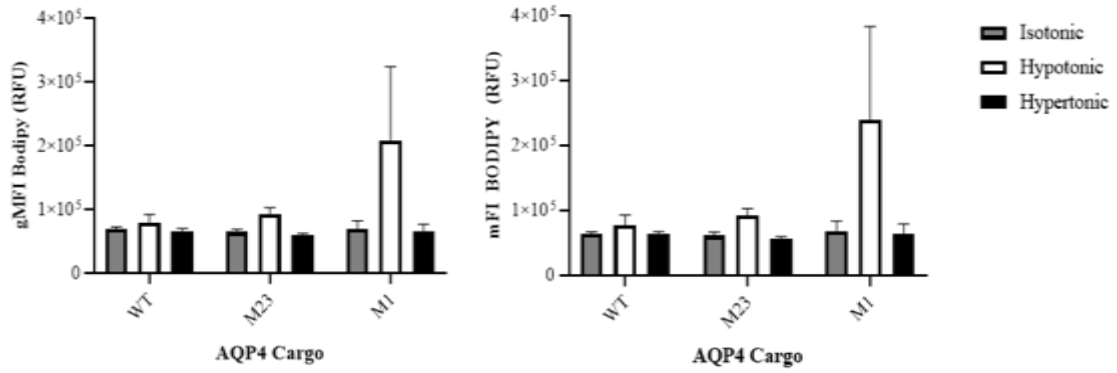

Figure 4.2 gMFI and mFI examples of BODIPY-FL emission data.

Bar charts show the gMFI and mFI of BIODIPY-FL Maleimide labelling of HeLa cell derived EV, measured by flow cytometry. Averages were calculated and compared (n=3).

4.2.4 Flow cytometry analysis of MDCK cell populations following tonic stress

Following tonic stress, MDCK cells were harvested and analysed using flow cytometry. Cells were analysed for signs of stress, apoptosis, and necrosis. The tonic conditions selected for use in this model, isotonic ~340mOsm, hypotonic ~110mOsm and hypertonic ~790mOsm, required validation. If cells became too stressed i.e., if they became apoptotic or necrotic, cells may release cellular components or apoptotic vesicles that could interfere with identification and analysis of EV. MDCK cell population data included, gMFI (Figure 4.4 A), the percentage of cells that express GFP (Figure 4.4 B), the relative size of cells (Figure 4.4 C), cell granularity (Figure 4.4 D) and total cell count (Figure 4.4 E).

As expected, M1 and M23 MDCK showed significantly higher levels of GFP expression than WT MDCK. Interestingly, M1 MDCK showed significantly higher GFP expression than M23- MDCK. No significant differences were observed within cell lines between tonic stress conditions. This corresponded with qualitative analysis of epifluorescence images.

The percentage of cells expressing AQP4-GFP differed significantly between cell lines. As expected, M1 and M23-AQP4 MDCK expressed significantly more GFP than WT MDCK. The mean percentage of M1 MDCK cells expressing GFP was 99% for each

tonic condition. The mean percentage of M23 MDCK cells expressing GFP was between 60-70% for each tonic condition. The percentage of cells expressing AQ4-GFP was considered in the analysis of EV derived from MDCK cells.

Significant differences were observed in the relative size of cells, estimated by their forward scatter properties (FSC-A). M1 MDCK cells are significantly larger in size in isotonic medium than WT MDCK. This observation was also made using light microscopy of cells in normal culture, prior to incubation in serum-free medium; M1 MDCK cells are significantly larger than WT MDCK. A significant difference was also seen in M1 MDCK in hypotonic medium compared with WT MDCK in hypotonic medium, though this difference was not as stark as seen in isotonic conditions. WT MDCK cells appeared to be slightly, but not significantly, larger following hypotonic and hypertonic stress compared to WT MDCK exposed to isotonic medium, this could provide an explanation for the reduced significance seen in hypotonic conditions but, the differences were small, and it is important to remember that, at the time of acquisition, all cells had been treated with trypsin and returned to isotonic medium.

No significant differences were seen in the granularity of cells, as estimated by mean SSC values (SSC-A), neither between cell lines, nor tonic conditions. Neither transfection nor tonic stress affected cell granularity.

No significant differences were observed in the total cell count either between cell lines or tonic conditions. High variation in counts was observed, and, though not statistically significant, M1 MDCK counts tended to be lower than other cell lines, across all tonic conditions this is likely because M1 MDCK were bigger and occupied a larger surface area than WT or M23 MDCK, meaning there were fewer M1 MDCK in a T75 flask than M23 and WT cells grown to confluency.

In summary, epifluorescence imaging and flow cytometry confirmed stable M1 and M23 AQP4-GFP expression in MDCK cells. AQP4-GFP relocalisation in this stable MDCK cell line had been published previously (Kitchen P, 2020). AQP4 MDCK cells did not appear to become apoptotic or necrotic, as no swelling or shrinkage was observed (Dive, 1992) and no differences in cell granularity were seen. These results were promising, cells did not appear to be apoptotic or necrotic and it was decided this model could be used to produce EV using the proposed tonic stress conditions.

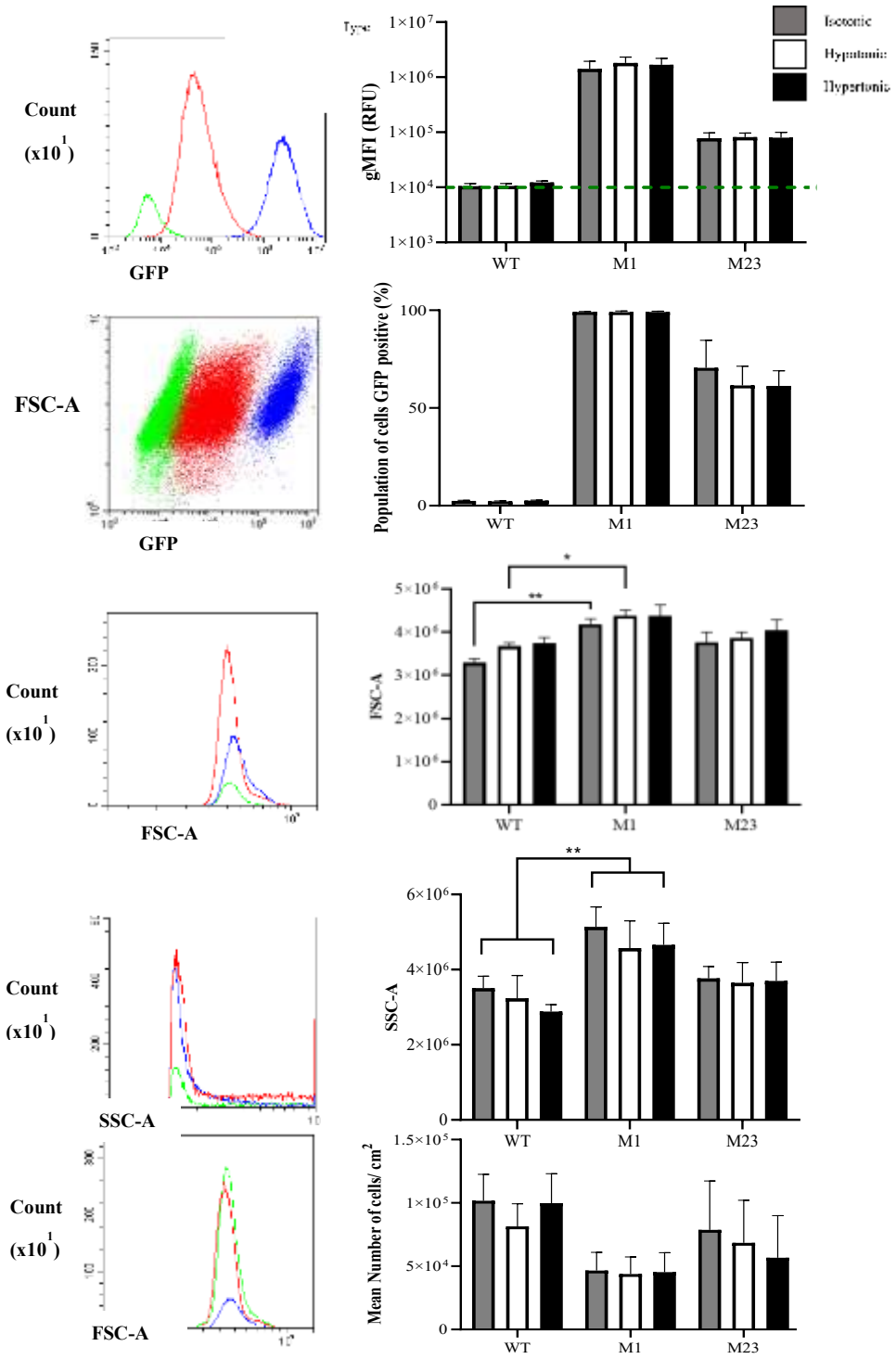

Figure 4.4 MDCK cell properties following tonic stress.

Representative flow cytometry frequency histograms and dot plots (lefthand column) show raw data from WT (green), M1-AQP4-GFP (blue) and M23-AQP4-GFP (red) MDCK cells. MDCK cell population data have been overlayed to clearly convey differences and similarities between cell populations. Bar charts (righthand column) show combined mean values (n=5) with SE for WT and AQP4 M1/M23-GFP MDCK cells following tonic stress with either isotonic (grey), hypotonic (white), or hypertonic (black) conditions. (A) Data show GFP expression (gMFI), the dashed green line represents where linear gate for fluorescence signal was drawn. (B) Percentage of cells expressing GFP. (C) Forward scatter area (correlates with cell size). (D) SSC area (correlates with granularity). (E) Total cell count. 2-way ANOVA was performed between both cell lines and tonic conditions for each cell property (using Sidak's or Tukey's multiple comparison tests, respectively. *=p<0.05, **=p<0.01).

4.2.5 Detection of MDCK-EV in SEC isolated samples

It was anticipated that cells would release EV, MDCK cells were subjected to tonic stress alongside serum starvation which has been shown to induce EV release. Cells release EV whether they are healthy, activated, stressed, apoptotic or necrotic but the type of EV, number of EV released, and EV cargo can vary greatly. To investigate these EV properties, EV release must first be confirmed.

First, EV samples were analysed using ultraviolet side scatter (UV-SSC) flow cytometry and detection of green fluorescence. The shorter wavelength of a violet laser (405 nm) allows detection of smaller particles than conventional flow cytometry including particles as small as ~100 nm in diameter (Gul, 2022). EV labelling a BODIPY dye gave EV green fluorescence properties. Still, EV detection using this method is not straightforward. First, a mixture of fluorescent calibration beads, of known sizes were analysed. The fluorescence properties and size variations of the beads made it possible to detect and group distinct populations of beads of defined sizes that could be distinguished from non-fluorescent background noise (Figure 4.5).

Detection parameters, such as the laser power and gain were optimised to enable bead detection and clear distribution of bead populations Bead populations had average diameters of 100 nm, 160 nm, 200 nm, 240 nm, 300 nm, 500 nm, and 900 nm (Figure 4.5 A). This range of sizes was designed, by the manufacturer, to correspond with the expected sizes of EV. The green fluorescence properties of beads allowed detection by excitation with a 488 nm laser and collection of green fluorescence emission as EV labelled with BODIPY also have green fluorescence properties (Figure 4.5 B). Thus, detection of EV was attempted using the detection parameters that enabled detection of fluorescent beads (van der Vlist, 2012).

BODIPY was used to label EV, BODIPY binds to free thiols on cysteine residues. It is presumed that larger EV will have more cargo and therefore, more thiol groups as such fluorescence increased with EV size. The smallest EV, which are the most difficult to detect based on size, also had the least fluorescence; this added to the difficulty in distinguishing them from non-fluorescent background. UV-SSC FC was used primarily to detect and count EV, rather than acquire exact size measurements.

4.2.6 Development of an EV gating protocol using UV-SSC FC

It was possible to detect BODIPY FL-labelled EV based on their green fluorescence properties, as only biological particles containing thiol groups were labelled green. EV were isolated in PBS, which introduced background noise that fell within the same 'green' region as fluorescent beads but not withing the EV 'cloud' (Figure 4.6 A). Therefore, EV were defined using a gating protocol. A gate was drawn around the 'cloud' of EV, to define an EV population and remove background noise from PBS (Figure 4.6 B). All EV data presented from here on in analyses EV populations defined using this gating method.

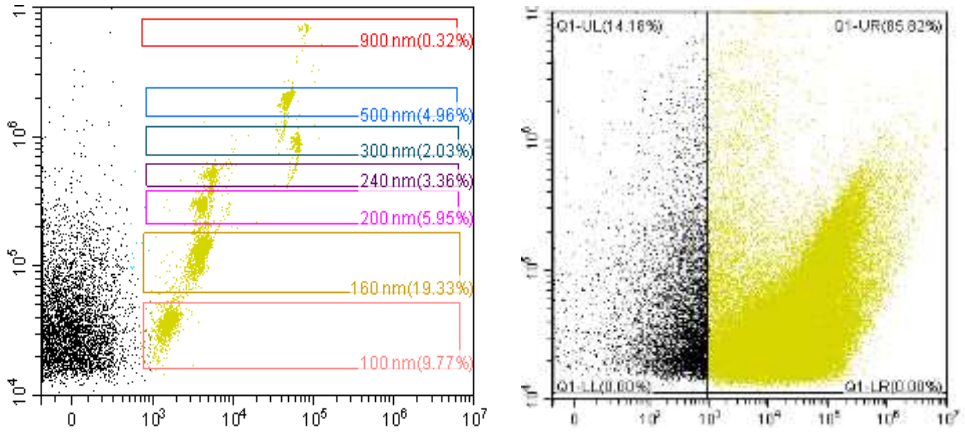

Figure 4.5 Optimisation of VSSC for EV detection

Representative flow cytometry dot plots show detection and discrimination of small fluorescent particles. (A) representative dot plot shows identification of calibration beads of know diameters, 100 nm, 160 nm, 200 nm, 240 nm, 300 nm, 500 nm and 900 nm to allow identification and estimation of EV size. (B) Representative dot plot of BODIPY-labelled EV detected using settings defined by optimisation of calibration bead detection.

BODIPY FL- labelled EV populations were defined using a second, linear gate. This 'BODIPY' gate was defined using green, fluorescent beads and confirmed with an unlabelled, EV population from WT cells, to ensure no green fluorescence was present (Figure 4.5 C). BODIPY FL- labelled EV populations were then measured using the same gate (Figure 4.5 D).

A UV-SSC FC protocol was set up for detection and analysis of BODIPY FL-labelled EV. This protocol removed non-fluorescent particles introduced by PBS and allowed quantification of green fluorescence. This protocol was used in all future EV analyses.

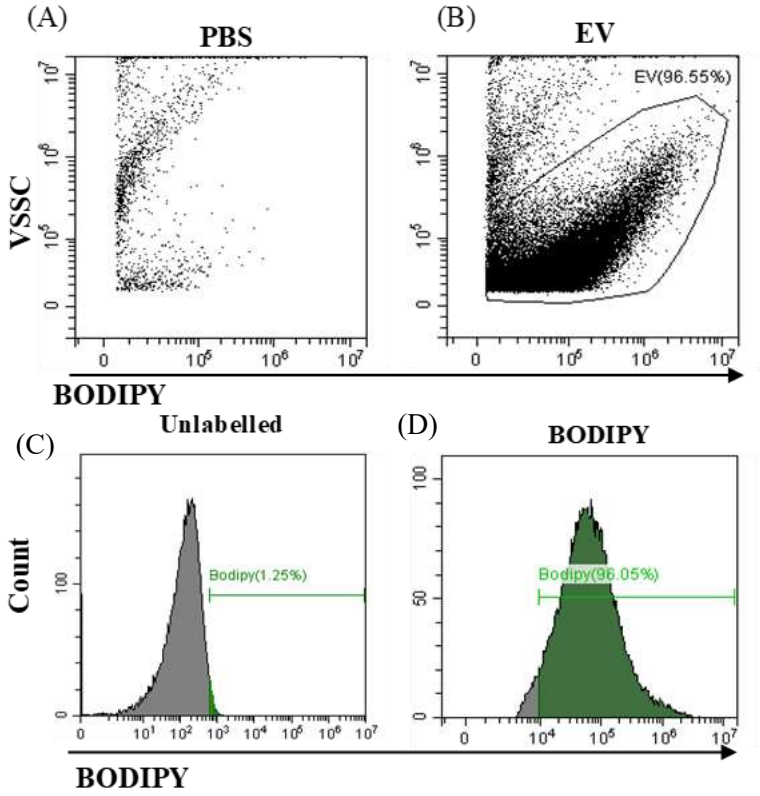

Figure 4.6 Defining EV populations using BODIPY labelling.

Representative dot plots show VSSC detection of small, EV-sized particles in (A) PBS and (B) isolated EV samples labelled with BODIPY FL. An 'EV' gate was drawn around the particle cloud to exclude background introduced by PBS. Representative frequency histograms show (C) unlabelled, WT EV with no green fluorescence, used to define a fluorescence positive population by drawing a 'BODIPY' gate. (D) BODIPY FL -labelled EV samples measured using the 'BODIPY' gate.

4.2.7 UV-SSC FC analysis of isolated EV fractions

EV samples were produced using 2nd generation (Gen 2) qEVoriginal 70 nm SEC columns (IZON Science LTD). According to the manufacturer's instructions, columns isolate EV-sized particles in a 2 mL fraction (fraction 2), following elution of a 3 mL 'buffer' fraction (fraction 1). Fraction 2 was then analysed for fluorescent particles using UV-SSC FC, as described in Figure 4.6.

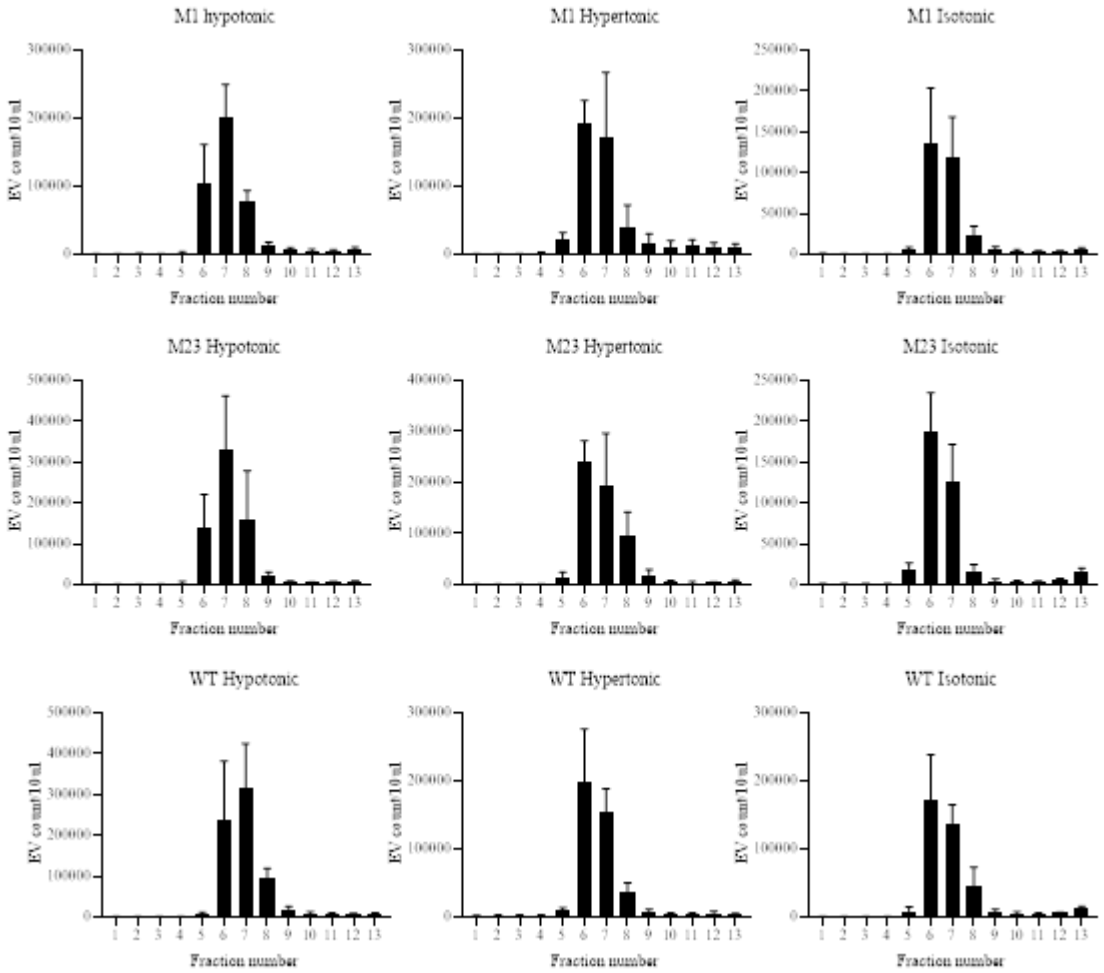

Figure 4.7 VSSC counting of fluorescent particles in MDCK derived eluate fractions.

Bar charts show mean fluorescent particle counts (EV) in 0.5 mL eluate fractions (1-13) from qEV columns, counted using VSSC flow cytometry, derived from M1, M23 and WT MDCK cells subjected to tonic stress. Mean and standard error shown. n=3.

The first attempt at isolating EV, using the manufacturer-recommended volumes, did not result in successful EV isolation. Although small numbers of particles were observed, the concentration was much lower than expected, and would not allow for accurate downstream EV analyses. Therefore, use of Gen2 columns required further optimisation. A more discreet elution protocol was designed; thirteen smaller, 0.5 mL, eluate fractions (fractions 1-13) were collected and analysed using UV-SSC FC. The number of particles in 10 µL of each fraction was counted in eluates derived from MDCK (Figure 4.7) cells following tonic stress.

Upon analysis of eluates from HeLa, fluorescent particles began to be eluted in fraction 5.; a number of MDCK eluates reflected this. All cell lines and conditions showed large numbers and, in some cases, peak counts, of fluorescent particles in fraction 6. This

explained the small number of particles counts observed in the original EV isolation attempt, following the manufacturer's instructions. The first 3 mL of eluate was discarded, this corresponds with fractions 1-6 of the 0.5 mL fractions. In the initial attempt, fractions 5 and 6 were discarded. Fractions 7 and 8 also contain EV, and large numbers in most cases. Therefore, fractions 5, 6, 7 and 8 were collected as a single, 2ml fraction in all future EV isolations. In some cases, such as M1, M23, and WT hypotonic MDCK eluates, more EV were counted in fraction 9 compared to fraction 5. This was because 2 mL of sample needed to be collected to keep the volume constant across samples, for accurate analysis. Also, as fraction numbers increase, particle size decreases and protein contaminants are more likely to be found in samples. Fractions 12 and 13 also showed high particle counts. Elution of these fractions correlated with elution of medium components (pink in colour) and are likely to contain unbound/ soluble BODIPY FL, rather than EV. Though all EV were eluted across fractions 5, 6, 7 & 8, differences were observed between elution profiles of particles. For example, hypotonic MDCK fractions contained fewer EV in fraction 6 than in fraction 7 while hypertonic MDCK fractions contained more EV in fraction 6 than in fraction 7. While these observations are interesting, because this may allude to differences in particle sizes between populations, particle elution is not an accurate measure of size. Therefore, these data were not analysed in more detail. They were however, considered in interpretation of more accurate sizing analyses in Chapter 5.

4.2.8 Confirmation of MDCK-EV release by cryoTEM

While it is logical to presume that the fluorescent particles counted in EV eluates are in-fact EV, because that have been labelled with BODIPY FL, a maleimide- binding dye, it is important to confirm that this is the case, before undertaking further EV analyses, electron microscopy accepted data. EV release was confirmed using cryogenic electron microscopy (Figure 4.8). CryoTEM confirmed that EV were successfully isolated from MDCK supernatants.

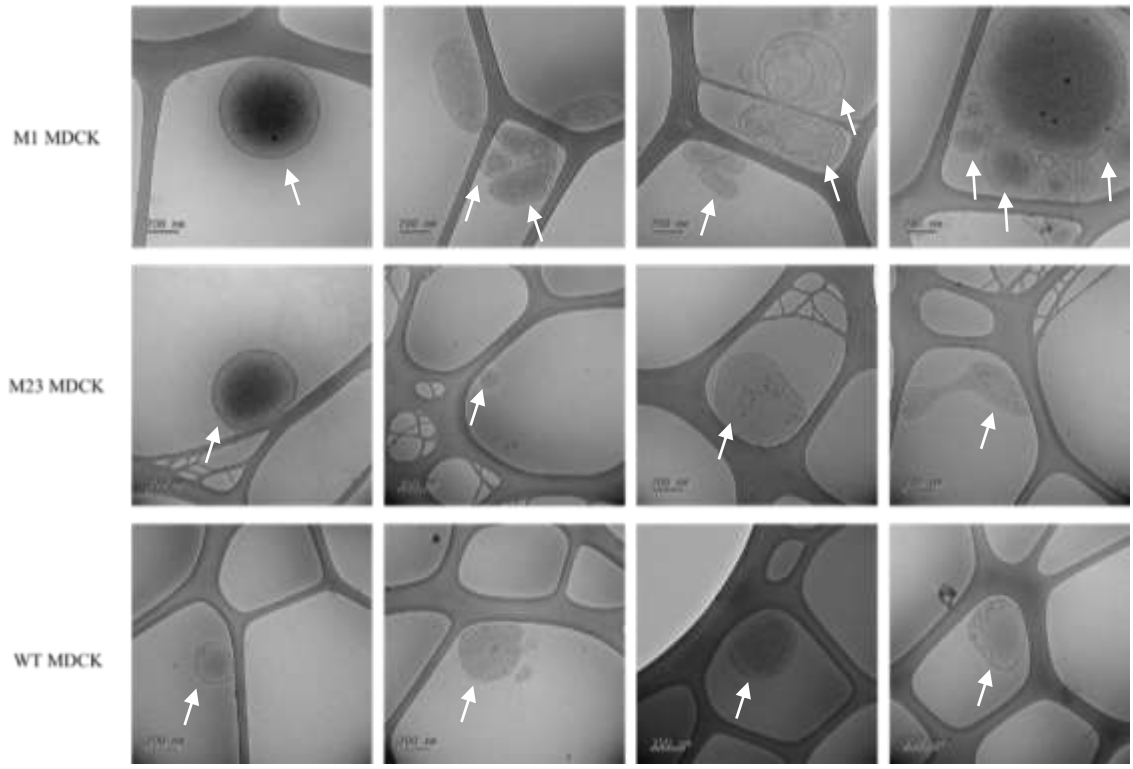

Figure 4.8 Cryogenic electron microscopy of MDCK -derived EV

Representative cryoTEM micrographs show EV released in hypotonic stress conditions by M1, M23 and WT MDCK. White arrows highlight EVs present in samples. Error bars measure 200 nm.

4.3 Development of an EV release model in HeLa cells

EV release by tonic stress was investigated in another cell line. A stable HeLa cell line was generated to investigate differences in EV released by cells expressing AQP4-GFP (AQP4 HeLa) with WT HeLa cells, expressing no AQP4 (WT HeLa).

4.3.1 Transient transfection of AQP4-GFP in HeLa cells.

To generate a stable HeLa cell line expressing AQP4-GFP, a transient transfection was first performed. The mammalian cell vector pDEST47, containing AQP4-GFP, was transiently transfected into HeLa cells. Successful transfection was confirmed by epifluorescence microscopy (Figure. 4.9).

AQP4-GFP was expressed in transfected cells. Variation was observed in AQP4-GFP concentration and localisation. Most cells were not successfully transfected; though the transfection efficiency was not quantified, qualitative analysis of fluorescence images shows a high number of cells without green fluorescence. High AQP4-GFP expression levels were observed in some cells. These cells were bright, round and losing

adherence. It is probable that high expression of exogenous AQP4-GFP killed these cells. As hoped, AQP4-GFP was expressed at lower levels in adherent, viable cells. These cells had intracellular and defined plasma membrane expression of AQP4-GFP (Figure 4.9 C) and were used to generate a stable HeLa cell line (AQP4 HeLa).

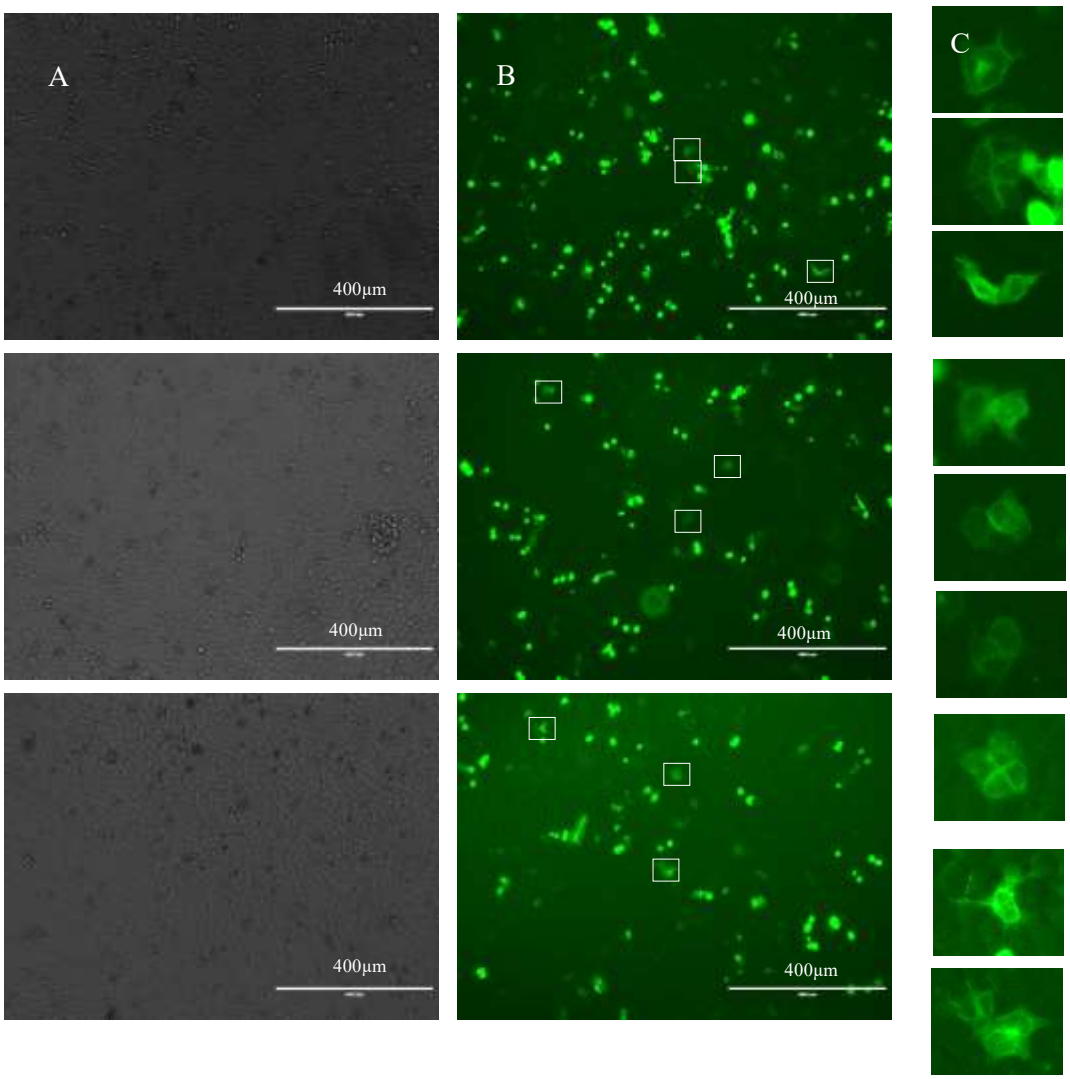

Figure 4.9 Transient transfection of AQP4-GFP in HeLa cells

Representative phase contrast and fluorescence micrographs show AQP4-GFP expression in HeLa cells 48h after transient transfection. (A) Phase contrast images show cell confluence. (B) Green fluorescence images represent AQP4-GFP expression. (C) Enhanced zoom images highlight examples of adherent cells with plasma membrane expression of AQP4-GFP (white boxes) Scale bar = 400 µm.

4.3.2 Optimisation of G418 concentration for use in antibiotic selection of transfected HeLa cells

Antibiotic selection was used to isolate cells expressing AQP4-GFP. Successfully transfected cells acquired G418 resistance, conferred by the pDEST47 vector which, contains a neomycin resistance gene. When incubated in G418 medium, only successfully transfected cells survived. This technique was used to increase the percentage of cells expressing AQP4-GFP. Antibiotic selection was optimised, to ensure all non-transfected cells (WT HeLa) were killed.

To determine the concentration of G418 required to kill all WT HeLa, and isolate AQP4 HeLa, a survival curve was established (Figure 4.10). WT HeLa were incubated with increasing concentrations of G418 in growth medium. Every 48 hours, cells were washed and G418 medium was renewed. After 14 days cells were stained with trypan blue and counted.

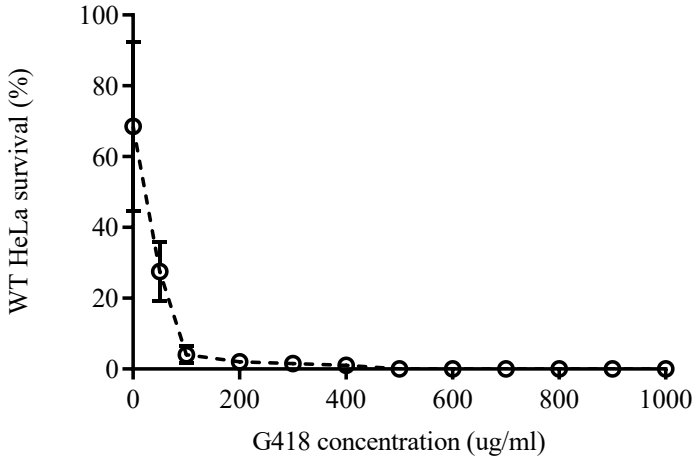

Figure 4.10 Determining concentration of G418 required to isolate AQP4 HeLa from WT HeLa

HeLa cells were treated with increasing concentrations of G418 to determine the minimum concentration required to kill all WT HeLa. 0, 50, 100, 200, 300, 300, 500, 600, 700, 800, 900 and 1000 µg/mL concentrations were measured. After 14 days of treatment, cells were stained with trypan blue and living cells were counted. The percentage of cells remaining was calculated. Mean values of three technical repeats shown with the standard deviation represented by the error bars.

It was determined that 500 µg/mL was the lowest concentration of G418 required to kill all WT HeLa; Lower concentrations did not kill all cells and use of higher concentrations is unnecessary and could also kill cells with useful levels of AQP4-GFP expression. 500 µg/mL G418 was selected and used to isolate AQP4 HeLa and generate a stable cell line.

4.3.3 Isolation of AQP4-GFP positive HeLa cells using G418 selection

Transiently transfected HeLa cells were incubated with 500 µg/ml G418 to kill WT HeLa, isolating AQP4 HeLa, and to create a stably transfected cell line.

Transfection efficiency was analysed 48 hours post transfection, using epifluorescence microscopy. Upon successful transfection, as described in Figure 3.1, HeLa were washed with PBS and incubated in 500 µg/mL G418 medium. Medium was renewed every 2 days to remove dead and/ or dying cells and replenish nutrients. After 14 days, cells were observed for colony formation and GFP expression using phase contrast and fluorescence microscopy. Colonies were resuspended using trypsin, diluted, and plated into ninety-six well plates at an average concentration of one cell per well. Cells were cultured in 500 µg/mL G418 medium until larger colonies formed, around one hundred cells per colony. Individual colonies were resuspended and plated into single wells in twenty-four well plates, then T75 flasks, to encourage proliferation, three different stable cell colonies were made in this process. Colonies were stored liquid nitrogen. One colony was selected and used for further study.

4.3.4 Confirmation of AQP4-GFP expression in stably transfected HeLa cells

Stable transfection of AQP4 HeLa was confirmed using a variety of methods. As AQP4-GFP is a fusion protein it is reasonable to suggest that GFP and AQP4 were expressed in equal concentrations. As such, detection of both AQP4 and GFP confirmed AQP4-GFP expression. GFP expression was confirmed using epifluorescence microscopy (Figure 4.11 A) and flow cytometry (Figure 4.11 B). AQP4 expression was confirmed by western blot (Figure 4.11 C).

Qualitative analysis of fluorescence micrographs showed clear differences in green expression were observed between WT- and AQP4 HeLa. It does not appear however, that 100% of the cell population express AQP4-GFP, despite the population originating from a single cell. GFP expression was confirmed by flow cytometry (Figure 4.11 B).

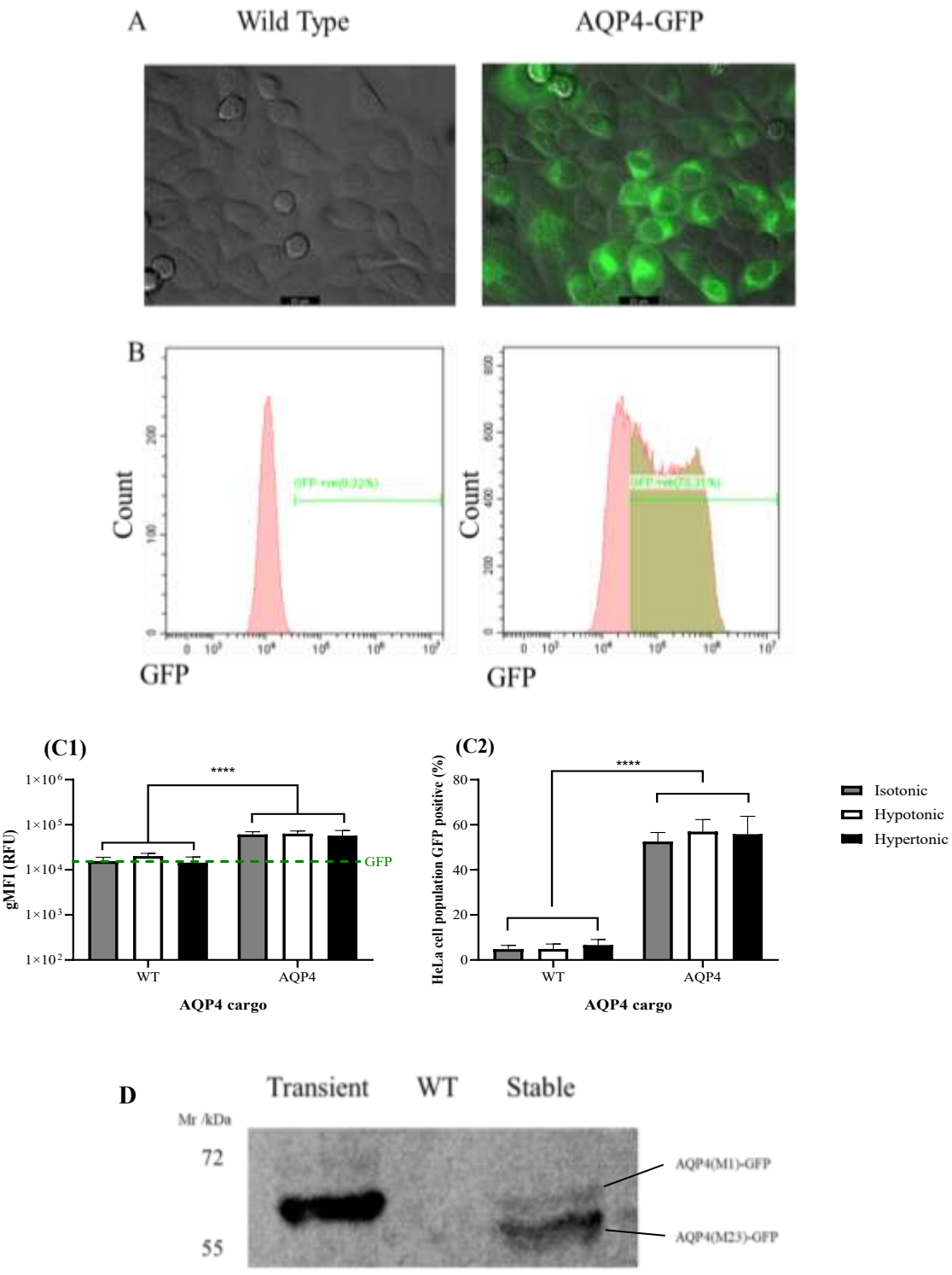

Figure 4.11 Confirmation of AQP4 expression in stably transfected HeLa cells

(A) Representative overlay micrographs and (B) representative flow cytometry frequency histograms show expression of GFP in non-transfected and stably transfected HeLa cells. (C) Bar charts show collated flow cytometry data, (1) gMFI of green fluorescence in HeLa cell populations and (2) percentage of HeLa cell populations positive for GFP expression. (D) Western Blot for AQP4 in transiently transfected, non-transfected (WT) and stably transfected HeLa cells. T-test, ****=p<0.001

The gMFI of cell populations was calculated. As anticipated, a significant difference was seen between WT and AQP4 HeLa populations, further confirming expression of AQP4-GFP. The mean percentage of cells within each population that appear positive for AQP4-GFP was also calculated, this confirms that around 70% of the transfected cell population express AQP4-GFP. Western blot was used to confirm AQP4-GFP expression by directly blotting for AQP4 (Figure 4.11 C).

Two bands were observed in the column containing AQP4 HeLa, these were the correct size for an AQP4-GFP fusion protein, 60kDa. These were presumed to correspond with two AQP4 isoforms, M1 (60kDa) and M23 (58kDa). The stably transfected HeLa cells expressed more M23-AQP4 than M1-AQP4 as the lower band, corresponding with the shorter isoform, was darker. The expression level of M1 and M23 AQP4 isoforms is interesting when considering their roles in EV. Transiently transfected HeLa cells appeared to express more M1-AQP4 than M23. No bands were observed in the column containing sample from WT HeLa.

M1 and M23 are naturally occurring AQP4 isoforms (Jung, 1994), it is not yet known how their expression is regulated. M1 has twenty two extra amino acids at its N-terminus (Jung, 1994). In lacking these amino acids, M23-AQP4 is able assemble, forming supramolecular structures known as orthogonal arrays of particles (OAPs) (Rash, 1998). M1 homotetramers do not form OAPs but do combine with M23 to form heterotetramers, and subsequently, small OAPs (Rash, 1998, Neely et al., 1999, Jin et al., 2011). OAPs vary in size (Jin, 2011) and it is unlikely that large OAPs cannot be released in small EV. Recently however, a study has been published, which showed the presence of M23 in supernatant derived from stressed glial cells (Simone, 2022). This is an interesting finding and has been considered in the analysis of the data presented in this thesis.

Previous studies have investigated the rapid relocalisation of M1 and M23 AQP4 isoforms in response to extracellular hypotonicity (Kitchen, 2015), suggesting roles for both isoforms in membrane water transport. There is, however, conflicting evidence regarding the cellular water permeability of M1 and M23 AQP4 isoforms. One study shows M23 is more permeable (Silberstein et al., 2004), another suggests M1 is more water permeable (Fenton, 2010), another finds similar permeability properties (Neely, 1999) . As discussed in Chapter 1, it has been suggested that the water channel role of AQP4 could also be important in EV. Therefore, the rapid relocalisation of AQP4 in stably transfected EV was investigated further.

4.3.5 Comparison of M1 and M23 AQP4 expression in HeLa cells

Western blot confirmation of AQP4-GFP expression showed that the M23 isoform was more abundantly in AQP4 HeLa than M1. Previous studies have shown punctate expression of M23-AQP4-GFP and smooth, membrane expression of M1-AQP4-GFP (Silberstein et al., 2004, Kitchen et al., 2015b). Epifluorescence microscopy was used for qualitative analysis of AQP4-GFP isoforms in HeLa cells to ascertain whether the visual expression profile of stably transfected HeLa, correlated with the result of the western blot (Figure 4.11). AQP4 HeLa were imaged and analysed alongside transiently transfected M1-AQP4, M23-AQP4 and WT-AQP4 (mix of M1 and M23) HeLa (Figure 4.12).

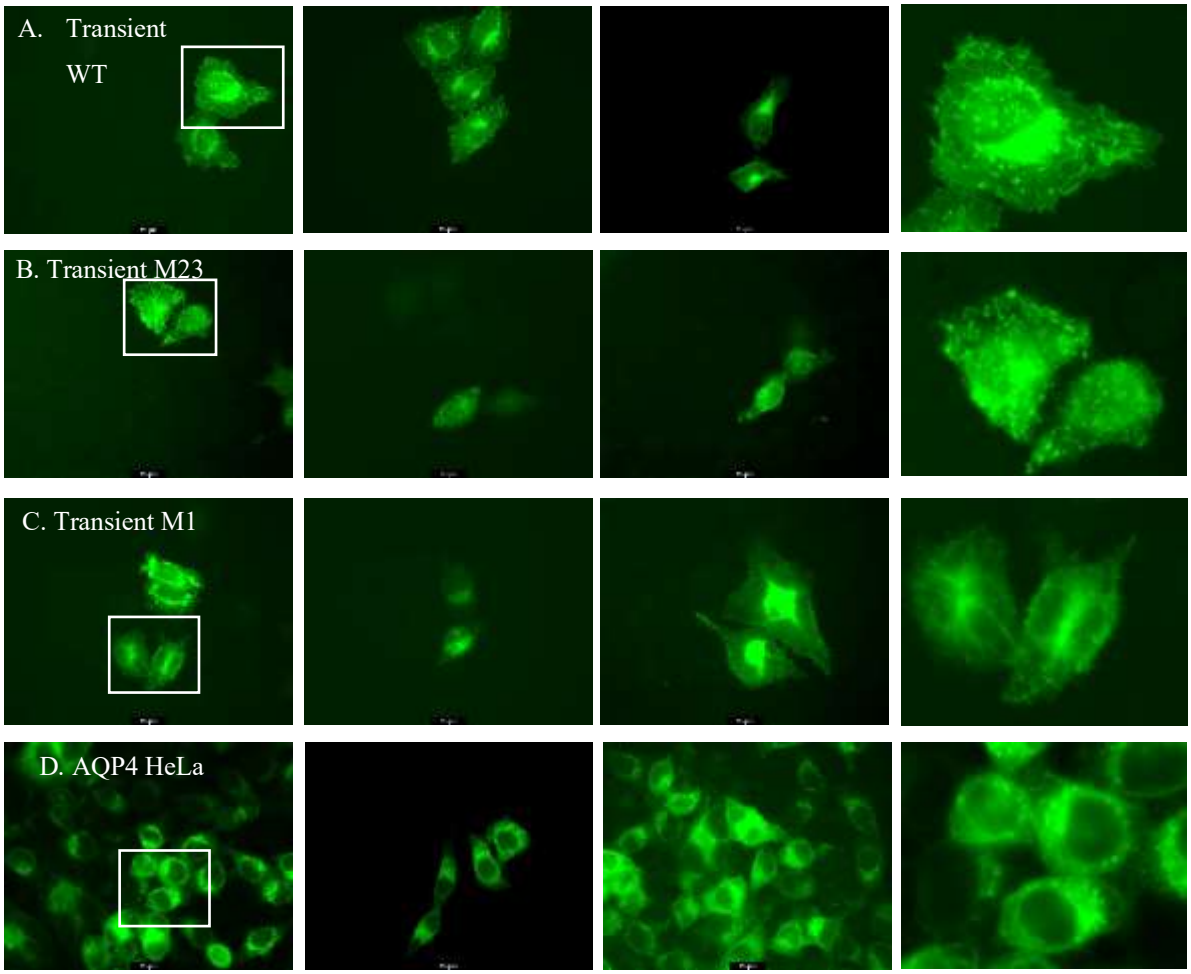

Figure 4.12 Localisation of AQP4 isotypes in live HeLa cells

Representative fluorescence micrographs show expression profiles and subcellular localisation of AQP4-GFP in AQP4 HeLa cells (stably transfected) and transiently transfected M1-AQP4, M23-AQP4 and WT-AQP4 HeLa cells. 3 representative images are shown per isotype. White boxes highlight areas used to create representative zoom images to show detail of subcellular localisation. Scale bars are 25 μm.

The expression and subcellular localisation of AQP4-GFP isoforms M1, M23, and WT (both M1 & M23) was compared with AQP4 HeLa. Qualitative analysis of cells showed variation in expression and localisation profiles between isoforms. Cells transfected with WT-AQP4 showed variation in expression profiles, some cells had more punctate expression and some more membrane expression (Figure 4.12 A). Cells transfected with M23 alone showed bright punctate expression with little membrane definition (Figure 4.12 B). Cells transfected with M1 alone also showed punctate expression, but also spindle-like structures and membrane definition (Figure 4.12 C). Interestingly, stably transfected cells appear to have to most defined membranes, compared to other isoform combinations. Intracellular and punctate expression was also observed and could account for the increased expression of M23 detected by western blot.

Epifluorescence imaging of stably transfected HeLa supported the findings of the AQP4 HeLa western blot (Figure 4.11 C), both M1 and M23 isoforms of AQP4 are expressed in AQP4 HeLa. It was considered important, when generating a cell line for use in an EV release model, that both M1 and M23 isoforms were expressed, as it was not known whether M23-AQP4 would be released in EV, at the time this model was established, no publications had shown the release of M23 in EV.

4.3.6 Rapid relocalisation of AQP4-GFP in response to extracellular hypotonicity

Stably transfected AQP4-GFP HeLa cells were subjected to increased extracellular hypotonicity to assess rapid relocalisation of AQP4-GFP from intracellular vesicles to the plasma membrane. The expression of AQP4 in the plasma membrane is essential for its function as a water channel. Relocalisation of AQP4 from intracellular vesicles is an important mechanism that increases AQP4 concentration in the plasma membrane. It has previously been shown that extracellular hypotonicity triggers rapid relocalisation and insertion of AQP4 to the plasma membrane, contributing to increased water uptake and cell swelling (Kitchen, 2015). AQP4 relocalisation, was measured to confirm the functionality of AQP4 in AQP4 HeLa as this was integral for use in an EV release model that sought to investigate AQP4 function in EV.

Epifluorescence imaging was used to acquire AQP4-GFP relocalisation data (Figure 4.12). AQP4 HeLa were grown in glass-bottomed dishes. Cells were imaged first in isotonic medium and then water was added incrementally to create increasingly hypotonic environments, cells were imaged in each environment. Water was added to

isotonic medium at ratios of 1:1, 2:1 and 3:1. AQP4-GFP relocalisation to the plasma membrane was quantified as the relative membrane expression (RME). FIJI image processing software was used to draw fluorescence intensity line profiles through cells, including extracellular space, plasma membrane and cell cytoplasm. Fluorescence values were exported to Microsoft Excel computer software and the mean membrane fluorescence was divided by the total fluorescence (membrane + intracellular fluorescence) to give the RME.

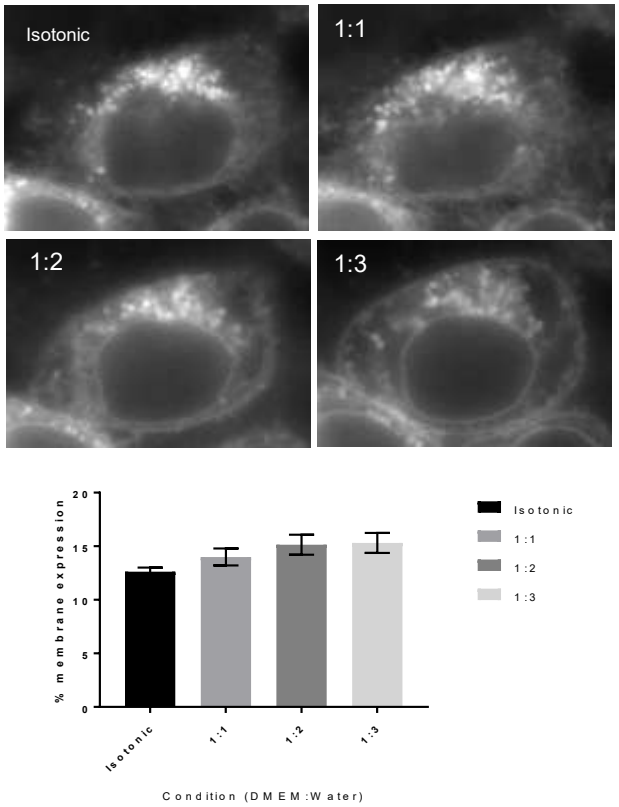

Figure 4.13 RME of AQP4-GFP in AQP-HeLa in response to extracellular hypotonicity

Representative fluorescence images show the localisation of AQP4-GFP in stably transfected HeLa cells in isotonic, and increasingly hypotonic environments. Water was added to isotonic culture medium. Final ratios of medium to water included 1:1, 1:2 and 1:3. GFP fluorescence was shown in grey scale to maximize contrast and visibility of AQP4-GFP signal. Bar chart shows the mean relative membrane expression (RME) of AQP4-GFP in HeLa cells following exposure to increasing hypotonicity. Standard error shown, n=1 with 3 technical replicates.

Qualitative analysis of cells in hypotonic conditions 2:1 and 3:1 showed clear cell swelling and increased membrane expression of AQP4-GFP (Figure 4.13). A significant increase in mean RME was observed in AQP4 HeLa exposed to 2:1 medium

compared to isotonic medium. This difference was more subtle than seen previously in other models, where bigger increases in RME were observed (Kitchen, 2015).

These findings were confirmed by way of a calcein AM swelling assay (Figure 4.14) (Kitchen P, 2020). All calcein AM loading data included in this thesis were generated by Lucas Unger, who devised and conducted the experiments and analysis (Unger, unpublished). HeLa cells were loaded with calcein AM, a cell-permeable dye that self-quenches when concentrated, producing increased and decreased fluorescence intensities in hypotonic and hypertonic conditions, respectively. Calcein AM signal was detected in isotonic (growth medium) and hypotonic (pure water) conditions. The rate constant (k) was calculated for each condition. AQP4 HeLa and WT HeLa were compared to another AQP4 stable cell line, AQP4-MDCK. AQP4-MDCK express either M1-AQP4, M23-AQP4 or no AQP4 (WT).

AQP4 HeLa had a mean swelling rate constant of $0.4s^{-1}$. This was significantly higher than WT HeLa which was $0.2s^{-1}$. The transfection of AQP4 into HeLa cells has significantly increased the swelling capacity of HeLa cells in a hypotonic environment, with a mean difference in swelling rate of $0.2s^{-1}$. This supports earlier findings (Figure 4.13) and confirms AQP4 is a functional water channel in AQP4 HeLa. M1 MDCK had a mean swelling rate constant of $0.65s^{-1}$, M23 had a mean swelling rate of $0.25s^{-1}$, and WT MDCK had a mean swelling rate of $0.1s^{-1}$. Both M1 and M23 MDCK had swelling rate contents significantly higher than WT MDCK, with mean differences of $0.55s^{-1}$ and $0.15s^{-1}$, respectively. This assay concluded that M1 MDCK cells had a much higher swelling capacity than M23 alone. M1 MDCK cells showed a bigger increase in swelling than AQP4 HeLa, when normalised to their respective WT counterparts. It is plausible that this result reflects the expression of endogenous AQP in these cell lines. MDCK cells express no endogenous AQP and have extremely low water permeability, whereas HeLa cells express AQPs 3, 6, 8, & 11 (Pellavio, 2017) functional water channels. Thus, WT HeLa cells had a higher mean swelling rate than WT MDCK cells. In addition, M1 MDCK had a higher mean swelling rate than AQP4 HeLa. Differences between HeLa and MDCK cells are discussed later in this chapter and this result is discussed in more detail.

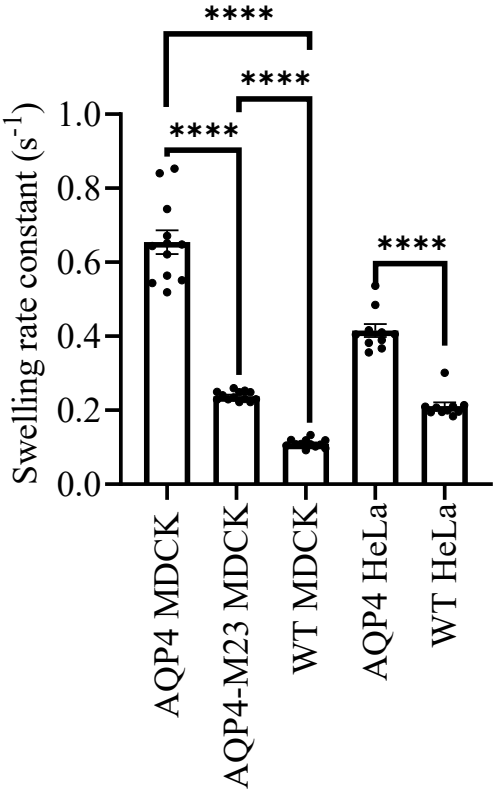

Figure 4.14 Swelling capacity of HeLa and MDCK cells in response to extracellular hypotonicity

Bar chart shows the mean swelling rate constant (k) for stably transfected MDCK cells expressing either M1, M23 or no AQP4 and stably transfected AQP4 expressing HeLa cells and WT-HeLa cells following exposure to a hypotonic environment (pure water) as measured by a calcein swelling assay. Individual values are plotted along with means and SE for each cell line. Statistical significance was determined by ANOVA (MDCK) with a Tukey's multiple comparison test and t-test (HeLa) Data provided by Lucas Unger with his permission. ****=p<0.001.

4.3.7 Validation of EV release model conditions in HeLa

AQP4 and WT HeLa were analysed following tonic stress. Hypo and hypertonic stress conditions were used to trigger EV release by HeLa cells. Hypotonic and hypertonic media were made following the method used to produce EV in MDCK cells. Cell culture medium was used as an isotonic control. All tonic conditions used serum-free cell culture medium to reduce contamination with serum EV. Cells were subjected to tonic stress for four hours, a time used previously by the research group to produce apoptotic EV. Cell health following tonic stress was analysed using flow cytometry. Properties measured included cell count, size, granularity and AQP4-GFP expression.

Table 3 Conditions used in EV release model - HeLa

Cell Line	AQP4 content	Tonic condition
HeLa	WT	isotonic
		hypotonic
		hypertonic
	AQP4	isotonic
		hypotonic
		hypertonic

4.3.8 Flow cytometry analysis of HeLa cell populations following tonic stress

Following tonic stress, AQP4 and WT HeLa were harvested and analysed to determine any effects. Cells were analysed for changes seen in relation to cell stress. Cell population data included, (Figure 4.15 A) the gMFI of GFP, (Figure 4.15 B) the percentage of cells that express GFP, (Figure 4.15 C) the relative size of cells, (Figure 4.15 D) cell granularity (Figure 4.15 E) and total cell count.

gMFI data were achieved using a 488 nm laser for GFP excitation. Fluorescence intensities of individual cells were recorded and the gMFI of the population calculated (Figure 4.15 A). The percentage of cells expressing GFP was calculated by counting the number of cells that fell within the 'GFP' gate as a percentage of the whole cell population (Figure 4.15 B). The relative size of cells was measured by taking the mean FSC-A values (Figure 4.15 C). As cells interact with a laser, they scatter the light, more FSC correlates with larger particles. Cell granularity was measured by taking SSC values (Figure 4.15 D). Laser light is scattered in a sideways direction when it interacts with intracellular structures, such as granules and proteins. Higher SSC-A values correlate with more granularity. Total cells count for each condition was normalised to the surface area (Figure 4.15 E).

As expected, AQP4 HeLa showed significantly higher levels of GFP expression than WT HeLa. No significant differences were observed within cell lines between tonic stress conditions. It was not expected that changes would be observed but it was an important parameter to check. Considering that these cells and conditions were used to make EV, it was important to know if AQP4 expression was altered by tonic stress.

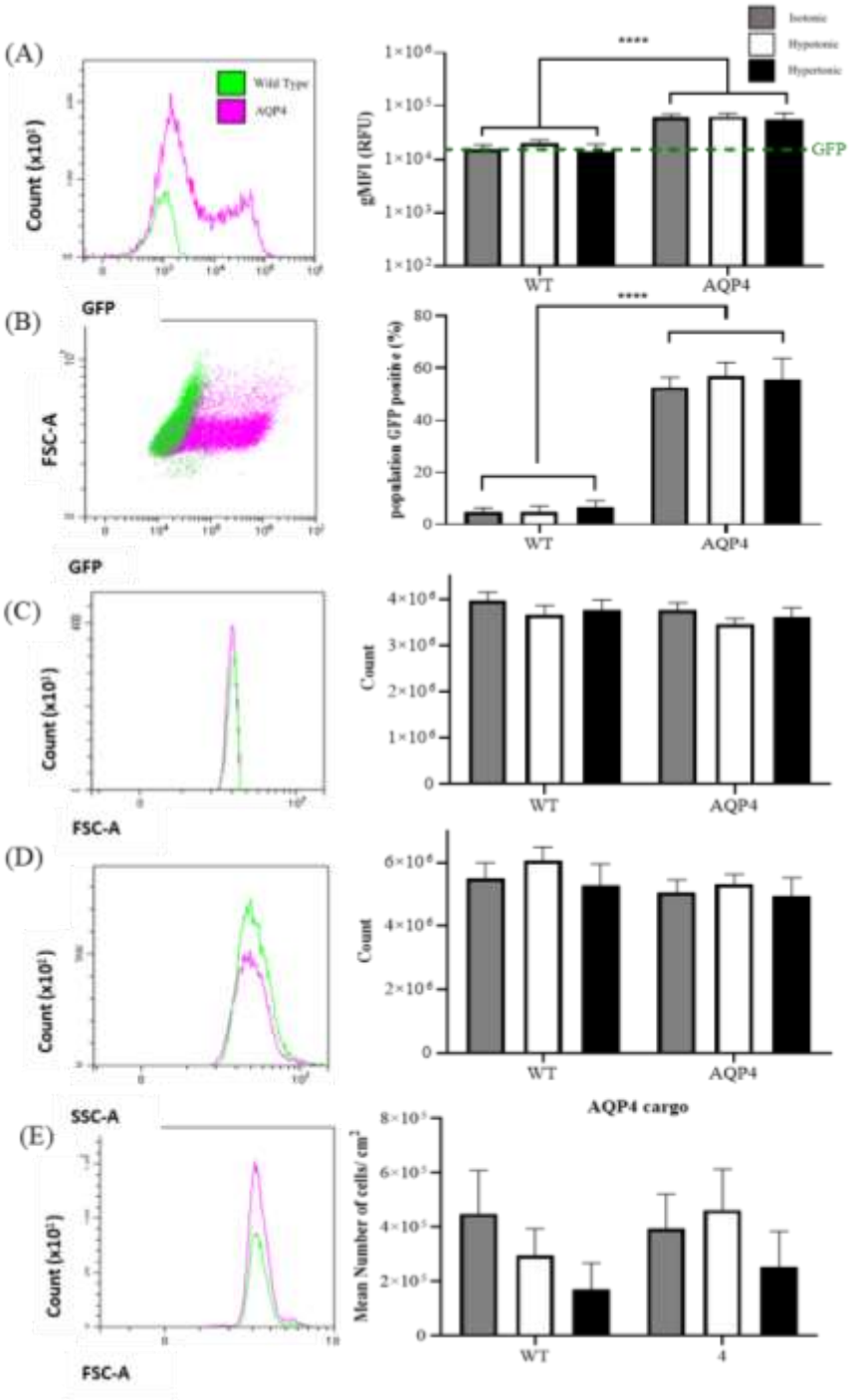

Figure 4.15 HeLa cell properties following tonic stress.

Representative flow cytometry frequency histograms and dot plots show raw data from WT (green) and AQP4-GFP expressing (pink) HeLa cell populations. Data overlayed to clearly convey differences and similarities between populations. Bar charts show combined mean values (n=5) with SE for WT and AQP4-GFP HeLa cells following tonic stress with either isotonic (grey), hypotonic (white), or hypertonic (black) conditions. (A) gMFI, dashed green line represents where linear gate for fluorescence signal was drawn. (B) Percentage of cells expressing GFP. (C) Forward scatter area (correlates with cell size). (D) SSC area (correlates with granularity). (E) Total cell count. 2-way ANOVA was performed between both cell lines and tonic conditions (Sidak and Tukey's tests, respectively) for each cell property. **** = P<0.001.

The percentage of cells expressing AQP4-GFP differed significantly between cell lines. As expected, significantly more AQP4 HeLa expressed GFP than WT HeLa. The mean percentage of AQP4 HeLa expressing GFP is ~60% for each tonic condition. This was considered in the analysis of EV derived from AQP4 HeLa.

No significant differences were observed in the relative size of cells (FSC-A), neither between cell lines nor conditions. Differences between cell lines would suggest that stable AQP4-GFP transfection influenced cell size. Differences in cell size between tonic conditions are not observed, cells do not appear to be swollen, for example due to necrosis or shrunken, as is seen in apoptotic cells (Dive, 1992).

No significant differences were seen in the granularity of cells (SSC-A), neither between cell lines, nor tonic conditions. Stress granules are made by cells in 'stressful' conditions and prevent apoptosis (Arimoto, 2008). They are commonly seen in cancer-derived cells and have been identified in HeLa cells (Timalsina, 2018). Granular necrosis is also observed in tumour- derived cells, as chromatin condenses (Samaratunga, 2020). Neither stable transfection nor tonic stress affected cell granularity.

No significant differences were observed in total cell count either between cell lines or tonic conditions but there was high variation in counts, and cell counts in hypertonic stress tended to be lower than other conditions, it is possible that cells have become rounded and lost adherence. For this reason, cell counts from hypotonic and hypertonic conditions was also normalised to isotonic cell counts (Figure 4.16).

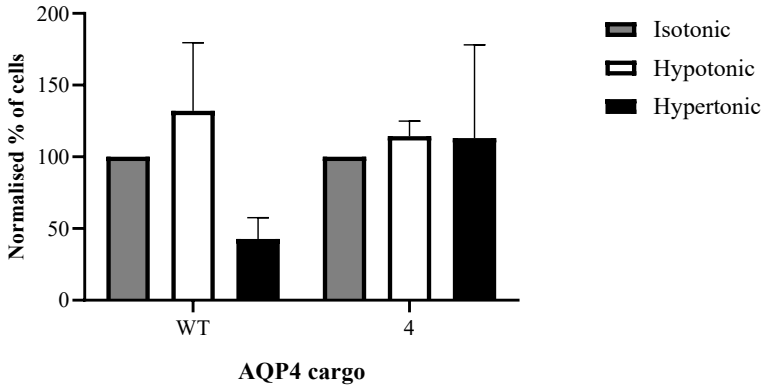

Figure 4.16 Normalised HeLa cell counts after tonic stress.

Mean cell counts were normalised to the isotonic control, where the number of cells present in the isotonic control was considered 'normal' and the number of cells present following exposure to hypertonic and hypertonic environments was compared. AQP4 and WT HeLa cell counts following hypotonic and hypertonic stress normalised to isotonic controls, where isotonic = 100%. Standard error shown. n=5-9.

After normalisation to isotonic cell counts, standard error values are still varied. It is clear however, that the mean number of WT HeLa cells is less than 50% of the equivalent isotonic cell count, following hypertonic stress. A 2-way ANOVA statistical analysis concluded this finding is not significant.

In summary, a stable HeLa cell line was made, expressing AQP4-GFP. Western blot showed greater expression of M23-AQP4 than M1-AQP4. Epifluorescence imaging confirmed expression of both; both punctate intracellular expression, and smooth plasma membrane expression was observed. AQP4-GFP relocalised to the plasma membrane in response to extracellular hypotonicity but the effect was smaller than observed in MDCK cells. AQP4-GFP HeLa were analysed after tonic stress. Findings conclude HeLa are resilient in tonic stress conditions, no swelling, or shrinkage was observed, suggesting cells did not become necrotic or apoptotic(Dive, 1992). No differences in cell granularity were seen, reinforcing findings that suggest cells are not necrotic. Though not significant, it is important to note that fewer HeLa cells are counted following hypertonic stress, compared to isotonic stress conditions. Overall, these results were promising, and it was decided that AQP4 and WT HeLa could be used to produce EV in a tonicity-linked model.

4.3.9 Confirmation of HeLa EV release by cryoTEM

CryoTEM imaging of EV confirmed EV release by both HeLa cell lines in hypertonic conditions.

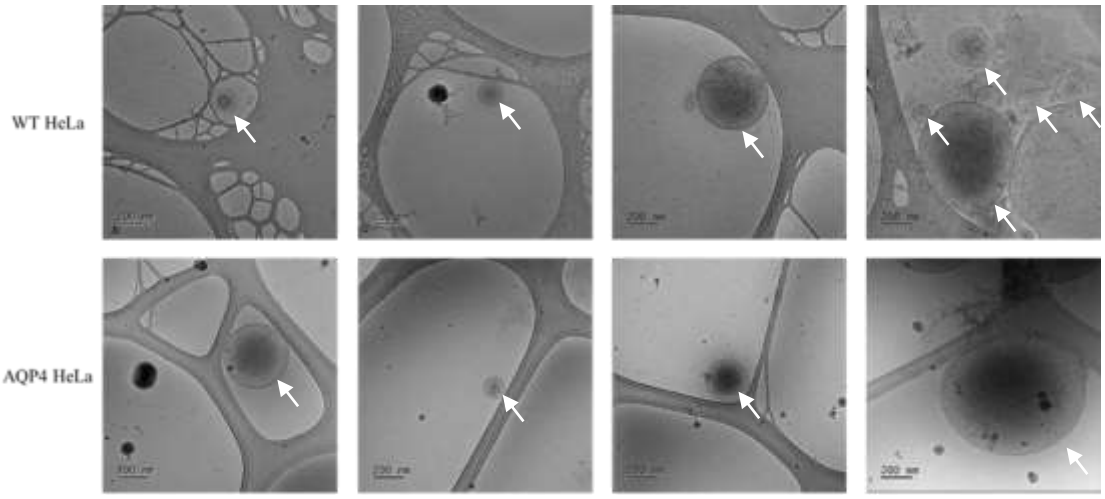

Figure 4.17 CryoTEM imaging of HeLa derived EV

Representative cryoTEM micrographs show EV released in hypertonic stress conditions by AQP4 and WT HeLa cells. White arrows highlight EV released. Scale bars measure 200 nm.

4.4 Discussion and Limitations

This chapter describes the development of a tonicity-linked EV release model. A tonicity-linked EV release model was devised using hypotonic, isotonic, and hypertonic conditions. A four-hour incubation time was selected. SEC was used to isolate vesicles and fraction analyses were performed to optimise EV collection. Fractions 5, 6, 7, and 8 were collected and combined. This ensured that all isolated EV were collected, and final fraction volumes were the same for all samples. However, this also resulted in dilution of EV samples, as fraction 5 contained lower numbers of EV than samples 6, 7, and 8. EV release was confirmed using cryoTEM. AQP4-GFP release in EV was confirmed using confocal microscopy, flow cytometry, and western blot.

HeLa cells were stably transfected with AQP4-GFP. AQP4-GFP expression and stable transfection was confirmed using fluorescence microscopy, flow cytometry and western blot. Western blot showed higher M23-AQP4 expression levels than M1-AQP4. Epifluorescence microscopy showed both punctate fluorescence (M23) smooth, membrane fluorescence (M1). Moreover, AQP4-GFP relocalised to the plasma membrane in response to extracellular hypotonicity and cells swelled as water uptake increased. Though M1 and M23 AQP4 were both expressed, it was unfortunate that stably transfected HeLa expressed more M23 than M1 AQP4. EV were released by HeLa cells in all tonic stress conditions used. AQP4-GFP was identified in EV released by all AQP4-GFP expressing cells. Thus, it was concluded that the tonicity-linked HeLa EV release model developed was fit for purpose and the conditions described were used to trigger EV release.

In conclusion, SEC successfully isolated EV, from AQP4 positive and AQP4 negative cells subjected to tonic stress. These EV were analysed and characterised further in Chapter 5.

Chapter 5 Characterising EV from AQP4-positive and AQP4-negative cells

5.1 Introduction

This chapter presents the results of investigations into the properties of EV derived from AQP4-positive and AQP4-negative HeLa cells, and M1-AQP4, M23-AQP4 and AQP4-negative MDCK cells, released under isotonic, hypotonic, and hypertonic conditions, as described in Chapter 4. Current EV research largely seeks to characterise EV and their cargoes, to better understand the mechanisms by which they are released, and their potential roles once released. EV can be categorised by properties such as their cargo composition, physical dimensions, and the rate at which they are released. AQP have been identified in EV from many cell types and many different roles have been suggested for AQP in EV, as reviewed here (Clarke-Bland et al., 2022). Studies that directly compare EV with and without AQP are few, and comparisons of EV with and without AQP4 even more so. This chapter describes the characterisation of EV, produced in Chapter 4, and outlines investigations into roles for AQP4 in EV, including roles in inflammatory processes, and EV survival in hypotonic environments. EV were characterised using western blot, UV-SSC FC, and nano-flow cytometry. Potential roles for EV in inflammatory processes were investigated using flow cytometry.

5.2 Characterisation and function of MDCK-derived EV

As with EV derived from HeLa cells populations, MDCK-EV were characterised. EV derived from M1-AQP4, M23-AQP4 positive AQP4-negative cells, MDCK cells, released under isotonic, hypotonic, and hypertonic extracellular conditions were analysed using a variety of experimental techniques to determine whether any differences in the characteristics or function of EV populations existed. It was possible that these EV contained different AQP4 cargo which, could affect EV properties and function. EV were analysed for differences in size, number of EV released, BODIPY labelling, and Annexin-V APC labelling using UV-SSC FC, and their possible role in inflammation was investigated.

5.2.1 Cargo analyses of MDCK-derived EV

MDCK-EV were analysed for their composition, including confirmation of AQP4 presence in EV, quantification of BODIPY labelling and analysis and quantification of Annexin-V labelling. To confirm and quantify EV cargoes, EV were analysed using western blot, UV-SSC FC, and Nano-flow cytometry.

5.2.1.1 Confirmation of AQP4 in MDCK-EV

The presence of M1 and M23 AQP4 in MDCK EV was confirmed in order study the function of AQP4 in EV further. AQP4 presence in MDCK-EV was detected by western blot, UV-SSC FC, and Nano-flow cytometry (Figure 5.1). Western blot analysis of MDCK-EV samples identified AQP4 M1 and M23 in corresponding samples (Figure 5.1 A). AQP4 was not detected in samples containing EV released by AQP4-negative, WT MDCK cells. AQP4-GFP release was detected using an anti-AQP4 antibody (ab128906, Abcam). GFP in EV was detected using UV-SSC FC (CytoFLEX, Beckman Coulter). Unlabelled EV (with no BODIPY) were measured for green fluorescence. The method used was outlined earlier, for HeLa EV (Figure 5.1B). GFP in EV was also detected using Nano-flow cytometry (Nano FCM) (Figure 5.1 C). These results confirm M1 and M23 AQP4 release in MDCK-EV.

5.2.1.2 BODIPY Labelling of MDCK EV

To identify and count MDCK-EV, EV were labelled with BODIPY. MDCK-EV labelling with BODIPY was quantified using UV-SSC FC and calculating the gMFI of green fluorescence in EV populations. BODIPY labelling of MDCK-derived EV was also analysed in multiple ways to ensure that any differences between conditions and/ or cell lines were identified (Figure 5.2).

First, BODIPY labelling of M1, M23 and WT (no transfected AQP4) MDCK-EV was analysed. gMFI for all tonic conditions were combined and analysed using the Welch's t-test (Figure 5.2 A) and no significant differences were observed.

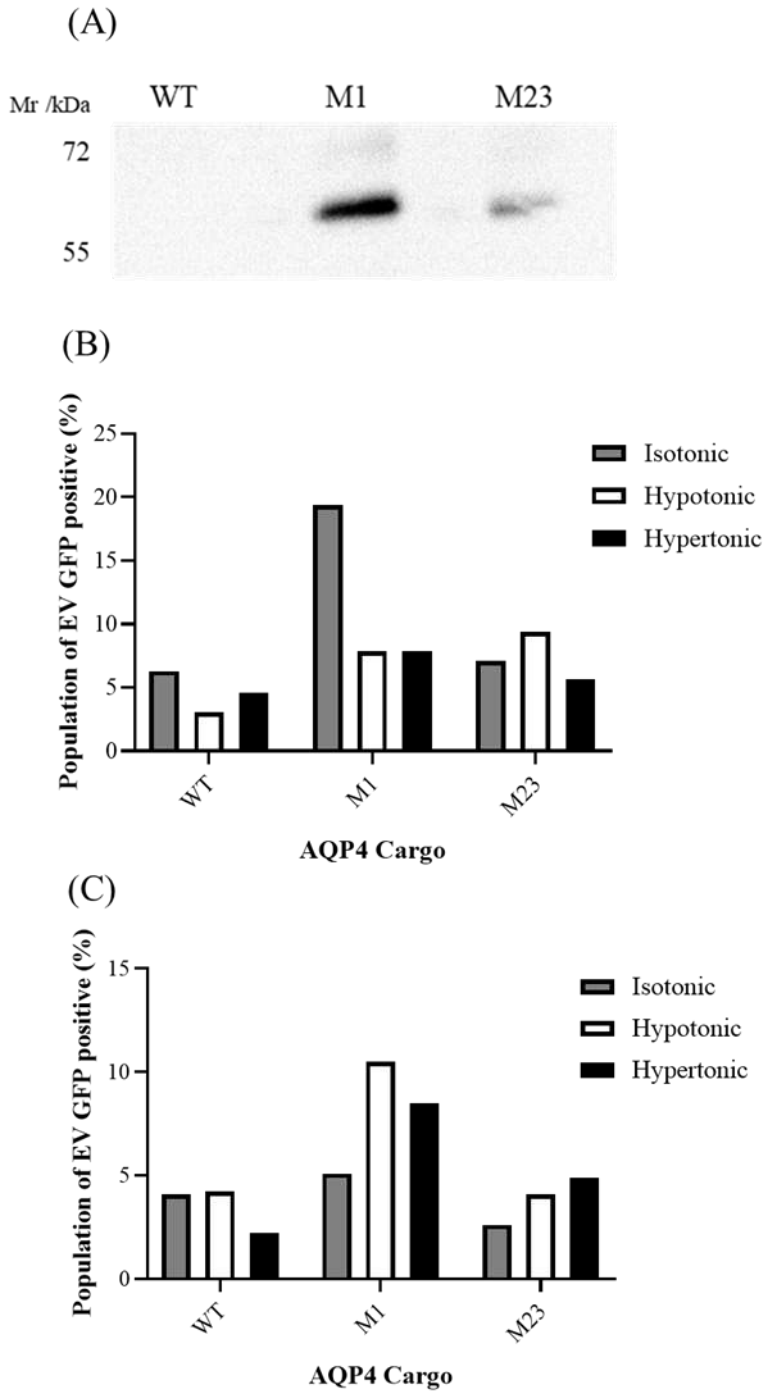

Figure 5.1 Confirmation of AQP4-GFP release in MDCK-EV

(A) Western Blot for AQP4 in EV derived from non-transfected (WT) and stably transfected M1-AQP4 and M23-AQP4 MDCK cells. AQP4 was detected using anti-AQP4 antibody. (B) Bar chart shows number of green, fluorescent EV in WT, M23 and M1 EV populations measured using VSSC flow cytometry. (n=1). (C) Bar chart shows number of green, fluorescent EV in WT, M23 and M1 EV populations measured using nano-flow cytometry. (n=1)

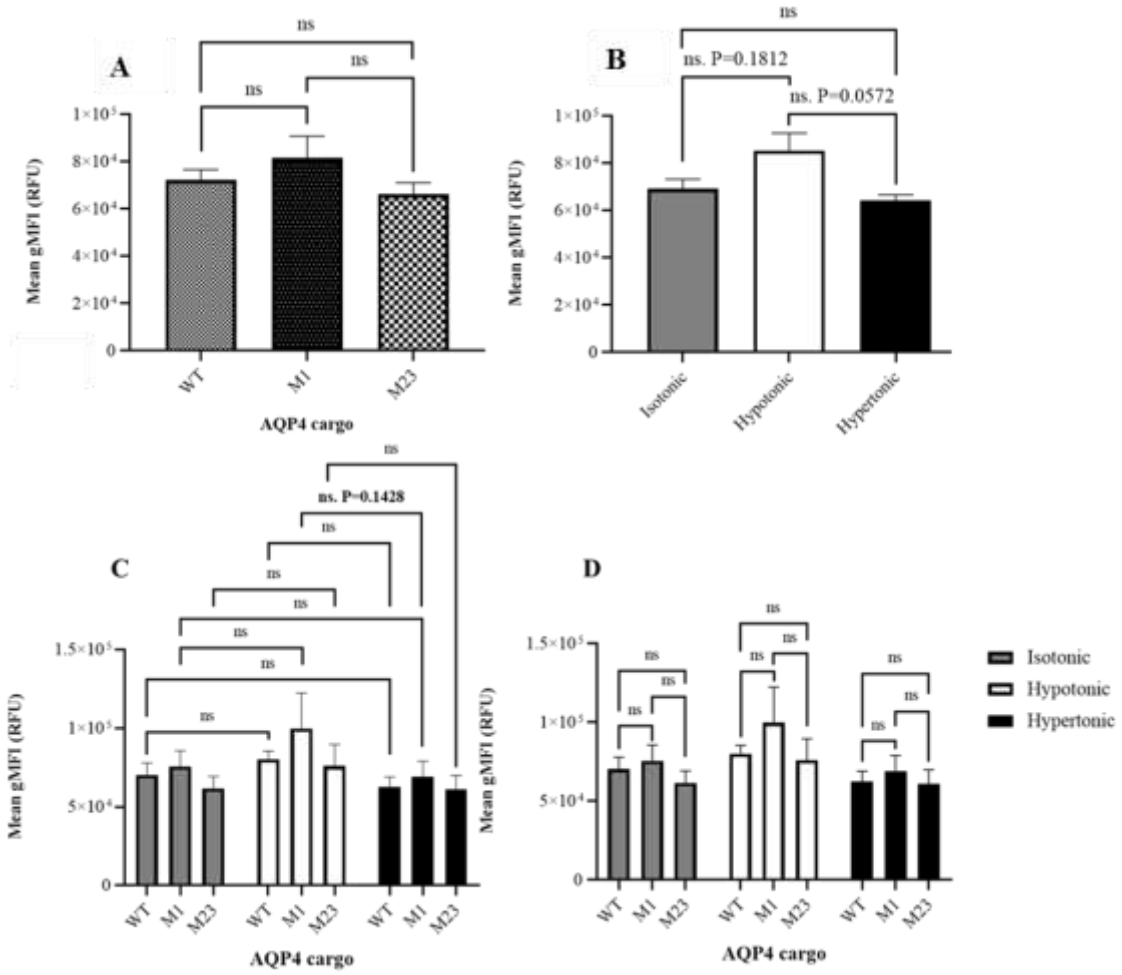

Figure 5.2 gMFI of MDCK-derived EV

BODIPY-FL labelling of MDCK-derived EV was measured using VSSC flow cytometry. Green fluorescence emission of BODIPY from EV sized particles was detected and quantified as relative fluorescence units (RFU). All panels show gMFI of EV and the standard error of the mean. All data are n=5-7. (A) Tonic condition data was combined to detect differences between WT, M1 and M23 EV populations. Data were analysed using a Welch's T-test to compare means. (B) WT, M1 and M23 data were combined to detect differences between tonic conditions. Data were analysed using 2-way ANOVA and Tukey's multiple comparison test. (C) Tonic conditions and AQP4 cargo were plotted individually, only experimental repeats were combined. Data from individual cell lines were compared across tonic conditions using by 2-way ANOVA and Sidak's multiple comparison test. (D) Tonic conditions and AQP4 cargo were plotted individually, only experimental repeats were combined. Data from different cell lines were compared in each tonic condition using by 2-way ANOVA and Sidak's multiple comparison test.

gMFI of EV released in different tonic conditions was calculated. gMFI of M1, M23 and WT MDCK-EV were combined, to allow statistical analysis of tonic conditions alone (Figure 5.2 B). A two-way ANOVA and Tukey's multiple comparison test, where each tonic condition was compared to every other tonic condition, was used to determine statistical significance of any differences between tonic conditions. No significant

differences were observed, however, when the gMFI EV released by cells in hypotonic conditions when compared with isotonic, control conditions, the P value given was 0.1812. Though this difference was not significant, EV made in hypotonic conditions had a slightly higher gMFI than EV made in isotonic conditions. No significant differences were observed between isotonic and hypertonic conditions. Despite this not being statistically significant, the P value was low, and some differences may have occurred, EV released in hypertonic conditions appeared to have a lower BODIPY gMFI than EV released in hypotonic conditions. These data follow a similar pattern to EV derived from HeLa cells; hypertonic HeLa-EV labelled significantly less than hypotonic EV derived from HeLa cells. The fact that this pattern is seen across both models suggests that something to do with the hypertonic condition causes reduced labelling of BODIPY.

Differences in gMFI of individual cell lines between different tonic conditions were analysed, a two-way ANOVA with Sidak's multiple comparison test was performed (Figure 5.2 C). When analysed individually, no significant differences were observed. The lowest P value calculated was between M1 in hypotonic and hypertonic conditions, where BODIPY labelling of EV released in hypertonic conditions was lower than EV released in hypotonic conditions, P=0.1428.

The gMFI of M1, M23 and EV derived from AQP4-negative cells in each tonic condition was calculated. A two-way ANOVA with Sidak's multiple comparison test was performed where gMFIs of EV derived from AQP4-negative cells counts were compared with gMFIs of M1 and M23 EV counts in each tonic condition (Figure 5.2 D). No significant differences were observed between cell lines in any tonic condition.

In conclusion, the data show that MDCK-derived EV made in hypertonic conditions appear to bind less BODIPY than EV made in hypotonic conditions, though these were not statistically significant. This is the same pattern observed in HeLa derived EV, where EV made in hypertonic conditions labelled significantly less for BODIPY than EV derived from HeLa cells released in isotonic and hypotonic conditions. It appears that EV produced in hypertonic conditions, regardless of the cell line from which they are derived, contain fewer free thiol groups than EV made in hypotonic and isotonic conditions. A likely explanation for this is reduction in the number of free thiol groups due to hypertonic stress. Hypertonic stress is known to increase the production of ROS by cells (Yang et al., 2005). *In vivo*, ROS release contributes to oxidative stress which, can damage cells and tissues. It is thought that free thiol groups interact with and scavenge ROS to reduce oxidative stress and subsequent damage. When free thiol

groups interact with ROS, they become oxidised and are no longer ‘free’ to bind other molecules, such as BODIPY. This would explain the reduced BODIPY FL labelling observed in EV released in hypertonic conditions and while it is a very plausible explanation, further experiments would have to be carried out, such as confirmation of an increase in ROS production, in order to confirm this finding.

5.2.1.3 Annexin-V labelling of MDCK derived EV

5.2.1.3.1 Establishing an Annexin-V labelling protocol

EV derived from HeLa cells were labelled with Annexin-V APC, a fluorescently conjugated compound which binds phosphatidylserine (PS) in the plasma membrane and emits light at wavelengths in the red range of the electromagnetic spectrum, with peak emission at 660 nm. Annexin-V labelling of EV is a well-established technique, used since EV were first identified (Heijnen et al., 1999).

For comparison of Annexin-V labelling of EV populations, both the percentage of EV Annexin-V positive EV, and the gMFI of EV populations was measured using UV-SSC FC. EV populations were labelled with Annexin-V following SEC isolation. Positive labelling of EV with Annexin-V was defined using a fluorescence gating method, similar to the one designed for BODIPY FL-Maleimide fluorescence. Annexin-V emission of unlabelled ‘Annexin-V-negative’ EV populations was measured and defined as background fluorescence (Figure 5.3 A). An ‘Annexin-V’-positive gate was drawn to include higher fluorescence intensities than the emission from the unlabelled populations and included around 2% of the unlabelled population, to ensure the full range of fluorescence signal was collected. This gate was used to confirm Annexin-V labelling of labelled EV populations and calculate the percentage of EV labelled positively with Annexin-V (Figure 5.3 B). A positive shift in fluorescence intensity was observed in EV populations labelled with Annexin-V (Figure 5.3 C). BODIPY labelling of EV was not affected by Annexin-V labelling, the fluorescence signal from BODIPY remained the same between Annexin-V negative and positive populations (Figure 5.3 D).

To quantify Annexin-V labelling of EV derived from HeLa cells, the percentage of EV labelled with Annexin-V was calculated for each population, by calculating the percentage of EV that fell within the positive ‘Annexin-V’ gate described above. To identify differences between populations, Annexin-V labelling of EV derived from HeLa

cells was analysed using the same method used for BODIPY-labelling data analyses.

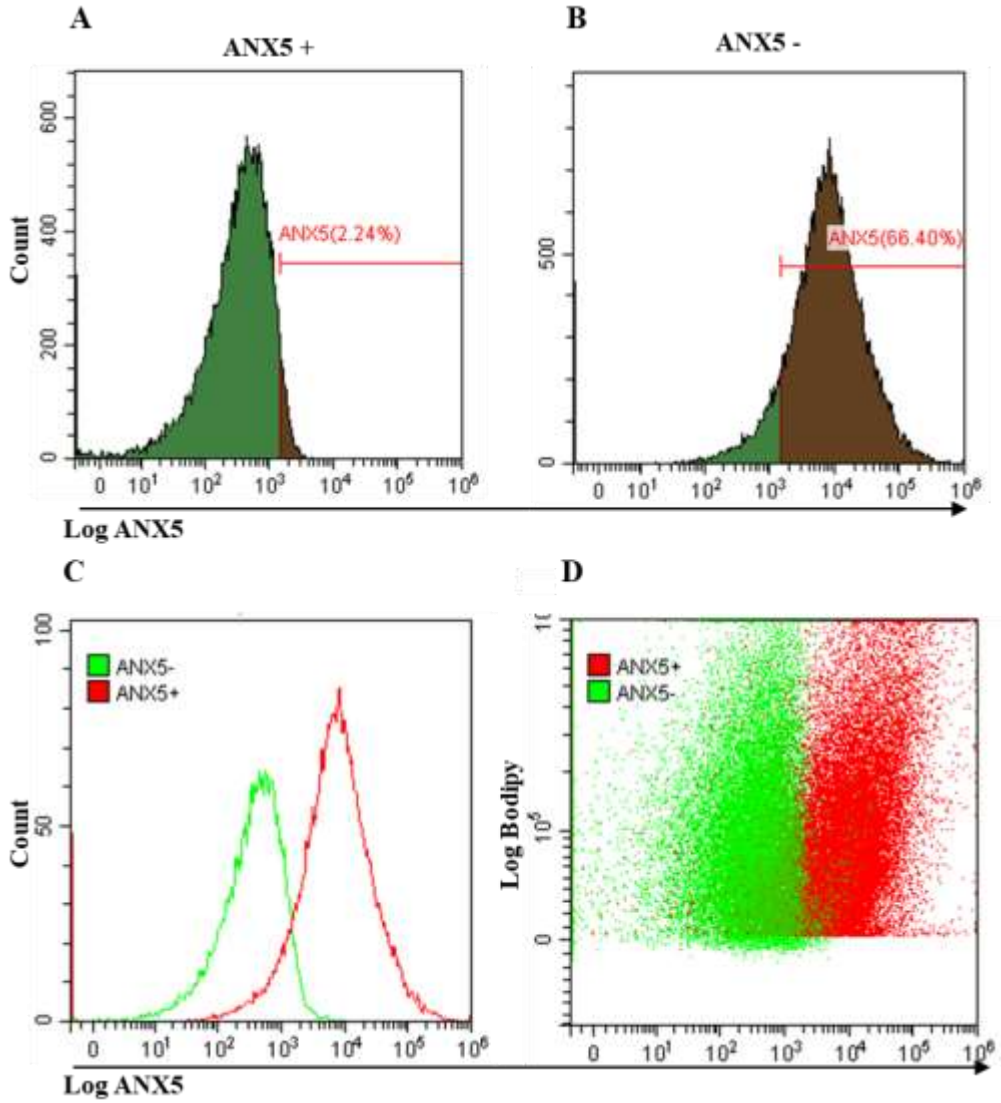

Figure 5.3 Annexin V gating protocol

Following BODIPY labelling and isolation by SEC, MDCK-EV were incubated with Annexin V APC. EV populations were defined using BODIPY labelling (Figure 3.12). (A) Representative histograms show the linear gate applied to define Annexin V labelling of BODIPY-labelled EV. This gate was drawn against an Annexin V APC -negative EV population. The gate was confirmed using an Annexin V positive EV population. (B) Representative overlay histogram shows APC fluorescence intensity of Annexin V negative and Annexin V positive EV populations. Representative overlay dot plot shows the BODIPY and Annexin V APC labelling profiles of Annexin V APC -negative and positive populations.

The same statistical analyses were applied to combinations of, and individual data sets to identify differences between cell lines, tonic conditions, and individual cell lines in each condition.

5.2.1.3.2 Annexin-V labelling of MDCK-EV – percentage population

MDCK-EV were labelled with Annexin-V following the same method used to label EV derived from HeLa cells. Annexin-V was used to fluorescently label PS in MDCK-EV. To identify any differences in PS content in M1, M23, and WT MDCK released in Isotonic, hypotonic, and hypertonic conditions, the percentage of EV labelled positively for Annexin-V and gMFI of Annexin-V in MDCK-EV populations was measured using UV-SSC FC (Figure 5.4).

5.2.1.4 Annexin-V labelling of MDCK EV– gMFI

The gMFI Annexin-V signal of each EV population was calculated to quantify the average amount of Annexin-V labelling per EV. Annexin-V labelling of MDCK-EV was analysed in multiple ways to ensure that any differences between conditions and cell lines were identified (Figure 5.5). The data show that there are no significant differences between either M1, M23 or WT EV or between tonic conditions.

The percentage of EV labelled with Annexin-V was calculated for each population. Annexin-V labelling of MDCK-EV was analysed in multiple ways to ensure that any differences between conditions and cell lines were identified as above. No significant differences were seen in the percentage of EV labelled with Annexin-V between M1, M23 and WT MDCK-EV, made in isotonic, hypotonic, or hypertonic conditions, regardless of how the data was analysed or which statistical analyses were used. The values calculated in this study align with those of previous studies which show that around 60% of HeLa populations label positively with Annexin-V. It does not appear that the presence nor absence of AQP4, or that any of the tonic conditions in which EV are made, alter the percentage of EV that were labelled with Annexin-V.

5.2.2 Quantifying MDCK-EV release

The number of EV released by M1, M23 and AQP4-negative HeLa cells, in different tonic stress conditions, was counted using UV-SSC FC (Figure 5.6). EV counts for each condition was normalised to the corresponding cell count. The number of EV released by M1, M23 and WT MDCK cells, in isotonic, hypotonic, and hypertonic conditions was calculated to determine whether the expression of AQP4 altered the number of EV released by cells in tonic stress. EV were labelled with BODIPY and counted using UV-SSC FC, as described in Figure 4.12. Cells were counted using flow

cytometry. The total number of EV per condition was calculated and normalised to the total number of cells. This was shown as EV released per cell.

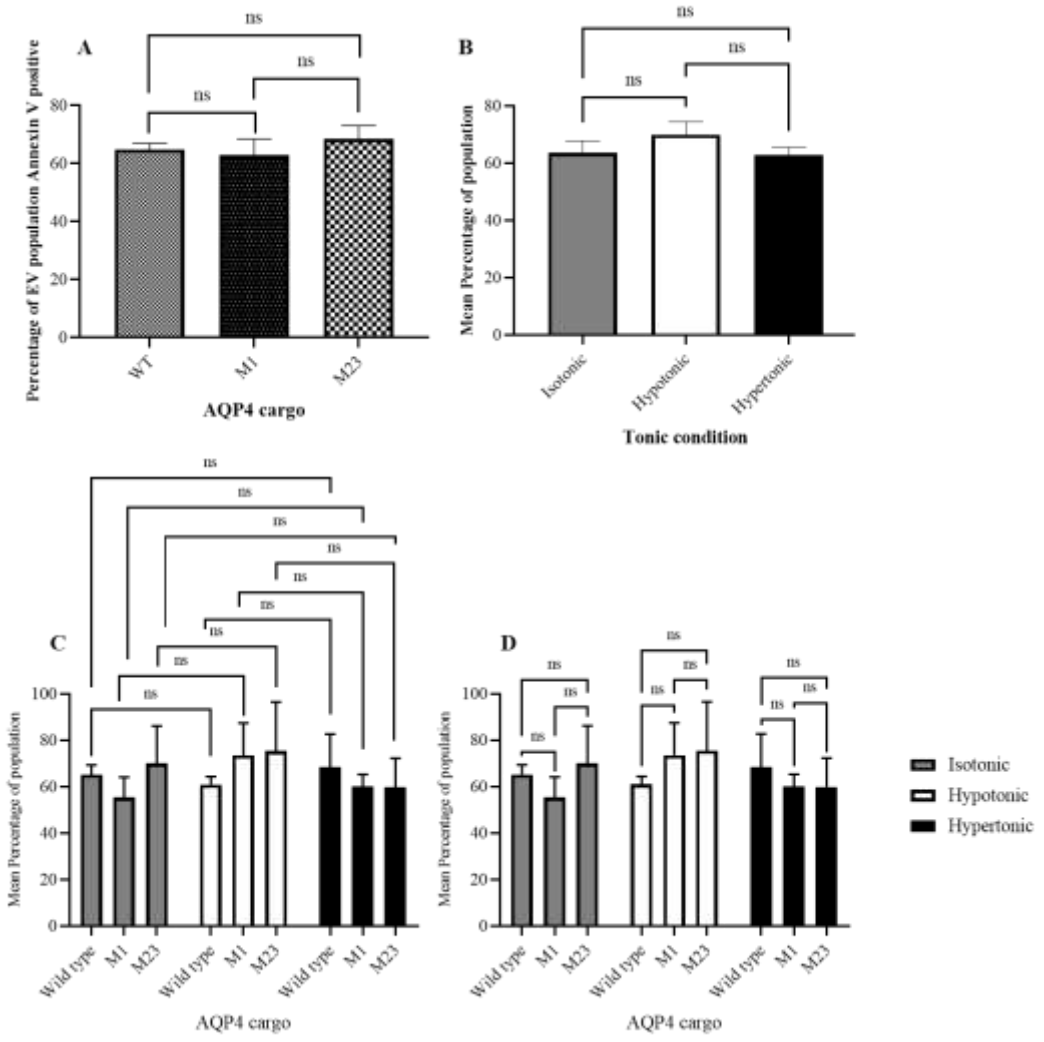

Figure 5.4 Annexin V APC labelling of EV derived from HeLa cells- Percentage Population

Annexin V APC Labelling of MDCK-derived EV was measured using VSSC flow cytometry. EV positive for emission of red fluorescence (Annexin V APC) were detected and counted. Number of EV with red fluorescence was shown as a percentage of the EV population. All panels show mean percentage of Annexin V labelled EV and standard error. All data are n=3. (A) Tonic condition data were combined to detect differences between WT, M1 and M23 EV populations. Data were analysed using a Welch's T-test to compare means. (B) WT, M1 and M23 EV data were combined to detect differences between tonic conditions. Data were analysed using 2-way ANOVA and Tukey's multiple comparison test. (C) Tonic conditions and AQP4 cargo were plotted individually, only experimental repeats were combined. Data from individual cell lines were compared across tonic conditions using by 2-way ANOVA and Sidak's multiple comparison test. (D) Tonic conditions and AQP4 cargo were plotted individually, only experimental repeats were combined. Data from different cell lines were compared in each tonic condition using by 2-way ANOVA and Sidak's multiple comparison test.

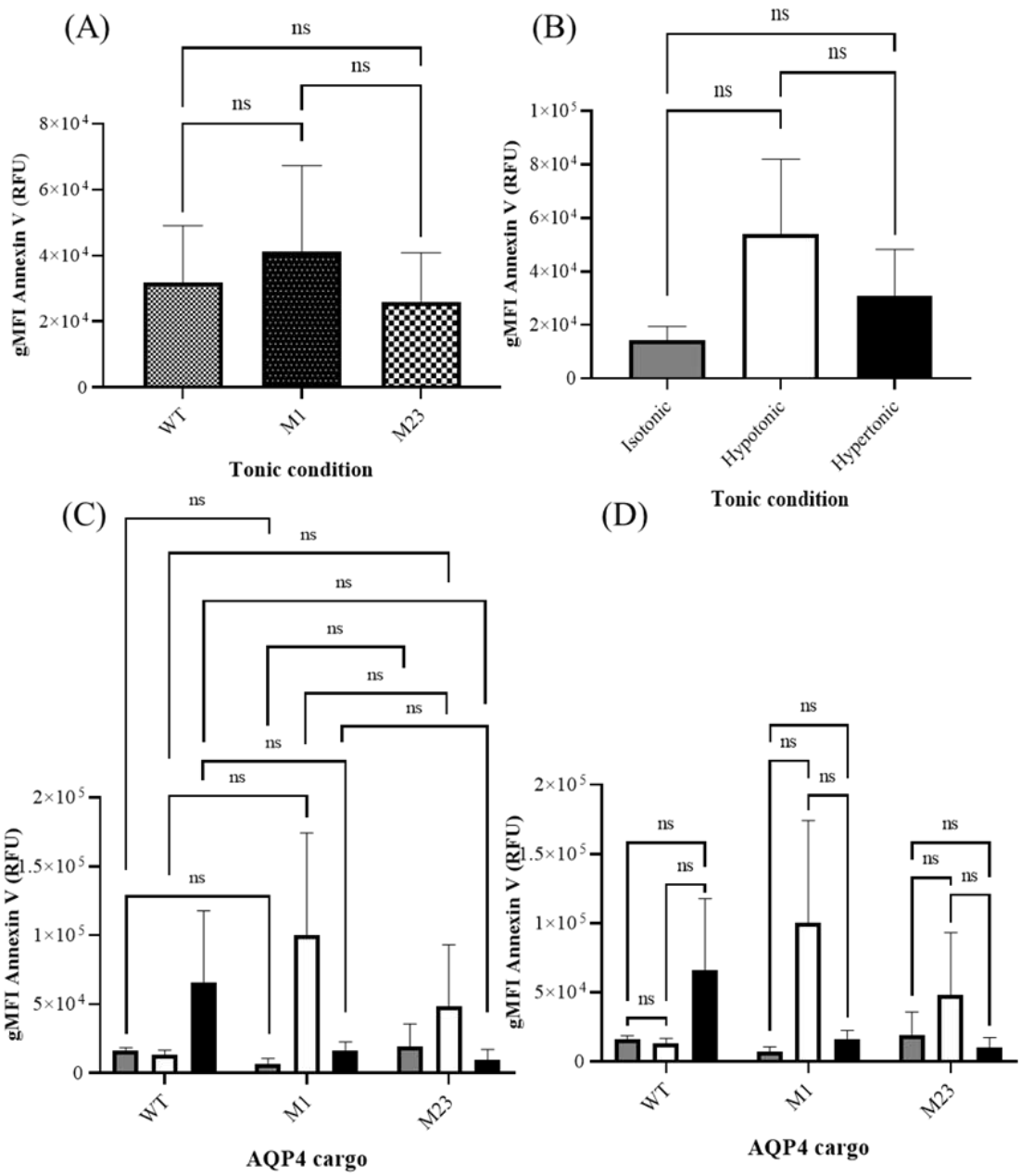

Figure 5.5 Annexin V APC labelling of MDCK-EV - gMFI

Annexin V APC Labelling of MDCK-derived EV was measured using VSSC flow cytometry. EV positive for emission of red fluorescence (Annexin V APC) were detected and fluorescence intensities were quantified. Red fluorescence was quantified as gMFIs. All panels show the gMFI of Annexin V labelled EV and standard error. All data are n=3. (A) Tonic condition data were combined to detect differences between WT, M1 and M23 EV populations. Data were analysed using a Welch's T-test to compare gMFI. (B) WT, M1 and M23 data were combined to detect differences between tonic conditions. Data were analysed using 2-way ANOVA and Tukey's multiple comparison test. (C) Tonic conditions and AQP4 cargo were plotted individually, only experimental repeats were combined. Data from individual cell lines were compared across tonic conditions using by 2-way ANOVA and Sidak's multiple comparison test. (D) Tonic conditions and AQP4 cargo were plotted individually, only experimental repeats were combined. Data from different cell lines were compared in each tonic condition using by 2-way ANOVA and Sidak's multiple comparison test.

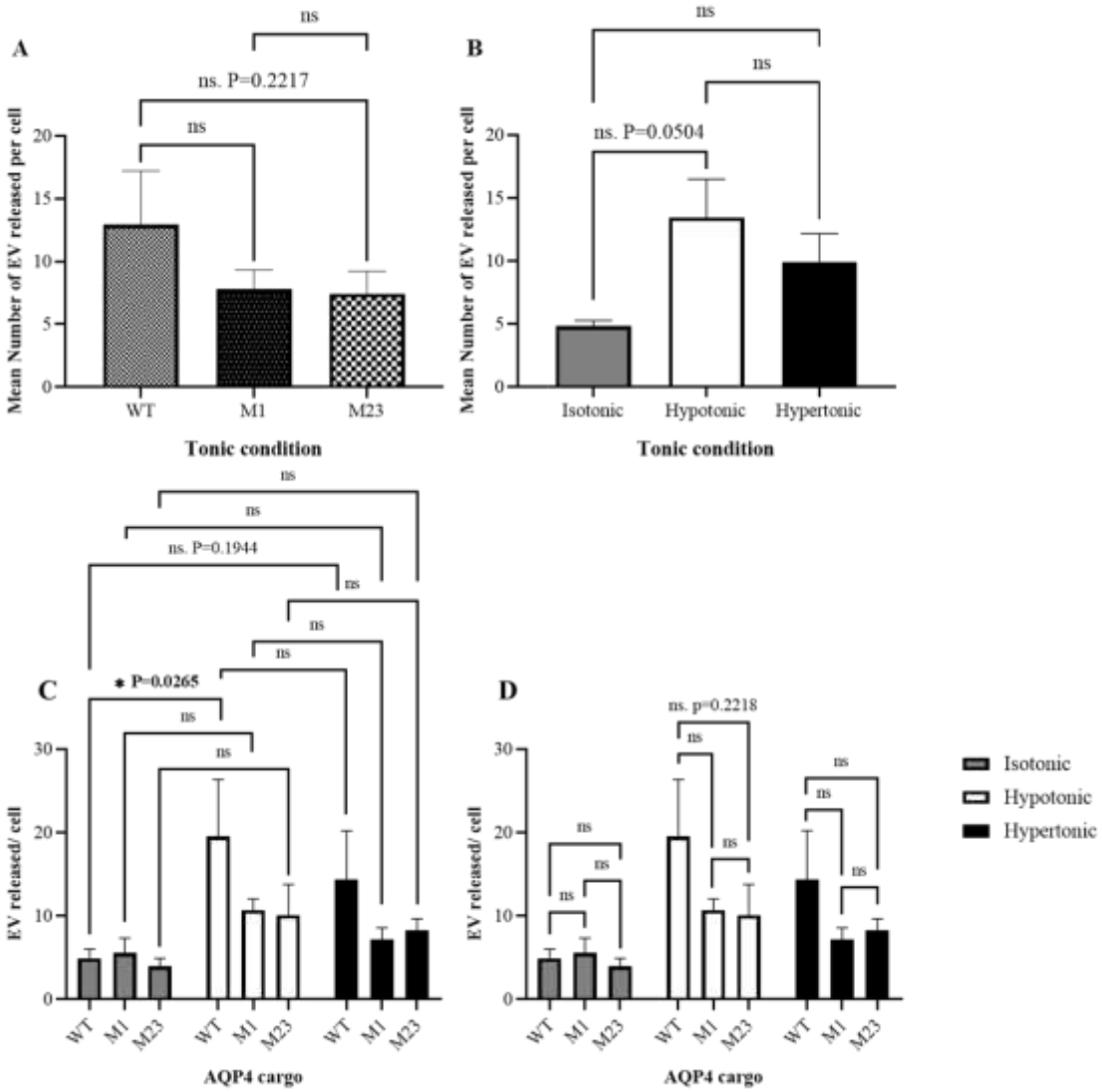

Figure 5.6 MDCK-EV counting by VSSC Flow Cytometry

MDCK-EV were counted using VSSC flow cytometry. EV positive for BODIPY-FL were detected and counted. The number of EV shown as the mean number of EV released per cell. All panels show mean number of EV released and the standard error. Isotonic and hypotonic data are n=5. Hypertonic data are n=3 (A) Tonic condition data were combined to detect differences between WT, M1 and M23 EV populations. Data were analysed using a Welch's T-test to compare means. (B) WT, M1 and M23 data were combined to detect differences between tonic conditions. Data were analysed using 2-way ANOVA and Tukey's multiple comparison test. (C) Tonic conditions and AQP4 cargo were plotted individually, only experimental repeats were combined. Data from individual cell lines were compared across tonic conditions using by 2-way ANOVA and Sidak's multiple comparison test. (D) Tonic conditions and AQP4 cargo were plotted individually, only experimental repeats were combined. Data from different cell lines were compared in each tonic condition using by 2-way ANOVA and Sidak's multiple comparison test. *=p<0.05.

MDCK-EV counts were analysed in multiple ways. M1, M23 and WT MDCK-EV counts were compared, regardless of tonic stress conditions. Mean cell counts for all tonic conditions were combined and data analysed using a Welch's t-test. No significant differences were seen between M1, M23 or WT MDCK-EV. The lowest P value calculated was between WT and M23 cell lines where P=0.2217. WT cells released more EV then M1 and M23 cells but the variation for WT cells was such that these observations are not statistically significant. (Figure 5.6 A)

The number of EV released in difference tonic conditions was calculated, data from M1, M23 and WT EV were combined (Figure 5.6 B). A two-way ANOVA and Tukey's multiple comparison test, where each tonic condition was compared to every other tonic condition, was used to determine statistical significance of differences between conditions. No significant differences were seen in the number of EV released by cells in any tonic conditions. Though upon comparison of hypotonic conditions with EV counts from isotonic, control conditions, though the P value calculated was 0.0504, which almost fell within the statistically significant range. More EV are released in hypotonic conditions than in isotonic conditions. EV released by cells in hypertonic conditions was not statistically different from either isotonic or hypertonic conditions.

To identify differences in EV release of individual cell lines between different tonic conditions, a two-way ANOVA with Sidak's multiple comparison test was performed (Figure 5.6 C). No significant differences were observed between conditions in most comparisons. However, a significant increase in EV release was observed in WT MDCK cells exposed to hypotonic conditions, compared to EV release by WT MDCK cells in isotonic conditions; the P value given was 0.0265. The P value calculated when WT EV released in isotonic conditions were compared with WT EV released in hypertonic conditions was 0.1944, this is not statistically significant, but it may be that there was an increase in the number of WT EV released in hypertonic conditions.

The number of EV released between cell lines was analysed in each tonic condition. A two-way ANOVA with Sidak's multiple comparison test was performed where means of M1, M23 and WT EV counts were compared in each condition (Figure 5.6 D). No significant differences were observed between cell lines in any tonic condition. The lowest P value calculated was between WT and M23 cell lines in hypotonic conditions, P=0.2218, where WT cells released more EV than M23 cells.

A number of differences in EV release were observed. Overall, it appeared the WT MDCK released more EV than M1 or M23 MDCK. When data were combined and tonic

conditions were analysed, it was seen that more EV are released in hypotonic conditions. Upon more detailed analysis, it was clear that WT cells exposed to hypotonic conditions, released the most EV and significantly more than WT cells in isotonic conditions. When compared with M1 and M23 MDCK cells, more variation is observed in the number of EV released by WT MDCK cells. M1 and M23 MDCK are less affected by hypotonic and hypertonic stress than WT MDCK cells. It is reasonable to conclude that M1 and M23 expression in MDCK cells has a protective effect for cells in tonic stress conditions. It has been shown that cells secret higher numbers of EV when stressed (Debbi et al., 2022). It is possible that the water channel property of AQP4 means cells AQP4-positive cells have better volumetric regulation and are less stressed, and therefore, do not release as many EV.

The number of EV released between cell lines was analysed in in each tonic condition. A two-way ANOVA with Sidak's multiple comparison test was performed where means of EV derived from AQP4-negative cells counts were compared with means of EV derived from AQP4-positive cells counts in each condition (Figure 5.6 D). No significant differences were observed between cell lines in any condition.

5.2.3 MDCK-EV size

The mean size of M1, M23, and WT MDCK-derived EV, made in isotonic, hypotonic, and hypertonic conditions was measured using UV-SSC FC, and nano-flow cytometry (Nano FCM).

5.2.3.1 MDCK EV mean size, UV-SSC FC

Mean UV-SSC measurements for all conditions were collected and compared using a variety of statistical analyses (Figure 5.7) The mean size of MDCK-derived EV populations was analysed . The mean size of MDCK-EV with M1, M23 and without AQP4 (WT) were compared, by combining UV-SSC data from all tonic conditions and comparing between cell lines (Figure 5.7 A). Data were analysed using Welch's t-test. A significant increase was observed in the mean size of EV containing M23-AQP4 compared to the mean size of M1-AQP4 and WT EV, P values were 0.0138 and 0.0120, respectively.

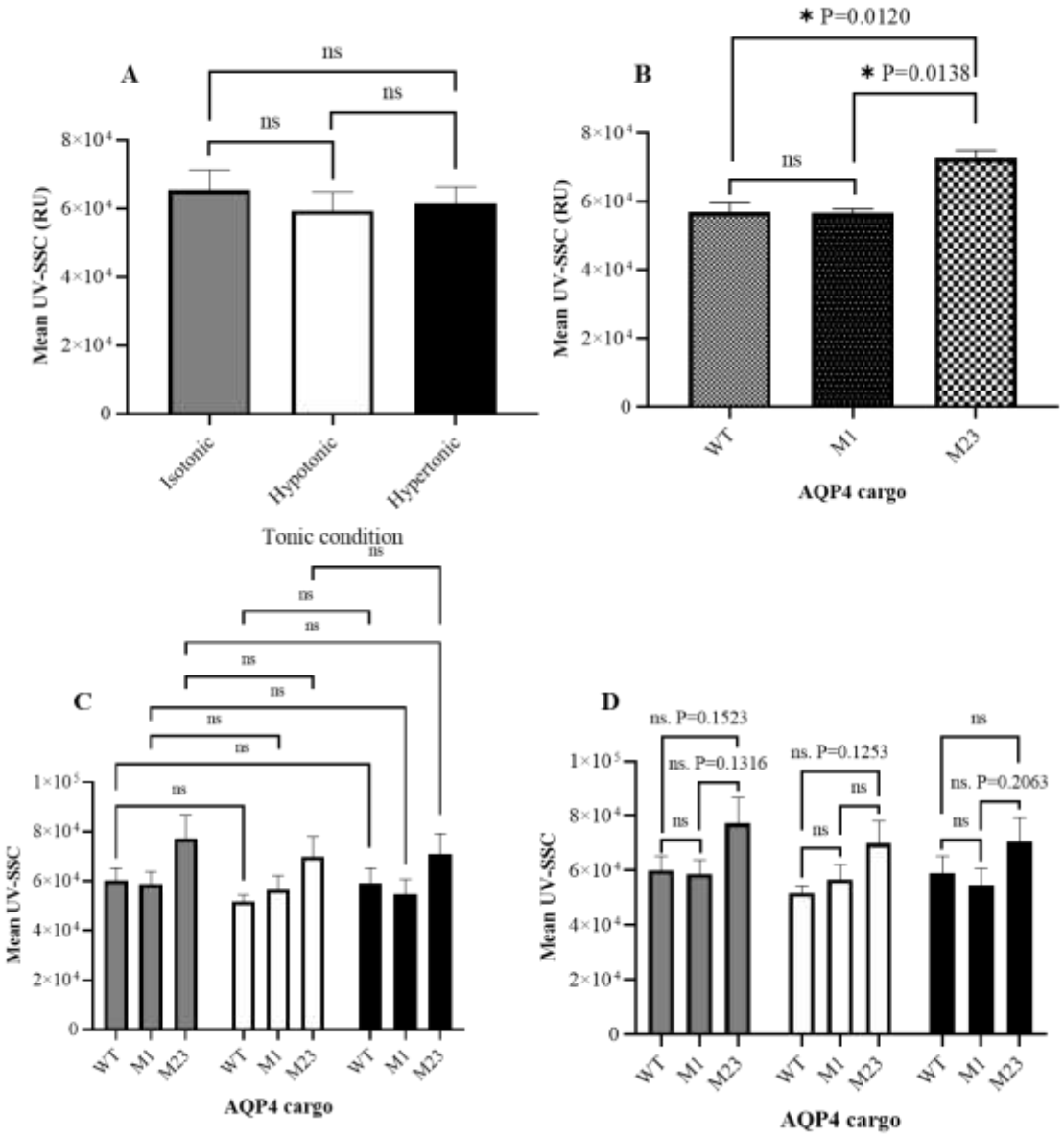

Figure 5.7 Mean size of EV derived from HeLa cells – VSSC Flow cytometry.

MDCK-EV were detected using VSSC flow cytometry. The mean VSSC values of EV populations were calculated. All panels show mean VSSC values and the standard error. All data are n=5-7. (A) Tonic condition data were combined to detect differences between WT, M1 and M23 EV populations. Data were analysed using a Welch's T-test to compare means. (B) WT, M1 and M23 data were combined to detect differences between tonic conditions. Data were analysed using 2-way ANOVA and Tukey's multiple comparison test. (C) Tonic conditions and AQP4 cargo were plotted individually, only experimental repeats were combined. Data from individual cell lines were compared across tonic conditions using by 2-way ANOVA and Sidak's multiple comparison test. (D) Tonic conditions and AQP4 cargo were plotted individually, only experimental repeats were combined. Data from different cell lines were compared in each tonic condition using by 2-way ANOVA and Sidak's multiple comparison test. *=p<0.05.

Next, the mean UV-SSC of EV released in different tonic conditions was calculated. M1, M23 and WT EV data were combined (Figure 5.7 B). A two-way ANOVA and Tukey's multiple comparison test of column data. No significant differences were seen in the size of EV in any tonic conditions.

EV release of individual cell lines between different tonic conditions, a two-way ANOVA with Sidak's multiple comparison test was performed (Figure 5.7 C). No significant differences in size were observed between tonic conditions for either M1, M23 or WT EV.

The mean size of EV for each cell line was compared in each tonic condition (Figure 5.7 D). A two-way ANOVA with Sidak's multiple comparison test was performed where the means of M1, M23 and WT EV counts were compared in each condition. No significant differences were observed between cell lines in any tonic condition.

In conclusion, UV-SSC FC analyses of EV size showed that EV released by M23 MDCK cells are bigger, on average, than EV from M1 and WT EV populations. There are a number of possible explanations for this. It may be that M23 cells are apoptotic. Apoptotic EV are generally bigger than exosomes or microvesicles, though qualitative analysis of raw UV-SSC data suggests that the size of M23 EV does not fall within the size range of apoptotic EV, around 500 -2000nm in diameter (Battistelli and Falcieri, 2020). In addition, no differences in Annexin-V labelling of M23 MDCK cell or EV were observed.

Another consideration is the predisposition of M23 AQP4 to form OAPs (Silberstein et al., 2004). Epifluorescence microscopy of M23 MDCK cells showed punctate expression of M23 AQP4, suggesting OAP formation. It was hypothesised that OAP formation in M23 MDCK cell membranes may limit the size of EV that cells can make, as the presence of OAP in cell membranes reduces the amount of OAP- free membrane and large OAPs will only be released in larger vesicles, due to their large size.

5.2.3.4 MDCK EV mean size -nano-flow cytometry

EV diameters were estimated using nano-flow cytometry, a technique capable of estimating particle size with higher resolution that UV-SSC FC (Figure 5.8). Analysis of EV size using nano- flow cytometry was completed one time and therefore the data

cannot be analysed confidently. These data can, however, be used alongside data produced by UV-SSC FC. Nano-flow data show an average smaller

particle size than UV-SSC FC. This could be explained in a number of ways. Both methods provide only estimates of size, and limitations of UV-SSC, such as calibration with polystyrene beads has been discussed previously. The data acquired by nano-flow cytometry data show consistent sizes between EV populations, whereas UV-SSC data show a bigger average particle size in M23 MDCK derived EV populations.

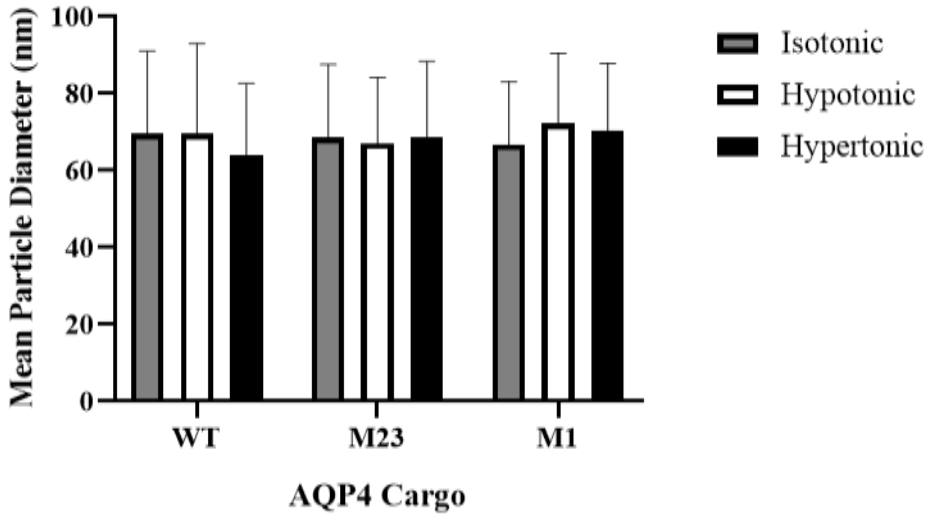

Figure 5.8 Mean Size of EV derived from HeLa cells – Nano FCM

The bar chart shows the mean particle diameter (nm) of MDCK-EV, produced in different tonic conditions, as measured by nano-flow cytometry (Nano FCM). Mean plus standard deviation shown, n=1.

5.2.4. MDCK-EV Interaction with THP-1 cells

5.2.4.1 MDCK EV Interaction - Percentage Population

MDCK-EV interaction and uptake by macrophages was measured, in the same way as HeLa EV. Flow cytometry was used to identify green fluorescence in differentiated THP-1 (macrophage) cells transferred by BODIPY labelled EV. The percentage of cell populations with green fluorescence and the gMFI of THP-1 cells was measured and analysed. The percentage of THP-1 cells that appeared positive for green fluorescence was measured following incubation with BODIPY-labelled EV. The percentage of THP-1 cells labelled with green fluorescence was calculated and compared to an EV-negative, and therefore non-fluorescent, THP-1 population (Figure 5.9).

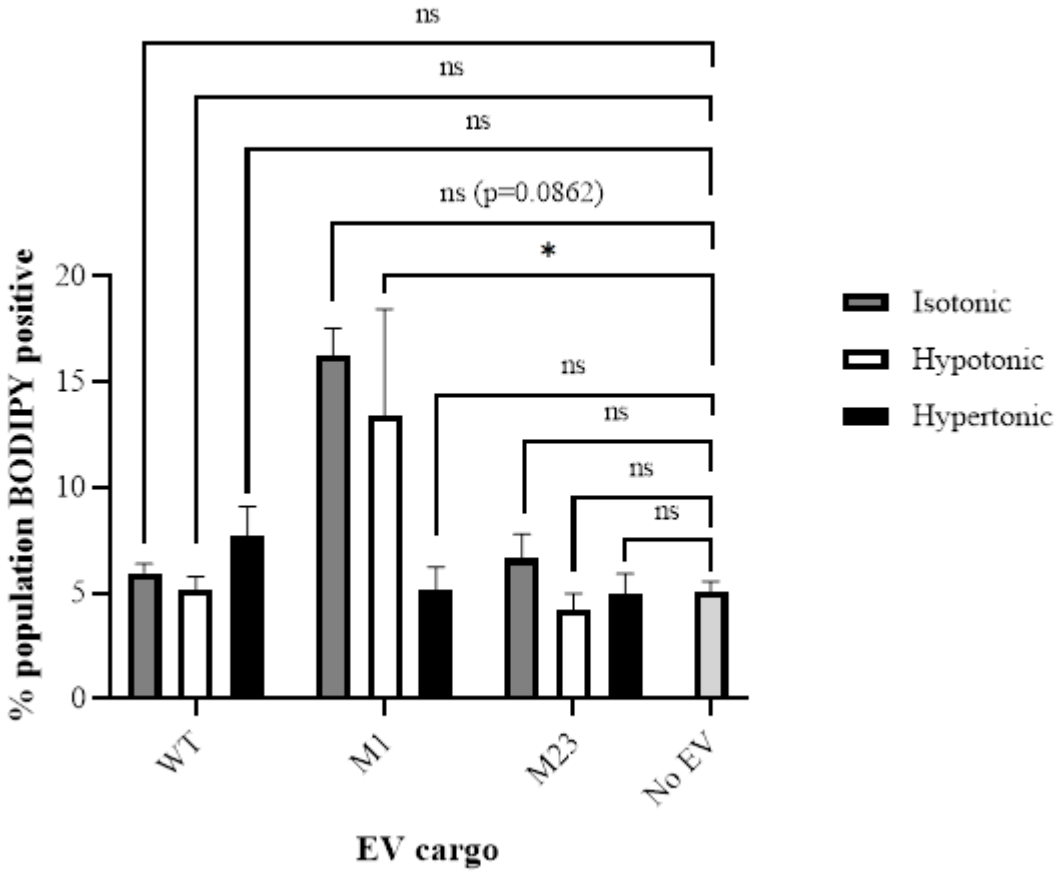

Figure 5.9 Interaction of EV derived from HeLa cells with THP-1 cells

Flow cytometry was used to measure the interaction between BODIPY FL- labelled MDCK-EV and THP-1 cells. Green fluorescence accumulation in THP-1 cells was measured and quantified the percentage of cells positive for green fluorescence. Populations were compared with a control THP-1 population, measured without incubation with EV. Statistical significance was determined using a 2-way ANOVA (with Sidak's and Tukey's multiple comparison tests). *=p<0.05. n=3

A 2-way ANOVA was used to analysed data for significant differences in THP-1 fluorescence after incubation with EV, compared with control THP-1. Most conditions did not show any significant differences when compare with control THP-1, meaning that there were no increases in THP-1 fluorescence and therefore, no/ little interaction observed. THP-1 cells derived EV, produced in hypotonic conditions showed a significant increase. M1 MDCK derived EV produced in isotonic conditions, showed a consistent but not statistically significant increase in fluorescence.

The results of this experiment suggest that THP-1 macrophages interact more readily with EV containing M1-AQP4 than M23-AQP4 positive EV and WT incubated with M1 MDCK however did increase in green fluorescence intensity. M1 MDCK EV, unless the EV are produced in hypertonic conditions, THP-1 macrophages do not appear interact with these EV, when compared to control THP-1. THP-1 cells were incubated with EV

at a 1:10 ratio. No differences between HeLa cell populations were observed using this method. It was initially thought that the experimental set up required optimisation. The clear differences seen between MDCK EV populations in interaction with THP-1 cells suggest there is a fundamental difference.

5.2.5 MDCK-EV Interaction -gMFI

The gMFI of THP-1 cells was measured as another way to assess uptake of green, fluorescent EV. Figure 5.10 shows the differences between uptake of EV from M1, M23 or MDCK cell expressing no AQP4, produced in isotonic, hypotonic, and hypertonic environments.

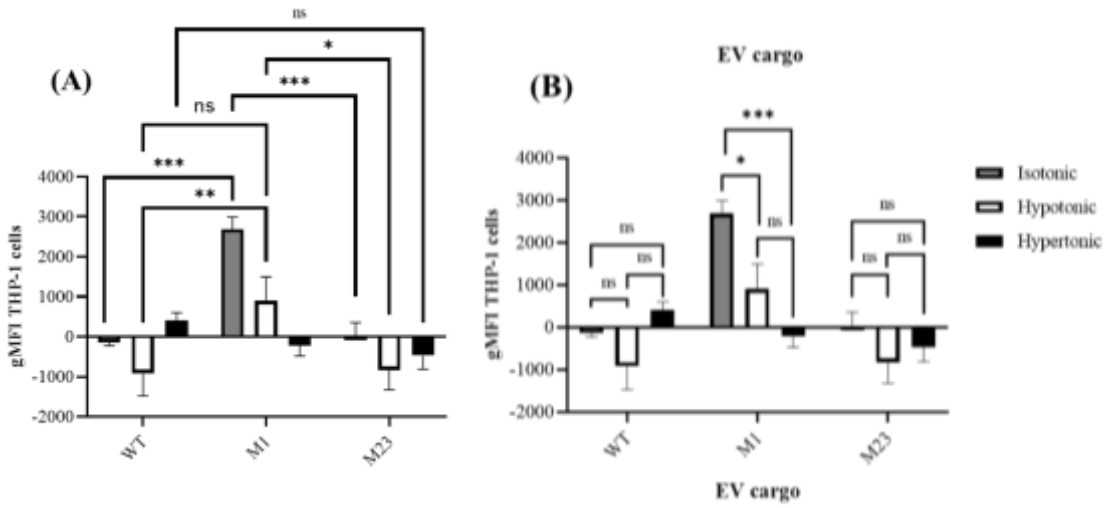

Figure 5.10 gMFI THP-1 MDCK interaction

Flow cytometry was used to measure the interaction between BODIPY FL- labelled MDCK-EV and THP-1 cells. Green fluorescence accumulation in THP-1 cells was measured and quantified as the gMFI of THP-1 cells. Populations were normalised to a control THP-1 population, measured without incubation with EV. n=3 A two-way ANOVA was performed to assess statistical significance (with Sidak's and Tukey's multiple comparison tests). *=p<0.05, **=p<0.01, ***=p<0.005, ****=p<0.001.

5.2.6 MDCK-EV hypotonic tolerance

MDCK-EV were counted before and after exposure to a hypotonic environment (Figure 5.11). One role suggested for AQP in EV is volumetric regulation of EV in changing tonic environments encountered after release by cells. To investigate whether the presence of M1 or M23 AQP4 in EV alters their ability to survive in hypotonic environments, EV were exposed to a hypotonic (2:1 water: DMEM) conditions and counted using UV-SSC FC.

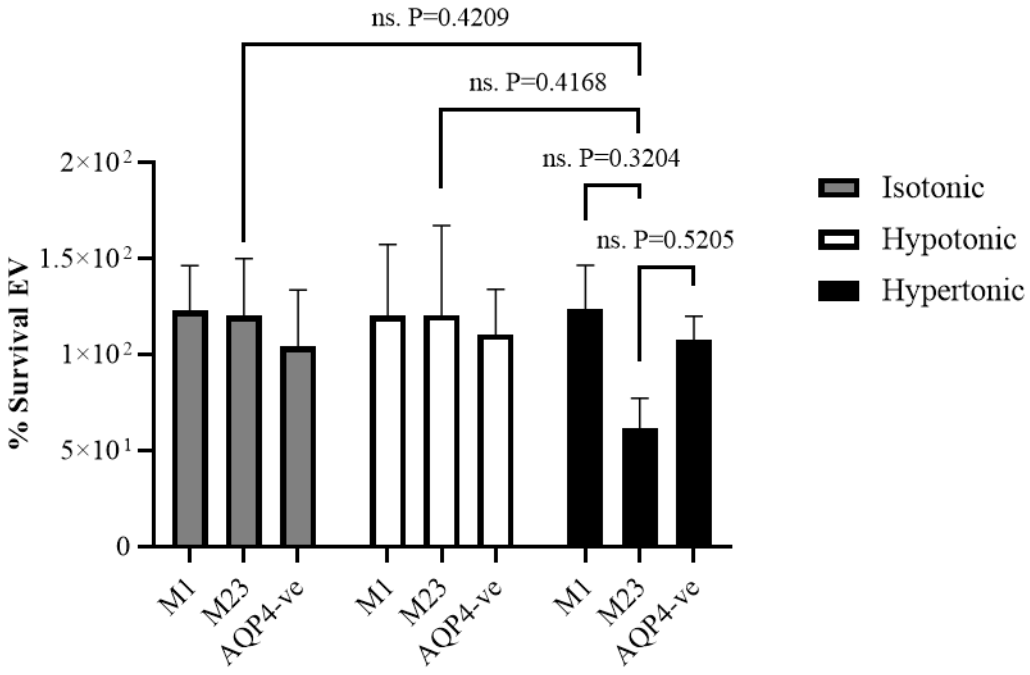

Figure 5.11 MDCK EV hypotonic tolerance

Bar chart shows the number of EV released by MDCK cells present following hypotonic exposure in a ~130 mOsM environment. Data are presented as a percentage of the equivalent in an isotonic environment. EV containing M1, M23 or no AQP4 are compared. EV produced in different environments are also compared. Statistical significance was determined using a two-way ANOVA (with Sidak's and Tukey's multiple comparison tests). n=3

No significant differences were observed between MDCK-EV populations exposed to hypotonic environments. There did appear to be a slight reduction in the number of m23 EV produced in hypertonic conditions present following hypotonic exposure. M23 EV were slightly larger in size that WT and M1 EV populations. It is possible that the size of EV plays a role in the different response to hypotonic environments.

5.3 Characterisation and function analyses of HeLa-derived EV

EV derived from WT, AQP4-negative and AQP4-positive stably transfected HeLa cells, released under isotonic, hypotonic, and hypertonic extracellular conditions were analysed using a variety of experimental techniques to determine whether any differences between EV derived from HeLa cells populations existed.

5.3.1 Cargo analyses of HeLa-EV

EV derived from HeLa cells were analysed for their cargoes including confirmation of AQP4 presence in EV, quantification of BODIPY labelling, and analysis and quantification of Annexin-V labelling. The composition of EV can indicate the state of the cell from which they are derived and provide insight into the release pathway via which EV were made. To confirm and quantify EV cargoes, EV were analysed using western blot, UV-SSC FC, and Nano-flow cytometry.

5.3.1.1 Confirmation of AQP4 in HeLa-EV

AQP4 in EV derived from stably transfected HeLa cells was investigated. The aim of creating an EV release model was to produce EV with and without AQP4 for further investigation, so confirmation of AQP4 was important. AQP4 presence was confirmed by UV-SSC FC, and nano-flow cytometry (Figure 5.12). GFP in EV was detected using UV-SSC FC (CytoFLEX, Beckman Coulter). Unlabelled EV (with no BODIPY) were measured for green fluorescence. The percentage of EV that fell within a 'green EV' gate was calculated. The gate was defined based on UV-SSC and green fluorescence, like the 'BODIPY' gate drawn in Figure 4.12. As these EV were unlabelled, any green fluorescence detected came from GFP presence (Figure 5.12 B). GFP in EV was also detected using Nano-flow cytometry (Nano FCM), a flow cytometry-based system, capable of analysing small particles more with higher resolution than UV-SSC FC (Figure 5.12 C). Combined, these results show that AQP4 release in EV derived from HeLa cells is unclear. UV-SSC show similar AQP4 content between EV derived from AQP4-negative and AQP4-positive cells. It is unusual that AQP4 appears to be present in EV derived from AQP4-negative cells. It is possible that the protein content is too low to analyse accurately using these methods. Nano-flow cytometry analysis of these EV does show differences in fluorescence properties of EV derived from AQP4-negative and AQP4-positive cells. These differences are very small, with a mean value of ~3% of EV derived from AQP4-positive cells positive for green fluorescence. Although the

differences in AQP4 content appeared small, these EV were studied further to identify any other possible differences. It was considered that any differences seen may not be due to the presence or absence of AQP4. It is also important to note that the detection methods used may not be sensitive enough to distinguish fluorescent EV from background particles when fluorescence levels are determined by cellular release of GFP in EV. The nature of the antibody used to detect AQP4 was considered,

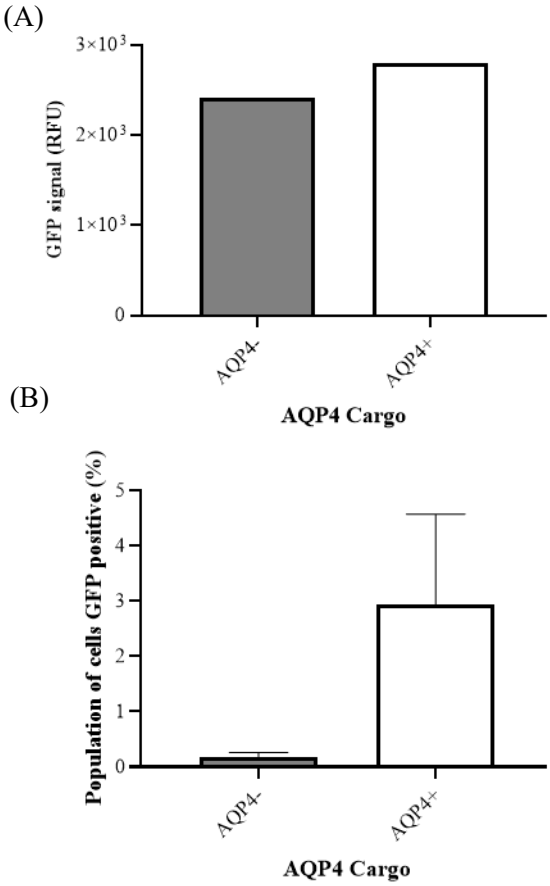

Figure 5.12 Detection of AQP4-GFP in EV derived from HeLa cells

(A) Western Blot of AQP4 in EV derived from non-transfected (WT) and stably transfected HeLa (AQP4+) cells. AQP4 was detected using an anti-AQP4 antibody (Abcam, ab128906). (B) VSSC detection of AQP4-GFP in EV derived from non-transfected and stably transfected HeLa (AQP4+) cells. GFP excited using 488nm laser and GFP emission detected using filter for green wavelengths. (C) Nano-flow cytometry detection of AQP4-GFP in EV derived from non-transfected (WT) and stably transfected (AQP4+) HeLa cells. GFP excited using 488nm laser and GFP emission detected using filter for green wavelengths.

5.3.1.2 BODIPY Labelling of HeLa EV

EV derived from HeLa cells were labelled with BODIPY for identification and counting. BODIPY is a fluorescent label that binds to free thiol groups, found on cysteine residues. As most proteins contain cysteine residues, it was reasonable to presume that BODIPY would label protein-containing EV. It was not known however whether BODIPY labelling would be consistent across all EV samples. To determine this, EV derived from HeLa cells were labelled with BODIPY and measured for BODIPY fluorescence using UV-SSC FC.

BODIPY labelling of EV derived from HeLa cells was analysed in multiple ways to ensure that any differences between tonic conditions and cell lines were identified, the same statistical analyses were applied across all UV-SSC data.

A Welch's t-test was used to analyse differences between BODIPY labelling of EV derived from AQP4-positive and AQP4-negative cells. Data from different tonic conditions were combined, and gMFI values calculated. This analysis was performed to identify any differences resulting from AQP4 presence in EV, without the influence of differences because of tonic stress. No significant differences were seen in BODIPY labelling of EV from aquaporin 4 positive and aquaporin for negative cells (Figure 5.13 A).

Next, the gMFI of EV released in difference tonic conditions was calculated; AQP4-negative and EV derived from AQP4-positive cells data were combined, in order to only compare differences based on tonic condition, and not cellular AQP4 content (Figure 5.13 B). A two- way ANOVA and Tukey's multiple comparison test was applied to identify and significant differences. Significant differences were observed between hypotonic and hypertonic conditions; The gMFI of EV released in hypertonic conditions was significantly lower than the gMFI of EV released in hypotonic conditions, P=0.0025.

No significant differences were observed in the gMFI of EV released by cells in hypotonic conditions when compared with isotonic, control conditions, the P value given was 0.1007. Though this difference was not significant, EV made in hypotonic conditions had a slightly higher gMFI than EV made in isotonic conditions. No significant differences were observed between isotonic and hypertonic conditions, P=0.1267, though EV released in hypertonic conditions did appear to have a slightly lower gMFI than EV made in isotonic conditions.

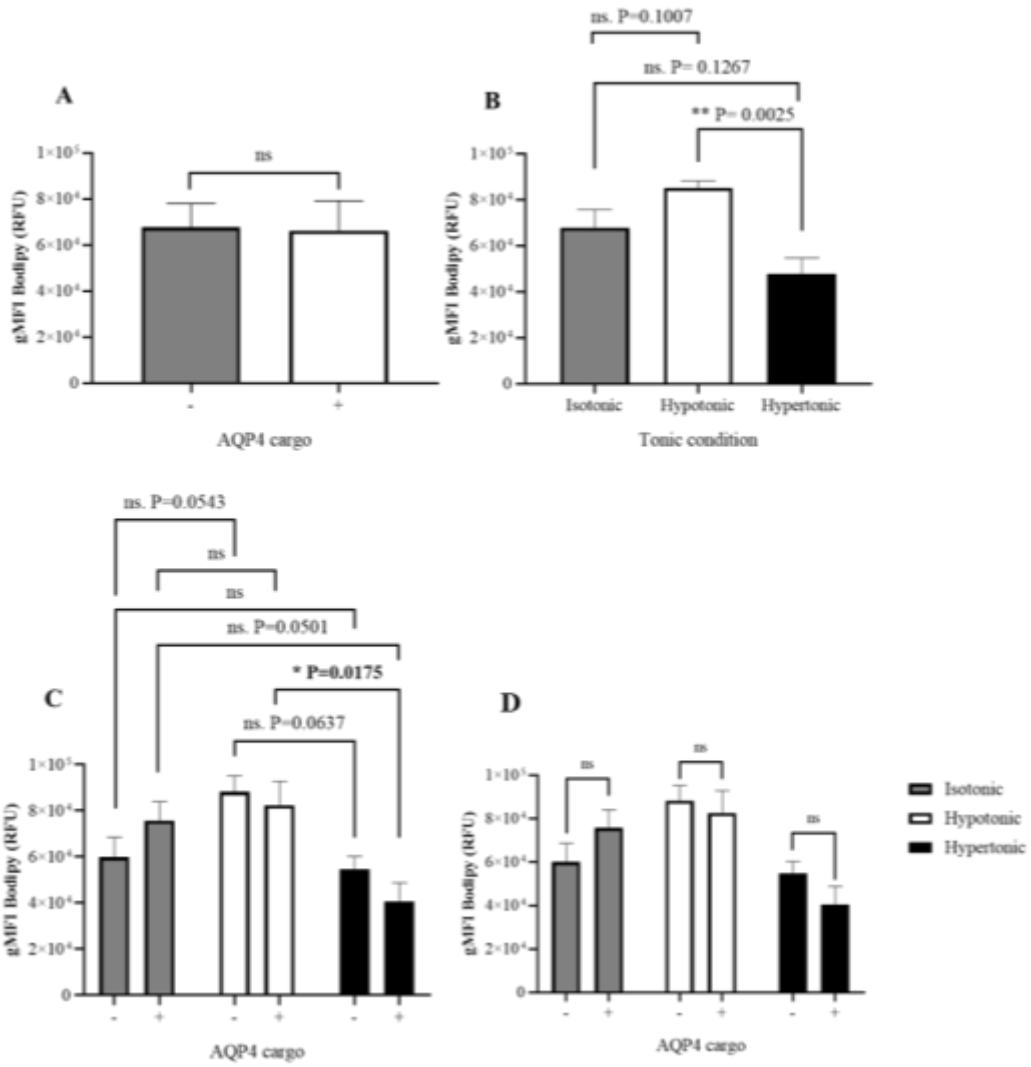

Figure 5.13 gMFI of BODIPY labelling of EV derived from HeLa cells

BODIPY-FL labelling of HeLa-derived EV was measured using VSSC flow cytometry. Green fluorescence emission of BODIPY from EV sized particles was detected and quantified as relative fluorescence units (RFU). All panels show geometric mean green fluorescence emission by EV and the standard error of the mean. All isotonic and hypotonic data are n=6. Hypertonic data are n=3. (A) Tonic condition data was combined to detect differences between AQP4-positive and AQP4-negative EV populations. Data were analysed using a Welch's T-test to compare means. (B) AQP4-positive and AQP4-negative data were combined to detect differences between tonic conditions. Data were analysed using 2-way ANOVA and Tukey's multiple comparison test. (C) Tonic conditions and AQP4 cargo were plotted individually, only experimental repeats were combined. Data from individual cell lines were compared across tonic conditions using by 2-way ANOVA and Sidak's multiple comparison test. (D) Tonic conditions and AQP4 cargo were plotted individually, only experimental repeats were combined. Data from different cell lines were compared in each tonic condition using by 2-way ANOVA and Sidak's multiple comparison test. *=p< 0.05, **=p< 0.01.

.

To interrogate these findings in more detail, each cell line and tonic condition was analysed individually. First, a two-way ANOVA with Sidak's multiple comparison test was performed to analyse the effect on tonic conditions on each cell line (Figure 5.13 C). When analysed individually, only EV derived from AQP4-positive cells, released in hypertonic stress conditions, showed a significant decrease in gMFI, when compared with EV derived from AQP4-postitive cells, made in hypotonic conditions, P=0.0175. EV derived from AQP4-positive cells, made in isotonic conditions, showed a higher gMFI than EV derived from AQP4-positive cells, made in hypertonic conditions, though this was not statistically significant P=0.0501. EV derived from AQP4-positive HeLa, made in isotonic and hypotonic conditions had showed no significant differences.

When analysed EV derived from AQP4-negative cells did not show significant differences between any conditions. Though, some slight differences were observed; EV derived from AQP4-negative cells, made in isotonic conditions, were compared with EV derived from AQP4-negative-cells made in hypotonic conditions, a slight increase in BODIPY labelling was observed and a P value of 0.0543 was calculated. EV derived from AQP4-negative-cells made in hypotonic conditions were compared with EV derived from AQP4-negative cells made in hypertonic conditions, a decrease in BODIPY labelling was observed, though again this was not statistically significant, P=0.063. No significant differences were observed between EV derived from AQP4-negative cells made in isotonic and hypotonic conditions.

The gMFI of AQP4-positive and EV derived from AQP4-negative cells in each tonic condition was calculated and compare (Fig 5.13 D). A two-way ANOVA with Sidak's multiple comparison test was performed where gMFIs of EV derived from AQP4-negative cells counts were compared with gMFIs of EV derived from AQP4-positive cells counts in each tonic condition. No significant differences were observed between cell lines in any tonic condition.

In conclusion, the data show that EV derived from HeLa cells, made in hypertonic conditions, appear to label with less BODIPY than EV made in isotonic and hypertonic conditions, independent of the presence or absence of AQP4 (Figure 5.13 B). There are a number of possible explanations for this.

As 92-97% of all eukaryotic proteins contain cysteine residues, on which free thiol groups are found. It is possible to assume that the amount of BODIPY labelling corresponds with the number of cysteine residues or amount of protein present in EV. Lower labelling EV released in hypertonic conditions may mean that fewer cysteine

residues are present in EV released in hypertonic conditions. It is possible that fewer cysteine-containing proteins are in these EV but, as most proteins contain cysteine residues, it is more likely that less protein is present EV released in hypertonic conditions. It has been shown that the concentration of protein in EV is altered in EV released in different conditions (Busatto et al., 2021, Ovchinnikova et al., 2021).

5.3.1.3 Annexin-V labelling of HeLa EV

5.3.1.3.2 Annexin-V labelling of HeLa EV- percentage population

Annexin-V labelling of EV derived from AQP4-positive and AQP4-negative HeLa cell lines were compared by combining tonic stress data and analysing using the Welch's t-test. No significant differences were seen in the percentage of EV labelled with Annexin-V between AQP4-positive and AQP4-negative HeLa-derived EV (Figure 5.14 A).

Next the percentage of positively labelled EV, released in different tonic conditions was calculated; AQP4-negative and EV derived from AQP4-positive cells data were combined (Figure 5.14 B). A two-way ANOVA and Tukey's multiple comparison test, where each tonic condition was compared to every other tonic condition, was used to determine statistical significance of differences between conditions. No significant differences were seen in the percentage of EV labelled with Annexin-V in hypotonic conditions when compared with isotonic, control conditions. No significant differences were observed between isotonic and hypertonic conditions. No significant differences were observed between hypotonic and hypertonic conditions.

To interrogate these findings in more details, by identifying differences in individual cell lines between different tonic conditions, a two-way ANOVA with Sidak's multiple comparison test was performed (Figure 5.14 C). When analysed individually, no significant differences were observed. When analysed, EV derived from AQP4-negative cells did not show significant differences between any conditions. No significant differences were observed between isotonic, and EV released in hypotonic conditions derived from AQP4-negative cells.

The mean percentage of Annexin-V labelled, AQP4-positive and EV derived from AQP4-negative cells was calculated in each tonic condition (Figure 5.14 D). A two-way ANOVA with Sidak's multiple comparison test was performed where percentages of positively labelled EV derived from AQP4-negative cells were compared with

percentages of EV derived from AQP4-positive cells counts in each tonic condition. No significant differences were observed between cell lines in any tonic condition.

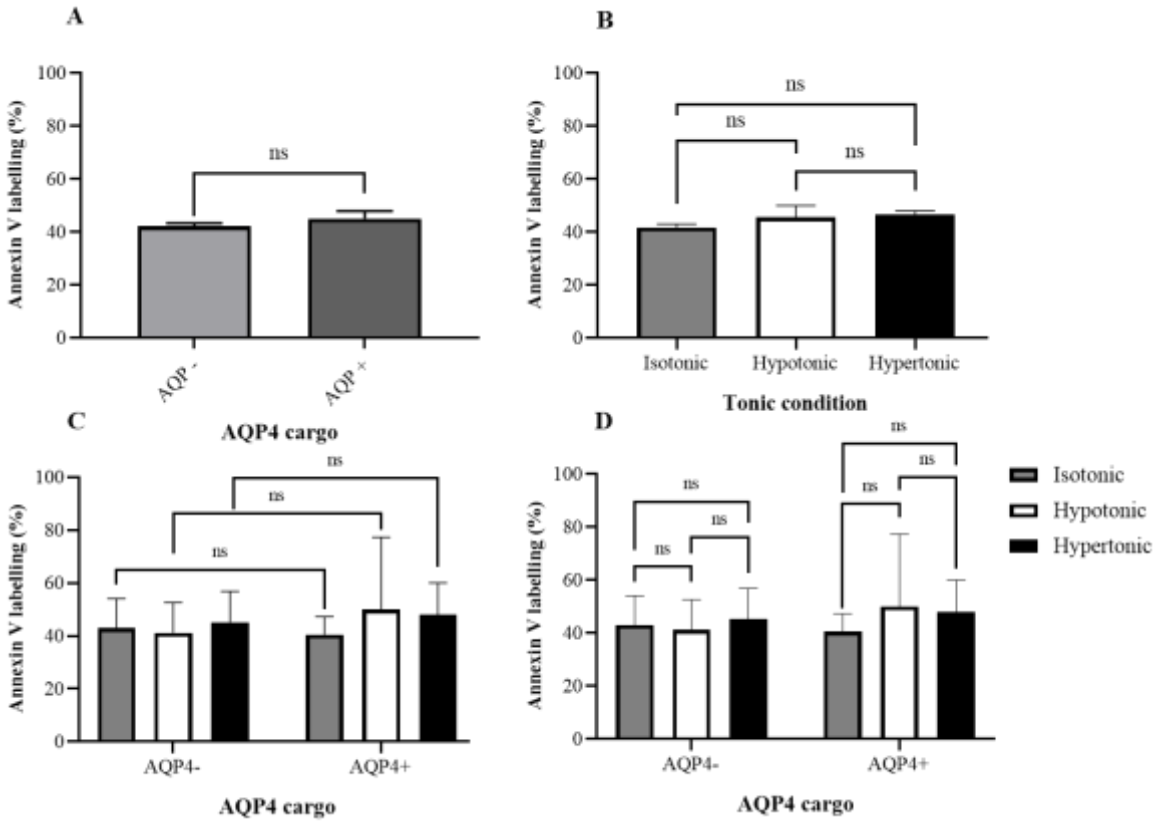

Figure 5.14 Annexin V APC labelling of EV derived from HeLa cells- Percentage Population

Annexin V APC Labelling of HeLa-derived EV was measured using VSSC flow cytometry. EV positive for emission of red fluorescence (Annexin V APC) were detected and counted. Number of EV with red fluorescence was shown as a percentage of the EV population. All panels show mean percentage of Annexin V labelled EV and standard error. All data are n=3. (A) Tonic condition data were combined to detect differences between AQP4-positive and AQP4-negative EV populations. Data were analysed using a Welch's T-test to compare means. (B) AQP4-positive and AQP4-negative data were combined to detect differences between tonic conditions. Data were analysed using 2-way ANOVA and Tukey's multiple comparison test. (C) Tonic conditions and AQP4 cargo were plotted individually, only experimental repeats were combined. Data from individual cell lines were compared across tonic conditions using by 2-way ANOVA and Sidak's multiple comparison test. (D) Tonic conditions and AQP4 cargo were plotted individually, only experimental repeats were combined. Data from different cell lines were compared in each tonic condition using by 2-way ANOVA and Sidak's multiple comparison test.

In conclusion, the data show that there are no significant differences in the percentage of EV derived from HeLa cells that label positively with Annexin-V. The values calculated in this study align with those of previous studies, showing that around 60% of HeLa populations label positively with Annexin-V, which reflected unpublished findings of other research group members. It does not appear that the presence or

absence of AQP4, or that any of the tonic conditions in which EV are made, alter the percentage of EV that were labelled with Annexin-V.

5.3.1.3.3 Annexin-V labelling of HeLa EV- gMFI

The gMFI of Annexin-V labelled EV derived from HeLa cells was calculated for each population. Similar numbers of EV appeared to label with Annexin-V all EV populations, but the amount of labelling per EV, must also be considered. Increases in gMFI of Annexin-V correspond with increased Annexin-V labelling (Figure 5.15). gMFI for all tonic conditions were combined and gMFI values of Hela derived from AQP4-positive and AQP4-negative cells were compared, regardless of tonic condition. gMFI were analysed using a Welch's t-test. No significant differences were seen in Annexin-V Maleimide labelling of AQP4-positive and EV derived from AQP4-negative cells (Figure 5.15 A).

Next, the gMFI of EV released in difference tonic conditions was calculated, irrelevant of their possible AQP4 content. AQP4-negative and EV derived from AQP4-positive cells data were combined (Figure 5.15 B). A two-way ANOVA and Tukey's multiple comparison test was used to determine statistical significance of differences between tonic conditions. No significant differences were seen between conditions.

Each cell line and tonic condition were analysed individually. A two-way ANOVA with Sidak's multiple comparison test was performed to analyse the effect on tonic conditions on each cell line (Figure 5.15 C). No significant differences were observed. The gMFI of AQP4-positive and EV derived from AQP4-negative cells in each tonic condition was calculated and compared (Fig 5.15 D). A two-way ANOVA with Sidak's multiple comparison test was performed where gMFIs of EV derived from AQP4-negative cells counts were compared with gMFIs of EV derived from AQP4-positive cells counts in each tonic condition. No significant differences were observed between cell lines in any tonic condition.

In conclusion, the data show that there are no significant differences in Annexin-V labelling of EV derived from HeLa cells. Both the percentage data and the gMFI values suggest that neither the cell line, nor the tonic condition affect EV labelling with Annexin-V. This in turn suggests that available PS is similar or the same across all conditions.

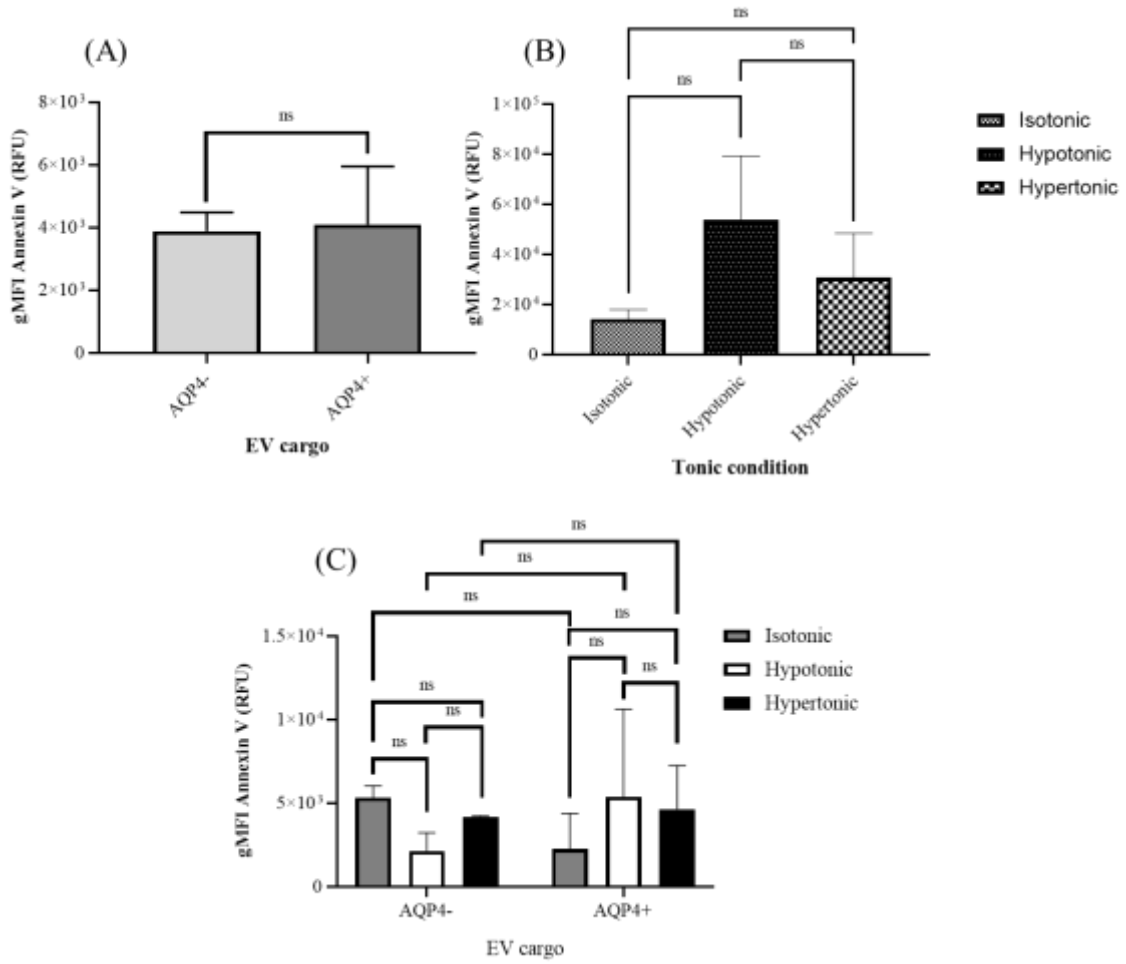

Figure 5.15 Annexin V APC labelling of EV derived from HeLa cells - gMFI

Annexin V APC Labelling of HeLa-derived EV was measured using VSSC flow cytometry. EV positive for emission of red fluorescence (Annexin V APC) were detected and fluorescence intensities were quantified. Red fluorescence was quantified as gMFIs. All panels show the gMFI of Annexin V labelled EV and standard error. All data are n=3. (A) Tonic condition data were combined to detect differences between AQP4-positive and AQP4-negative EV populations. Data were analysed using a Welch's T-test to compare geometric means. (B) AQP4-positive and AQP4-negative data were combined to detect differences between tonic conditions. Data were analysed using 2-way ANOVA and Tukey's multiple comparison test. (C) Tonic conditions and AQP4 cargo were plotted individually, only experimental repeats were combined. Data from individual cell lines were compared across tonic conditions using by 2-way ANOVA and Sidak's multiple comparison test. (D) Tonic conditions and AQP4 cargo were plotted individually, only experimental repeats were combined. Data from different cell lines were compared in each tonic condition using by 2-way ANOVA and Sidak's multiple comparison test.

5.3.2 HeLa EV release quantification

The number of EV released by AQP4-positive and AQP4-negative HeLa cells was quantified. It has been shown that external changes, such as hypoxia, acidity and starvation, can trigger and increase EV release by cells and can reflect the health and/ or state of the cells from which they are derived (Debbi et al., 2022). To determine whether hypotonic or hypertonic stress increase EV release by HeLa cells, BODIPY labelled EV were counted using UV-SSC FC. EV counts for each condition were normalised to corresponding cell counts, measured using flow cytometry. The total number of EV per condition was calculated and normalised to the total number of cells. This was expressed as EV released/ cell (Figure 5.16).

HeLa EV counts were analysed in multiple ways as above. Mean EV counts for all tonic conditions were combined and possible differences between cell lines, independent of tonic stress, were analysed using a Welch's t-test. No significant differences were seen between the number of EV released by AQP4-positive and AQP4-negative cell lines (Figure 5.16 A).

Next the number of EV released in difference tonic conditions was calculated, data from EV derived from AQP4-negative and AQP4-positive cells were combined to analyse tonic conditions, irrespective of AQP content (Figure 5.16 B). A two-way ANOVA and Tukey's multiple comparison test, where each tonic condition was compared to every other tonic condition, was used to determine statistical significance of differences between conditions. No significant differences were seen in the number of EV released by cells in hypotonic conditions when compared with EV counts from isotonic, control conditions. Significant differences were observed between hypertonic and isotonic conditions (P=0.0415) and between hypertonic and hypotonic conditions (P=0.0310).

Differences in EV release by AQP4- positive and AQP4 negative cell lines were analysed with a two-way ANOVA with Sidak's multiple comparison test was performed (Figure 5.16 C). Though an increase in the mean number of EV released by AQP4-negative cells was observed in hypertonic conditions compared to isotonic and hypotonic conditions, these differences were not statistically significant. P values were 0.0901 and 0.0747, respectively. No differences were observed in numbers of EV released by AQP4-negative cells in isotonic and hypotonic conditions. AQP4-positive cell EV release followed the same pattern as AQP4-negative cells, where an increase in numbers of EV released was observed in hypertonic conditions compared to isotonic

and hypotonic conditions. These increases were not statistically significant, P values were 0.2611 and 0.2241, respectively. No differences were observed in numbers of EV released by AQP4-positive cells in isotonic and hypotonic conditions.

Any differences in the number of EV released between AQP4-positive and AQP4-negative cells in different tonic conditions were analysed (Figure 5.16 D). A two-way ANOVA with Sidak's multiple comparison test was performed where means of EV derived from AQP4-negative cells counts were compared with means of EV derived from AQP4-positive cells counts in each condition. No significant differences were observed between cell lines in any tonic condition.

In conclusion, more EV are released in hypertonic stress conditions than in isotonic and hypotonic conditions. This increase in EV release is not dependent on AQP4 expression. This suggests that HeLa cells are more sensitive to hypertonic stress than hypotonic stress. HeLa cells express endogenous AQP water channel, AQP1 (Pellavio et al., 2017) therefore, both WT and AQP4 HeLa express water channel AQP. It is possible that HeLa cells are not sensitive to hypotonic stress because they express endogenous AQP1 (Pellavio et al., 2017) that protects them in hypotonic conditions. This could account for the lack of increase in EV release observed in hypotonic conditions when compared to hypertonic conditions in both AQP4-negative and AQP4-positive cells.

Cell counts, for both AQP4 negative and AQP4-positive cells, are lower after hypertonic stress. The number of EV released following hypertonic stress increased significantly compared to other conditions. As EV numbers are normalised to cell counts, the number of EV released per cells were higher. Upon analysis of EV populations, EV produced in hypertonic conditions were consistently more concentrated than EV produced in isotonic and hypotonic conditions, before any normalisation, suggesting that the increase in EV release is not purely because of a reduction in cell number.

5.3.3 HeLa EV size estimation

The mean size AQP4-positive and AQP4-negative HeLa EV, made in isotonic, hypotonic, and hypertonic conditions was measured using UV-SSC FC , and nano-flow cytometry (Nano FCM).

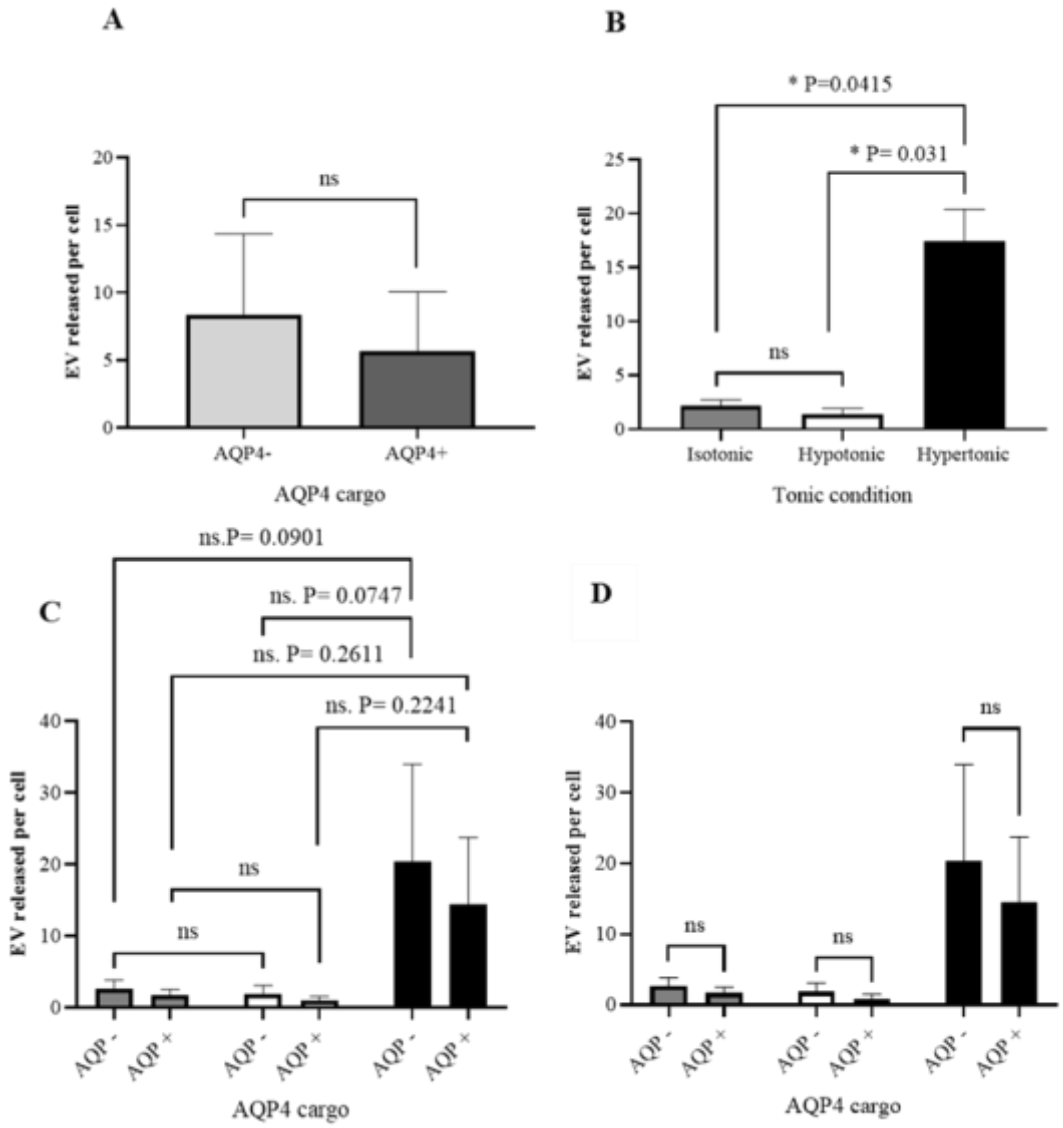

Figure 5.16 EV derived from HeLa cells counting by VSSC Flow Cytometry

EV derived from HeLa cells were counted using VSSC flow cytometry. EV positive for BODIPY-FL were detected and counted. The number of EV shown as the mean number of EV released per cell. All panels show mean number of EV released and the standard error. Isotonic and hypotonic data are n=5. Hypertonic data are n=3 (A) Tonic condition data were combined to detect differences between AQP4-positive and AQP4-negative EV populations. Data were analysed using a Welch's T-test to compare means. (B) AQP4-positive and AQP4-negative data were combined to detect differences between tonic conditions. Data were analysed using 2-way ANOVA and Tukey's multiple comparison test. (C) Tonic conditions and AQP4 cargo were plotted individually, only experimental repeats were combined. Data from individual cell lines were compared across tonic conditions using by 2-way ANOVA and Sidak's multiple comparison test. (D) Tonic conditions and AQP4 cargo were plotted individually, only experimental repeats were combined. Data from different cell lines were compared in each tonic condition using by 2-way ANOVA and Sidak's multiple comparison test. *=$p<0.05$.

5.3.3.1 HeLa EV mean size -UV-SSC FC

The mean size of AQP4-negative and AQP-4 positive EV derived from HeLa cells, made in isotonic, hypotonic, and hypertonic conditions was measured. The size of EV can give insight into how EV are released; exosomes, for example, are typically smaller than microvesicles. Apoptotic blebs may also be released in stress condition and are generally larger than both types of EV. EV populations were identified and counted using UV-SSC FC. The mean UV-SSC values, which corresponds with EV size (Bohren, 2008), was calculated for all conditions, and compared using a variety of statistical analyses (Figure 5.17).

The size of HeLa-derived EV populations was analysed in multiple ways, as above. EV derived from cells AQP4-negative and AQP4-positive HeLa were compared. UV-SSC data from all tonic conditions was combined and compared. Data were analysed using Welch's t-test. No significant differences in size were seen between AQP4-positive and AQP4-negative HeLa-derived EV (Figure 5.17 A).

Next, the mean UV-SSC of EV released in different tonic conditions was calculated. AQP4-positive and negative EV data were combined (Figure 5.17 B). A two-way ANOVA and Tukey's multiple comparison test of column data, where each tonic condition was compared to every other tonic condition, was used to determine statistical significance of differences between conditions. No significant differences were seen in the size of EV in any tonic conditions.

To interrogate these findings in more detail and identify differences in EV release of individual cell lines and tonic conditions, a two-way ANOVA with Sidak's multiple comparison test was performed (Figure 5.17 C). No significant differences were observed between tonic conditions for either AQP4-positive or AQP4-negative cells.

The mean size of EV for each cell line was in each tonic condition. A two-way ANOVA with Sidak's multiple comparison test was performed where means of EV derived from AQP4-negative cells counts were compared with means of EV derived from AQP4-positive cells counts in each condition (Figure 5.17 D). No significant differences were observed between cell lines in any tonic condition.

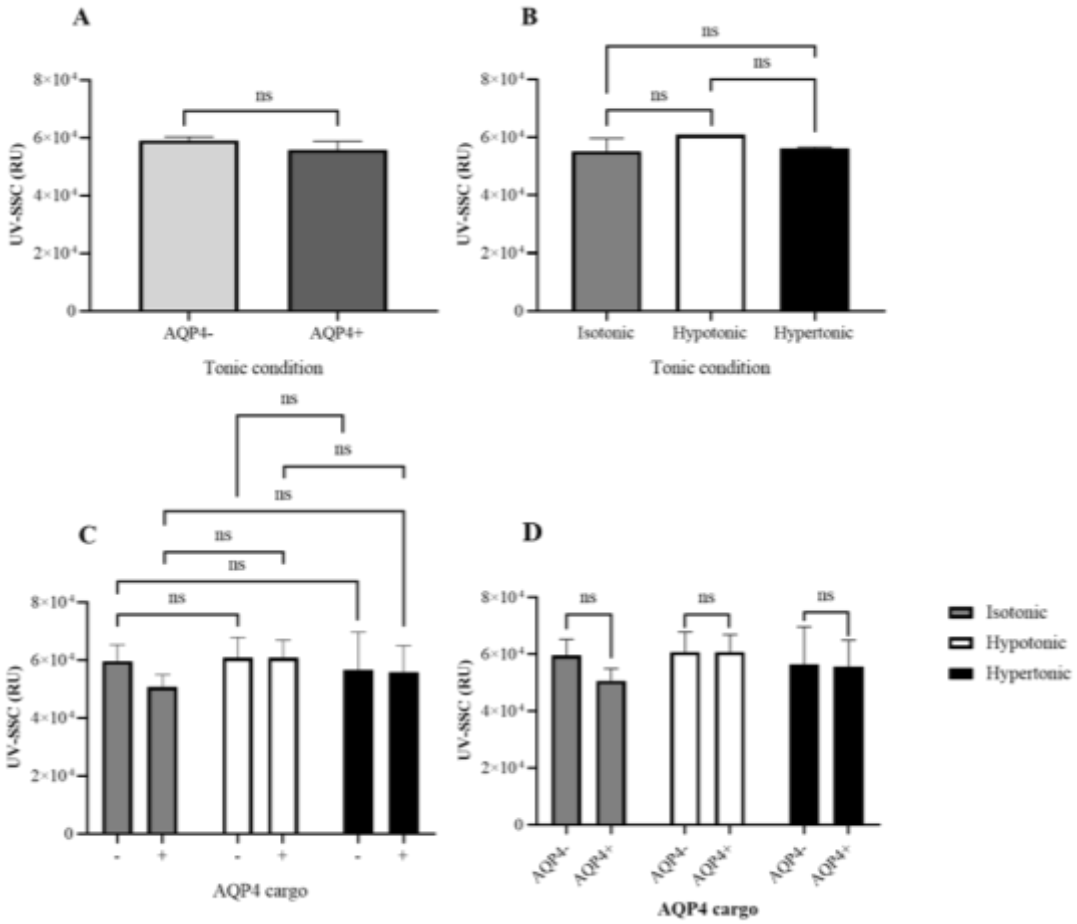

Figure 5.17 Mean size of EV derived from HeLa cells – VSSC Flow cytometry.

EV derived from HeLa cells were detected using VSSC flow cytometry. The mean VSSC values of EV populations were calculated. All panels show mean VSSC values and the standard error. Isotonic and hypotonic data are n=6. Hypertonic data are n=3 (A) Tonic condition data were combined to detect differences between AQP4-positive and AQP4-negative EV populations. Data were analysed using a Welch's T-test to compare means. (B) AQP4-positive and AQP4-negative data were combined to detect differences between tonic conditions. Data were analysed using 2-way ANOVA and Tukey's multiple comparison test. (C) Tonic conditions and AQP4 cargo were plotted individually, only experimental repeats were combined. Data from individual cell lines were compared across tonic conditions using by 2-way ANOVA and Sidak's multiple comparison test. (D) Tonic conditions and AQP4 cargo were plotted individually, only experimental repeats were combined. Data from different cell lines were compared in each tonic condition using by 2-way ANOVA and Sidak's multiple comparison test.

In conclusion, there were no significant differences in sizes of EV released by AQP4-positive and AQP4-negative cells. Neither AQP4 expression nor tonic stress changed the mean size of EV released. If the size of EV does correspond with the type of EV released by HeLa cells, then according to these findings, the type of EV released is not altered by AQP4 expression or by hypotonic or hypertonic stress.

According to this method EV are released within both the **size** range of exosomes and microvesicles across all populations. These findings are not however exhaustive; the limitations of the analysis method must be considered when interpreting these data. EV sizes are estimated based on the size of calibration beads, these are made of polystyrene and have a different refractive index, as discussed earlier. In addition, the sensitivity of the method limits the detection of smaller particles, with the smallest particles reliably detected being 100nm, a limitation of conventional and UV-SSC FC. While this method of EV detection can give a measure of EV size, more accurate particle sizing methods are available.

5.3.3.2 HeLa EV mean size -nano-flow cytometry

The mean diameters of EV release from HeLa cell populations were investigated using nano-flow cytometry (Figure 5.18). This technique is capable of estimating particle size with more accuracy than UV-SSC FC.

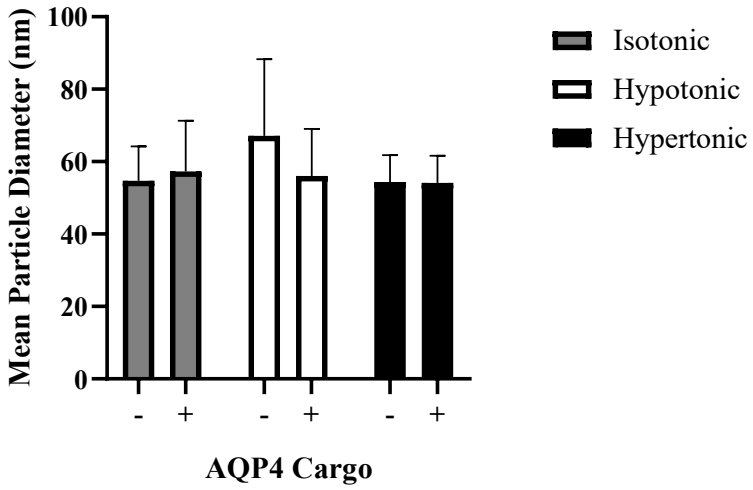

Figure 5.18 Mean Size of EV derived from HeLa cells – Nano FCM

Bar chart shows the mean particle diameter of EV released by AQP4 -positive and AQP4-negative HeLa cells released in isotonic, hypotonic, and hypertonic conditions, measured by nano-flow cytometry. n=1

Nano-flow cytometry was performed with the aim of strengthening EV size data. UV-SSC FC detection of particles can estimate their size based on calibration with fluorescent polystyrene beads. As discussed earlier, there are limitations to this method that affect the accuracy of size estimation. Nano-flow cytometry overcomes some of these limitations using sensitive detectors and smaller flow volumes. This technique also estimates particle size by calibration against beads. The data show no significant

differences in particle diameter between EV populations, though it must be considered that this data is n=1. Overall, the mean diameter of particles appeared to be lower than the mean diameter estimated by UV-SSC FC.

5.3.4 HeLa EV- THP-1 interaction

Interactions and uptake of HeLa -derived EV by macrophage cells (THP-1) were investigated to see whether there are any differences in interaction properties between EV populations. One important role for EV is in communication, where they interact with, are taken up and processes by neighbouring cells. It has been shown that interaction of immune cells with EV can illicit or dampen immune responses *in vivo*. Interaction of macrophage cells with EV can activate macrophage cells, switching their phenotype and initiating inflammatory cascades. The first steps in this process are the interaction and uptake of EV by macrophages. Flow cytometry was used to identify green fluorescence in differentiated THP-1 cells. Upon interaction with BODIPY labelled EV, THP-1 should become fluorescent. This increase in fluorescence can be detected. THP-1 cells were incubated with EV populations and green fluorescence in cells was quantified. The percentage of THP-1 populations with green fluorescence and the gMFI of THP-1 cells was measured and analysed. The gMFI of cell populations were normalised to the gMFI of control THP-1 populations without EV incubation. No significant differences were observed between control THP-1 cells and THP-1 cells incubated with any HeLa EV population (Figure 5.19).

There were a number of attempts to optimise this experiment to increase interaction between EV populations and THP-1 cells, in order to identify any differences between populations. Incubation times were increased. Cells were incubated for 5, 15, 30 and 45 minutes before measurement, but no differences in uptake were observed. In the data presented cells were incubated with EV at a 1:10 ratio, this ratio was increase to 1:20, 1:40 and 1:80 but not difference in EV uptake were observed. It is not known why no interaction or uptake was observed, it is possible that fluorescence was lost in the EV uptake process. Labelling EV with a different fluorophore and live cell fluorescence imaging may help to elucidate this.

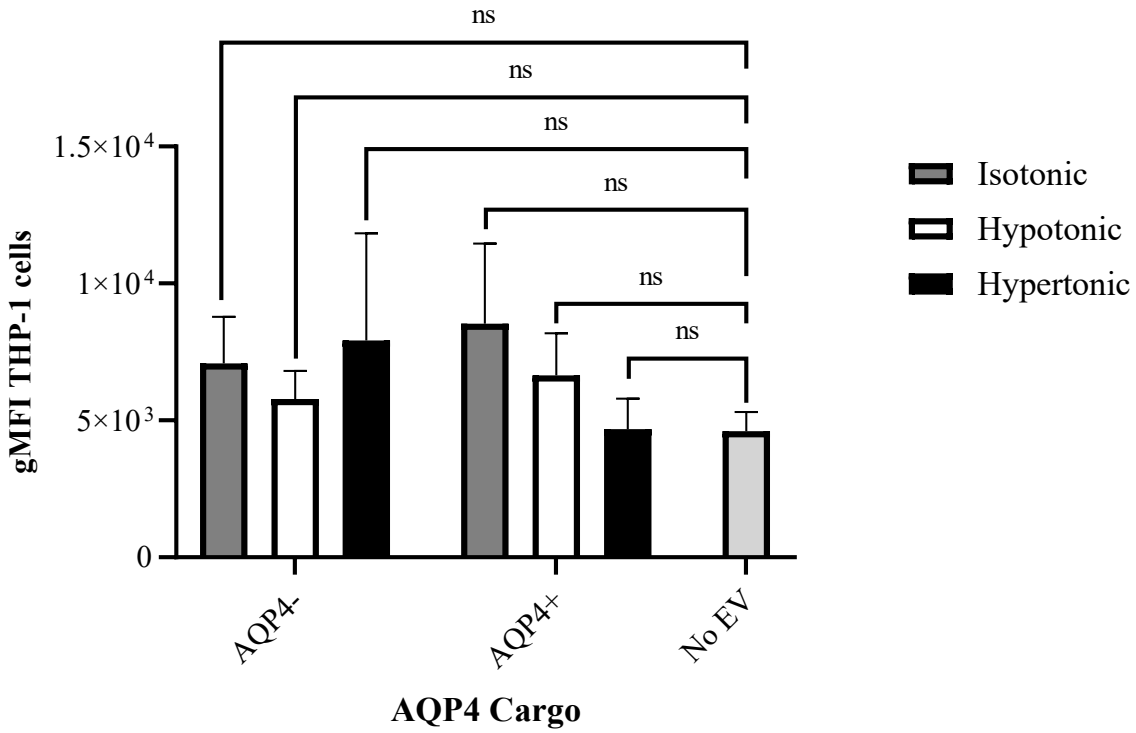

Figure 5.19 Interaction of EV derived from HeLa cells with THP-1 cells

Flow cytometry was used to measure the interaction between BODIPY FL- labelled EV and THP-1 cells. Green fluorescence accumulation in THP-1 cells was measured and quantified as mean green fluorescence of THP-1 populations. The mean green fluorescence intensity of control THP-1 cells, with no exposure to EV, was measured and compared to the mean green fluorescence intensity of cells incubated with EV. Data from different cell lines were compared in each tonic condition using by 2-way ANOVA and Sidak's multiple comparison test.

5.4 Discussion

A number of experiments were conducted to characterise and investigate the potential roles of AQP4-containing EV released in different tonic conditions. Some differences in EV populations were identified. AQP4 presence in MDCK EV was confirmed and correlated with the amount of AQP4 protein observed in the cells from which the EV are derived. GFP release was detected using UV-SSC FC and Nano-flow cytometry.

BODIPY labelling of EV was measured and quantified (Figure 5.2 & 5.13). Differences were observed in both HeLa and MDCK-EV populations. Less BODIPY labelling was observed in EV released in hypertonic conditions. It is possible that hypertonicity reduces the number of free thiols and consequently results in reduced levels of. The reduction in free thiols may be due to the increased release of ROS by stressed cells, which binds to and oxidises free thiol groups, thus inhibiting BODIPY binding (St-Louis et al., 2012).

The number of EV released in each condition was counted (Figure 5.6 & 5.16). EV counts were normalised to cell counts and presented as the number of EV released per cell. All EV were collected after a 4h incubation, so this is the number of EV released per cell in 4 hours. Differences in the EV released rate were observed. HeLa cells released significantly more EV in hypertonic conditions compared to isotonic and hypotonic conditions. The presence or absence of AQP4 in HeLa did not affect this result. It was hypothesised that the presence of water channel proteins in both WT and AQP4 HeLa cells had a protective effect in hypotonic conditions, allowing volumetric regulation, and so increased numbers of EV were not observed. Hypertonicity appeared to increase stress in cells and subsequently EV release.

The average size of EV was estimated using UV-SSC FC (Figures 5.7 & 5.17). Differences were observed only in MDCK-EV, where M23 EV were significantly larger than WT and M1 EV. Only one other recent publication identifies AQP4 M23 in EV (Simone et al., 2022) this paper confirms the presence of AQP4 M23 in glial-derived EV, in a range of sizes. It does not count the number of EV in each size fraction collected but it does seek to quantify the amount of AQP4-M23 in each fraction. Not surprisingly, more M23 is detected in larger vesicles.

MDCK released similar numbers of EV in isotonic and hypertonic conditions. Increased levels of EV release were observed in hypotonic conditions. When cell lines and tonic conditions were analysed individually, the data show that WT MDCK cell, containing no functional water channels, released significantly more EV in hypotonic conditions than M1-AQP4 expressing cells. This is an interesting finding which suggests that the presence of M1 in MDCK cells has a protective effect in hypotonic environments. It is hypothesised that AQP4 provides volumetric regulation capabilities in MDCK cells. It is plausible that WT MDCK release increased numbers of EV in hypotonic environments to control cell volume. A theory that has been suggested in other studies (Blanc et al., 2009)

The average size of EV was initially measured using UV-SSC FC. No differences in mean EV size were observed, other than that EV derived from M23 positive MDCK cell populations were significantly larger than EV derived from WT and M1 MDCK populations, when analysed using UV-SSC FC. The same observations were not made from nano-flow cytometry data.

MDCK EV containing M1 AQP4, produced in isotonic and hypotonic conditions, interacted more with THP-1 macrophage cells than all other EV populations, suggesting M1 presence in EV increases macrophage uptake (Figure 5.19).

In conclusion, a variety of experiments were performed to characterise EV and identify potential roles for AQP4.

Chapter 6 - Discussion

The overall aim of this thesis was to characterise AQP4 in both intracellular and EV, the connection between these two mechanisms has been summarised in Figure 6.1. Identifying AQP4 trafficking between the astrocyte cell surface and intracellular vesicles *in vivo* required the development of robust imaging methods. The characterisation of AQP4 in EV required the development of *in vitro* models that would enable the first quantitative analysis of EV from AQP4-positive cells.

6.1 General Discussion

Subcellular AQP4 localisation following SCI.

In order to determine whether there were any observable differences in the subcellular localization of AQP4 *in vivo*, a rat spinal cord injury model was used. Previously, it had been observed *in vitro* that TFP, a CaM inhibitor, and H89, a PKA inhibitor, prevented translocation of AQP4 from intracellular vesicles to the plasma membrane in response to changes in extracellular tonicity that somewhat mimic changes observed following ischemic injury (Kitchen et al., 2020, Salman et al., 2017). These observations had been made in *in vitro* models but needed to be confirmed in an *in vivo* model. A rat spinal crush injury model was used to investigate AQP4 expression and localisation by IHC and confocal microscopy. A large part of this project involved optimisation of this technique to ensure successful labelling and image analysis.

AQP4 is expressed throughout astrocytes in rat spinal cord tissue and expression increases following SCI. IHC and confocal microscopy confirmed AQP4 expression in rat spinal cord tissue (Figure 3.2). GFAP labelling and DAPI staining were used to confirm the location of astrocytes. AQP4 was identified in the membranes of astrocytic cell bodies, processes and endfeet (Figure 3.5). Difficulties were encountered in identifying different parts of astrocytes due to their 3D nature and star shape. Cell bodies were easily identified by the presence of nuclei labelled by DAPI but processes and endfeet could not be distinguished from one another. It appeared that cell bodies and processes overlapped and so accurate quantification of AQP4 expression at the subcellular level was not possible. AQP4 expression was quantified in 2D images, the mean fluorescence value for each image was calculated and compared (Figure 3.4). AQP4 expression increased following SCI but this was not seen in tissue treated with TFP or H89 (Figure 3.4). Previously, it had been shown that AQP4 is expressed

specifically at astrocytic endfeet (Nielsen et al., 1997b). This present study identified AQP4 expression throughout the plasma membrane of astrocytes, including endfeet, cell bodies, and processes. It was hypothesized that the endfoot localisation of AQP4 to astrocytic endfeet was important in the movement of water into astrocytes following injury. Here AQP4 was identified throughout astrocytes. In order to investigate the hypothesis further, AQP4 localisation following injury was calculated. AQP4 is localised to astrocytic endfeet following crush injury. This study showed increased concentration of AQP4 at the endfeet of astrocytes in rat spinal cord tissue following injury (Figure 3.8). IHC and confocal microscopy showed increased AQP4 expression around vascular endothelial cells following SCI (Figure 3.8). Identification of endfeet was a difficult process that required a number of optimisation steps. An image analysis protocol was devised, whereby endfeet were identified based on their proximity to endothelial cell labelling (Figure 3.9). Aspects of this method could have been improved to remove subjectivity and increase accuracy, such as the manual selection and drawing of ROIs that identified and quantified endfeet. Nonetheless, the results of this experiment clearly showed differences between AQP4 localisation to endfeet prior to and following SCI (Figure 3.10). This correlates well with previous studies that have identified AQP4 in endfeet and demonstrated that AQP4 is responsible for movement of water into the brain. (Haj-Yasein et al., 2011). This finding supports the hypothesis that the localisation of AQP4 to astrocytic endfeet is a potential target for reduction of injury associated oedema.

AQP4 endfoot localisation following SCI was inhibited following treatment with TFP and H89. AQP4 localisation in rat spinal cord tissue, treated with either TFP or H89 was quantified using the method described above. No increase in endfoot expression of AQP4 following treatment with TFP or H89 was observed. This showed inhibition of endfoot localisation of AQP4 following treatment with either TFP or H89. No significant differences were observed between the uninjured control tissue and treated tissue. Significant differences were observed when compared with injured, untreated tissue (Figure 3.8). Following publication of these findings (Kitchen et al., 2020), a number of studies have shown possible therapeutic uses for TFP in the reduction of oedema in CNS pathologies including stroke (Sylvain et al., 2021), apoptosis and inflammation (Xing et al., 2023) and epilepsy (Szu and Binder, 2022). H89 had previously been identified as an inhibitor of AQP4 phosphorylation, and subsequent membrane relocalisation, by PKA in gastric cells (Carmosino et al., 2007) and astrocytes *in vitro* (Kitchen et al., 2015b). The results of this study confirm and expand on previous

finding, confirming the AQP4 the AQP4 trafficking mechanism and roles of CaM and PKA *in vivo*. Possible clinical uses for H89 are less likely; PKA inhibition is a broad effect that could have multiple negative side effects. These findings are in line with the hypothesis that TFP and H89 treatment would prevent the relocalisation of AQP4 to endfeet following injury.

AQP4 localisation to endfeet correlates with oedema. Further experiments performed by Dr Andrea Halsey, University of Birmingham, and that analysed tissue following SCI showed increased oedema, which was reduced following treatment with TFP or H89 (Kitchen et al., 2020). Animals were also assessed for their ability to walk across a ladder, an assessment of SCI recovery. Animals treated with TFP or H89 recovered significantly more quickly than injured, untreated animals (Kitchen et al., 2020). These findings correlate with previous studies that investigated the role of AQP4 relocalisation in SCI (Manley et al., 2000b, Kimura et al., 2010, Saadoun et al., 2002). These experiments were key in confirming the hypothesis that treatment with TFP or H89 reduces expression and endfoot localisation of AQP4 and subsequent oedema. This solidifies the hypothesis that these agents could be used to target AQP4 and reduce oedema and associated secondary injury following ischemic injury cause by CNS pathologies such as TBI.

Development of a tonicity induce EV release model

AQP4 had previously been identified in EV derived from CNS cells in a number of CNS pathologies and a number of roles for AQP in EV has been proposed (Clarke-Bland et al., 2022). One objective of this thesis was to create an *in vitro* method, by which AQP4 expression and the role of changes in extracellular tonicity, could be analysed in the context of EV production.

Stable cell lines were used for *in vitro* EV release**.** An *in vitro* EV release model was created using MDCK and HeLa cells in order to study possible roles for AQP4 in EV, and possible effects of tonic stress on EV release. An *in vitro* model was chosen for EV release to maximize homogeneity of EV populations. Use of *in vitro* models to produce and analyse EV has been published (Lenzini et al., 2020, Simone, 2022) Other methods, such as isolation of EV from animal and/or human samples produces heterogeneous EV populations, derived from different cell lines, and containing different cargoes. While it has not been shown that all EV released by AQP4-positive cells, contain AQP4, the production of EV from a single cell line with homogeneous AQP4 expression, should reduce EV variation. AQP4 expression in MDCK and HeLa

cells were confirmed, but homogeneity of AQP4 expression was not observed in all cell lines. Variation in the percentage of cells within a population that expressed AQP4-GFP, and in the average intensities of AQP4-GFP expression of individual cells within cell populations, were observed. This was likely to affect the homogeneity of EV populations and was considered when analysing EV release data.

EV release by HeLa and MDCK cells was induced using isotonic, hypotonic, and hypertonic stress. Previously no studies have been published that analyse AQP function in EV and use tonic stress as a release trigger. One study uses hypo and hypertonicity to induce 'exocytosis of vesicles' production by chromaffin cells. This study identifies an increase in vesicles released in hypotonic conditions (Amatore et al., 2007). Another study utilizes hypotonicity to lyse cells for vesicle extraction (Thamphiwatana et al., 2017).

EV were released in serum free medium, to avoid sample contamination with serum-derived vesicles (Wang et al., 2021). Serum starvation triggers EV release (Wang et al., 2021). EV release was observed in all tonic conditions tested, this is presumed to be triggered by serum starvation; it may also be that the cells used release EV at the same rate without serum starvation, though it was not possible to confirm this.

EV are released in response to stress (Ludwig et al., 2020), Specifically EV are release in response to a range of external triggers such as hypoxia, (Bister et al., 2020), serum starvation (Wang et al., 2021) and acoustic waves (Ambattu et al., 2020), to name a few (Debbi et al., 2022). Increased EV release had been observed in multiple CNS pathologies. These pathologies are complex and characterized by multiple changes in the cellular environment, such as physical damage, hypoxia, and extracellular tonicity. In this study, one of these environmental changes, extracellular tonicity, was investigated.

The tonic conditions chosen for this study had been published previously (Conner et al., 2012, Kitchen et al., 2015b). These conditions had shown cell swelling (hypotonic) and cell shrinkage (hypertonic) and trafficking of AQP to and from plasma membranes, respectively. This shows that these conditions illicit a mechanistic

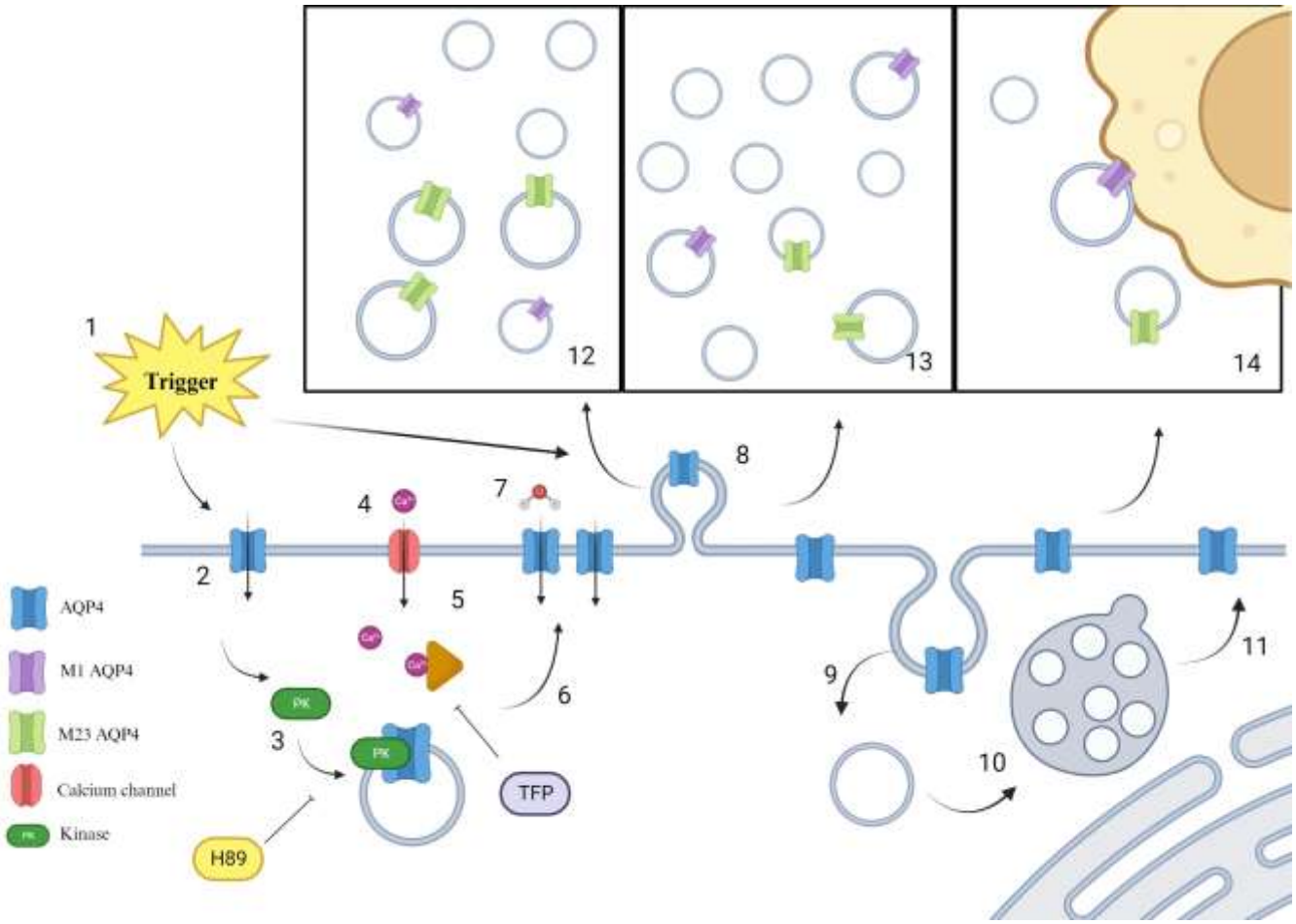

Figure 6.1 Roles for AQP4 in intracellular and extracellular vesicles

Schematic shows the roles for AQP4 in intracellular and EV identified in this study. 1. External triggers such as hypotonicity and hypoxia. 2. water influx into cells through AQP4 in the plasma membrane. 3. Phosphorylation of AQP4 by PKA. 4. Influx of extracellular calcium into cells. 5. Activation of calmodulin. 6. Trafficking of AQP4 in intracellular vesicles to the plasma membrane. 7. Increased water influx into cells. PKA phosphorylation of AQP4 is inhibited by H89. Calmodulin activity is inhibited by TFP. 8. External trigger causes release of microvesicles and 9. Production of exomes by endocytosis. 10. Formation of MVB. 11. Release of exosomes. 12. EV derived from cells expressing M23 AQP4 are larger than WT and M1 EV. 13. WT cells release more EV in hypotonicity. 14. EV from M1 AQP4 cells interact with THP-1 cells.

response that controls the concentration of AQP4 in the plasma membrane, and therefore cell water permeability. In previously conducted experiments, cells were subjected to tonic stress for shorter time periods, around 5 minutes, and changes in cell volume were observed within this time frame.

A 4-hour time period was selected for EV production in this study, a number of studies use this time frame to induce EV release and it is used within the research group to produce apoptotic EV (Essien et al., 2023) (Crescitelli et al., 2013, Di Rocco et al., 2016). On reflection, 4-hour incubation may not have been optimal for EV production using tonic stress as the number of EV released were generally lower than observed in UV-induced EV production. In this study, the maximum number of EV released was ~20EV per cell in 4 hours. Methods that use UV light as a trigger for EV release produce ~10x as many EV in the same time frame. For ease of analysis, higher numbers of EV release are desirable. The literature suggests that EV production, induced using a variety of methods, utilise longer incubation periods, up to 24 hours (Debbi et al., 2022). Though it has not been confirmed, it must be considered that a longer incubation may have allowed for the collection and isolation of higher numbers of EV. It was not known, prior to incubation for EV release, what affect the chosen tonic conditions would have on cells incubated for longer time periods; a 4-hour incubation time was conducted in this study and cells were analysed for signs of stress prior to confirmation of a successful EV release model. While it is possible that the rate of EV would have been increased had a longer incubation time been used, it is also possible that longer incubation periods could have affected cell viability and caused release of more apoptotic vesicles, for example.

To conclude, EV were released during a 4-hour incubation time, incubation of EV for longer time periods may have resulted in increased numbers of EV release and may have also resulted other in changes to EV populations, such as the type of EV released. Testing longer incubation times, assessing cell viability, and analysing EV populations could provide more detailed information about an optimal incubation time.

MDCK and HeLa EV were successfully isolated using SEC. UV-SSC analysis of fractions collected from SEC columns following attempted isolation of EV confirmed isolation of BODIPY- labelled particles within the expected EV size range (Figure 4.7). Second generation (Gen 2) SEC columns from IZON Inc. were used. Initially EV isolation was attempted following the manufacturer's instructions which specified that a

'buffer' fraction of 3 mL should be collected and discarded, followed by a 2 mL 'EV positive' fraction and 3.5 mL 'protein' fraction, which would contain particles smaller than EV. This method did not result in successful isolation of EV; UV-SSC FC analyses of EV fractions identified very few green, fluorescent particles. In order to optimise this protocol, 13 smaller, 0.5 mL fractions were collected consecutively, including the 'buffer', 'EV positive', and 'protein' fractions defined in the manufacturer's protocol (fractions 1-13). These smaller fractions were analysed using UV-SSC FC. Green, fluorescent particles were identified in fractions 5, 6, 7, and 8. The EV isolation method was adapted, and a 2 mL 'buffer' fraction, 2 mL 'EV positive' fraction and 3.5mL 'protein' was collected instead. Hypertonic HeLa EV were not subjected to more detailed analyses of smaller fractions, as this condition was added to the investigation following optimisation of EV isolation. It is assumed that EV derived from HeLa cells, produced in hypertonic conditions are released in fractions 5-8, in line with results of MDCK derived EV release across all tonic conditions (Figures 4.7).

While green, fluorescent particles were observed in samples isolated using SEC, confirmation of EV release required a more exact method, where EV could be visualised, rather than representative events on a dot plot, as seen in UV-SSC FC. This is a more reliable method as it allows visualisation of the morphology particles in samples and rules out the possibility of contamination.

In this study cryoTEM imaging of EV allowed identification of EV, phospholipid bilayers, actin, and surface proteins. EM and cryoTEM are often used to confirm EV presence (Chuo et al., 2018). These techniques are recommended in the Minimal Information for Studies of EV (MISEV) guidelines (Thery et al., 2018). In this study EV were successfully visualised in samples from all cell lines using cryoTEM, confirming EV release from cells (Figure 4.8 & 4.17). EV release by all cell lines was confirmed as EV were visualised in all populations. Confirmation of EV release using cryoTEM is reliable but has its drawbacks, it is not high throughput and is labour intensive and expensive. For this reason, not all tonic conditions were imaged. In order to visualise EV using cryoTEM, samples had to concentrated 200x more than for UV-SSC FC analyses and were still difficult to locate. Other possible observations were made, such as possible interactions between EV containing M1 AQP4, or continued EV release of smaller EV by larger EV. As this experiment was performed only one time, and a limited number of images were taken, this has not been confirmed. Further cryoTEM imaging would need to be performed.

Characterisation of EV

AQP4-GFP release in MDCK EV derived from M1 and M23 MDCK was confirmed (Figure 5.1). Three independent techniques were used to detect AQP4-GFP. Western blot for AQP4 confirmed the presence of AQP4-GFP, with bands visible around 55-60 kDa confirming M1 and M23 AQP4 release in EV. GFP was detected in EV derived from M1 and M23 positive MDCK cells using UV-SSC and nano-flow cytometry techniques. AQP4-GFP release in HeLa derived EV was less clear (Figure 5.12). UV-SSC and nano-flow cytometry showed small differences in GFP detection in EV derived from AQP4-positive HeLa cells. It is not known what differences in HeLa EV populations were difficult to detect. Differences in HeLa cell populations were clear, but this was not reflected in EV. AQP4 detection using western blot was unsuccessful in both cells and EV (data not shown), though GFP detection by western blot was consistently successful and produced a band of around 55-60 kDa, correlating with the size of the AQP4-GFP fusion protein. It was considered, that the AQP4 epitope of the anti-AQP4 antibody used was not accessible, due to changes in protein folding, though this was not confirmed. The inability to detect AQP4 in EV directly using western blot is likely due to the same issue.

In summary, M1 and M23 AQP4-GFP were detected in MDCK EV, and clear differences in AQP4-GFP content was observed when compared to EV released by WT MDCK cells. AQP4-GFP detection in HeLa EV was unreliable. AQP4 could not be detected by western blot and differences in GFP detection using UV-SSC and nano-flow cytometry were small. While differences in the populations do confirm release of AQP4-GFP, they also suggest that overall differences in the AQP4 content of HeLa EV populations may be inconsequential when discussing any differences in EV release by AQP4 positive and WT HeLa cells.

Studies have shown the selective release of AQP into EV, where levels of EV AQP do not correlate with the levels of cellular expression (Oshikawa-Hori et al., 2019). This does not appear to be the case in this instance. The total protein concentration loaded for SDS-PAGE was not quantified. It is presumed that the number of EV in M1 and M23 samples was similar as samples were processed in the same way and M1 and M23 samples consistently contained similar numbers of EV.

BODIPY Maleimide labelling of HeLa derived EV was decreased in EV produced in hypertonic environments, suggesting that hypertonicity changes affect BODIPY-labelling of EV (Figure 5.13). It is thought that free thiol groups, present on proteins in EV membranes will have been oxidised and are no longer available for binding by BODIPY Maleimide (St-Louis et al., 2012). If cells are stressed, they may produce ROS such as H_2O_2 to which, free thiol groups are sensitive. Oxidised thiol groups will not bind to BODIPY Maleimide. Hypertonic stress had been shown to induce oxidative damage in cells and release of ROS (Kultz, 2004, Naziroglu et al., 2013)

BODIPY Maleimide is a dye commonly used to label EV, conferring green fluorescence properties that allow for EV identification against background noise. A reduction in binding of BODIPY Maleimide results in reduced fluorescence properties of EV and may complicate identification of EV. This must be considered when using BODIPY maleimide to identify and quantify EV populations. This experiment does not confirm these findings however, this experiment only identifies a reduction in BODIPY labelling of EV in hypertonic conditions and the literature to support this theory is sparse and there are potentially contradictory findings the show the successful use of hypertonic solutions to reduce oxidative stress *in vivo* (Mojtahedzadeh et al., 2014, Nunes et al., 2021), though the mechanisms of this are not yet fully understood.

Annexin-V labelling, on the other hand, appeared to label all EV populations consistently (Figure 5.4, 5.5, 5.14 & 5.15). Annexin-V labelling of EV is well-established (Perez et al., 2023). These findings suggest that Annexin-V labelling of EV may be a better method of EV identification. Also, that Annexin-V was added following EV isolation by SEC, which introduces the potential for Annexin-V aggregates to be introduced to the sample, and that Annexin-V labelling of BODIPY labelled events was calculated, Annexin-V was not used to identify EV, but Annexin-V labelling of EV was measured. It must also be considered that this technique relies on PS exposure in EV membranes. PS is a phospholipid, abundant in the membranes of eukaryotic cells. PS is exposed, or 'flipped' inside out during apoptosis and acts as and 'eat me' signal, recruiting immune cells (Nagata et al., 2020) and exposed PS has also been identified on EV (Perez et al., 2023). Though there are no observable differences in PS exposure between EV populations in this study, it is interesting that PS is released in EV. Exposure of PS is considered the first step in EV release (Bevers et al., 1983, Fadok et al., 1992, Zwaal and Schroit, 1997). And that the majority, if not all EV, contain exposed PS (Lacroix et al., 2012, Morel et al., 2011). Exposed PS on the outer surface of cells remains exposed when release as EV acting as circulating 'eat me' signals

(Matsumoto et al., 2017). Circulating EV, with no exposed PS are not taken up by macrophages as quickly as EV exposing PS (Matsumoto et al., 2021).

WT MDCK cells released EV at a faster rate than M1 MDCK cells in hypotonic environments (Figure 5.6). This suggests that hypotonicity is a trigger for EV release in cells that do not contain AQP4, or other AQP water channel proteins. It has been shown that most cells do not express aquaporins, as there is no need if membranes are permeable to water and osmotic changes are small (Verkman, 2013). In some pathologies such as ischemic injury however, tonic changes are rapid and it has been proposed that EV are released as a mechanism of cell volume regulation (Blanc et al., 2009), and it is reasonable to consider that AQP-negative cells may release higher numbers of EV in response to extracellular tonicity as a mechanism of volumetric control.

HeLa cells released more EV in hypertonic conditions than isotonic or hypotonic conditions, regardless of AQP4 content, though AQP4 content of EV appeared to be negligible (Figure 5.12). Methods used to detect differences in AQP4-GFP levels in EV derived from AQP4-positivr and AQP4-negative HeLa cells showed only small changes. It may be that there are no significant differences in the amount of AQP released in HeLa EV. It is also possible that any differences were too small to detect using the methods applied in this study. It is possible that the hypertonic condition used caused cell stress and triggered EV release. Hypertonicity shown to affect vesicle production pathways (Carpentier et al., 1989) and intracellular trafficking of AQP2 (Hasler et al., 2008). There is more information around hypoxia and EV. Many studies that assess the effects of hypoxia on EV release do so in cancer cell lines and most studies that measure EV release by hypoxic cells report increases in EV numbers compared to normoxic controls, reviewed here (Bister et al., 2020). There is an important link between hypoxia and extracellular tonicity *in vivo* and following TBI. Hypoxia occurs in tissue following interruption of blood supplies (ischemia) and contributes to oedema severity. Previous studies have shown trafficking of AQP4 in response to hypoxia (Kitchen et al., 2015b, Markou et al., 2022) Hypoxia negatively affects energy dependent solute balances (Bordone et al., 2019), causing cytotoxic oedema and causing water influx into astrocytes and subsequent cell swelling. Use of a model where the tonicity of the extracellular environment is altered is expected to mimic disruption in solute homeostasis caused by hypoxia.

UV-SSC FC analysis of MDCK EV showed an average larger size of EV containing M23 AQP4, when compared with EV derived from WT and M1 MDCK cells (Figure 5.7). Studies that identify M23-AQP4 in EV are limited. Recent published evidence showed higher levels of M23-AQP4 were observed in larger EV, but western blot of smaller EV, <100 nm, also confirmed AQP4 presence . These samples were isolated by ultracentrifugation at 100,000x g and may therefore still contain small, soluble protein aggregates.

It is hypothesised that M23-MDCK EV are larger because the formation of OAPs in cell membranes, which could reduce the capacity of cells to produce small vesicles. Only one clear band was observed for M23 using western blot, at a size of around 60 kDa, the size of an AQP4-GFP monomer. The presence of large OAPs in EV was not investigated, the maximum size of molecules that could be detected in the western blot that was undertaken was 250kDa. An older study has shown the presence of M23 in membrane vesicles of varying sizes, including the presence of a range of OAP sizes in vesicles with diameters over 200 nm, using western blot (Simone et al., 2022).

In conclusion, it is plausible that the average size of EV released by cells expressing M23 AQP4 is higher than the average size of EV released by cells expressing no, or M1 AQP4 because M23 forms OAPs which are planar structures that cannot easily fit into smaller particles. Although this study, and previous studies do show the presence of AQP4 M23 in smaller EV, it is apparent that M23 OAPs were only found in larger EV (Smith et al., 2014) This study has not attempted to identify larger OAPs in EV and so it has not been confirmed that OAP presence in EV is responsible for the increased average EV diameter in M23 EV. It is also important to note however, that the methods used to detect EV are not reliable measurements of size, due to the limitations of detection of particles under 100nm in diameter using UV-SSC FC. It is also possible that this technique is not sensitive enough to reliably detect differences in size of EV populations. Other, more specific methods could be used, such as further imaging with cryoTEM, or the use of techniques that directly measure particle size such as tuneable resistive pulse sensing (TRPS) which measures the disruption of electric currents by single particles (Smith et al., 2014). This technique was attempted but manufacturing issues made essential hardware components unreliable, and the data acquired were not used.

As discussed earlier, interactions between EV and immune cells can have pro- or anti-inflammatory effects. Circulating EV act as messengers and deliver cargo to recipient cells. Transfer of functional AQP has been demonstrated (Weatherall and Willmott, 2015). It has been suggested that vesicle swelling facilitates vesicle fusion with plasma membranes (Street et al., 2011). It is possible that the presence of AQP in EV facilitates EV swelling and therefore fusion with recipient cells, though at this point in time, this is speculative. EV uptake derived from M1 MDCK were more readily interacted with by macrophage type, THP-1 cells when compared with EV derived from WT or M23 MDCK (Figure 5.9 & 5.10). This was observed with EV produced in isotonic and hypotonic, but not in hypertonic conditions. It is not known why this was the case. It has previously been shown that the interaction between immune cells and EV can depend on EV cargo, and it is possible that there are differences between MDCK derived from M1 cells that promote interaction. It is also possible that M1-AQP4 promotes interaction of THP-1 cells with MDCK derived EV. It is interesting that this phenomenon is not observed in EV produced in hypertonic environments. Other analyses performed as part of this study did not identify differences in MDCK derived EV produced in hypertonic conditions, compared with those produced in hypotonic or isotonic conditions. It is possible that the fluorescence signal of EV is lost in the process of EV uptake by macrophages, fluorescence could be degraded.

6.2 Limitations of the study

Confocal microscopy analysis of AQP4 expression and localisation showed clear differences between samples, but more accurate analyses could have been performed by including 3D data collection and analyses, rather than analysis of 2D images. In addition, image resolution could have been enhanced by using more advanced microscopy techniques such as super resolution imaging, or expansion microscopy (Kelly et al., 2004).

There appeared to be some non-specific labelling with the RECA-1 antibody (Figure 3.7), as some cells that were labelled did not appear to be endothelial. There are areas of subjectivity in the data analysis method, specifically in the endfoot identification, brighter areas of expression are easier to identify and likely to be included in data

analyses. This would be improved if endothelial cell labelling were more specific, and all areas around red labelling were included for every field of view.

HeLa and MDCK cells were used to make EV. These cell lines do not express endogenous AQP4 (Chen et al., 2015, Pellavio et al., 2017). and are not cells of the CNS (Kitchen et al., 2016, Scherer et al., 1953). There were attempts to use astrocytes to produce EV. An experiment was designed to create an AQP4 knockdown model in human primary astrocytes, but a number of issues were encountered that made this unrealistic. Preliminary investigations using rat primary astrocytes confirmed EV release by astrocytes and the presence of AQP4 in EV. In order to use this cell line effectively, AQP4-positive, and AQP4-negative cell lines were required. This required a lot of optimisations and at this time, the UK COVID-19 lockdown came into effect. The university building was closed for 3-6 months, followed by a long period of restricted access where these experiments would not have been possible. Instead, in order to keep the project moving, a stable HeLa cell line was produced, requiring less time on campus.

Later in the project, when normality was resumed, there was an attempt to create an EV release model using IPSC-derived astrocytes. An experiment was designed to create an AQP4 knockdown. Unfortunately, the very slow growth rate of these cells made EV production inefficient. Cells had to be grown for a long time in order generate enough cells to make EV. In addition, these cells could only be used to a low passage number (~3). Cells had to be expanded before a knockdown transfection could be performed and cells had to be expanded again to create different tonic conditions. Following attempts to grow enough cells to produced EV from WT IPSC-derived HeLa, it was deemed that it was not feasible to optimise this model and generate EV within the time frame remaining to complete the project. Therefore, stably transfected MDCK cells, which were already available and had been established using other experiments, were used instead. Though MDCK cells do not express endogenous AQP4 they are kidney cells, often exposed to changes in extracellular tonicity. They are quick to replicate and easy to grow. AQP4 isoforms M1 and M23 had previously been stably transfected into MDCK cells and a WT control was available for comparison (Gaush et al., 1966).

Numbers of EV released were enough to perform analyses, but it is possible that optimisation of tonic conditions would have yielded more EV, and a variety of tonic

conditions could have been trialled to investigate this further. The hypotonic condition used was selected based on previous trafficking experiments, intracellular AQP4-GFP relocalised to the plasma membrane of HeLa cells, demonstrating a cellular response to hypotonic stress.

There are multiple ways to isolate EV and recent studies seek to find the most effective. SEC is expensive and time consuming. In in addition, prior to isolation, samples must be concentrated using centrifugal concentration filters, to reduce sample volume to 500 µL for SEC. This technique is well suited to the concentration of large volumes but is not ideal when multiple EV samples are being used. Using this technique to isolate fifteen different EV samples was especially time-consuming and used large amounts of costly consumables. This technique was used successfully to isolate EV, but it is not known how efficient it was i.e., what percentage of the starting number of EV were collected. In addition, the size of EV analysed was determined by the SEC isolation. The minimum and maximum sizes of EV collected using this method are 70 nm to 1000 nm, respectively.

Alternative ways to isolate EV could have been used, differential ultracentrifugation (dUC) is commonly used for EV isolation. EV are centrifuged at increasing speeds to separate and isolate small particles which, pellet at higher speeds. This is a multistep and time-consuming process. Also, while larger particles such as cell debris and apoptotic bodies can be removed, EV are not separated from smaller particles such as soluble protein (Kitchen et al., 2016). dUC of EV was attempted briefly in this study but resulted in low EV-yield. On reflection, as 15 EV conditions were made for each experiment, optimisation of dUC, would have made a viable alternative to SEC.

A UV-SSC FC gating protocol was designed using polystyrene calibration beads and detection of green fluorescence. Gates were drawn manually and were as such, subjective. EV populations were at times, difficult to determine, as EV fall within a similar size to other debris and medium components.

The small size of EV pushes this technique to the limit of detection and small EV will not have been counted. Some particles introduced by PBS fell within the ‘EV’ and ‘BODIPY’ gates and could not be excluded from EV measurements, fortunately these particle numbers were small relative to EV numbers.

Polystyrene beads were used to successfully set up a UV-SSC EV detection protocol based on size and green fluorescence intensity. It was possible to detect and count EV

using this protocol. The size of EV was measured relative to polystyrene beads which, had different laser refraction properties, and give and only an estimate of size, not an accurate measurement. Though three distinct methods of detection were used to confirm AQP4-GFP release in EV, each method was performed only one time, so statistical analyses could not be applied. Western blot of AQP4 release in EV was not quantified, the method required to produce EV was laborious and required a large number of EV, for each condition ten T75 flasks of cells were required, ~8.4 x 10^7 cells. Sample volume was concentrated 1000x and, while AQP4 expression could have been normalised to the cell and/ or EV counts, or to total protein counts, it was decided that the priority was to confirm, rather than quantify AQP4-GFP release in EV and so, the entire sample was used for western blot, rather than protein quantification methods. For this reason, it was not possible to analyse EV from all tonic conditions. To produce EV derived from HeLa cells for western blot, hypertonic conditions were used. For MDCK, EV were released in hypotonic medium, as the most EV were released in these conditions. Future studies may show differences between cellular expression and EV release of AQP4.

UV-SSC and nano-flow cytometry were used for GFP detection in EV. While these techniques were able to confirm the presence of GFP in EV, the quantification of GFP in EV was not possible as these techniques do not provide an accurate measure of fluorescence. It was not possible to compare relative fluorescence intensities of EV in each condition as the background caused by unlabelled and low/ non-fluorescent EV was high and overshadowed any differences seen between populations. The percent of EV populations was also too low to convey any differences. Instead, a gate was drawn around the area where fluorescent EV would normally appear and the number of EV that fell within this gate were counted.

Data from UV-SSC FC were presented as average relative UV-SSC values, rather than actual size units, such as nanometres. This is because the size of EV can only be estimated using UV-SSC FC and any attempt to measure actual size would be inaccurate. As highlighted earlier, the size of EV was estimated by calibrating against fluorescent polystyrene beads of mixed sizes which, can be used to ensure detection of a range of fluorescent beads, from 100 nm to 1000 nm diameter. Though the size of beads can be presented in nanometres, the size of EV that fall within the same size range cannot. UV-SSC FC relies on measurement of the scattering of the UV laser to give a measurement of size. As the polystyrene calibration beads and EV are made of

different materials, they give different light scattering properties that are not related to particle size.

6.3 Future Work

These data were published in *Cell* and the use of TFP to prevent oedema following TBI has now progressed to Stage 1 clinical trials. There are more than 230 publications that cite this paper including topics such as, further investigation into components of the AQP4 trafficking pathway , development of new drug delivery technologies (Helwa et al., 2017) and investigations around the role of AQP4 in the glymphatic system . Work around identifying and optimising treatments that target the AQP4 trafficking mechanism to prevent oedema and secondary injury is ongoing in the research group.

The stable HeLa cell line produced has been adopted by other research group members and is currently being used to investigate AQP4 in HeLa cells, work is focussed on the high levels of M23 expression. Further optimisation of the parameters used in this model could lead to optimised EV release, and alternative triggers, such as hypoxia, which also important in AQP4 localisation and function, could be used to trigger EV release in this model.

For any future EV studies, it would be sensible to optimise EV isolation methods. Studies that produce multiple populations of EV and use SEC columns for EV isolation require a large number of costly consumables, optimisation of an alternative EV isolation technique, such as UC would require fewer resources. In addition, UC would allow for separation of EV of different sizes and densities within EV populations, and would allow analysis of EV of all sizes, and different types of EV.

Many more analyses could be performed on EV released by MDCK and HeLa cells using this model. Many roles for AQP4 in EV had been suggested and the experiments outlined in this thesis go only a small way to exploring a few of these potential roles. Future work could include investigation into the membrane properties of EV, investigation into the ability of EV to change shape and move through extracellular matrices. More detailed investigations into the interaction of immune cells would be of interest, next steps could include analysis into macrophage phenotypes following interaction with EV and assessment of pro and/ or anti-inflammatory properties of EV. EV uptake and transfer of EV cargo to neighbouring cells is another interesting concept

that could provide insight into AQP4 function in EV. A range of possible roles for AQP in EV have been suggested (Kitchen et al., 2020) such as the transfer of functional AQP to neighbouring cells.

Ultimately, the goal would be to better understand the role of AQP4 in EV following TBI. The findings of this study offer preliminary findings that could be explored further, such as the increased interaction between EV from M1 AQP4 MDCK cells compared to EV derived from WT and M23. Perhaps the presence of M1 AQP4 in EV increases recruitment of immune cells to sites of injury. It has been demonstrated that numbers of CNS-derived EV containing AQP4 are increased following TBI (Tureckova et al., 2023). It has been suggested that AQP4 in EV could be used as a biomarker for TBI severity but no hypotheses regarding the function of AQP4 in these EV have, as yet been investigated.

6.4 Summary

This thesis demonstrates that the subcellular localisation of AQP4 is important to its function, both AQP4 localisation to astrocytic endfeet following SCI, and the release of AQP4 in EV following tonic stress have interesting downstream effects. The findings of this thesis are translational findings have contributed to the discovery of a potential AQP4 translocation inhibitor that may prevent CNS oedema following injury in human patients. Investigations into potential roles for AQP4 in EV were more preliminary, the findings of these investigations could be applied to a wide variety of EV fields, such as the intro development and optimisation of EV *in vitro* of EV, EV as biomarkers, drug delivery by EV and understanding the role of AQP in EV release further.

Bibliography.

ABDEEN, A., SONODA, H., EL-SHAWARBY, R., TAKAHASHI, S. & IKEDA, M. 2014. Urinary excretion pattern of exosomal aquaporin-2 in rats that received gentamicin. *Am J Physiol Renal Physiol,* 307**,** F1227-37.

ABELS, E. R., MAAS, S. L. N., NIELAND, L., WEI, Z., CHEAH, P. S., TAI, E., KOLSTEEG, C. J., DUSOSWA, S. A., TING, D. T., HICKMAN, S., EL KHOURY, J., KRICHEVSKY, A. M., BROEKMAN, M. L. D. & BREAKEFIELD, X. O. 2019. Glioblastoma-Associated Microglia Reprogramming Is Mediated by Functional Transfer of Extracellular miR-21. *Cell Rep,* 28**,** 3105-3119 e7.

ABIR-AWAN, M., KITCHEN, P., SALMAN, M., CONNER, M., CONNER, A. & BILL, R. 2018. Inhibitors of Mammalian Aquaporin Water Channels. *International Journal of Molecular Science***,** 1589.

AGRE, P., KING, L. S., YASUI, M., GUGGINO, W. B., OTTERSEN, O. P., FUJIYOSHI, Y., ENGEL, A. & NIELSEN, S. 2002. Aquaporin water channels--from atomic structure to clinical medicine. *J Physiol,* 542**,** 3-16.

AKERS, J. C., RAMAKRISHNAN, V., KIM, R., PHILLIPS, S., KAIMAL, V., MAO, Y., HUA, W., YANG, I., FU, C. C., NOLAN, J., NAKANO, I., YANG, Y., BEAULIEU, M., CARTER, B. S. & CHEN, C. C. 2015. miRNA contents of cerebrospinal fluid extracellular vesicles in glioblastoma patients. *J Neurooncol,* 123**,** 205-16.

AMATORE, C., ARBAULT, S., BONIFAS, I., LEMAITRE, F. & VERCHIER, Y. 2007. Vesicular exocytosis under hypotonic conditions shows two distinct populations of dense core vesicles in bovine chromaffin cells. *Chemphyschem,* 8**,** 578-85.

AMBATTU, L. A., RAMESAN, S., DEKIWADIA, C., HANSSEN, E., LI, H. & YEO, L. Y. 2020. High frequency acoustic cell stimulation promotes exosome generation regulated by a calcium-dependent mechanism. *Commun Biol,* 3**,** 553.

ANDREI, C., DAZZI, C., LOTTI, L., TORRISI, M. R., CHIMINI, G. & RUBARTELLI, A. 1999. The secretory route of the leaderless protein interleukin 1beta involves exocytosis of endolysosome-related vesicles. *Mol Biol Cell,* 10**,** 1463-75.

ARIMOTO, K., FUKUDA, H., IMAJOH-OHMI, S., SAITO, H., & TAKEKAWA, M. 2008. Formation of stress granules inhibits apoptosis by suppressing stress-responsive MAPK pathways. . *Nature cell biology,* 10**,** 1324–1332.

ARROYO, J. D., CHEVILLET, J. R., KROH, E. M., RUF, I. K., PRITCHARD, C. C., GIBSON, D. F., MITCHELL, P. S., BENNETT, C. F., POGOSOVA-AGADJANYAN, E. L., STIREWALT, D. L., TAIT, J. F. & TEWARI, M. 2011. Argonaute2 complexes carry a population of circulating microRNAs independent of vesicles in human plasma. *Proc Natl Acad Sci U S A,* 108**,** 5003-8.

ASVAPROMTADA, S., SONODA, H., KINOUCHI, M., OSHIKAWA, S., TAKAHASHI, S., HOSHINO, Y., SINLAPADEELERDKUL, T., YOKOTA-IKEDA, N., MATSUZAKI, T. & IKEDA, M. 2018. Characterization of urinary exosomal release of aquaporin-1 and -2 after renal ischemia-reperfusion in rats. *Am J Physiol Renal Physiol,* 314**,** F584-F601.

AUGUSTE, K. I., JIN, S., UCHIDA, K., YAN, D., MANLEY, G. T., PAPADOPOULOS, M. C. & VERKMAN, A. S. 2007. Greatly impaired migration of implanted aquaporin-4-deficient astroglial cells in mouse brain toward a site of injury. *FASEB J,* 21**,** 108-16.

BAI, C., FUKUDA, N., SONG, Y., MA, T., MATTHAY, M. A. & VERKMAN, A. S. 1999. Lung fluid transport in aquaporin-1 and aquaporin-4 knockout mice. *J Clin Invest,* 103**,** 555-61.

BATRAKOVA, E. V. & KIM, M. S. 2015. Using exosomes, naturally-equipped nanocarriers, for drug delivery. *J Control Release,* 219**,** 396-405.

BATTISTELLI, M. & FALCIERI, E. 2020. Apoptotic Bodies: Particular Extracellular Vesicles Involved in Intercellular Communication. *Biology (Basel),* 9.

BEARD, K., MEANEY, D. F. & ISSADORE, D. 2020. Clinical Applications of Extracellular Vesicles in the Diagnosis and Treatment of Traumatic Brain Injury. *J Neurotrauma,* 37**,** 2045-2056.

BEITZ, E., WU, B., HOLM, L. M., SCHULTZ, J. E. & ZEUTHEN, T. 2006. Point mutations in the aromatic/arginine region in aquaporin 1 allow passage of urea, glycerol, ammonia, and protons. *Proc Natl Acad Sci U S A,* 103**,** 269-74.

BEJEROT, S., HESSELMARK, E., MOBARREZ, F., WALLEN, H., HIETALA, M. A., NYBOM, R. & WETTERBERG, L. 2019. Neuromyelitis optica spectrum disorder with increased aquaporin-4 microparticles prior to autoantibodies in cerebrospinal fluid: a case report. *J Med Case Rep,* 13**,** 27.

BESER, A., SORJONEN, K., WAHLBERG, K., PETERSON, U., NYGREN, A. & ASBERG, M. 2014. Construction and evaluation of a self rating scale for stress-induced exhaustion disorder, the Karolinska Exhaustion Disorder Scale. *Scand J Psychol,* 55**,** 72-82.

BEVERS, E. M., COMFURIUS, P. & ZWAAL, R. F. 1983. Changes in membrane phospholipid distribution during platelet activation. *Biochim Biophys Acta,* 736**,** 57-66.

BEWICKE-COPLEY, F., MULCAHY, L. A., JACOBS, L. A., SAMUEL, P., AKBAR, N., PINK, R. C. & CARTER, D. R. F. 2017. Extracellular vesicles released following heat stress induce bystander effect in unstressed populations. *J Extracell Vesicles,* 6**,** 1340746.

BISTER, N., PISTONO, C., HUREMAGIC, B., JOLKKONEN, J., GIUGNO, R. & MALM, T. 2020. Hypoxia and extracellular vesicles: A review on methods, vesicular cargo and functions. *J Extracell Vesicles,* 10**,** e12002.

BLANC, L., LIU, J., VIDAL, M., CHASIS, J. A., AN, X. & MOHANDAS, N. 2009. The water channel aquaporin-1 partitions into exosomes during reticulocyte maturation: implication for the regulation of cell volume. *Blood,* 114**,** 3928-34.

BOHREN, C. F. H., D.R. 2008. *Absorption and scattering of light by small particles,* New York, Wiley Interscience.

BORDONE, M. P., SALMAN, M. M., TITUS, H. E., AMINI, E., ANDERSEN, J. V., CHAKRABORTI, B., DIUBA, A. V., DUBOUSKAYA, T. G., EHRKE, E., ESPINDOLA DE FREITAS, A., BRAGA DE FREITAS, G., GONCALVES, R. A., GUPTA, D., GUPTA, R., HA, S. R., HEMMING, I. A., JAGGAR, M., JAKOBSEN, E., KUMARI, P., LAKKAPPA, N., MARSH, A. P. L., MITLOHNER, J., OGAWA, Y., PAIDI, R. K., RIBEIRO, F. C., SALAMIAN, A., SALEEM, S., SHARMA, S., SILVA, J. M., SINGH, S., SULAKHIYA, K., TEFERA, T. W., VAFADARI, B., YADAV, A., YAMAZAKI, R. & SEIDENBECHER, C. I. 2019. The energetic brain - A review from students to students. *J Neurochem,* 151**,** 139-165.

BUSATTO, S., IANNOTTA, D., WALKER, S. A., DI MARZIO, L. & WOLFRAM, J. 2021. A Simple and Quick Method for Loading Proteins in Extracellular Vesicles. *Pharmaceuticals (Basel),* 14.

CARMOSINO, M., PROCINO, G., TAMMA, G., MANNUCCI, R., SVELTO, M. & VALENTI, G. 2007. Trafficking and phosphorylation dynamics of AQP4 in histamine-treated human gastric cells. *Biol Cell,* 99**,** 25-36.

CARPENTIER, J. L., SAWANO, F., GEIGER, D., GORDEN, P., PERRELET, A. & ORCI, L. 1989. Potassium depletion and hypertonic medium reduce "non-coated" and clathrin-coated pit formation, as well as endocytosis through these two gates. *J Cell Physiol,* 138**,** 519-26.

CASSIDY, D. J., LJ, C., PELOSO, P., BORG, J., VON HOLST, H., HOLM, L., KRAUS, J. & CORONADO, V. 2004. INCIDENCE, RISK FACTORS AND PREVENTION OF MILD TRAUMATIC OF MILD TRAUMATIC BRAIN INJURY: RESULTS OF THE WHO COLLABORATING CENTRE TASK FORCE ON MILD TRAUMATIC BRAIN INJURY. *Journal of rehabilitation medicine***,** 28-60.

CHEN, F., TILLBERG, P. W. & BOYDEN, E. S. 2015. Optical imaging. Expansion microscopy. *Science,* 347**,** 543-8.

CHEN, J. Q., ZHANG, C. C., JIANG, S. N., LU, H. & WANG, W. 2016. Effects of Aquaporin 4 Knockdown on Brain Edema of the Uninjured Side After Traumatic Brain Injury in Rats. *Med Sci Monit,* 22**,** 4809-4819.

CHEN, Q. & DUAN, E. K. 2011. Aquaporins in sperm osmoadaptation: an emerging role for volume regulation. *Acta Pharmacol Sin,* 32**,** 721-4.

CHENG, Y., PEREIRA, M., RAUKAR, N., REAGAN, J. L., QUESENEBERRY, M., GOLDBERG, L., BORGOVAN, T., LAFRANCE, W. C., JR., DOONER, M., DEREGIBUS, M., CAMUSSI, G., RAMRATNAM, B. & QUESENBERRY, P. 2019. Potential biomarkers to detect traumatic brain injury by the profiling of salivary extracellular vesicles. *J Cell Physiol,* 234**,** 14377-14388.

CHUO, S. T., CHIEN, J. C. & LAI, C. P. 2018. Imaging extracellular vesicles: current and emerging methods. *J Biomed Sci,* 25**,** 91.

CIREGIA, F., URBANI, A. & PALMISANO, G. 2017. Extracellular Vesicles in Brain Tumors and Neurodegenerative Diseases. *Front Mol Neurosci,* 10**,** 276.

CLARKE-BLAND, C. E., BILL, R. M. & DEVITT, A. 2022. Emerging roles for AQP in mammalian extracellular vesicles. *Biochim Biophys Acta Biomembr,* 1864**,** 183826.

COLEMAN, B. M., HANSSEN, E., LAWSON, V. A. & HILL, A. F. 2012. Prion-infected cells regulate the release of exosomes with distinct ultrastructural features. *FASEB J,* 26**,** 4160-73.

CONNER, M. T., CONNER, A. C., BLAND, C. E., TAYLOR, L. H., BROWN, J. E., PARRI, H. R. & BILL, R. M. 2012. Rapid aquaporin translocation regulates cellular water flow: mechanism of hypotonicity-induced subcellular localization of aquaporin 1 water channel. *J Biol Chem,* 287**,** 11516-25.

CONNER, M. T., CONNER, A. C., BROWN, J. E. & BILL, R. M. 2010. Membrane trafficking of aquaporin 1 is mediated by protein kinase C via microtubules and regulated by tonicity. *Biochemistry,* 49**,** 821-3.

CRESCITELLI, R., LASSER, C., SZABO, T. G., KITTEL, A., ELDH, M., DIANZANI, I., BUZAS, E. I. & LOTVALL, J. 2013. Distinct RNA profiles in subpopulations of extracellular vesicles: apoptotic bodies, microvesicles and exosomes. *J Extracell Vesicles,* 2.

CUI, Y. & BASTIEN, D. A. 2011. Water transport in human aquaporin-4: molecular dynamics (MD) simulations. *Biochem Biophys Res Commun,* 412**,** 654-9.

CVJETKOVIC, A., JANG, S. C., KONECNA, B., HOOG, J. L., SIHLBOM, C., LASSER, C. & LOTVALL, J. 2016. Detailed Analysis of Protein Topology of Extracellular Vesicles-Evidence of Unconventional Membrane Protein Orientation. *Sci Rep,* 6**,** 36338.

D'ASTI, E., CHENNAKRISHNAIAH, S., LEE, T. H. & RAK, J. 2016. Extracellular Vesicles in Brain Tumor Progression. *Cell Mol Neurobiol,* 36**,** 383-407.

DAS, M., MOHAPATRA, S. & MOHAPATRA, S. 2012. New perspectives on central and peripheral immune responses to acute traumatic brain injury. *Journal of Neuroinflammation*.

DAY, R. E., KITCHEN, P., OWEN, D. S., BLAND, C., MARSHALL, L., CONNER, A. C., BILL, R. M. & CONNER, M. T. 2014. Human aquaporins: regulators of transcellular water flow. *Biochim Biophys Acta,* 1840**,** 1492-506.

DE GROOT, B. L., ENGEL, A. & GRUBMULLER, H. 2001. A refined structure of human aquaporin-1. *FEBS Lett,* 504**,** 206-11.

DEBBI, L., GUO, S., SAFINA, D. & LEVENBERG, S. 2022. Boosting extracellular vesicle secretion. *Biotechnol Adv,* 59**,** 107983.

DENKER, B. M., SMITH, B. L., KUHAJDA, F. P. & AGRE, P. 1988. Identification, purification, and partial characterization of a novel Mr 28,000 integral membrane protein from erythrocytes and renal tubules. *J Biol Chem,* 263**,** 15634-42.

DENVER, P., D'ADAMO, H., HU, S., ZUO, X., ZHU, C., OKUMA, C., KIM, P., CASTRO, D., JONES, M. R., LEAL, C., MEKKITTIKUL, M., GHADISHAH, E., TETER, B., VINTERS, H. V., COLE, G. M. & FRAUTSCHY, S. A. 2019. A Novel Model of Mixed Vascular Dementia Incorporating Hypertension in a Rat Model of Alzheimer's Disease. *Front Physiol,* 10**,** 1269.

DI ROCCO, G., BALDARI, S. & TOIETTA, G. 2016. Towards Therapeutic Delivery of Extracellular Vesicles: Strategies for In Vivo Tracking and Biodistribution Analysis. *Stem Cells Int,* 2016**,** 5029619.

DING, T., MA, Y., LI, W., LIU, X., YING, G., FU, L. & GU, F. 2011. Role of aquaporin-4 in the regulation of migration and invasion of human glioma cells. *Int J Oncol,* 38**,** 1521-31.

DIVE, C., GREGORY, C. D., PHIPPS, D. J., EVANS, D. L., MILNER, A. E., & WYLLIE, A. H.. 1992. Analysis and discrimination of necrosis and apoptosis (programmed cell death) by multiparameter flow cytometry. *Biochimica et biophysica acta,* 1133**,** 275–285.

DUMONT, R. J., OKONKWO, D. O., VERMA, S., HURLBERT, R. J., BOULOS, P. T., ELLEGALA, D. B. & DUMONT, A. S. 2001. Acute spinal cord injury, part I: pathophysiologic mechanisms. *Clin Neuropharmacol,* 24**,** 254-64.

EITAN, E., HUTCHISON, E. R., MAROSI, K., COMOTTO, J., MUSTAPIC, M., NIGAM, S. M., SUIRE, C., MAHARANA, C., JICHA, G. A., LIU, D., MACHAIRAKI, V., WITWER, K. W., KAPOGIANNIS, D. & MATTSON, M. P. 2016. Extracellular Vesicle-Associated Abeta Mediates Trans-Neuronal Bioenergetic and Ca(2+)-Handling Deficits in Alzheimer's Disease Models. *NPJ Aging Mech Dis,* 2**,** 16019-.

ELLIOT, S., GOLDSMITH, P., KNEPPER, M., HAUGHEY, M. & OLSON, B. 1996. Urinary excretion of aquaporin-2 in humans: a potential marker of collecting duct responsiveness to vasopressin. *J Am Soc Nephrol,* 7**,** 403-9.

ERIKSSON, U. K., FISCHER, G., FRIEMANN, R., ENKAVI, G., TAJKHORSHID, E. & NEUTZE, R. 2013. Subangstrom resolution X-ray structure details aquaporin-water interactions. *Science,* 340**,** 1346-1349.

ESSIEN, S. A., AHUJA, I. & EISENHOFFER, G. T. 2023. Macrophage Migration Inhibitory Factor on Apoptotic Extracellular Vesicles Regulates Compensatory Proliferation. *bioRxiv*.

FADOK, V. A., VOELKER, D. R., CAMPBELL, P. A., COHEN, J. J., BRATTON, D. L. & HENSON, P. M. 1992. Exposure of phosphatidylserine on the surface of apoptotic lymphocytes triggers specific recognition and removal by macrophages. *J Immunol,* 148**,** 2207-16.

FENTON, R. M., HB. MACAULAY, N. 2010. Differential water permeability and regulation of three aquaporin-4 isoforms. *Cell and Molecular Life Sciences,* 67**,** 829-840.

FLAMION, B. & SPRING, K. R. 1990. Water permeability of apical and basolateral cell membranes of rat inner medullary collecting duct. *Am J Physiol,* 259**,** F986-99.

FRUHBEIS, C., FROHLICH, D., KUO, W. P. & KRAMER-ALBERS, E. M. 2013. Extracellular vesicles as mediators of neuron-glia communication. *Front Cell Neurosci,* 7**,** 182.

FUKUDA, A. M., ADAMI, A., POP, V., BELLONE, J. A., COATS, J. S., HARTMAN, R. E., ASHWAL, S., OBENAUS, A. & BADAUT, J. 2013. Posttraumatic reduction of edema with aquaporin-4 RNA interference improves acute and chronic functional recovery. *J Cereb Blood Flow Metab,* 33**,** 1621-32.

GAUSH, C. R., HARD, W. L. & SMITH, T. F. 1966. Characterization of an established line of canine kidney cells (MDCK). *Proc Soc Exp Biol Med,* 122**,** 931-5.

GHAJAR, J. 2000. Traumatic brain injury. *Lancet,* 356**,** 923-9.

GOETZL, E. J., ELAHI, F. M., MUSTAPIC, M., KAPOGIANNIS, D., PRYHODA, M., GILMORE, A., GORGENS, K. A., DAVIDSON, B., GRANHOLM, A. C. & LEDREUX, A. 2019. Altered levels of plasma neuron-derived exosomes and their cargo proteins characterize acute and chronic mild traumatic brain injury. *FASEB J,* 33**,** 5082-5088.

GONZALEZ-MOLINA, L. A., VILLAR-VESGA, J., HENAO-RESTREPO, J., VILLEGAS, A., LOPERA, F., CARDONA-GOMEZ, G. P. & POSADA-DUQUE, R. 2021. Extracellular Vesicles From 3xTg-AD Mouse and Alzheimer's Disease Patient Astrocytes Impair Neuroglial and Vascular Components. *Front Aging Neurosci,* 13**,** 593927.

GOSSELIN, R. D., MEYLAN, P. & DECOSTERD, I. 2013. Extracellular microvesicles from astrocytes contain functional glutamate transporters: regulation by protein kinase C and cell activation. *Front Cell Neurosci,* 7**,** 251.

GOULD, S. J. & RAPOSO, G. 2013. As we wait: coping with an imperfect nomenclature for extracellular vesicles. *J Extracell Vesicles,* 2.

GRANT, L. R., MILIC, I. & DEVITT, A. 2019. Apoptotic cell-derived extracellular vesicles: structure-function relationships. *Biochem Soc Trans,* 47**,** 509-516.

GUL, B., SYED, F., KHAN, S., IQBAL, A., & AHMAD, I. 2022. Characterization of extracellular vesicles by flow cytometry: Challenges and promises. *Micron*.

GUO, Q., SAYEED, I., BARONNE, L. M., HOFFMAN, S. W., GUENNOUN, R. & STEIN, D. G. 2006. Progesterone administration modulates AQP4 expression and edema after traumatic brain injury in male rats. *Exp Neurol,* 198**,** 469-78.

HAHM, J. K., J. PARK, J. 2021. Strategies to Enhance Extracellular Vesicle Production. *Tissue Engineering & Regenerative Medicine,* 18**,** 513-524.

HAJ-YASEIN, N. N., VINDEDAL, G. F., EILERT-OLSEN, M., GUNDERSEN, G. A., SKARE, O., LAAKE, P., KLUNGLAND, A., THOREN, A. E., BURKHARDT, J. M., OTTERSEN, O. P. & NAGELHUS, E. A. 2011. Glial-conditional deletion of aquaporin-4 (Aqp4) reduces blood-brain water uptake and confers barrier function on perivascular astrocyte endfeet. *Proc Natl Acad Sci U S A,* 108**,** 17815-20.

HASEGAWA, H., MA, T., SKACH, W., MATTHAY, M. A. & VERKMAN, A. S. 1994. Molecular cloning of a mercurial-insensitive water channel expressed in selected water-transporting tissues. *J Biol Chem,* 269**,** 5497-500.

HASLER, U., NUNES, P., BOULEY, R., LU, H. A., MATSUZAKI, T. & BROWN, D. 2008. Acute hypertonicity alters aquaporin-2 trafficking and induces a MAPK-dependent accumulation at the plasma membrane of renal epithelial cells. *J Biol Chem,* 283**,** 26643-61.

HAYAKAWA, K., ESPOSITO, E., WANG, X., TERASAKI, Y., LIU, Y., XING, C., JI, X. & LO, E. H. 2016. Transfer of mitochondria from astrocytes to neurons after stroke. *Nature,* 535**,** 551-5.

HAZELTON, I., YATES, A., DALE, A., ROODSELAAR, J., AKBAR, N., RUITENBERG, M. J., ANTHONY, D. C. & COUCH, Y. 2018. Exacerbation of Acute Traumatic Brain Injury by Circulating Extracellular Vesicles. *J Neurotrauma,* 35**,** 639-651.

HEIJNEN, H. F., SCHIEL, A. E., FIJNHEER, R., GEUZE, H. J. & SIXMA, J. J. 1999. Activated platelets release two types of membrane vesicles: microvesicles by surface shedding and exosomes derived from exocytosis of multivesicular bodies and alpha-granules. *Blood,* 94**,** 3791-9.

HELWA, I., CAI, J., DREWRY, M. D., ZIMMERMAN, A., DINKINS, M. B., KHALED, M. L., SEREMWE, M., DISMUKE, W. M., BIEBERICH, E., STAMER, W. D., HAMRICK, M. W. & LIU, Y. 2017. A Comparative Study of Serum Exosome Isolation Using Differential Ultracentrifugation and Three Commercial Reagents. *PLoS One,* 12**,** e0170628.

HINSON, S. R., ROMERO, M. F., POPESCU, B. F., LUCCHINETTI, C. F., FRYER, J. P., WOLBURG, H., FALLIER-BECKER, P., NOELL, S. & LENNON, V. A. 2012. Molecular outcomes of neuromyelitis optica (NMO)-IgG binding to aquaporin-4 in astrocytes. *Proc Natl Acad Sci U S A,* 109**,** 1245-50.

HORSEFIELD, R., NORDEN, K., FELLERT, M., BACKMARK, A., TORNROTH-HORSEFIELD, S., TERWISSCHA VAN SCHELTINGA, A. C., KVASSMAN, J., KJELLBOM, P., JOHANSON, U. & NEUTZE, R. 2008. High-resolution x-ray structure of human aquaporin 5. *Proc Natl Acad Sci U S A,* 105**,** 13327-32.

HYDER, A., WUNDERLICH, C., PUVANACHANDRA, P., GURURAJ, G. & KOBUSINGYE, O. 2007. The impact of traumatic brain injuries: a global perspective. *Neurorehabilitation,* 22**,** 341-53.

IGARASHI, H., HUBER, V. J., TSUJITA, M. & NAKADA, T. 2011. Pretreatment with a novel aquaporin 4 inhibitor, TGN-020, significantly reduces ischemic cerebral edema. *Neurol. Sci* 113-116.

ILLINGWORTH, A. 2023. *What is MFI and how is it calculated?* [Online]. International Clinial Cytometry Society. Available: https://www.cytometry.org/web/q_view.php?id=152&filter=Analysis%20Techniques [Accessed 2023].

JENNETT, B. 1998. Epidemiology of head injury. *Archives of Disease in Childhood,* 78**,** 403-6.

JIN, B. J., ROSSI, A. & VERKMAN, A. S. 2011. Model of aquaporin-4 supramolecular assembly in orthogonal arrays based on heterotetrameric association of M1-M23 isoforms. *Biophys J,* 100**,** 2936-45.

JIN, B. J., ROSSI, A., & VERKMAN, A. S. 2011. Model of aquaporin-4 supramolecular assembly in orthogonal arrays based on heterotetrameric association of M1-M23 isoforms. *Biophysical journal,* 100**,** 2936–2945.

JUNG, H. J. & KWON, T. H. 2016. Molecular mechanisms regulating aquaporin-2 in kidney collecting duct. *Am J Physiol Renal Physiol,* 311**,** F1318-F1328.

JUNG, J. S., BHAT, R. V., PRESTON, G. M., GUGGINO, W. B., BARABAN, J. M., & AGRE, P. 1994. Molecular characterization of an aquaporin cDNA from brain: candidate osmoreceptor and regulator of water balance. *Proceedings of the National Academy of Sciences,* 91**,** 3056.

JUNG, J. S., PRESTON, G. M., SMITH, B. L., GUGGINO, W. B. & AGRE, P. 1994. Molecular structure of the water channel through aquaporin CHIP. The hourglass model. *J Biol Chem,* 269**,** 14648-54.

KE, C., POON, W., NG, H., LAI, F., TANG, N. & PANG, J. 2002. Impact of experimental acute hyponatremia on severe traumatic brain injury in rats: influences on injuries, permeability of blood-brain barrier, ultrastructural features, and aquaporin-4 expression. *Experimental Neurology***,** 194-206.

KELLY, M. L., CHO, W. J., JEREMIC, A., ABU-HAMDAH, R. & JENA, B. P. 2004. Vesicle swelling regulates content expulsion during secretion. *Cell Biol Int,* 28**,** 709-16.

KIENING, K., VAN LANDEGHEM, F., SCHREIBER, S., THOMALE, U., VON DEIMLING, A., UNTERBERG, A. & JF, S. 2002. Decreased hemispheric Aquaporin-4 is linked to evolving brain edema following controlled cortical impact injury in rats. *Neuroscience letters***,** 105-108.

KIMURA, A., HSU, M., SELDIN, M., VERKMAN, A. S., SCHARFMAN, H. E. & BINDER, D. K. 2010. Protective role of aquaporin-4 water channels after contusion spinal cord injury. *Ann Neurol,* 67**,** 794-801.

KING, L. S. & AGRE, P. 1996. Pathophysiology of the aquaporin water channels. *Annu Rev Physiol,* 58**,** 619-48.

KISHIDA, K., KURIYAMA, H., FUNAHASHI, T., SHIMOMURA, I., KIHARA, S., OUCHI, N., NISHIDA, M., NISHIZAWA, H., MATSUDA, M., TAKAHASHI, M., HOTTA, K., NAKAMURA, T., YAMASHITA, S., TOCHINO, Y. & MATSUZAWA, Y. 2000. Aquaporin adipose, a putative glycerol channel in adipocytes. *J Biol Chem,* 275**,** 20896-902.

KITCHEN, P., CONNER, M. T., BILL, R. M. & CONNER, A. C. 2016. Structural Determinants of Oligomerization of the Aquaporin-4 Channel. *J Biol Chem,* 291**,** 6858-71.

KITCHEN, P., DAY, R. E., SALMAN, M. M., CONNER, M. T., BILL, R. M. & CONNER, A. C. 2015a. Beyond water homeostasis: Diverse functional roles of mammalian aquaporins. *Biochim Biophys Acta,* 1850**,** 2410-21.

KITCHEN, P., DAY, R. E., TAYLOR, L. H., SALMAN, M. M., BILL, R. M., CONNER, M. T. & CONNER, A. C. 2015b. Identification and Molecular Mechanisms of the Rapid Tonicity-induced Relocalization of the Aquaporin 4 Channel. *J Biol Chem,* 290**,** 16873-81.

KITCHEN, P., DAY, R. E., TAYLOR, L. H., SALMAN, M. M., BILL, R. M., CONNER, M. T., & CONNER, A. C. 2015. Identification and Molecular Mechanisms of the Rapid Tonicity-induced Relocalization of the Aquaporin 4 Channel. *The Journal of biological chemistry,* 290**,** 16873–16881.

KITCHEN, P., SALMAN, M. M., HALSEY, A. M., CLARKE-BLAND, C., MACDONALD, J. A., ISHIDA, H., VOGEL, H. J., ALMUTIRI, S., LOGAN, A., KREIDA, S., AL-JUBAIR, T., WINKEL MISSEL, J., GOURDON, P., TORNROTH-HORSEFIELD, S., CONNER, M. T., AHMED, Z., CONNER, A. C. & BILL, R. M. 2020. Targeting Aquaporin-4 Subcellular Localization to Treat Central Nervous System Edema. *Cell,* 181**,** 784-799 e19.

KITCHEN P, S. M., ABIR-AWAN M, AL-JUBAIR T, TÖRNROTH-HORSEFIELD S, CONNER AC, BILL RM. 2020. Calcein Fluorescence Quenching to Measure Plasma Membrane Water Flux in Live Mammalian Cells. *STAR protocols,* 1.

KNEPPER, M. A., KWON, T. H. & NIELSEN, S. 2015. Molecular Physiology of Water Balance. *N Engl J Med,* 373**,** 196.

KONOSHENKO, M. L., EA. VLASSOV, AV. LAKTIONOV, PP. 2018. Isolation of Extracellular Vesicles: General Methodologies and. *BioMed Research International,* 2018.

KRIZ, J. 2006. Inflammation in ischemic brain injury: timing is important. *Crit Rev Neurobiol,* 18**,** 145-57.

KULTZ, D. 2004. Hyperosmolality triggers oxidative damage in kidney cells. *Proc Natl Acad Sci U S A,* 101**,** 9177-8.

KUMAR, A., STOICA, B. A., LOANE, D. J., YANG, M., ABULWERDI, G., KHAN, N., KUMAR, A., THOM, S. R. & FADEN, A. I. 2017. Microglial-derived microparticles mediate neuroinflammation after traumatic brain injury. *J Neuroinflammation,* 14**,** 47.

LACROIX, R., JUDICONE, C., PONCELET, P., ROBERT, S., ARNAUD, L., SAMPOL, J. & DIGNAT-GEORGE, F. 2012. Impact of pre-analytical parameters on the measurement of circulating microparticles: towards standardization of protocol. *J Thromb Haemost,* 10**,** 437-46.

LEE, J., MCKINNEY, K. Q., PAVLOPOULOS, A. J., HAN, M. H., KIM, S. H., KIM, H. J. & HWANG, S. 2016. Exosomal proteome analysis of cerebrospinal fluid detects biosignatures of neuromyelitis optica and multiple sclerosis. *Clin Chim Acta,* 462**,** 118-126.

LENNON, V. A., KRYZER, T. J., PITTOCK, S. J., VERKMAN, A. S. & HINSON, S. R. 2005. IgG marker of optic-spinal multiple sclerosis binds to the aquaporin-4 water channel. *J Exp Med,* 202**,** 473-7.

LENZINI, S., BARGI, R., CHUNG, G. & SHIN, J. W. 2020. Matrix mechanics and water permeation regulate extracellular vesicle transport. *Nat Nanotechnol,* 15**,** 217-223.

LI, L., ZHANG, H., VARRIN-DOYER, M., ZAMVIL, S. S. & VERKMAN, A. S. 2011. Proinflammatory role of aquaporin-4 in autoimmune neuroinflammation. *FASEB J,* 25**,** 1556-66.

LO SICCO, C., REVERBERI, D., BALBI, C., ULIVI, V., PRINCIPI, E., PASCUCCI, L., BECHERINI, P., BOSCO, M. C., VARESIO, L., FRANZIN, C., POZZOBON, M., CANCEDDA, R. & TASSO, R. 2017. Mesenchymal Stem Cell-Derived Extracellular Vesicles as Mediators of Anti-Inflammatory Effects: Endorsement of Macrophage Polarization. *Stem Cells Transl Med,* 6**,** 1018-1028.

LOANE, D. & KUMAR, L. 2015. Microglia in the TBI Brain: The Good, The Bad, And The Dysregulated. *Experimental Neurology,* 275**,** 316-327.

LOEB, J. 1920. On the Cause of the Influence of Ions on the Rate of Diffusion of Water through Collodion Membranes. I. *J Gen Physiol,* 2**,** 387-408.

LOITTO, V. M., FORSLUND, T., SUNDQVIST, T., MAGNUSSON, K. E. & GUSTAFSSON, M. 2002. Neutrophil leukocyte motility requires directed water influx. *J Leukoc Biol,* 71**,** 212-22.

LOZANO, D., GONZALES-PORTILLO, G., ACOSTA, S., DE LA PENA, I., TAJIRI, N. & KANEKO, Y. A. B. C. 2015. Neuroinflammatory responses to traumatic brain injury: etiology, clinical consequences, and therapeutic opportunities. *Neuropsychiatric disease and treatment,* 11**,** 97-106.

LUDWIG, N., YERNENI, S. S., MENSHIKOVA, E. V., GILLESPIE, D. G., JACKSON, E. K. & WHITESIDE, T. L. 2020. Author Correction: Simultaneous Inhibition of Glycolysis and Oxidative Phosphorylation Triggers a Multi-Fold Increase in Secretion of Exosomes: Possible Role of 2',3'-cAMP. *Sci Rep,* 10**,** 14027.

MAAS, S. L. N., ABELS, E. R., VAN DE HAAR, L. L., ZHANG, X., MORSETT, L., SIL, S., GUEDES, J., SEN, P., PRABHAKAR, S., HICKMAN, S. E., LAI, C. P., TING, D. T., BREAKEFIELD, X. O., BROEKMAN, M. L. D. & EL KHOURY, J. 2020. Glioblastoma hijacks microglial gene expression to support tumor growth. *J Neuroinflammation,* 17**,** 120.

MAGNI, F., SARTO, C., TICOZZI, D., SOLDI, M., BOSSO, N., MOCARELLI, P. & KIENLE, M. G. 2006. Proteomic knowledge of human aquaporins. *Proteomics,* 6**,** 5637-49.

MAIKOS, J. T., ELIAS, R. A. & SHREIBER, D. I. 2008. Mechanical properties of dura mater from the rat brain and spinal cord. *J Neurotrauma,* 25**,** 38-51.

MANLEY, G., FUJIMURA, M., MA, T., NOSHITA, N., FILIZ, F., BOLLEN, A., CHAN, P. & VERKMAN, A. 2000a. Aquaporin-4 deletion in mice reduces brain edema after acute water intoxication and ischemic stroke. *Nature Medicine***,** 159-163.

MANLEY, G. T., BINDER, D. K., PAPADOPOULOS, M. C. & VERKMAN, A. S. 2004. New insights into water transport and edema in the central nervous system from phenotype analysis of aquaporin-4 null mice. *Neuroscience,* 129**,** 983-91.

MANLEY, G. T., FUJIMURA, M., MA, T., NOSHITA, N., FILIZ, F., BOLLEN, A. W., CHAN, P. & VERKMAN, A. S. 2000b. Aquaporin-4 deletion in mice reduces brain edema after acute water intoxication and ischemic stroke. *Nat Med,* 6**,** 159-63.

MARKOU, A., UNGER, L., ABIR-AWAN, M., SAADALLAH, A., HALSEY, A., BALKLAVA, Z., CONNER, M., TORNROTH-HORSEFIELD, S., GREENHILL, S. D., CONNER, A., BILL, R. M., SALMAN, M. M. & KITCHEN, P. 2022. Molecular mechanisms governing aquaporin relocalisation. *Biochim Biophys Acta Biomembr,* 1864**,** 183853.

MARPLES, D., KNEPPER, M. A., CHRISTENSEN, E. I. & NIELSEN, S. 1995. Redistribution of aquaporin-2 water channels induced by vasopressin in rat kidney inner medullary collecting duct. *Am J Physiol,* 269**,** C655-64.

MARTINEZ-BALLESTA, M. C., GARCIA-IBANEZ, P., YEPES-MOLINA, L., RIOS, J. J. & CARVAJAL, M. 2018. The Expanding Role of Vesicles Containing Aquaporins. *Cells,* 7.

MATSUMOTO, A., TAKAHASHI, Y., NISHIKAWA, M., SANO, K., MORISHITA, M., CHAROENVIRIYAKUL, C., SAJI, H. & TAKAKURA, Y. 2017. Role of Phosphatidylserine-Derived Negative Surface Charges in the Recognition and Uptake of Intravenously Injected B16BL6-Derived Exosomes by Macrophages. *J Pharm Sci,* 106**,** 168-175.

MATSUMOTO, A., TAKAHASHI, Y., OGATA, K., KITAMURA, S., NAKAGAWA, N., YAMAMOTO, A., ISHIHAMA, Y. & TAKAKURA, Y. 2021. Phosphatidylserine-deficient small extracellular vesicle is a major somatic cell-derived sEV subpopulation in blood. *iScience,* 24**,** 102839.

MIDDELDORP, J. & HOL, E. M. 2011. GFAP in health and disease. *Prog Neurobiol,* 93**,** 421-43.

MOJTAHEDZADEH, M., AHMADI, A., MAHMOODPOOR, A., BEIGMOHAMMADI, M. T., ABDOLLAHI, M., KHAZAEIPOUR, Z., SHAKI, F., KUOCHAKI, B. & HENDOUEI, N. 2014. Hypertonic saline solution reduces the oxidative stress responses in traumatic brain injury patients. *J Res Med Sci,* 19**,** 867-74.

MOREL, O., JESEL, L., FREYSSINET, J. M. & TOTI, F. 2011. Cellular mechanisms underlying the formation of circulating microparticles. *Arterioscler Thromb Vasc Biol,* 31**,** 15-26.

MUGHEES, M., KUMAR, K. & WAJID, S. 2021. Exosome vesicle as a nano-therapeutic carrier for breast cancer. *J Drug Target,* 29**,** 121-130.

NAGATA, S., SAKURAGI, T. & SEGAWA, K. 2020. Flippase and scramblase for phosphatidylserine exposure. *Curr Opin Immunol,* 62**,** 31-38.

NAZIROGLU, M., YOLDAS, N., UZGUR, E. N. & KAYAN, M. 2013. Role of contrast media on oxidative stress, Ca(2+) signaling and apoptosis in kidney. *J Membr Biol,* 246**,** 91-100.

NEELY, J. D., CHRISTENSEN, B. M., NIELSEN, S. & AGRE, P. 1999. Heterotetrameric composition of aquaporin-4 water channels. *Biochemistry,* 38**,** 11156-63.

NEELY, J. D., CHRISTENSEN, B. M., NIELSEN, S., & AGRE, P. 1999. Heterotetrameric composition of aquaporin-4 water channels. *Biochemistry,* 38**,** 11156–11163.

NEKLUDOV, M., BELLANDER, B. M., GRYTH, D., WALLEN, H. & MOBARREZ, F. 2017. Brain-Derived Microparticles in Patients with Severe Isolated TBI. *Brain Inj,* 31**,** 1856-1862.

NESVEROVA, V. & TORNROTH-HORSEFIELD, S. 2019. Phosphorylation-Dependent Regulation of Mammalian Aquaporins. *Cells,* 8.

NGOLAB, J., TRINH, I., ROCKENSTEIN, E., MANTE, M., FLORIO, J., TREJO, M., MASLIAH, D., ADAME, A., MASLIAH, E. & RISSMAN, R. A. 2020. Correction to: Brain-derived exosomes from dementia with Lewy bodies propagate alpha-synuclein pathology. *Acta Neuropathol Commun,* 8**,** 123.

NIELSEN, S., DIGIOVANNI, S. R., CHRISTENSEN, E. I., KNEPPER, M. A. & HARRIS, H. W. 1993a. Cellular and subcellular immunolocalization of vasopressin-regulated water channel in rat kidney. *Proc Natl Acad Sci U S A,* 90**,** 11663-7.

NIELSEN, S., MARPLES, D., BIRN, H., MOHTASHAMI, M., DALBY, N. O., TRIMBLE, M. & KNEPPER, M. 1995. Expression of VAMP-2-like protein in kidney collecting duct intracellular vesicles. Colocalization with Aquaporin-2 water channels. *J Clin Invest,* 96**,** 1834-44.

NIELSEN, S., NAGELHUS, E., AMIRY-MOGHADDAM, M., BOURQUE, C., AGRE, P. & OTTERSEN, O. 1997a. Specialized membrane domains for water transport in glial cells: high-resolution immunogold cytochemistry of aquaporin-4 in rat brain. *Neuroscience***,** 171-80.

NIELSEN, S., NAGELHUS, E. A., AMIRY-MOGHADDAM, M., BOURQUE, C., AGRE, P. & OTTERSEN, O. P. 1997b. Specialized membrane domains for water transport in glial cells: high-resolution immunogold cytochemistry of aquaporin-4 in rat brain. *J Neurosci,* 17**,** 171-80.

NIELSEN, S., SMITH, B. L., CHRISTENSEN, E. I., KNEPPER, M. A. & AGRE, P. 1993b. CHIP28 water channels are localized in constitutively water-permeable segments of the nephron. *J Cell Biol,* 120**,** 371-83.

NOZAKI, K., ISHII, D. & ISHIBASHI, K. 2008. Intracellular aquaporins: clues for intracellular water transport? *Pflugers Arch,* 456**,** 701-7.

NUNES, G., RAMOS FIGUEIRA, E. R., ROCHA-FILHO, J. A., LANCHOTTE, C., NACIF, L. S., FERREIRA, D. M., ROMANO, V. C., ABDO, E. E., D'ALBUQUERQUE, L. A. C. & GALVAO, F. H. F. 2021. Hypertonic saline solution decreases oxidative stress in liver hypothermic ischemia. *Surgery,* 169**,** 1512-1518.

OGATA, K. & KOSAKA, T. 2002. Structural and quantitative analysis of astrocytes in the mouse hippocampus. *Neuroscience***,** 221-233.

OKLINSKI, M. K., LIM, J. S., CHOI, H. J., OKLINSKA, P., SKOWRONSKI, M. T. & KWON, T. H. 2014. Immunolocalization of Water Channel Proteins AQP1 and AQP4 in Rat Spinal Cord. *J Histochem Cytochem,* 62**,** 598-611.

OLIVEIRA, R. A., DINIZ, L. F., TEOTONIO, L. O., LIMA, C. G., MOTA, R. M., MARTINS, A., SANCHES, T. R., SEGURO, A. C., ANDRADE, L., SILVA, G. B., JR., LIBORIO, A. B. & DAHER, E. F. 2011. Renal tubular dysfunction in patients with American cutaneous leishmaniasis. *Kidney Int,* 80**,** 1099-106.

OSHIKAWA-HORI, S., YOKOTA-IKEDA, N., SONODA, H. & IKEDA, M. 2019. Urinary extracellular vesicular release of aquaporins in patients with renal transplantation. *BMC Nephrol,* 20**,** 216.

OVCHINNIKOVA, L. A., TEREKHOV, S. S., ZIGANSHIN, R. H., BAGROV, D. V., FILIMONOVA, I. N., ZALEVSKY, A. O. & LOMAKIN, Y. A. 2021. Reprogramming Extracellular Vesicles for Protein Therapeutics Delivery. *Pharmaceutics,* 13.

PAPADOPOULOS, M., SAADOUN, S., DAVIES & BELL, B. 2001. Emerging molecular mechanisms of brain tumour oedema. *BRITISH JOURNAL OF NEUROSURGERY* 101-108.

PAPADOPOULOS, M. C. & VERKMAN, A. S. 2013. Aquaporin water channels in the nervous system. *Nat Rev Neurosci,* 14**,** 265-77.

PATHOMPORN, P., ANANCHANOK, S., YODYING, P., SRISULUCK, K. & DURSAKORN, W. 2018. Serum electrolyte imbalance and prognostic factors of postoperative death in adult traumatic brain injury patients: A prospective cohort study. *Medicine*.

PELLAVIO, G., RUI, M., CALIOGNA, L., MARTINO, E., GASTALDI, G., COLLINA, S. & LAFORENZA, U. 2017. Regulation of Aquaporin Functional Properties Mediated by the Antioxidant Effects of Natural Compounds. *Int J Mol Sci,* 18.

PELLAVIO, G., RUI, M., CALIOGNA, L., MARTINO, E., GASTALDI, G., COLLINA, S., & LAFORENZA, U. 2017. Regulation of Aquaporin Functional Properties

Mediated by the Antioxidant Effects of Natural Compounds. *International journal of Molecular sciences,* 18.

PEREZ, G. I., BERNARD, M. P., VOCELLE, D., ZAREA, A. A., SALEH, N. A., GAGEA, M. A., SCHNEIDER, D., BAUZON, M., HERMISTON, T. & KANADA, M. 2023. Phosphatidylserine-Exposing Annexin A1-Positive Extracellular Vesicles: Potential Cancer Biomarkers. *Vaccines (Basel),* 11.

PETERS, P. J., BORST, J., OORSCHOT, V., FUKUDA, M., KRAHENBUHL, O., TSCHOPP, J., SLOT, J. W. & GEUZE, H. J. 1991. Cytotoxic T lymphocyte granules are secretory lysosomes, containing both perforin and granzymes. *J Exp Med,* 173**,** 1099-109.

POSTOLACHE, T. T., WADHAWAN, A., CAN, A., LOWRY, C. A., WOODBURY, M., MAKKAR, H., HOISINGTON, A. J., SCOTT, A. J., POTOCKI, E., BENROS, M. E. & STILLER, J. W. 2020. Inflammation in Traumatic Brain Injury. *J Alzheimers Dis,* 74**,** 1-28.

RAJENDRAN, L., HONSHO, M., ZAHN, T. R., KELLER, P., GEIGER, K. D., VERKADE, P. & SIMONS, K. 2006. Alzheimer's disease beta-amyloid peptides are released in association with exosomes. *Proc Natl Acad Sci U S A,* 103**,** 11172-7.

RAPOSO, G., NIJMAN, H. W., STOORVOGEL, W., LIEJENDEKKER, R., HARDING, C. V., MELIEF, C. J. & GEUZE, H. J. 1996. B lymphocytes secrete antigen-presenting vesicles. *J Exp Med,* 183**,** 1161-72.

RASH, J. Y., T. HUDSON, CS. AGRE, P. NIELSEN, S. 1998. Direct immunogold labeling of aquaporin-4 in square arrays of astrocyte and ependymocyte plasma membranes in rat brain and spinal cord. *PNAS U S A.,* 95**,** 11981-6.

SAADOUN, S., BELL, B. A., VERKMAN, A. S. & PAPADOPOULOS, M. C. 2008. Greatly improved neurological outcome after spinal cord compression injury in AQP4-deficient mice. *Brain,* 131**,** 1087-98.

SAADOUN, S., PAPADOPOULOS, M. C., DAVIES, D. C., KRISHNA, S. & BELL, B. A. 2002. Aquaporin-4 expression is increased in oedematous human brain tumours. *J Neurol Neurosurg Psychiatry,* 72**,** 262-5.

SAGARE, A. P., BELL, R. D., ZHAO, Z., MA, Q., WINKLER, E. A., RAMANATHAN, A. & ZLOKOVIC, B. V. 2013. Pericyte loss influences Alzheimer-like neurodegeneration in mice. *Nat Commun,* 4**,** 2932.

SALMAN, M. M., KITCHEN, P., WOODROOFE, M. N., BROWN, J. E., BILL, R. M., CONNER, A. C. & CONNER, M. T. 2017. Hypothermia increases aquaporin 4 (AQP4) plasma membrane abundance in human primary cortical astrocytes via a calcium/transient receptor potential vanilloid 4 (TRPV4)- and calmodulin-mediated mechanism. *Eur J Neurosci,* 46**,** 2542-2547.

SAMARATUNGA, H., DELAHUNT, B., SRIGLEY, J. R., BERNEY, D. M., CHENG, L., EVANS, A., FURUSATO, B., LEITE, K. R. M., MACLENNAN, G. T., MARTIGNONI, G., MOCH, H., PAN, C. C., PANER, G., RO, J., THUNDERS, M., TSUZUKI, T., WHEELER, T., VAN DER KWAST, T., ET AL 2020. Granular necrosis: a distinctive form of cell death in malignant tumours. *Pathology,* 52(5)**,** 507–514.

SAMPEY, G. C., MEYERING, S. S., ZADEH, M. A., SAIFUDDIN, M., HAKAMI, R. M. & KASHANCHI, F. 2014. Exosomes and their role in CNS viral infections. *J Neurovirol,* 20**,** 199-208.

SATO, D. K., NAKASHIMA, I., TAKAHASHI, T., MISU, T., WATERS, P., KURODA, H., NISHIYAMA, S., SUZUKI, C., TAKAI, Y., FUJIHARA, K., ITOYAMA, Y. & AOKI, M. 2013. Aquaporin-4 antibody-positive cases beyond current diagnostic criteria for NMO spectrum disorders. *Neurology,* 80**,** 2210-6.

SCHERER, W. F., SYVERTON, J. T. & GEY, G. O. 1953. Studies on the propagation in vitro of poliomyelitis viruses. IV. Viral multiplication in a stable strain of human malignant epithelial cells (strain HeLa) derived from an epidermoid carcinoma of the cervix. *J Exp Med,* 97**,** 695-710.

SIDEL, V. W. & SOLOMON, A. K. 1957. Entrance of water into human red cells under an osmotic pressure gradient. *J Gen Physiol,* 41**,** 243-57.

SILBERSTEIN, C., BOULEY, R., HUANG, Y., FANG, P., PASTOR-SOLER, N., BROWN, D. & VAN HOEK, A. N. 2004. Membrane organization and function of M1 and M23 isoforms of aquaporin-4 in epithelial cells. *Am J Physiol Renal Physiol,* 287**,** F501-11.

SIMONE, L., PISANI, F., BINDA, E., FRIGERI, A., VESCOVI, A. L., SVELTO, M. & NICCHIA, G. P. 2022. AQP4-dependent glioma cell features affect the phenotype of surrounding cells via extracellular vesicles. *Cell Biosci,* 12**,** 150.

SIMONE, L. P., F. BINDA, E. FRIGERI, A. VESCOVI, AL. SVELTO, M. NICCHIA, GP. 2022. AQP4-dependent glioma cell features affect the phenotype of surrounding cells via extracellular vesicles. *Cell & Bioscience,* 12.

SMITH, A. J., JIN, B. J., RATELADE, J. & VERKMAN, A. S. 2014. Aggregation state determines the localization and function of M1- and M23-aquaporin-4 in astrocytes. *J Cell Biol,* 204**,** 559-73.

SOLENOV, E., WATANABE, H., MANLEY, G. & VERKMAN, A. 2004. Sevenfold-reduced osmotic water permeability in primary astrocyte cultures from AQP-4-deficient mice, measured by a fluorescence quenching method. *American Journal of Physiology***,** 426–432.

SOLOMON, A. K., CHASAN, B., DIX, J. A., LUKACOVIC, M. F., TOON, M. R. & VERKMAN, A. S. 1983. The aqueous pore in the red cell membrane: band 3 as

a channel for anions, cations, nonelectrolytes, and water. *Ann N Y Acad Sci,* 414**,** 97-124.

ST-LOUIS, R., PARMENTIER, C., RAISON, D., GRANGE-MESSENT, V. & HARDIN-POUZET, H. 2012. Reactive oxygen species are required for the hypothalamic osmoregulatory response. *Endocrinology,* 153**,** 1317-29.

STIEFEL, M., TOMITA, Y. & MARMAROU, A. 2005. Secondary ischemia impairing the restoration of ion homeostasis following traumatic brain injury. *Journal of Neurosurgery*.

STIVER, S. 2009. Complications of decompressive craniectomy for traumatic brain injury. *Journal of Neurosurgery*.

STREET, J. M., BIRKHOFF, W., MENZIES, R. I., WEBB, D. J., BAILEY, M. A. & DEAR, J. W. 2011. Exosomal transmission of functional aquaporin 2 in kidney cortical collecting duct cells. *J Physiol,* 589**,** 6119-27.

SUN, M., HONEY, C., BERK, C., WONG, N. & TSUI, J. 2003. Regulation of aquaporin-4 in a traumatic brain injury model in rats. *Neurosurgery***,** 565-569.

SYLVAIN, N. J., SALMAN, M. M., PUSHIE, M. J., HOU, H., MEHER, V., HERLO, R., PEELING, L. & KELLY, M. E. 2021. The effects of trifluoperazine on brain edema, aquaporin-4 expression and metabolic markers during the acute phase of stroke using photothrombotic mouse model. *Biochim Biophys Acta Biomembr,* 1863**,** 183573.

SZATMARI, T., KIS, D., BOGDANDI, E. N., BENEDEK, A., BRIGHT, S., BOWLER, D., PERSA, E., KIS, E., BALOGH, A., NASZALYI, L. N., KADHIM, M., SAFRANY, G. & LUMNICZKY, K. 2017. Extracellular Vesicles Mediate Radiation-Induced Systemic Bystander Signals in the Bone Marrow and Spleen. *Front Immunol,* 8**,** 347.

SZU, J. I. & BINDER, D. K. 2022. Mechanisms Underlying Aquaporin-4 Subcellular Mislocalization in Epilepsy. *Front Cell Neurosci,* 16**,** 900588.

THAMPHIWATANA, S., ANGSANTIKUL, P., ESCAJADILLO, T., ZHANG, Q., OLSON, J., LUK, B. T., ZHANG, S., FANG, R. H., GAO, W., NIZET, V. & ZHANG, L. 2017. Macrophage-like nanoparticles concurrently absorbing endotoxins and proinflammatory cytokines for sepsis management. *Proc Natl Acad Sci U S A,* 114**,** 11488-11493.

THERY, C., OSTROWSKI, M. & SEGURA, E. 2009. Membrane vesicles as conveyors of immune responses. *Nat Rev Immunol,* 9**,** 581-93.

THERY, C., WITWER, K. W., AIKAWA, E., ALCARAZ, M. J., ANDERSON, J. D., ANDRIANTSITOHAINA, R., ANTONIOU, A., ARAB, T., ARCHER, F., ATKIN-SMITH, G. K., AYRE, D. C., BACH, J. M., BACHURSKI, D., BAHARVAND, H., BALAJ, L., BALDACCHINO, S., BAUER, N. N., BAXTER, A. A., BEBAWY, M.,

BECKHAM, C., BEDINA ZAVEC, A., BENMOUSSA, A., BERARDI, A. C., BERGESE, P., BIELSKA, E., BLENKIRON, C., BOBIS-WOZOWICZ, S., BOILARD, E., BOIREAU, W., BONGIOVANNI, A., BORRAS, F. E., BOSCH, S., BOULANGER, C. M., BREAKEFIELD, X., BREGLIO, A. M., BRENNAN, M. A., BRIGSTOCK, D. R., BRISSON, A., BROEKMAN, M. L., BROMBERG, J. F., BRYL-GORECKA, P., BUCH, S., BUCK, A. H., BURGER, D., BUSATTO, S., BUSCHMANN, D., BUSSOLATI, B., BUZAS, E. I., BYRD, J. B., CAMUSSI, G., CARTER, D. R., CARUSO, S., CHAMLEY, L. W., CHANG, Y. T., CHEN, C., CHEN, S., CHENG, L., CHIN, A. R., CLAYTON, A., CLERICI, S. P., COCKS, A., COCUCCI, E., COFFEY, R. J., CORDEIRO-DA-SILVA, A., COUCH, Y., COUMANS, F. A., COYLE, B., CRESCITELLI, R., CRIADO, M. F., D'SOUZA-SCHOREY, C., DAS, S., DATTA CHAUDHURI, A., DE CANDIA, P., DE SANTANA, E. F., DE WEVER, O., DEL PORTILLO, H. A., DEMARET, T., DEVILLE, S., DEVITT, A., DHONDT, B., DI VIZIO, D., DIETERICH, L. C., DOLO, V., DOMINGUEZ RUBIO, A. P., DOMINICI, M., DOURADO, M. R., DRIEDONKS, T. A., DUARTE, F. V., DUNCAN, H. M., EICHENBERGER, R. M., EKSTROM, K., EL ANDALOUSSI, S., ELIE-CAILLE, C., ERDBRUGGER, U., FALCON-PEREZ, J. M., FATIMA, F., FISH, J. E., FLORES-BELLVER, M., FORSONITS, A., FRELET-BARRAND, A., et al. 2018. Minimal information for studies of extracellular vesicles 2018 (MISEV2018): a position statement of the International Society for Extracellular Vesicles and update of the MISEV2014 guidelines. *J Extracell Vesicles,* 7**,** 1535750.

TIMALSINA, S., ARIMOTO-MATSUZAKI, K., KITAMURA, M., XU, X., WENZHE, Q., ISHIGAMI-YUASA, M., KAGECHIKA, H., & HATA, Y. 2018. Chemical compounds that suppress hypoxia-induced stress granule formation enhance cancer drug sensitivity of human cervical cancer HeLa cells. *Journal of biochemistry,* 164**,** 381–391.

TOLLIS, S., DART, A. E., TZIRCOTIS, G. & ENDRES, R. G. 2010. The zipper mechanism in phagocytosis: energetic requirements and variability in phagocytic cup shape. *BMC Syst Biol,* 4**,** 149.

TRAMS, E. G., LAUTER, C. J., SALEM, N., JR. & HEINE, U. 1981. Exfoliation of membrane ecto-enzymes in the form of micro-vesicles. *Biochim Biophys Acta,* 645**,** 63-70.

TURECKOVA, J., HERMANOVA, Z., MARCHETTI, V. & ANDEROVA, M. 2023. Astrocytic TRPV4 Channels and Their Role in Brain Ischemia. *Int J Mol Sci,* 24.

VAN DER POL, E., BOING, A. N., HARRISON, P., STURK, A. & NIEUWLAND, R. 2012. Classification, functions, and clinical relevance of extracellular vesicles. *Pharmacol Rev,* 64**,** 676-705.

VAN DER VLIST, E. J., NOLTE-'T HOEN, E. N., STOORVOGEL, W., ARKESTEIJN, G. J., & WAUBEN, M. H. 2012. Fluorescent labeling of nano-sized vesicles released by cells and subsequent quantitative and qualitative analysis by high-resolution flow cytometry. *Nature protocols,* 7**,** 311–1326.

VERKMAN, A. S. 2013. Aquaporins. *Curr Biol,* 23**,** R52-5.

VERKMAN, A. S. & MITRA, A. K. 2000. Structure and function of aquaporin water channels. *Am J Physiol Renal Physiol,* 278**,** F13-28.

VESICLEPEDIA. 2023. *Vesiclepedia* [Online]. Available: http://microvesicles.org/ [Accessed 26/09/2023 2023].

VON BARTHELD, C. S. & ALTICK, A. L. 2011. Multivesicular bodies in neurons: distribution, protein content, and trafficking functions. *Prog Neurobiol,* 93**,** 313-40.

WALLENSTEN, J., NAGER, A., ASBERG, M., BORG, K., BESER, A., WILCZEK, A. & MOBARREZ, F. 2023. Author Correction: Leakage of astrocyte-derived extracellular vesicles in stress-induced exhaustion disorder: a cross-sectional study. *Sci Rep,* 13**,** 10211.

WANG, F., CERIONE, R. A. & ANTONYAK, M. A. 2021. Isolation and characterization of extracellular vesicles produced by cell lines. *STAR Protoc,* 2**,** 100295.

WEATHERALL, E. & WILLMOTT, G. R. 2015. Applications of tunable resistive pulse sensing. *Analyst,* 140**,** 3318-34.

WITWER, K. W., BUZAS, E. I., BEMIS, L. T., BORA, A., LASSER, C., LOTVALL, J., NOLTE-'T HOEN, E. N., PIPER, M. G., SIVARAMAN, S., SKOG, J., THERY, C., WAUBEN, M. H. & HOCHBERG, F. 2013. Standardization of sample collection, isolation and analysis methods in extracellular vesicle research. *J Extracell Vesicles,* 2.

WOLF, P. 1967. The nature and significance of platelet products in human plasma. *Br J Haematol,* 13**,** 269-88.

XIN, D., LI, T., CHU, X., KE, H., LIU, D. & WANG, Z. 2021. MSCs-extracellular vesicles attenuated neuroinflammation, synapse damage and microglial phagocytosis after hypoxia-ischemia injury by preventing osteopontin expression. *Pharmacol Res,* 164**,** 105322.

XING, R., CHENG, J., YU, J., LI, S., MA, H. & ZHAO, Y. 2023. Trifluoperazine reduces apoptosis and inflammatory responses in traumatic brain injury by preventing the accumulation of Aquaporin4 on the surface of brain cells. *Int J Med Sci,* 20**,** 797-809.

YANEZ-MO, M., SILJANDER, P. R., ANDREU, Z., ZAVEC, A. B., BORRAS, F. E., BUZAS, E. I., BUZAS, K., CASAL, E., CAPPELLO, F., CARVALHO, J., COLAS, E., CORDEIRO-DA SILVA, A., FAIS, S., FALCON-PEREZ, J. M., GHOBRIAL, I. M., GIEBEL, B., GIMONA, M., GRANER, M., GURSEL, I., GURSEL, M., HEEGAARD, N. H., HENDRIX, A., KIERULF, P., KOKUBUN, K., KOSANOVIC, M., KRALJ-IGLIC, V., KRAMER-ALBERS, E. M., LAITINEN, S., LASSER, C., LENER, T., LIGETI, E., LINE, A., LIPPS, G., LLORENTE, A., LOTVALL, J., MANCEK-KEBER, M., MARCILLA, A., MITTELBRUNN, M., NAZARENKO, I., NOLTE-'T HOEN, E. N., NYMAN, T. A., O'DRISCOLL, L., OLIVAN, M.,

OLIVEIRA, C., PALLINGER, E., DEL PORTILLO, H. A., REVENTOS, J., RIGAU, M., ROHDE, E., SAMMAR, M., SANCHEZ-MADRID, F., SANTAREM, N., SCHALLMOSER, K., OSTENFELD, M. S., STOORVOGEL, W., STUKELJ, R., VAN DER GREIN, S. G., VASCONCELOS, M. H., WAUBEN, M. H. & DE WEVER, O. 2015. Biological properties of extracellular vesicles and their physiological functions. *J Extracell Vesicles,* 4**,** 27066.

YANG, C. H., QUAN, Z. X., WANG, G. J., HE, T., CHEN, Z. Y., LI, Q. C., YANG, J. & WANG, Q. 2022. Elevated intraspinal pressure in traumatic spinal cord injury is a promising therapeutic target. *Neural Regen Res,* 17**,** 1703-1710.

YANG, T., ZHANG, A., HONEGGAR, M., KOHAN, D. E., MIZEL, D., SANDERS, K., HOIDAL, J. R., BRIGGS, J. P. & SCHNERMANN, J. B. 2005. Hypertonic induction of COX-2 in collecting duct cells by reactive oxygen species of mitochondrial origin. *J Biol Chem,* 280**,** 34966-73.

YUYAMA, K., SUN, H., MITSUTAKE, S. & IGARASHI, Y. 2012. Sphingolipid-modulated exosome secretion promotes clearance of amyloid-beta by microglia. *J Biol Chem,* 287**,** 10977-89.

YUYAMA, K., SUN, H., SAKAI, S., MITSUTAKE, S., OKADA, M., TAHARA, H., FURUKAWA, J., FUJITANI, N., SHINOHARA, Y. & IGARASHI, Y. 2014. Decreased amyloid-beta pathologies by intracerebral loading of glycosphingolipid-enriched exosomes in Alzheimer model mice. *J Biol Chem,* 289**,** 24488-98.

YUYAMA, K., SUN, H., USUKI, S., SAKAI, S., HANAMATSU, H., MIOKA, T., KIMURA, N., OKADA, M., TAHARA, H., FURUKAWA, J., FUJITANI, N., SHINOHARA, Y. & IGARASHI, Y. 2015. A potential function for neuronal exosomes: sequestering intracerebral amyloid-beta peptide. *FEBS Lett,* 589**,** 84-8.

ZWAAL, R. F. & SCHROIT, A. J. 1997. Pathophysiologic implications of membrane phospholipid asymmetry in blood cells. *Blood,* 89**,** 1121-32.

Appendix 1

FASTA sequence of PDest 47

n>pcDNA-DEST47

GACGGATCGGGAGATCTCCCGATCCCCTATGGTGCACTCTCAGTACAATCTGCTCTG
ATGCCGCATAGTTAAGCCAGTAT

CTGCTCCCTGCTTGTGTGTTGGAGGTCGCTGAGTAGTGCGCGAGCAAAATTTAAGCT
ACAACAAGGCAAGGCTTGACCGA

CAATTGCATGAAGAATCTGCTTAGGGTTAGGCGTTTTGCGCTGCTTCGCGATGTACG
GGCCAGATATACGCGTTGACATT

GATTATTGACTAGTTATTAATAGTAATCAATTACGGGGTCATTAGTTCATAGCCCAT
ATATGGAGTTCCGCGTTACATAA

CTTACGGTAAATGGCCCGCCTGGCTGACCGCCCAACGACCCCCGCCCATTGACGTC
AATAATGACGTATGTTCCCATAGT

AACGCCAATAGGGACTTTCCATTGACGTCAATGGGTGGAGTATTTACGGTAAACTG
CCCACTTGGCAGTACATCAAGTGT

ATCATATGCCAAGTACGCCCCCTATTGACGTCAATGACGGTAAATGGCCCGCCTGG
CATTATGCCCAGTACATGACCTTA

TGGGACTTTCCTACTTGGCAGTACATCTACGTATTAGTCATCGCTATTACCATGGTG
ATGCGGTTTTGGCAGTACATCAA

TGGGCGTGGATAGCGGTTTGACTCACGGGGATTTCCAAGTCTCCACCCCATTGACG
TCAATGGGAGTTTGTTTTGGCACC

AAAATCAACGGGACTTTCCAAAATGTCGTAACAACTCCGCCCCATTGACGCAAATG
GGCGGTAGGCGTGTACGGTGGGAG

GTCTATATAAGCAGAGCTCTCTGGCTAACTAGAGAACCCACTGCTTACTGGCTTATC
GAAATTAATACGACTCACTATAG

GGAGACCCAAGCTGGCTAGTTAAGCTTGATCAAACAAGTTTGTACAAAAAAGCTGA
ACGAGAAACGTAAAATGATATAAA

TATCAATATATTAAATTAGATTTTGCATAAAAAACAGACTACATAATACTGTAAAA
CACAACATATCCAGTCACTATGGC

GGCCGCATTAGGCACCCCAGGCTTTACACTTTATGCTTCCGGCTCGTATAATGTGTG
GATTTTGAGTTAGGATCCGTCGA

GATTTTCAGGAGCTAAGGAAGCTAAAATGGAGAAAAAAATCACTGGATATACCAC
CGTTGATATATCCCAATGGCATCGT

AAAGAACATTTTGAGGCATTTCAGTCAGTTGCTCAATGTACCTATAACCAGACCGTT
CAGCTGGATATTACGGCCTTTTT

AAAGACCGTAAAGAAAAATAAGCACAAGTTTTATCCGGCCTTTATTCACATTCTTG
CCCGCCTGATGAATGCTCATCCGG

AATTCCGTATGGCAATGAAAGACGGTGAGCTGGTGATATGGGATAGTGTTCACCCT
TGTTACACCGTTTTCCATGAGCAA

ACTGAAACGTTTTCATCGCTCTGGAGTGAATACCACGACGATTTCCGGCAGTTTCTA
CACATATATTCGCAAGATGTGGC

GTGTTACGGTGAAAACCTGGCCTATTTCCCTAAAGGGTTTATTGAGAATATGTTTTT
CGTCTCAGCCAATCCCTGGGTGA

GTTTCACCAGTTTTGATTTAAACGTGGCCAATATGGACAACTTCTTCGCCCCCGTTT
TCACCATGGGCAAATATTATACG

CAAGGCGACAAGGTGCTGATGCCGCTGGCGATTCAGGTTCATCATGCCGTTTGTGA
TGGCTTCCATGTCGGCAGAATGCT

TAATGAATTACAACAGTACTGCGATGAGTGGCAGGCGGGGCGTAATCTAGAGGATC
CGGCTTACTAAAAGCCAGATAACA

GTATGCGTATTTGCGCGCTGATTTTTGCGGTATAAGAATATATACTGATATGTATAC
CCGAAGTATGTCAAAAAGAGGTA

TGCTATGAAGCAGCGTATTACAGTGACAGTTGACAGCGACAGCTATCAGTTGCTCA
AGGCATATATGATGTCAATATCTC

CGGTCTGGTAAGCACAACCATGCAGAATGAAGCCCGTCGTCTGCGTGCCGAACGCT
GGAAAGCGGAAAATCAGGAAGGGA

TGGCTGAGGTCGCCCGGTTTATTGAAATGAACGGCTCTTTTGCTGACGAGAACAGG
GGCTGGTGAAATGCAGTTTAAGGT

TTACACCTATAAAAGAGAGAGCCGTTATCGTCTGTTTGTGGATGTACAGAGTGATA
TTATTGACACGCCCGGGCGACGGA

TGGTGATCCCCCTGGCCAGTGCACGTCTGCTGTCAGATAAAGTCCCCCGTGAACTTT
ACCCGGTGGTGCATATCGGGGAT

GAAAGCTGGCGCATGATGACCACCGATATGGCCAGTGTGCCGGTCTCCGTTATCGG
GGAAGAAGTGGCTGATCTCAGCCA

CCGCGAAAATGACATCAAAAACGCCATTAACCTGATGTTCTGGGGAATATAAATGT
CAGGCTCCCTTATACACAGCCAGT

CTGCAGGTCGACCATAGTGACTGGATATGTTGTGTTTTACAGTATTATGTAGTCTGT
TTTTTATGCAAAATCTAATTTAA

TATATTGATATTTATATCATTTTACGTTTCTCGTTCAGCTTTCTTGTACAAAGTGGTT
CGATCTAGAATGGCTAGCAAAG

GAGAAGAACTTTTCACTGGAGTTGTCCCAATTCTTGTTGAATTAGATGGTGATGTTA
ATGGGCACAAATTTTCTGTCAGT

GGAGAGGGTGAAGGTGATGCTACATACGGAAAGCTTACCCTTAAATTTATTTGCAC
TACTGGAAAACTACCTGTTCCATG

GCCAACACTTGTCACTACTTTCTCTTATGGTGTTCAATGCTTTTCCCGTTATCCGGAT
CATATGAAACGGCATGACTTTT

TCAAGAGTGCCATGCCCGAAGGTTATGTACAGGAACGCACTATATCTTTCAAAGAT
GACGGGAACTACAAGACGCGTGCT

GAAGTCAAGTTTGAAGGTGATACCCTTGTTAATCGTATCGAGTTAAAAGGTATTGA
TTTTAAAGAAGATGGAAACATTCT

CGGACACAAACTCGAGTACAACTATAACTCACACAATGTATACATCACGGCAGACA
AACAAAAGAATGGAATCAAAGCTA

ACTTCAAAATTCGCCACAACATTGAAGATGGATCCGTTCAACTAGCAGACCATTAT
CAACAAAATACTCCAATTGGCGAT

GGCCCTGTCCTTTTACCAGACAACCATTACCTGTCGACACAATCTGCCCTTTCGAAA
GATCCCAACGAAAAGCGTGACCA

CATGGTCCTTCTTGAGTTTGTAACTGCTGCTGGGATTACACATGGCATGGATGAGCT
CTACAAATAATGAATTAAACCCG

CTGATCAGCCTCGACTGTGCCTTCTAGTTGCCAGCCATCTGTTGTTTGCCCCTCCCCC
GTGCCTTCCTTGACCCTGGAAG

GTGCCACTCCCACTGTCCTTTCCTAATAAAATGAGGAAATTGCATCGCATTGTCTGA
GTAGGTGTCATTCTATTCTGGGG

GGTGGGGTGGGGCAGGACAGCAAGGGGGAGGATTGGGAAGACAATAGCAGGCAT
GCTGGGGATGCGGTGGGCTCTATGGC

TTCTGAGGCGGAAAGAACCAGCTGGGGCTCTAGGGGGTATCCCCACGCGCCCTGTA
GCGGCGCATTAAGCGCGGCGGGTG

TGGTGGTTACGCGCAGCGTGACCGCTACACTTGCCAGCGCCCTAGCGCCCGCTCCTT
TCGCTTTCTTCCCTTCCTTTCTC

GCCACGTTCGCCGGCTTTCCCCGTCAAGCTCTAAATCGGGGGCTCCCTTTAGGGTTC
CGATTTAGTGCTTTACGGCACCT

CGACCCCAAAAAACTTGATTAGGGTGATGGTTCACGTAGTGGGCCATCGCCCTGAT
AGACGGTTTTTCGCCCTTTGACGT

TGGAGTCCACGTTCTTTAATAGTGGACTCTTGTTCCAAACTGGAACAACACTCAACC
CTATCTCGGTCTATTCTTTTGAT

TTATAAGGGATTTTGCCGATTTCGGCCTATTGGTTAAAAAATGAGCTGATTTAACAA
AAATTTAACGCGAATTAATTCTG

TGGAATGTGTGTCAGTTAGGGTGTGGAAAGTCCCCAGGCTCCCCAGCAGGCAGAAG
TATGCAAAGCATGCATCTCAATTA

GTCAGCAACCAGGTGTGGAAAGTCCCCAGGCTCCCCAGCAGGCAGAAGTATGCAA
AGCATGCATCTCAATTAGTCAGCAA

CCATAGTCCCGCCCCTAACTCCGCCCATCCCGCCCCTAACTCCGCCCAGTTCCGCCC
ATTCTCCGCCCCATGGCTGACTA

ATTTTTTTTATTTATGCAGAGGCCGAGGCCGCCTCTGCCTCTGAGCTATTCCAGAAG
TAGTGAGGAGGCTTTTTTGGAGG

CCTAGGCTTTTGCAAAAAGCTCCCGGGAGCTTGTATATCCATTTTCGGATCTGATCA
AGAGACAGGATGAGGATCGTTTC

GCATGATTGAACAAGATGGATTGCACGCAGGTTCTCCGGCCGCTTGGGTGGAGAGG
CTATTCGGCTATGACTGGGCACAA

CAGACAATCGGCTGCTCTGATGCCGCCGTGTTCCGGCTGTCAGCGCAGGGGCGCCC
GGTTCTTTTTGTCAAGACCGACCT

GTCCGGTGCCCTGAATGAACTGCAGGACGAGGCAGCGCGGCTATCGTGGCTGGCCA
CGACGGGCGTTCCTTGCGCAGCTG

TGCTCGACGTTGTCACTGAAGCGGGAAGGGACTGGCTGCTATTGGGCGAAGTGCCG
GGGCAGGATCTCCTGTCATCTCAC

CTTGCTCCTGCCGAGAAAGTATCCATCATGGCTGATGCAATGCGGCGGCTGCATAC
GCTTGATCCGGCTACCTGCCCATT

CGACCACCAAGCGAAACATCGCATCGAGCGAGCACGTACTCGGATGGAAGCCGGT
CTTGTCGATCAGGATGATCTGGACG

AAGAGCATCAGGGGCTCGCGCCAGCCGAACTGTTCGCCAGGCTCAAGGCGCGCAT
GCCCGACGGCGAGGATCTCGTCGTG

ACCCATGGCGATGCCTGCTTGCCGAATATCATGGTGGAAAATGGCCGCTTTTCTGG
ATTCATCGACTGTGGCCGGCTGGG

TGTGGCGGACCGCTATCAGGACATAGCGTTGGCTACCCGTGATATTGCTGAAGAGC
TTGGCGGCGAATGGGCTGACCGCT

TCCTCGTGCTTTACGGTATCGCCGCTCCCGATTCGCAGCGCATCGCCTTCTATCGCC
TTCTTGACGAGTTCTTCTGAGCG

GGACTCTGGGGTTCGCGAAATGACCGACCAAGCGACGCCCAACCTGCCATCACGAG
ATTTCGATTCCACCGCCGCCTTCT

ATGAAAGGTTGGGCTTCGGAATCGTTTTCCGGGACGCCGGCTGGATGATCCTCCAG
CGCGGGGATCTCATGCTGGAGTTC

TTCGCCCACCCCAACTTGTTTATTGCAGCTTATAATGGTTACAAATAAAGCAATAGC
ATCACAAATTTCACAAATAAAGC

ATTTTTTTCACTGCATTCTAGTTGTGGTTTGTCCAAACTCATCAATGTATCTTATCAT
GTCTGTATACCGTCGACCTCTA

GCTAGAGCTTGGCGTAATCATGGTCATAGCTGTTTCCTGTGTGAAATTGTTATCCGC
TCACAATTCCACACAACATACGA

GCCGGAAGCATAAAGTGTAAAGCCTGGGGTGCCTAATGAGTGAGCTAACTCACATT
AATTGCGTTGCGCTCACTGCCCGC

TTTCCAGTCGGGAAACCTGTCGTGCCAGCTGCATTAATGAATCGGCCAACGCGCGG
GGAGAGGCGGTTTGCGTATTGGGC

GCTCTTCCGCTTCCTCGCTCACTGACTCGCTGCGCTCGGTCGTTCGGCTGCGGCGAG
CGGTATCAGCTCACTCAAAGGCG

GTAATACGGTTATCCACAGAATCAGGGGATAACGCAGGAAAGAACATGTGAGCAA
AAGGCCAGCAAAAGGCCAGGAACCG

TAAAAAGGCCGCGTTGCTGGCGTTTTTCCATAGGCTCCGCCCCCCTGACGAGCATC
ACAAAAATCGACGCTCAAGTCAGA

GGTGGCGAAACCCGACAGGACTATAAAGATACCAGGCGTTTCCCCCTGGAAGCTCC
CTCGTGCGCTCTCCTGTTCCGACC

CTGCCGCTTACCGGATACCTGTCCGCCTTTCTCCCTTCGGGAAGCGTGGCGCTTTCT
CATAGCTCACGCTGTAGGTATCT

CAGTTCGGTGTAGGTCGTTCGCTCCAAGCTGGGCTGTGTGCACGAACCCCCCGTTCA
GCCCGACCGCTGCGCCTTATCCG

GTAACTATCGTCTTGAGTCCAACCCGGTAAGACACGACTTATCGCCACTGGCAGCA
GCCACTGGTAACAGGATTAGCAGA

GCGAGGTATGTAGGCGGTGCTACAGAGTTCTTGAAGTGGTGGCCTAACTACGGCTA
CACTAGAAGAACAGTATTTGGTAT

CTGCGCTCTGCTGAAGCCAGTTACCTTCGGAAAAAGAGTTGGTAGCTCTTGATCCG
GCAAACAAACCACCGCTGGTAGCG

GTGGTTTTTTTGTTTGCAAGCAGCAGATTACGCGCAGAAAAAAAGGATCTCAAGAA
GATCCTTTGATCTTTTCTACGGGG

TCTGACGCTCAGTGGAACGAAAACTCACGTTAAGGGATTTTGGTCATGAGATTATC
AAAAAGGATCTTCACCTAGATCCT

TTTAAATTAAAAATGAAGTTTTAAATCAATCTAAAGTATATATGAGTAAACTTGGTC
TGACAGTTACCAATGCTTAATCA

GTGAGGCACCTATCTCAGCGATCTGTCTATTTCGTTCATCCATAGTTGCCTGACTCC
CCGTCGTGTAGATAACTACGATA

CGGGAGGGCTTACCATCTGGCCCCAGTGCTGCAATGATACCGCGAGACCCACGCTC
ACCGGCTCCAGATTTATCAGCAAT

AAACCAGCCAGCCGGAAGGGCCGAGCGCAGAAGTGGTCCTGCAACTTTATCCGCCT
CCATCCAGTCTATTAATTGTTGCC

GGGAAGCTAGAGTAAGTAGTTCGCCAGTTAATAGTTTGCGCAACGTTGTTGCCATT
GCTACAGGCATCGTGGTGTCACGC

TCGTCGTTTGGTATGGCTTCATTCAGCTCCGGTTCCCAACGATCAAGGCGAGTTACA
TGATCCCCCATGTTGTGCAAAAA

AGCGGTTAGCTCCTTCGGTCCTCCGATCGTTGTCAGAAGTAAGTTGGCCGCAGTGTT
ATCACTCATGGTTATGGCAGCAC

TGCATAATTCTCTTACTGTCATGCCATCCGTAAGATGCTTTTCTGTGACTGGTGAGT
ACTCAACCAAGTCATTCTGAGAA

TAGTGTATGCGGCGACCGAGTTGCTCTTGCCCGGCGTCAATACGGGATAATACCGC
GCCACATAGCAGAACTTTAAAAGT

GCTCATCATTGGAAAACGTTCTTCGGGGCGAAAACTCTCAAGGATCTTACCGCTGTT
GAGATCCAGTTCGATGTAACCCA

CTCGTGCACCCAACTGATCTTCAGCATCTTTTACTTTCACCAGCGTTTCTGGGTGAG
CAAAAACAGGAAGGCAAAATGCC

GCAAAAAAGGGAATAAGGGCGACACGGAAATGTTGAATACTCATACTCTTCCTTTT
TCAATATTATTGAAGCATTTATCA

GGGTTATTGTCTCATGAGCGGATACATATTTGAATGTATTTAGAAAAATAAACAAA
TAGGGGTTCCGCGCACATTTCCCC

GAAAAGTGCCACCTGACGTC